Electronic Characterization of Mass-Selected Acyclic, Polycyclic and Oxygenated Hydrocarbons in Neon Matrices

INAUGURALDISSERTATION

zur

Erlangung der Würde eines Doktors der Philosophie

vorgelegt der

Philosophisch-Naturwissenschaftlichen Fakultät

der Universität Basel

von

Arghya Chakraborty

aus Westbengal, Indien

Basel, 2016

Genehmigt von der Philosophisch-Naturwissenschaftlichen Fakultät

auf antrag von

Dissertationsleiter: Prof. Dr. John. P. Maier
Korreferent: Prof. Dr. Stefan Willitsch

Basel, 23 Februar 2016

Prof. Dr. J. Schibler
Dekan

Electronic Characterization of Mass-Selected Acyclic, Polycyclic and Oxygenated Hydrocarbons in Neon Matrices

---

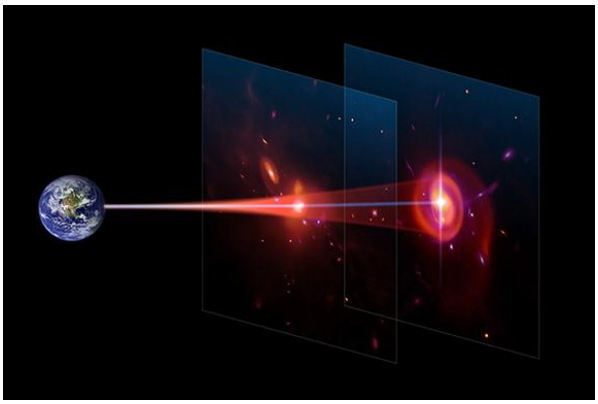

PhD THESIS

Of

ARGHYA CHAKRABORTY

Basel 2016

Acknowledgements

A researcher needs a healthy working atmosphere to be productive. The work and personal life in Basel would not have been so pleasant without the guidance and support of several individuals. First of all, I would like to thank Prof. John Paul Maier for his constant endorsement, supervision and providing world class experimental facilities in laboratory. Beside science, I have learned lots of technical skills from him and hopefully will apply them in my entire career.

I am very much thankful to Prof. Stefan Willitsch for being the co-referee of my thesis. Prof. Markus Meuwly is thanked for accepting to be the chair in my PhD defense.

Heartiest thank of mine goes to Dr. Jan Fulara for teaching me the essentials of the matrix isolation set-up, sharing his deep knowledge on spectroscopy and helping with his computational skill. Special thanks are also addressed to Dr. Corey Rice for his advices, explanations and experimental ideas. I am highly privileged to him for being the proof reader of my thesis.

I would like to thank my lab mates Karol Philiposki and Dr. Rainer Dietsche for providing a pleasant work atmosphere inside the laboratory and their readiness to help in experiments. I am also grateful to my other group members for being nice to me.

I also appreciate the constant support and advise which I received from the people who are technically involved in the experiments. Grischa Martin, Philipp Knöpfel and Dieter Wild from mechanical workshop are thanked. Georg Holderied is thanked for his expertise on electronics and Jacques Lecoultre for synthesizing many of the chemicals which played crucial role in the success of respective projects. I am thankful to Jean-Pierre Ramseyer for his technical supports, especially for online ordering of the chemicals and taking care of crucial things inside lab. I am also grateful to Dr. Anatoly Johnson for his help with laser set-ups and LabView programming. I want to thank Mike Devereux for his technical help with computers.

Very special thanks go to Snigdha Ghosh for her mental support throughout my PhD and also for being partial proof reader of my thesis. I am also grateful to my parents and friends for their love, strength and encouragement.

Finally, I would like to thank Swiss National Science Foundation and University of Basel for the financial support.

Dedicated to

My parents and Snigdha

Abstract

Interstellar chemistry embarked with the discovery of CH, CH^+, and CN in extraterrestrial clouds. Presently, a large number of molecules have been identified in different galactic environments mostly by millimeter-wave and infrared spectroscopy. Molecular complexity and the spectral features dramatically depend on the particle density and the temperature of the astronomical region where they reside. Hence, spectroscopic analysis of extraterrestrial molecules has a valid mean to probe the physical and chemical condition and history of galactic media.

Life on Earth is carbon based and surprisingly, similar tendency has been found in interstellar molecules. Almost 80 percent of detected species contain carbon as a major constituent. Hence, a better characterization of the molecular universe may elucidate the origin of terrestrial life.

Two long standing riddles in molecular astrophysics are the diffuse interstellar absorption lines in the visible and the broad emission features in the mid-infrared. Carbonaceous systems ranging from small acyclic to polycyclic aromatics are considered to be the carriers of these absorption and emission bands. To recognize individual molecules responsible for these transitions, spectroscopic analysis of astrophysically relevant species in the laboratory is needed; comparison studies between astronomical measurements and laboratory spectra are the way for identification. These exotic molecules may be stable in galactic clouds under very cold and low density conditions but are extremely short-lived in the laboratory framework. Therefore, noncontemporary synthesizing and sensitive characterizing methods are required.

The matrix isolation spectroscopy is considered as an outdated-technique after the discovery of laser-based experiments but in combination with theory, it still serves a pivotal role in characterization of transient species. Exotic organics are synthesized in electrical discharge for the respective precursors. The ions of interest are co-deposited with neon on a cold surface (6 K) after mass-selection. Neutrals are generated in the matrix by UV irradiation.

The acyclic unsaturated organics possess very unique structural flexibility. By mass selective deposition of a particular *m/z* ratio in solid neon, several isomers have been detected. An advantage of the matrix isolation technique is that all possible electronic transitions of

trapped species in the experimental measurement range can be recorded at once. Rare gases provide an environment in which the guest-host interactions slightly perturb the experimental band positions as compared to the gas-phase. Still matrix isolated spectrum is a good starting point for high resolution study and thence astrophysical findings.

Moderately intense absorptions are observed both in the visible and UV for $C_7H_n^{+/0}$ and $C_5H_n^{+/0}$, and charged oxygen containing polycarbon chains $H_2C_6O^+$, HC_7O^+, and $C_4O_2^+$ in neon matrices. The structural assignments of the electronic systems have been made on the basis of calculated ground-state stabilities with DFT and MP2 level of theory and computed excitation energies with TD DFT, SAC-CI, and CASPT2 methods. However, some of these ions and radicals have strong possibility to be the carriers of diffuse interstellar bands. The neutral oxygenated hydrocarbons are excluded as the carriers because no transition was detected after irradiation of the matrix. Theory explains that they possess strong transition in the deep UV. In addition, protonated PAHs and their oxygen containing analogs, which are credited for unidentified emission features, have been studied. Strong optical transitions suggest that they could be carriers of diffuse interstellar bands as well. A key species in combustion chemistry likely responsible for PAHs formation via mass-growth processes, fulvenallenyl radical, has been electronically characterized.

A part of this dissertation is devoted to physical organic chemistry. Reaction intermediates are too short-lived to probe. Nevertheless, identification of these species helps to infer a probable synthetic mechanism. Vibrationally resolved electronic spectra of fluorenylium, phenalenylium and fluorenyl radical have been measured in a neon matrix.

This electronic transition database of transient molecules created in the thesis can be used for their further gas-phase analysis and *in situ* detection in reaction or combustion systems.

Contents

PART-B: RESULTS

3. ELECTRONIC TRANSITIONS OF C_7H_n (3-5) CATIONS AND RADICALS

4. ELECTRONIC CHARACTERIZATION OF OXYGEN CONTAINING ACYCLIC HYDROCARBON CATIONS: ION-MOLECULE REACTION PRODUCT

5. SPECTROSCOPY OF PRONOTATED POLYCYCLIC AROMATICS

ACRONYMS AND ABBREVIATIONS

0_0^0	Origin band of electronic transition [**A** (v'=0) ← **X** (v''=0)]
AC	Alternating current
ASW	Amorphous solid water
AGB	Asymptotic giant branch
CASPT2	Complete active space with second-order perturbation theory
CASSCF	Complete active space self-consistent field
CCD	Charge-coupled device
cc-pV(D/T)Z	Correlation consistent polarized valence-(double/triple)-zeta, basis-set
CCSD(T)	Couple-cluster singles, doubles (triples) method
CI	Chemical ionization
CIS	Configuration interaction singles
DC	Direct current
DIB	Diffuse interstellar band
DBT	2,3,6,7 dibenzotropone
EI	Electron impact Ionization
ESR	Electron spin resonance
FA	Fulvenallenyl radical
FL	9-fluorenone
FT	Fluoranthene
FUV	Far ultraviolet
in situ	'in position' (Latine)
ISM	Interstellar medium
IR	Infrared
MI	Matrix isolation
MP2	Moller-Plesset perturbation theory of 2^{nd} order
MRD-CI	Multi-reference double-excitation/configuration interaction
MS	Mass spectrometry
MW	Microwave
Nd:YAG	Neodynium(III)-doped yttrium aluminum garnet [Nd^{+3}: $Y_3Al_5O_{12}$]
NMR	Nuclear magnetic resonance
NTT	New technology telescope
PAH	Polycyclic aromatic hydrocarbon
PDR	Photodissociation/Photondominated region
PES	Potential energy surface

PH	Phenantherene
PNe	Planetary nebulae
PMT	Photomultiplier tube
QMS	Quadrupole mass analyser
R2P2CI	two-color two-photon ionization
Sg	Sagittarius
SAC-CI	Symmetry adapted cluster/configuration interaction
TD DFT	Time dependent density functional theory
TMC	Taurus Molecular Cloud
UIR	Unidentified infrared band
VLT	Very large telescope
YSO	Young stellar object
ZPL	Zero phonon line

History of Astronomy: How it all started?

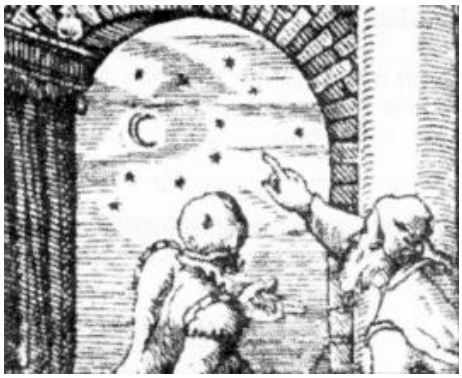

Astronomy is the oldest natural science. Celestial phenomena had multifaceted influence on ancient human life. Mankind was horrified by numerous light spots in the dark sky and their sudden disappearance during the day. Early human culture reckoned the celestial objects as a super-power controlling rain, drought, seasons, and tides on Earth. A substantial role of stars and planets in religious functions, mythology and even in antediluvian calendrical systems has been identified. Being the brightest ones in the sky, the Sun and Moon had drawn more importance. According to archeological evidences, humans have got some impression on solar and lunar cycles in the Bronze Age.

Art has long been a way to mankind for expressing their thoughts. The **Nebra sky disk**, founded by archeological thieves in 1999 and recovered in 2002 in Switzerland, is Bronze Age art and the earliest (2000 BC) known depiction of celestial phenomena.[1] The gold decoration on the disk shows a full Moon and a crescent Moon along with stars (**Figure A.1**). This could be a foot print of astronomy in ancient world. The **Kokino**, a Bronze Age archaeological site now in the Republic of Macedonia, represents an astronomical observatory constructed around 1900 BC and was continuously serving until 700 BC (**Figure A.2**).[2] The archeologists interpreted that this place equipped with special stones was for tracking the movement of Sun and Moon.

1

2

Figure A. 1) Nebra sky disk, 2000 BC; **2)** Kokino Observatory, 1900 BC

Mesopotamia, India and China have major contribution in ancient astronomy. The eastern observers, especially China, successfully tracked the appearance of new stars in sky. It has been claimed that the Chinese had seen the Halley's Comet around 240 BC and possibly in 1059 BC too.[3]

Astronomical studies in Indian subcontinent can be found in the Indus Valley Civilization. They used calendar in 3rd millennium BC.[4] The oldest surviving Indian astronomical document is the Vedanga Jyotisha, which demonstrates how to track solar and lunar motions for rituals.[5]

Western history of astronomy starts with the ancient Greek civilization about 600 BC. The root of western astronomy can be found in Mesopotamia. The Babylonian astronomy was the basis of the Greek and Hellenistic astronomy. In this regime, the motion of celestial objects had been treated with mathematics.[6,7] **Pythagoras of Samos**, the great Greek mathematician, is the founder of the movement called Pythagoreanism.[7] The three-dimensional models for explaining the apparent motions of planets were developed in the 4th century BC by **Eudoxus of Cnidus** and **Callippus of Cyzicus**. Around 220 BC **Eratosthenes** claimed the Earth as a sphere based on its shadow on the Moon during lunar eclipses which is one of the eminent hypothesis ever made by any philosopher from ancient world.[7] He also calculated the circumference of the Earth to be 40320 km which is very close to the real value (40075 km).

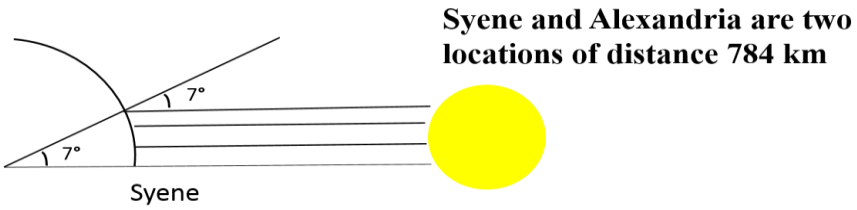

The ratio of the distance between two places to the circumference of Earth (R) should be equal to 7/360.

784 / R km = 7° /360°

Hence, R= **40320** km

Contemporaneously, **Aristotle** and his student **Plato** attempted to pursue quantitative study on the Earth's motion. The Aristotelian cosmology was geocentric – Earth was considered at the center of the universe. From the observations with naked eye and philosophical imaginations, this geocentric model was well accepted until the 15th century AD.

16th century is called as the period of *renaissance* in astronomy and Nicolaus Copernicus was the key character. For the first time, he proposed the heliocentric model (sun in the middle) of the universe (solar system).[8] There was a political dispute regarding the acceptance of the new model. Undoubtedly, this work is a revolutionary step towards modern cosmology. The hypothesis was defended and modified later by **Galileo Galilei** and **Johannes Kepler**. On the technological front, one of the foundation for the leap forward is the manufacture of telescope by Galileo Galilei.[9] It is apposite to say that he is the first modern scientist who not only proposed a model but also defended by real observations. Sunspots, mountains on the Moon, satellites of Jupiter (Io, Europa, Ganymede and Callisto) and Saturn's ring were discovered by him.[10] Until then, mathematical and philosophical approaches were serving astronomy. The importance of spectroscopy has been introduced by **Isaac Newton** with his prism experiment, where he showed that white light is a combination of seven different wavelengths of light.[11] Detection of atomic absorption by **Gustav Kirchhoff** and **Robert Bunsen** in 18th century is also one of the greatest works that exemplified the essence of spectroscopy in astronomy.[12]

By the use of increasingly advanced telescopes, in the period between 17th to 19th centuries, a number of planets and stars were discovered and a rough image of the Milky Way was more or less established.

Edwin Hubble has huge contribution in modern astronomy. He has identified Andromeda and other spiral nebulae as star systems. Hubble and Milton made the pioneer discovery in 1929 that the universe is expanding,[13] changing the approach of astrophysical research. It indicates that the information of young universe is lying on the infrared (IR) domain because visible light emitted from early stars after Big Bang is now stretched to the IR due to this expansion of space. Few years later in 1950s, the invention of radio-astronomy[14] has facilitated the characterization of outer space.

BIBLIOGRAPHY

[1] D. Welle, *The Sky Disc of Nebra: Bronze Age Sky Disc Deciphered,* **2002**: http://www.bibliotecapleyades.net/arqueologia/nebra_disk.htm

[2] *Archaeo-astronomical Site Kokino*, UNESCO World Heritage, **2009**: http://whc.unesco.org/en/tentativelists/5413/

[3] M. Kidger, *Astronomical Enigmas: Life on Mars, the Star of Bethlehem, and Other Milky Way Mysteries.* The Johns Hopkins University Press, **2005**.

[4] P-Y. Bely, C. Christian and J-R Roy, *A Question and Answer Guide to Astronomy*. Cambridge University Press. **2010**.

[5] M. K. V. Bappu, S. K. Biswas, D. C. V. Mallik and C. V. Vishveshwara, *Cosmic Perspective (Chapter 2: Indian astronomy)*. Cambridge University Press, **1989**.

[6] J. Gribbin, *The scientists: A history of Science told through the lives of its greatest inventors*. New York: Random House, **2004**.

[7] J. Burnet, *Early Greek Philosophy*. A. and C. Black, **1892**.

[8] J. Gribbin, *The science: A history 1543-2001*. London: Penguin Books Ltd, **1987**.

[9] The telescope. The Galileo Project: http://galileo.rice.edu/sci/instruments/telescope.html

[10] https://cosmology.carnegiescience.edu/timeline/1610

[11] I. Newton, *Phil. Trans. R. Soc. London* **1672**, *6*, 3075.

[12] R. Bunsen and G. Kirchhoff, *Ann. Phys. Chem.* **1860**, *110*, 161.

[13] E. Hubble, *Proc. Natl. Acad. Sci.* **1929**, *3*, 168.

[14] G. Westerhout, *Ann. New York Acad. Sci.* **1972**, *189*, 21.

PART-A:

Astrochemistry and Matrix Isolation Background

Chapter 1

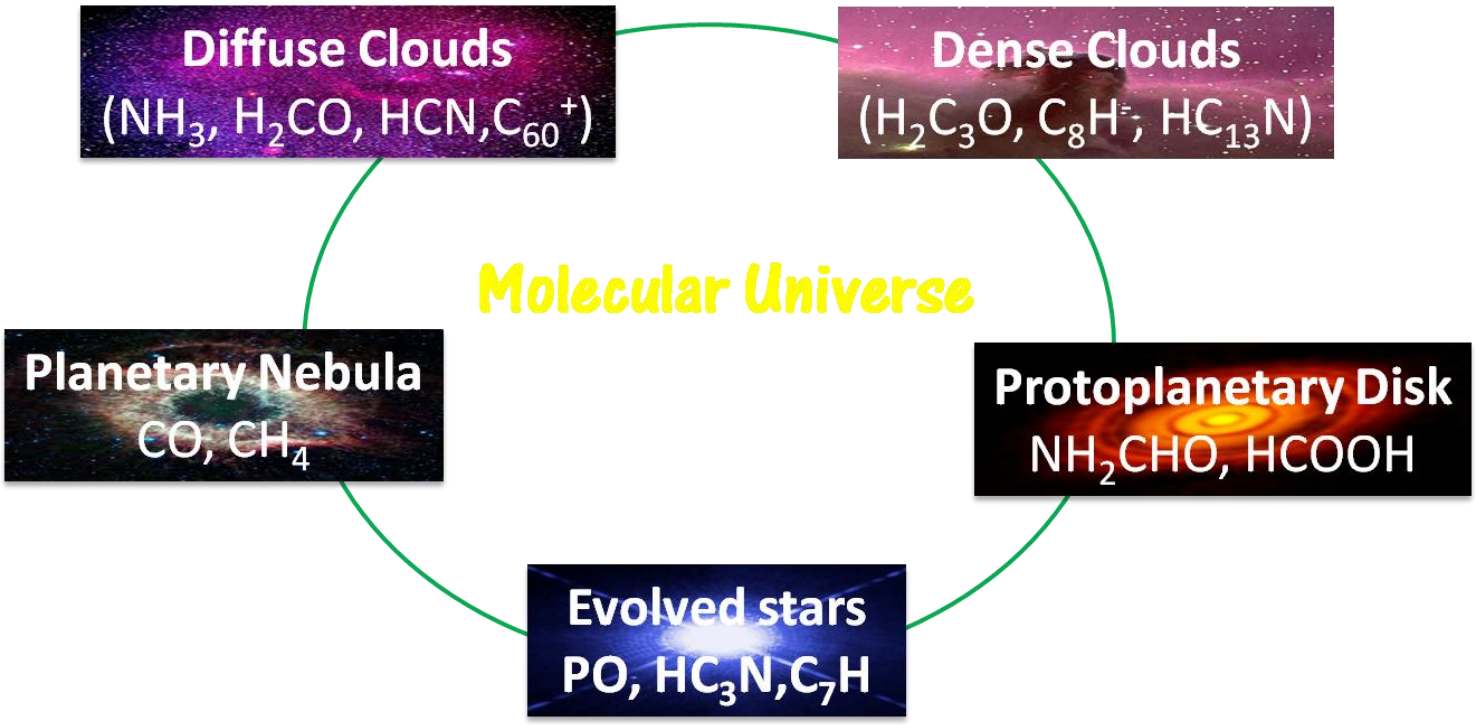
Diffuse Clouds
(NH_3, H_2CO, HCN,C_{60}^+)
Dense Clouds
(H_2C_3O, C_8H^-, $HC_{13}N$)
Molecular Universe
Planetary Nebula
CO, CH_4
Protoplanetary Disk
NH_2CHO, HCOOH
Evolved stars
PO, HC_3N,C_7H

INTRODUCTION

1

1.1 Structure of the Universe

Interstellar matter is concentrated into large organizations known as galaxies which can be termed as the building blocks of the universe.[1] Galaxies can be of various shapes – spiral, elliptical, lenticular and lastly irregular. Our galaxy, the Milky Way, has a normal spiral structure with radius around 30 kiloparsec (1 parsec =3.26 light years) and the solar system is located in a planar spiral arm approximately 8.5 kiloparsec away from the galactic center. Stars are the most compact galactic objects in the universe and the regions between them are not void. The interstellar regions consist of gas and dust. The formation of stars from dust and gas, and their deterioration to interstellar material is the fundamental aspect of galactic ecology. Currently, physical and chemical evolution of galactic and extragalactic matter is a topic of research. The introduction is focused on our own galaxy (universe) because know-how on complex interstellar processing of cosmic matter is confined to the Milky Way.

The universe is extremely heterogeneous – it consists of patchy, clumsy environments with a broad range of particle densities and temperature. The large galactic structures (1-200 parsec) are called as interstellar clouds. Depending on the density of the cosmic matter, these clouds can be classified as dense or diffuse. The particle density in the dense medium has been estimated around 10^6 cm^{-3} while in diffuse one ~ 10^2 cm^{-3}; these are the two limiting values.[2] The diffuse clouds have low extinction ($A_v < 1$) in optical domain,[3] therefore, telescopic observations of low density mediums are quite satisfactory. Temperature in the diffuse medium typically ranges from 50 to 150 K. Chemical characteristic of these clouds is mostly atomic. Diffuse or dense condition is actually two fundamental physical arrangements of interstellar matter. As the particle density increases within the cloud, diffuse one transforms first to translucent and then to dense medium (cloud). This density is controlled by motions of interstellar materials, random perturbations, stellar winds, and shock waves.[4,5]

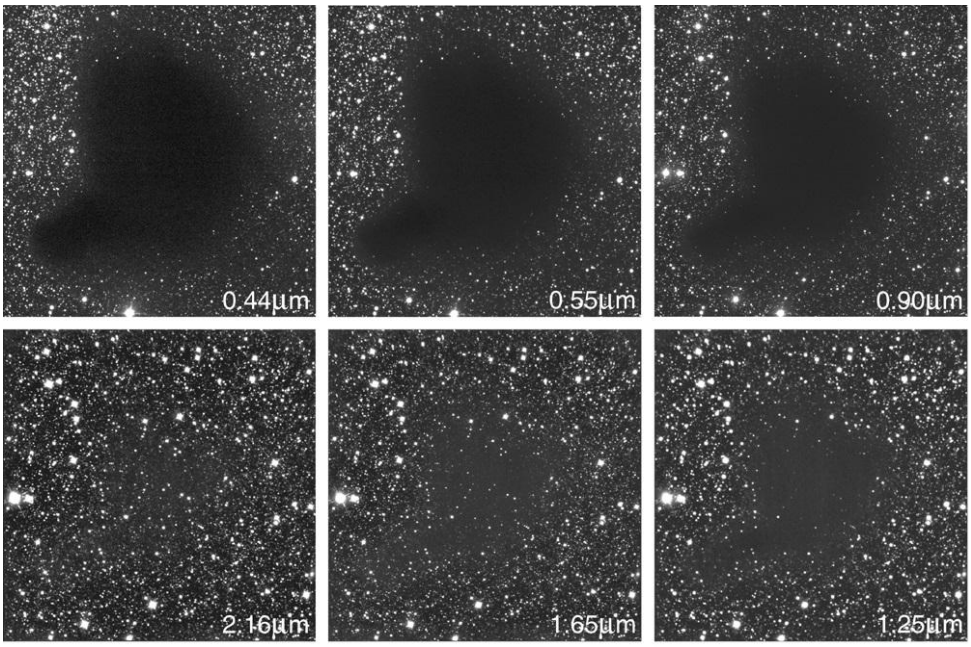

Figure 1.1: Images of the Dark Cloud B68-taken at six wavebands by NTT and VLT telescope.

Dense media possess large visible extinction due to high particle density. Light from stars is scattered from the outer layer which results very low temperature (10-30 K) inside the clouds. As these dense regions remain non-detectable in visible domain, therefore, they are called **dark clouds**. However, the dark clouds do not extinguish the radiofrequency photons because of the wavelength of the radiation (scattering $\eta \propto 1/\lambda^4$). Hence, investigation in infrared (IR) and microwave (MW) domain is the viable approach for the exploration of the darkest parts of the universe. Additionally, as interstellar gases in dark clouds are extremely cold, they emit in shorter wavelength, and therefore, the detection is facile in IR/MW region. Images of B68 dark cloud recorded at various wavelengths are shown in **Figure 1.1** (credit to ESO)**.** The background stars become visible at shorter wavelengths, 1.25−2.16 µm.

Astronomical structure of size 50-200 parsec containing dark clouds, bright nebulae, giant stars, and young stellar objects are called as molecular cloud. Vast assemblage of molecular gases can be seen in such cloud; H_2 and CO are the most dominant.[2] Molecular clouds are the stellar nursery and synthetic laboratory for cosmic molecules. Molecular clouds allow exotic chemical reactions which are not characteristics of terrestrial chemistry. The view of the Milky Way captured by telescopes at the present time elucidates the heterogeneous characteristic of the

cosmos. CCD image of interstellar medium (ISM) recorded by Adam Block[6] at the Caelum Observatory showing different astronomical environments is given below (**Figure 1.2)**.

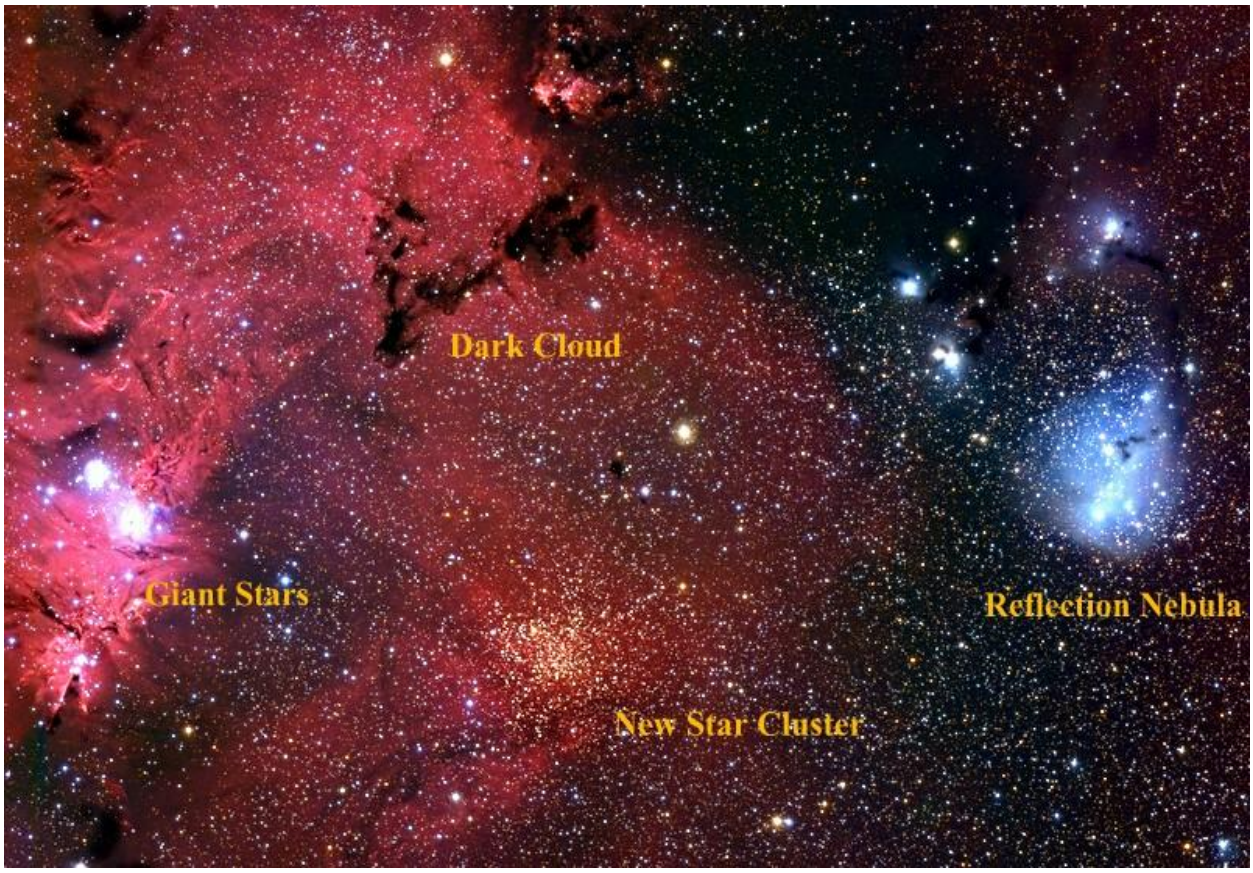

Figure 1.2: The CCD image of interstellar medium taken by Adam Block and Tim Pucket at the Caelum Observatory. The different galactic media are assigned.[6]

- The red colored portion is known as **H II** region which comprises of ionized gas. The origin of color is the H-α emission. **H II** regions associate with a giant star and the UV flux of the nearby star photoionizes the interstellar gases. **H II regions** are also known as emission nebulae.
- **Refection nebula** can be seen in blue at the right of the **Figure 1.2**. The scattering of nearby starlight by the dust grains are responsible for such color. The energy of the nearest stellar light is insufficient to ionize gases of this cloud to form an emission nebula.

- A newly formed stellar cluster can be found at lower center of the figure.
- Millions of stars are in reddish color.
- The black spots at the middle of this image floating over the reddish background are **dark clouds**.

Neighborhood of H II region, the outer environment of molecular clouds, refection nebulae, diffused/translucent clouds, protoplanetary disk atmosphere, clouds around active galactic nucleus are classified as photon-dominated or photodissociation region (PDR) where far UV photons (FUV: $\lambda < 200$ nm) of nearby stars predominate and alter the physical and chemical compositions (molecular complexity) of the medium.[7] PDRs have a significant contribution in interstellar chemistry. Atomic and molecular gases co-exist here.

Chemical processes in different galactic objects are unique and governed by temperature, density, and stellar UV flux (cosmic ray). Thus, it is not easy to understand the overall chemistry of ISM. The concept of polyatomic molecular universe is new, it started with the detection of NH_3 in 1968.[8] This discovery has established that the identification of molecules in space has validity to characterize the universe. High resolution spectra of interstellar molecules render densities, temperatures and information on chemical evolution of the clouds. Molecular abundance can be calculated with a model approach once the temperature and chemical nature of the surroundings are known. But, a major limitation in constructing accurate astrophysical models is the non-availability of low-temperature, low-pressure data, therefore, laboratory studies in a condition resemble to outer space are required.

In last five decades by the dedicated spectroscopic analysis, almost 180 molecules have been detected in space (**Table 1.1**). Theoretical and experimental investigation on their formation pathway is a hot-topic in modern astrochemistry. However, before going into the details, the generation of elements (nucleosynthesis) in the universe must be discussed.

1.2 Nucleosynthesis: Chemistry of Stars

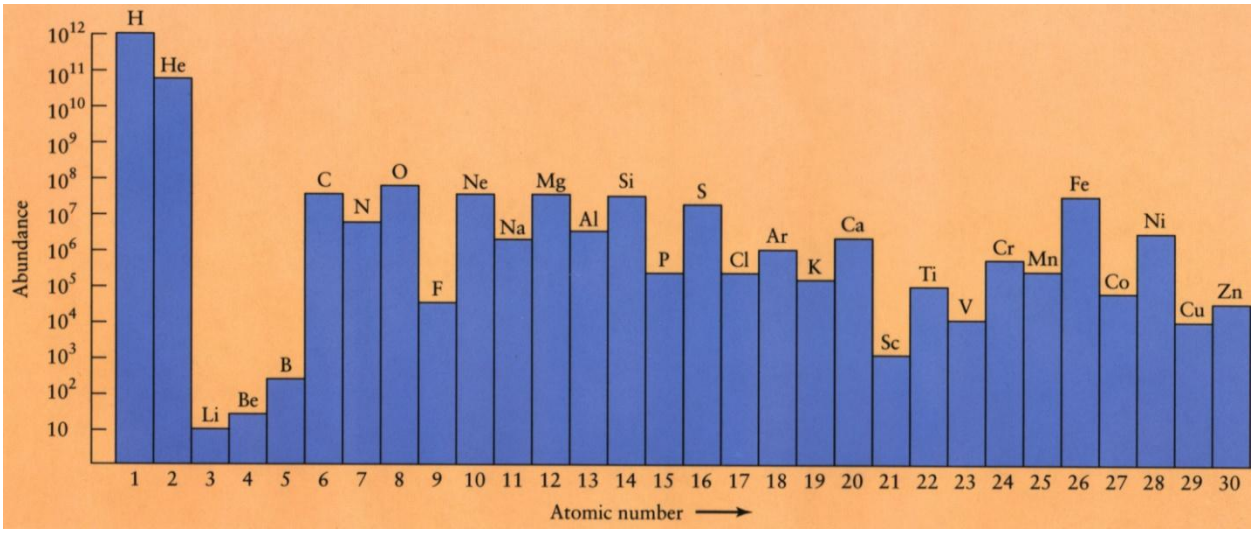

Figure 1.3: Cosmic abundance of elements Z≤30

According to the Big Bang cosmological model[9] almost entirely hydrogen and helium with trace amount of lithium and beryllium are the primordial elements generated during the cooling of the universe from initial expansion. All other elements were formed in stars through various sequences of processes involving nuclear burning or bombardment of heavy nuclei by smaller ones.[10] The cosmic abundance of elements ≤ 30 atomic number has been shown in **Figure 1.3**.

Stars are composed of mostly hydrogen and the fusion of hydrogen into helium is their source of energy. The low- and middle-mass stars (0.5-10 $M_{\odot}$; $M_{\odot}$ = mass of Sun) at the last phase of their lives, because of the outage of hydrogen in core, contract and the central temperature increases. In this phase, stars begin to fuse the existing helium and synthesize carbon and other elements. Formation of carbon by the fusion of helium is known as *triple alpha process*.[11] Stellar wind ejects the outer layer of star and expels products into ISM. Planetary nebulae contain those elements.

Triple alpha process: This involves three alpha particles - helium nuclei.

$$^{4}_{2}\mathrm{He} + {}^{4}_{2}\mathrm{He} \rightarrow {}^{8}_{4}\mathrm{Be}$$

$$^{8}_{4}\mathrm{Be} + {}^{4}_{2}\mathrm{He} \rightarrow {}^{12}_{6}\mathrm{C}$$

As byproduct oxygen has also been synthesized where $^{12}_{6}C$ further fuses with $^{4}_{2}He$. This process could proceed further to produce heavier elements (Ne, Mg, Si, etc). Carbon and oxygen are the major product of the nucleosynthesis in stars, only a small fraction is converted to neon or higher elements.

$$^{12}_{6}C + {}^{4}_{2}He \rightarrow {}^{16}_{8}O$$

Fusion pathway generates the nuclides up to nickel-56. Heavier elements after Ni occur by core-collapse supernova.

***Supernova explosion*:** The stars with mass > 20 $M_{\odot}$ end in a supernova explosion;[12] core of the high-mass star at the last phase becomes so dense ($5x10^{17}$ kg m^{-3}) that it can be compared with the density of atomic nuclei. The core becomes extremely unstable and blows off materials from outer layer in shock waves or an explosion. Heavier elements than iron (^{56}Fe) is formed via neutron capture during the supernova.

1.3 Chemistry of the Interstellar Medium: Molecule Formation

Given the strength of stellar radiation flux in unshielded environments, it is very unlike to form or exist any molecules in the vicinity of stars.[2] Therefore, elements being produced in stars, disperse into intersteller medium and generate molecules *via* various operations. In cold astronomical regions, exothermic reactions do not proceed without high kinetic energy of reactants to provide the required activation energy. The chemistry in the ISM is mostly controlled by cosmic rays, UV photons and shock waves.[13] According to present understanding, gas-phase reactions and solid-phase synthesis on dust grains are the two major pathways for the generation of molecules in space. The maximum number of molecules are identified in the gas-phase although a solid-phase origin of few species has been recently established. The list of molecules detected in space is given in **Table 1.1** (solid phase ones are in blue).

Table 1.1: Molecules detected in Space

2 atoms	3	4	5	6	7	8	9
H_2	C_3	*c*-C_3H	C_5	C_5H	C_6H	CH_3C_3N	CH_3C_4H
AlF	C_2H	*l*- C_3H	C_4H	*l*-C_2H_4	CH_2CHCN	$OCHOCH_3$	CH_3CH_2CN
AlCl	C_2O	C_3N	C_4Si	C_2H_4	CH_3C_2H	CH_3COOH	C_2H_6O
C_2	C_2S	C_3O	*l*-C_3H_2	CH_3CN	HC_5N	C_7H	C_2H_5OH
CH	CH_2	C_3S	c-C_3H_2	CH_3NC	CH_3CHO	C_6H_2	HC_7N
CH^+	HCN	C_2H_2	H_2C_2N	CH_3OH	CH_3NH_2	$C_2H_4O_2$	C_8H
CN	HCO	NH_3	CH_4	CH_3SH	*c*-C_2H_4O	*l*-HC_6H	C_2H_5NO
CO	HCO^+	HC_2N	HC_3N	HC_3NH^+	H_4C_2O	C_4H_3N	C_8H^-
CO^+	HCS^+	H_2CN^+	HC_2NC	C_2H_2O	C_6H^-	$H_4C_2N_2$	C_3H_6
CP	HOC^+	HNCO	HCO_2H	NH_3CO	CH_3NCO	$C_2H_5N_2$	C_2H_5SH
SiC	H_2O	HNCS	H_2CNH	C_5N			
HCl	H_2S	$HOCO^+$	H_2C_2O	*l*-HC_4H			
KCl	HNC	H_2CO	H_2CN_2	*l*-HC_4N			
NH	OCN^-	H_2CN	HNC_3	*c*-H_2C_3O			
NO	MgCN	H_2CS	SiH_4	C_5N^-			
NS	MgNC	H_3O^+	H_2COH^+	HNCHCN			
NaCl	N_2H^+	*c*-SiC_3	C_4H^-	HNCHCN			
OH	N_2O	CH_3	OCHCN				
PN	NaCN	C_3N^-	HNCNH				
SO	OCS	PH_3	CH_3OH				
SO^+	SO_2	HCNO	NH_4^+				
SiN	*c*-SiC_2	HOCN	NH_2CO^+				
SiO	CO_2	HSCN	$NCCNH^+$				
SiS	NH_2	H_2O_2					
CS	H_3^+	C_3H^+					
HF	SiCN	HMgCN					
HD	AlNC	HC_2O					
ArH^+	Si_2C						
O_2	C_2N						
CF	TiO_2			**10**	**11**	**12**	**> 12**
PO	FeCN			CH_3C_5N	HC_9N	*c*-C_6H_6	$HC_{11}N$
AlO	H_2O^+			$(CH_3)_2CO$	CH_3C_6H	*n*-C_3H_7CN	C_{60}
OH^+	SiNC			$(CH_2OH)_2$	$C_3H_6O_2$	*i*-C_3H_7CN	C_{70}
CN^-	AlOH			C_3H_6O	$C_3H_6O_2$	C_3H_8O	C_{60}^+
SH^+	CCP						
TiO^+	HCP						
HCl^+	KCN						
SH	H_2Cl^+						

Gas-phase Synthesis:

Gas-phase chemistry in space can be introduced with the generation of H_2 from atomic H. Previously, radiative association of H atoms on dust grains was thought to be a viable pathway.[14] Laboratory investigation has shown that the rate coefficient of H_2 formation *via* radiative association is extremely low and does not explain the high abundance of H_2 in the universe. Ionic combination ($H^+ + H^-$) can be an alternative route for the formation of cosmic H_2.[14] However, the high abundance of H_2 in the ISM is still an enigma to astrochemists.

The probable mechanisms for the gas-phase synthetic of extraterrestrial molecules are: **i)** ion-molecule, **ii)** neutral-neutral, **iii)** radiative association, **iv)** photodissociation, and **v)** dissociative recombination reaction.[7,13] These pathways have been ascribed after pursuing laboratory studies under interstellar conditions.[15]

i) **Ion-molecule reaction**

This is an important pathway in extremely cold astronomical regions. These reactions need zero activation energy and perhaps, predominate inside dark clouds where cosmic rays initiate the process by ionizing gases. Such a process also prevails in the planetary ionosphere.

$$H^+ + O \rightarrow O^+ + H$$

$$O^+ + H_2 \rightarrow OH + H^+$$

$$C^+ + OH \rightarrow CO^+ + H$$

$$CO^+ + H_2 \rightarrow \mathbf{HCO^+} + H$$

$$H_2 + H_2^+ \rightarrow \mathbf{H_3^+} + H$$

$$O_2^+ + NO \rightarrow NO^+ + O_2 \text{ (in atmosphere of Venus)}$$

The **proton transfer** process is a subsidiary ion-neutral reaction in the ISM. H_3^+ having very low H^+-detachment energy is considered as efficient protonating agent. H_3^+ is almost present everywhere in space, hence, can be initiator of chain reactions in astronomical clouds which lead to form complex species.

$$CO + H_3^+ \rightarrow HCO^+ + H_2$$

ii) **Neutral-neutral combination**

This process dominates in warm regions (>300 K). Radicals have high tendency to react with atoms; for instance, atomic oxygen does not efficiently react with many stable neutrals but combines readily with radicals. Laboratory analysis has unveiled a high rate coefficient for neutral-neutral reactions, leading interstellar molecular synthetic processes.

$$O + OH \rightarrow O_2 + H$$

$$C + OH \rightarrow CO + H$$

$$OH + H_2 \rightarrow H_2O + H$$

iii) **Radiative association**

This mechanism is most important for the generation of polyatomic species. The rate of radiative association inversely proportional to temperture, therefore, in cold astronomical regions, it is efficient. Experimental and theoretical studies predict that in a dark cloud, radiative association of molecular and atomic ions to hydrogen may produce CH_3^+, CH_5^+ and C_nH^- species.

$$C^+ + H_2 \rightarrow CH_2^+ + h\nu$$

$$CH^+ + H_2 \rightarrow CH_3^+ + h\nu$$

$$CH_3^+ + H_2 \rightarrow CH_5^+ + h\nu.$$

$$C_n^- + H \rightarrow \mathbf{C_nH^-} + h\nu$$

iv) **Photodissociation**

Photodissociation of molecules is a characteristic of unshielded clouds (PDR) illuminated by the radiation field of nearby stars. Molecules dissociated by UV photons produce reactive fragments. These fragments either react with atoms/molecules or dispersing into the PDR interface participate in chain reactions and form complex systems.

The rate of these processes depends on the photoionisation cross-section of the absorbing species and the radiation flux. The calculated rate of dissociation in ISM is ~ 10^{-10} s^{-1}.

$$h\nu + H_2O \rightarrow H + OH;\ h\nu + C \rightarrow C^+$$

$$C^+ + OH \rightarrow \mathbf{HOC^+} / CO^+ + H$$

$$CO^+ + H_2 \rightarrow \mathbf{HCO^+} + H$$

iv) **Dissociative recombination**

According to chemical point of view, this mechanism can form metastable species.

$$e^- + HCNH^+ \rightarrow HCN + H \text{ or } HNC + H$$

$$e^- + HCO^+ \rightarrow H + CO$$

Solid-phase synthesis

Earlier gas-phase reactions were solely conceived as the route for the formation of interstellar molecules. Therefore, a substantial amount of laboratory and computation studies have been carried out, but the gas-phase approach has failed to explain the abundance and formation pathways of many extreterrestrial molecules. Hence, over the last two decades solid-state synthesis in interstellar ices has been invoked as a solution to the astrochemical community.

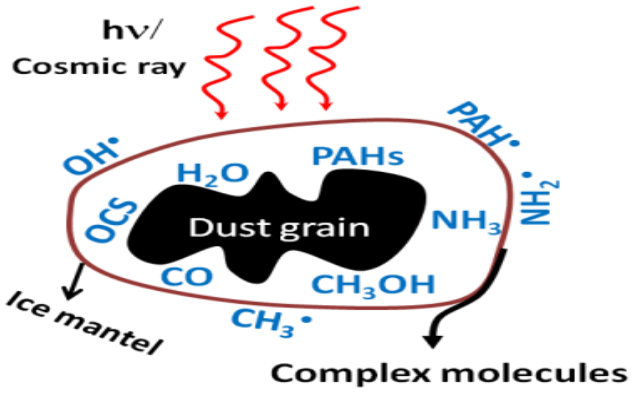

Figure 1.4: Generation of complex molecules *via* energetic processing (VUV/cosmic ray irradiation) of ices on interstellar dust grain.

The solid-phase synthesis of molecules is characteristic of dense clouds, disk of young stellar objects (YSOs) and icy planet surface where temperature range around 10-40 K. Ices on top of micrometer sized dust grains, originating from accretion of gas-phase species over millions of years, offer a molecular reservoir. These molecular ices upon cosmic ray or VUV photon exposure generate radicals which by reacting with each other during the warming up of the mantel form several complex species (**Figure 1.4**).[16] Thereafter, , they are delivered to gas-phase during the evaporation of ices.

Multi-component ices have been observed in space, largely by the Infrared Space Observatory (ISO) and Spitzer space telescopes.[17] The main component is amorphous solid water (ASW) but also other constituents have been identified: CO, CO_2, CH_3OH, CH_4, OCS, and NH_3. Some 12-15 molecules are assigned, and it is likely that many more species are embedded in cosmic ices.[17]

1.4 Oultine of Molecular Diversity in the ISM

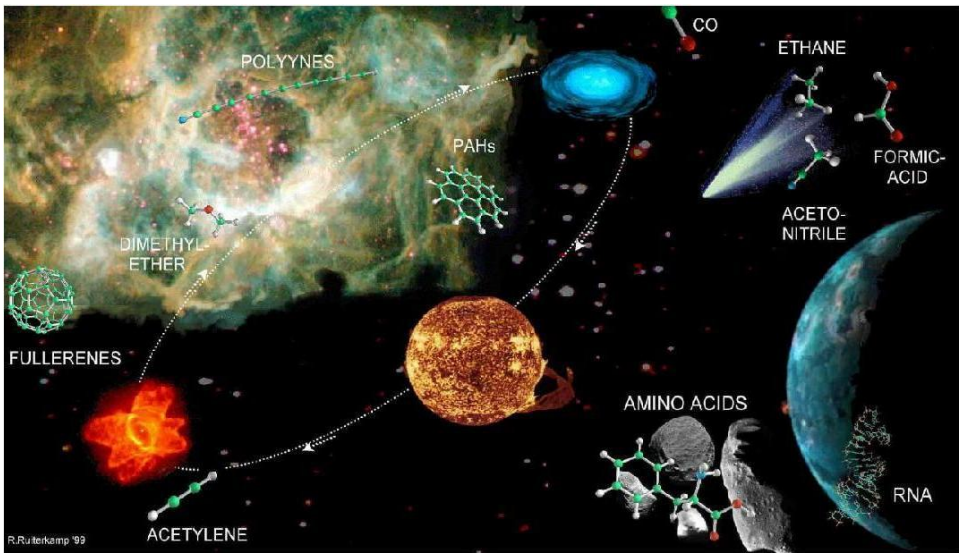

Figure 1.5: Space considering as diverse molecular factory

Most of the detected extraterrestrial molecules are organic in nature. As an example, 100% of these species with atomicity ≥ 6 contain carbon. The galactic clouds where molecules have been substantially detected are protoplanetary nebulae, cold interstellar cores, hot corinos, lukewarm corinos, circumstellar envelopes and outflow. Significant molecular diversity has been observed from these astronomical objects. So far, no complex molecules have been identified in protoplanetary disk. A large variety of molecules have been found in the hot core Sg B2 (N) cloud which is the richest molecular inventory in the Milky Way. Acetone (CH_3COCH_3), ethylene glycol ($HOCH_2CH_2OH$), glycolaldehyde ($HOCH_2CHO$), cyclopropenone (c-H_2C_3O) and N-containing organics have been identified herein.[18] Methanol (CH_3OH), acetadehyde (CH_3CHO), propylene (CH_3CHCH_2) like terrestrial molecues have been detected in Taurus Molecular Cloud (TMC-1).[19] Since the species C_nH anions/radicals and cyanopolynes are found in TMC-1,[20-23] cold cores are considered as a significant resorvior and nursery of complex

organic systems Hot corinos, low-mass version of hot core, which are closer to the stellar radiation are rich in hydrogen and contain mostly saturated organics ($HCOOCH_3$, CH_3OCH_3, CH_3CH_2CN) while unsaturated species predominate in cold galactic clouds. A number of unsaturated species are also abundant in lukewarm corino L1512 (~30 K).[24] Rich organic chemistry has been identified in circumstellar envelopes of evolved stars. Disk of asymptotic giant branch (AGB) star IRC+10216 has shown chemisry similar to TMC-1;[25] C_4H^-, C_nH radicals, C_4Si, H_2CS have been found.[26,27] In such disk, larger aromatics can be generated *via* combustion of acetylenic molecules.[28] Protoplanetary nebula CRL 618 also possesses emerging organic chemistry.[29] Benzene has been identified only in CRL 618 within the Milky Way.[30] $HCOOCH_3$, HCOOH, CH_3CN and ethanol (C_2H_5OH) are found in outflow[31] and more heteroatomic species (incresing complexcity) can be detected here. Signature of larger organics has been observed towards young stellar objects *via* infrared observation.[32]

Planetary bodies also play crucial role in the enhancement of molecular complexity. More than 20 complex systems (aromatics, polymers, N-bearing species) have been discovered either in cometary coma or on the surface of icy bodies.[33-35] The Rosetta mission on 67P/Churyumov–Gerasimenko (67P/C-G) comet is successful and will surely unveil extratrestrial origin of many new species. CH_3NCO has been recently identified both in Sg B2N region in gas-phase and on the 67P/C-G in solid-phase.[35,36] Some of the molecules identified in comets have astrobiological imporatance. It is still believed that precursor of life was delivered on Earth by comets. Extensive organic chemistry has been found in Saturn's moon Titan.[37] Jupiter's moon Europa and Io have also drawn attention of astrochemist with their exotic surface chemistry.[38] The artist's imagination on the molecular diversity in the universe is shown in **Figure 1.5.**

Benzene (C_6H_6), triacetylene (HC_6H), methylacetylene (CH_3CCH), methylamine (CH_3NH_2) type complex organics have been identified in external galaxies.[39,40]

In addition, unidentified infrared emission features and diffused interstellar bands, the two riddles of interstellar spectroscpy, hold singnature of several molecules.

1.5 The carrier of UIR emission bands: Characteristics of PAHs

A new subfield of molecular astrophysics has been developed with the radio-astronomical observations of galactic clouds. In 1970s for the first time, broad emission features in the mid-IR spectra of planetary nebulae, refection nebulae and H II emission nebulae were detected.[41] Recently, Infrared- and *Spitzer*- Space Observatory missions have shown that these emission bands are dominant in all astronomical clouds associated with dust, gas and illuminated by stellar flux.[42,43] The IR interstellar emission spectrum is dominated by bands at 3.3, 6.2, 7.7, 8.6, 11.2, 12.7, 16.4 μm. There are also weaker peaks at 3.4, 3.5, 5.25, 5.75, 6.0, 6.9, 7.5, 10.5, 11.0, 13.5, 14.2, 17.4 and 18.9 μm. All these features are situated on broad plateaus ranging from 3.2-3.6, 6-9, 11-14 and 15-19 μm **(**Figure 1.6**)**. The emitters are still unknown and thus, these features are known as unidentified infrared (UIR) emission bands. The richness and diversity in the spectrum imply that UIR bands hold information of enormous interstellar molecules.

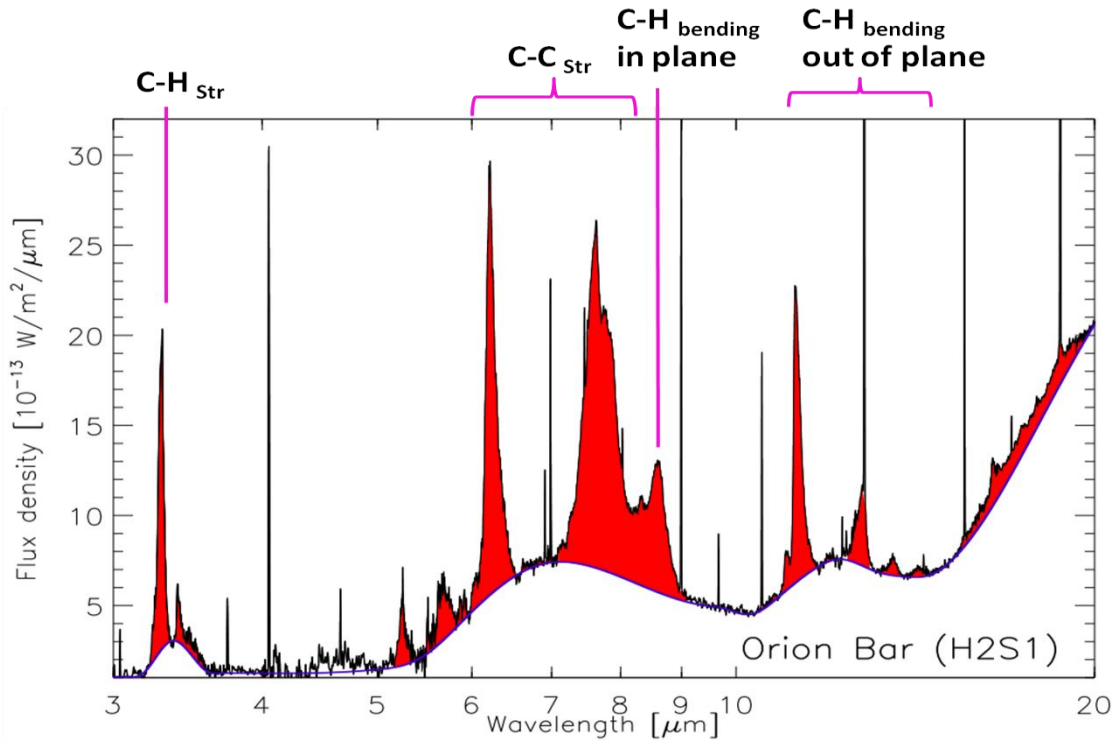

Figure 1.6: The mid IR emission features obtained in the spectrum of PDR region of Orion Bar. The richness of the spectrum and their probable assignments are indicated.[44]

UIR fluorescence dominates in brighter galactic clouds which demonstrates that these emissions originate *via* three consecutive processes:

1) Excitation of the species by the absorption of a single UV/visible photon from nearby stars,
2) Whole or partial redistribution of absorbed photon energy over available vibrational modes in time scale 10^{-12} – 10^{-10} s, and
3) Radiative relaxation through IR emission.

The high feature-to-continuum ratio in this mid-IR spectrum suggests their molecular origin. Though there are variance in intensity and width of the peaks but the overall band profiles are quite similar implying a single class of molecules as the carrier. There is no firm conclusion but it is strongly conceived that IR fluorescence of aromatic molecules is responsible. Actually, two classes of molecules were considered 1) gas-phase polycyclic aromatic hydrocarbons,[45,46] 2) carbonaceous grain with partly aromatic nature.[47] PAHs model has gained immense attention because experimental and theoretical studies shows that C-C and C-H vibrations of polycyclic aromatics have close resemblance to UIR bands.[48] The acyclic acetylenic hydrocarbons were excluded for the consideration because the C≡C vibrations lie around 4.8-5.5 μm where UIRs are not so pronounced.[49]

The 2nd class of species, carbonaceous larger grains, were also ruled out from the possible UIR emitter because timescale for absorbed photon energy to diffuse needs to be shorter than the IR emission timescale.[42]

The proposition, "UV excitation of PAHs causing UIRs," is questioned by recently astronomical observations on vdB 133, a reflection nebulae exposed to UV-poor photons.[50,51] Surprisingly, the intensities of UIR bands detected here are as strong as seen from the sources associated with intense UV flux. This observation appeals for slightly different types of PAHs to be the UIR emitter as well. The electronic absorption edge is known to be red-shifted either by the increase of PAHs size or upon ionization,[52] therefore polycyclic aromatic cations have received significant attention in recent years.

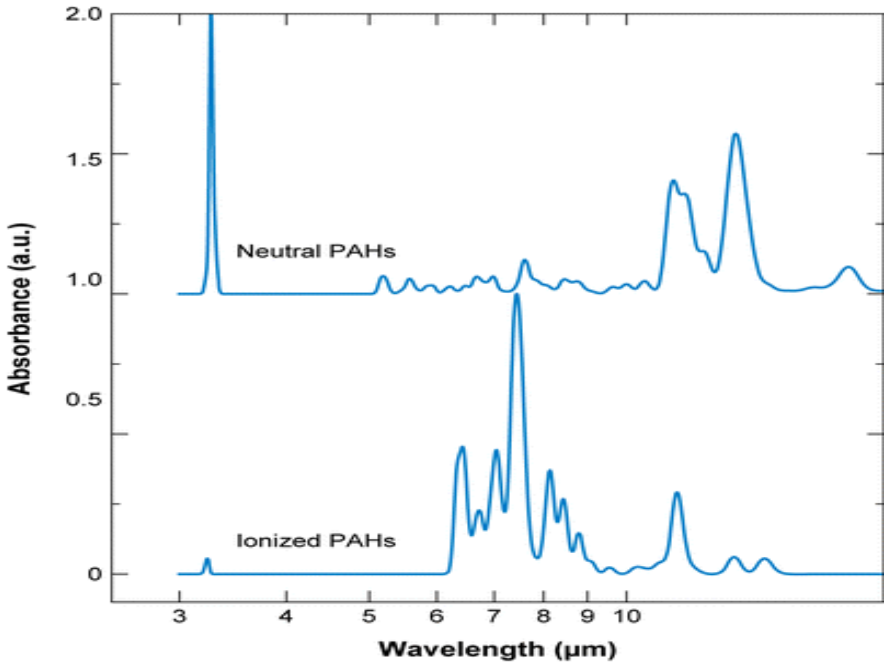

Fig 1.7: The spectrum of a mixture of PAHs (upper trace) compared with the transition of the cationic species of the same PAHs (lower trace). CC modes increased noticeably compared to CH modes with ionization. Figure taken from Allamandola *et al*.[48]

Variance of UIR bands strength towards different astronomical sources has been attributed to the charge-state of PAHs.[48] The laboratory experiment undertaken by Allamandola *et al*. proved that C-C stretching vibration increases manifold by ionization of PAH molecule. The ionization also has influence on stretching and out-of-plane bending vibrations of C-H bond (**Figure 1.7**).

Alongside PAHs/$PAHs^+$, their derivatives such as methyl substituted PAHs, nitrogen-, silicon-containing PAHs can also be carrier of UIR bands.[28] Protonated PAHs (H^+-PAHs) are very promising because of the $–CH_2$ group and strong electronic absorption in visible regions (*vide infra*). The PAHs anions are unlikely to be the carrier as their stability in photon-dominated region is not convicing.

However, laboratory studies like matrix isolation spectroscopy, multiphoton dissociation, high resolution infrared characterization along with computational investigation are going on for the better insight into the spectroscopy of larger aromatics.[28, 53. 54.]

Extraterrestrial origin of PAHs / H^+-PAHs and their derivatives:

Combustion of small hydrocarbons in terrestrial condition has established that the formation of larger organics is a characteristic of high temperature chemistry.[55] In astronomical setting, carbon rich AGB stars provide such sooting environments. UIR features have been detected in the post-AGB envelops and planetary nebulae (PNe). No IR emission has been observed in the outflow of carbon rich AGB stars. This could be due to the absence of UV-pumping photons as these stars are cooler than 4000 K. However, the detection of UIRs in PNe and post-AGB objects strengthens the speculation that the late-type stars are the birthplace of cosmic PAHs. The reaction in circumstellar disks is mainly governed by the pyrolysis of C_2H_2 (in hydrogen dominated condition).[28] The generation of PAHs in the soot of the acetylenic hydrocarbon flames has been well established.[55] The propargyl ($\bullet CH_2–C\equiv CH$) and fulvenallenyl ($\bullet C_5H_4C\equiv CH$) recombination mechanism have been proposed as the most viable pathways of PAHs formation.[56-59] HCN and C_2H_2 are thought to be the precursor of PNAHs (Nitrogen containing PAHs) in ISM.[28]

The plausible mechanisms of molecular growth in sooting environment are shown below.

$^{\bullet}CH_2–C\equiv CH + {}^{\bullet}CH_2–C\equiv CH \rightarrow C_6H_6 \rightarrow C_6H_5^{\bullet} + H$ (*propargyl recombination process*)

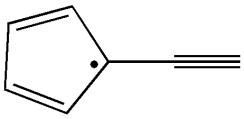

Fulvenallenyl radical

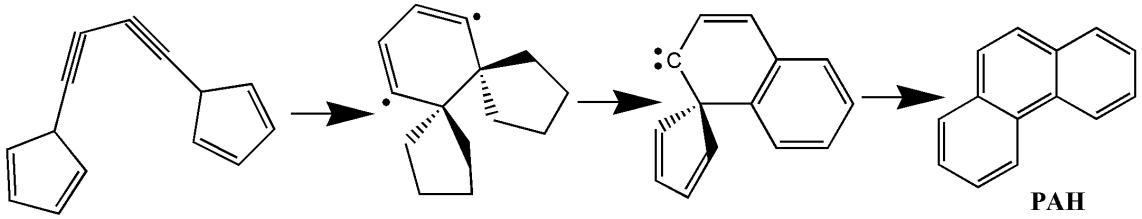

Interstellar shocks may also have role in PAHs generation. Supernova explosions generate shock waves which propagate though the interstellar gas and grains. The grain-grain collisions triggered by the shock wave has an important role in the interstellar grain-size distribution and a typical shock $v_s \sim 100$ km s^{-1} may transform 10% of the existing carbon of the shocked medium into carbon cluster. These clusters can produce PAHs through further chemical processing.[28]

Interstellar PAHs can be altered by cosmic rays and UV radiation. Sputtering of PAHs condensed on icy grains by atomic ions (cosmic ray) can generate variety of hydrocarbons.

H^+-PAHs which have recently been considered as the probable carrier of 6.2 μm UIR feature represent a special class of molecules. The study done by Olah *et al.*[60] established that protonation of aromatics generates σ-complex rather than π-addition adduct, therefore, a $–CH_2$ (aliphatic C-H stretching) group existing in the protonated PAHs can be responsible for 6.2 μm band. In extraterrestrial clouds, H^+-PAHs could be formed *via* the addition of H_2 to H-deficient PAH cation or by the reaction between neutral PAHs and H_3^+; experimental evidences demonstrate that difference in proton affinity between donor and accepter more than 100 kJ mol^{-1} exhibits dissociative proton transfer.[61] Hence, this process is viable only for large aromatics. In addition, H^+-PAHs being electronically closed shell species are unreactive towards further reactions and possess low lying electronic states.

1.6 Decoding of Diffuse Interstellar Bands

Unique absorption features observed in the optical domain (400-900 nm) of various stellar spectra (**Figure 1.8**) are classified as diffuse interstellar bands (DIBs). It is called "diffuse" to address that they are much broader compared to stellar absorption lines. Their interstellar nature has been understood from the facts that strength of DIBs are roughly proportional to the extinction and the bands are independent of the radial velocity of the light source (stars).[62] The prominent characteristics of DIBs are: the density of the lines increases towards the near IR region, they do not perfectly correlate with each other, line widths are also not uniform–some DIBs show fine profile which is attributed to the rotational and vibrational sub-structures. These aforesaid observations (especially the band sub-structure) appeal for the molecular origin of DIBs.[62-65]

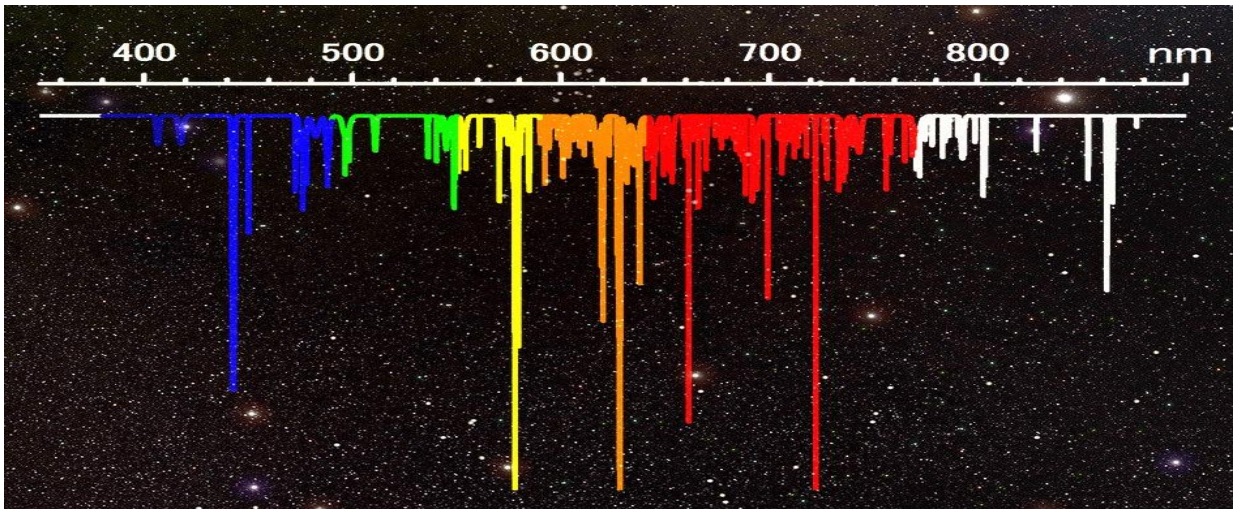

Figure 1.8: The diffuse interstellar bands.

Suspicious features in the spectrum of stellar objects were first observed in 1922 by Mary Heger at Lick Observatory[66] although a systematic investigation on DIBs was led up by Merrill a decade later in 1934.[67] Around 1930s, existence of gas-phase molecules (even triatomic) with measureable population in interstellar medium was far away from the imagination of astronomers because they believed that physical conditions in diffuse clouds are too harsh to host larger than diatomic species. Thus, various ingenious solid-state systems were considered for the carrier of this bands.[68-77] But eventually they were excluded because the expected solid-state effects are absent in DI lines. With the advancement of astronomical observations like the inclusion of CCD detector and high resolution spectrograph (around 1960s-1980s), it has been observed that the width and the position of the absorption lines are independent of the sight-line. This illustrates that DIBs are the transition of interstellar gas-phase molecules. An abnormal behavior on DIB strength was noticed by Adamson, Whittet & Ouley when they were recording the light from different stars transversing through a relatively dense cloud.[78] According to Beer-Lambert law, one should expect stronger DI features when light is passing through a dense cloud because of a higher concentrations of absorbers. But the observational finding was reserve. This phenomenon has revealed that the DIB carriers are located at the extreme outer layer of interstellar clouds where the stellar radiation flux is reduced by the cloud interior. This is known as "skin effect".[79,80]

Presently, almost 600 DIBs have been recorded and very few have been assigned.[81] The bands at 661.4, 628.4, 443.0 nm are quite strong. A huge number of molecules are responsible for DIBs. Hence, decoding of DI lines has potential to render a rough image of the molecular universe. Several classes of molecules such as fullerene, porphyrins, PAHs, hydrocarbon/carbon chains have been considered as carriers of DIBs.[82-84] Nevertheless, the molecular recognition of DIBs has still not been very successful.

Fullerenes: Fullerene has been considered as a probable carrier of DIBs because of its extremely high stability particularly in an environment similar to PDR. As the carriers of DIBs are habitant of diffuse interstellar space, hence, they should be exposed to harsh stellar radiation. C_{60} can survive in such astronomical circumstance. C_{60} and C_{70} have a first ionization potential around 7.6 eV and for that, the corresponding cations have been also conceived as DIBs carrier. In 2015 C_{60}^{+} was identified as the carrier of 963.27 and 957.75 nm DIBs.[85]

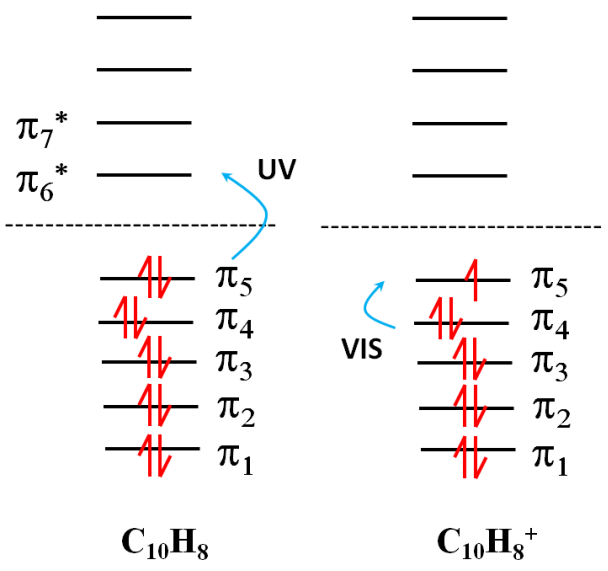

Figure 1.9: Schematic diagram of the π energy levels involved in the electronic transitions of Naphthalene and its cation.

b) ***PAHs***: PAHs as DIB carrier is still an enigma in interstellar spectroscopy. Astronomers have advocated for PAHs on the basis of three crucial aspects: i) photostability in the interstellar radiation field, ii) abundance of cosmic carbon in interstellar material can provide an enough column density for PAHs, iii) visible electronic transitions (C atom ~ 40) with high oscillator strengths. Small PAHs cations, protonated PAHs, dehydrogenated PAHs also have strong absorption in visible. The shift of absorption wavelength from UV to visible with ionization for the smallest PAH naphthalene has been shown in **Figure 1.9**.

c) ***Bare Carbon chains and Hydrocarbons****:* Douglas and Snow proposed that perhaps the polycarbon chain such as C_5, C_7, or C_9 could exist under interstellar conditions by internal

conversion.[82,86] Transitions to a short-lived excited state by a relaxation process precludes dissociation. Theory predicts their absorptions lie around 400-500 nm and are considered as the strong contender for the 438.77 nm DIB. Recent laboratory research on polycarbon chain cations has shown a transition around 440 nm (see **Chapter 3**).

1.7 The Motivation and Structure of the Thesis

Acyclic hydrocarbons with high carbon to hydrogen ratio have drawn attention as the carrier of DIBs because of two reasons: i) they possess strong absorptions in the visible domain, ii) polar carbon chains have been already identified in dense galactic clouds. A Rotational analysis of 579.71 nm DIB has revealed that species containing five to seven heavy atoms could be carrier.[87] The 438.77 nm DIB has been already predicted to be the transition of carbon chain species.[82] Spectroscopic studies of $HC_{2n+1}H^{+/0}$ and $HC_{2n}H^{+/0}$ classes of molecules have been carried out and they are not the carrier.[88,89] Hence, a slightly different system $C_7H_n^{+/0}$ (n=3-5) have been undertaken for electronic characterization in 6 K neon matrices [**Chapter 3**]. Absorption spectra of $C_5H_n^{+/0}$ (n=1,3) species have been recorded (**Appendix).** The spin-off of these characterizations is: electronic spectra of $C_7H_n^{+/0}$ or $C_5H_n^{+/0}$ can be used for their *in situ* detection in hydrocarbon flames. In the soot of acetylenic hydrocarbons, larger aromatics have been commonly identified, but mechanism of this molecular aggregation is still unknown. $C_7H_n^{+/0}$ or $C_5H_n^{+/0}$ are resonance stabilized hydrocarbon ions and radicals and are conceived as the probable intermediate in the mass-growth process.

Carbon and oxygen have similar cosmic abundance which indicates their rich chemistry in space. According to kinetic studies bare carbon chains and unsaturated hydrocarbon species possess high affinity towards oxygen. A number of unsaturated organics have been found in the ISM (**Table 1.1**); therefore, one could expect the oxygenated hydrocarbon chains as well. This proposition became more apposite with the identification of H_2C_3O in Sg B2N molecular cloud where c-H_2C_3 was detected earlier. Therefore, electronic transitions of $H_2C_6O^+$, HC_7O^+, and $C_4O_2^+$ have been measured, facilitating gas-phase studies and astronomical comparisons [**Chapter 4**].

UIR bands have been tentatively assigned to the vibrational emissions of UV-excited PAHs; their derivatives, such as dehydrogenated, protonated or oxygen, silicon, nitrogen containing PAHs, are also under consideration. Despite the spectroscopic analysis on numerous PAHs and

their cations, assignment of individual polycyclic aromatics to any UIR emission or DIB was not possible to make. The recent identification of C_{60}^+ in a diffuse cloud[85] has again appealed for the existence of larger aromatics in outer space. With this concern, a slightly different PAHs from the already emphasized ones, protonated fluorenone (H^+-$C_{13}H_8O$), protonated dibenzotropone (H^+-$C_{15}H_{10}O$) and protonated fluoranthene (H^+-$C_{16}H_{10}$), have been studied in neon matrices [**Chapter 5**]. The structure of fluoranthene is similar to the backbone of C_{60}. Fluorenone has extraterrestrial origin, being found in meteoritic residue.

Spectral analysis of fluorenyl cation ($C_{13}H_9^+$) was a long standing goal because of its high reactivity. Recently, in amorphous ice a broad absorption of fluorenyl cation has been reported. In this concern, $C_{13}H_9^+$ cations have been deposited in neon matrix to record vibrationally structured electronic absorptions. Fluorenylium, phenalenylium and benz[f]indenylium cations and the radicals are identified [**Chapter 6**].

BIBLIOGRAPHY

[1] G. O. Abell, D. Morrison and S. C. Wolf, *Philadelphia: Saunders Coll.* **1993**.

[2] K.M. Ferrière, *Rev. Mod. Phys.* **2001**, *73*, 1031.

[3] T. J. Millar and D.A. Williams, *Philadelphia: Saunders Coll.* **1993**.

[4] J. M. Shull, *ESA SP-263* **1986**, 511.

[5] A. P. Jones, A. G. G. M. Tielens, D. J. Hollenbach, and C. F. McKee, *Astrophys. J.* **1994**, *433*, 797.

[6] http://www.caelumobservatory.com/gallery/apogee.shtml

[7] D. J. Hollenbach and A. G. G. M. Tielens, *Rev. Mod. Phys.* **1999**, *71*, 173.

[8] A. C. Cheung, D. M. Rank, C. H. Townes, D. D. Thornton and W. J. Welch, *Phys. Rev. Lett.* **1968**, *21*, 1701.

[9] S. Singh, *Big Bang: The Origin of the Universe*. Harper Perennial. **2005**, 560.

[10] S.E. Woosley and A. Heger, *Phys. Rep.* **2007**, *442*, 269.

[11] E. E. Salpeter, *Astrophys. J.* **1952**, *115*, 326.

[12] A. Heger, C. L. Fryer, S. E. Woosley, N. Langer and D. H. Hartmann, *Astrophys. J.* **2003**, *591*, 288.

[13] T. P. Snow and V. M. Bierbaum, *Annu. Rev. Anal. Chem.* **2008**. *1*, 229.

[14] W. D, Watson, *Rev. Mod. Phys.* **1976**, *48*, 513.

[15] E. Herbst, Annu. Rev. Phys. Chem. **1995**, *46*, 27.

[16] H. Linnartz, S. Ioppolo and G. Fedoseev, *Int. Rev. Phys. Chem*. **2015**, *34*, 205.

[17] S. Bottinelli et al. *Astrophys. J.* **2010**, *718*, 1100.

[18] L. E. Snyder, *Proc. Natl. Acad. Sci.* **2006**, *103*, 12243.

[19] N. Marcelino, J. Cernicharo, M. Agúndez, E. Roueff, M. Gerin, J. Martín-Pintado, R. Mauersberger and C. Thum, *Astrophys. J. Lett.* **2007**, *665*, L127.

[20] H. Suzuki, S. Yamamoto, M. Ohishi, N. Kaifu, S. Ishikawa, *Astrophys. J.* **1992**, *392*, 551.

[21] N. Sakai, T. Sakai, Y. Osamura and S. Yamamoto, *Astrophys. J.* **2007**, *667*, L65.

[22] S. Brünken, H. Gupta, C. A. Gottlieb, M. C. McCarthy and P. Thaddeus, *Astrophys. J.* **2007,** *664*, L43.

[23] E. Herbst and E. F. van Dishoeck, *Annu. Rev. Astron. Astrophys.* **2009**, *47*, 427.

[24] N. Sakai, T. Sakai, Y. Osamura and S. Yamamoto, *Astrophys. J. Lett.* **2007,** *667*, L65.

[25] R. Sahai and C. K. Chronopoulos, *Astrophys. J. Lett.* **2010,** *711*, L53.

[26] M. Ohishi, N. Kaifu, K. Kawaguchi, A. Murakami, S. Saito, S. Yamamoto, S.-I. Ishikawa, Y. Fujita, Y. Shiratori and W. M. Irvine, *Astrophys. J.* **1989**, *345*, L83.

[27] M. Agúndez, J. P. Fonfría Expósito, J. Cernicharo, J. R. Pardo and M. Guélin, *Astron. Astrophys.* **2008**, *479*, 493.

[28] A. G. G. M. Tielens, *Annu. Rev. Astron. Astrophys.* **2008**, *46*, 289.

[29] J. R. Pardo, J. Cernicharo, J. R. Goicoechea, M. Guélin and A. A. Ramo, *Astrophys. J.* **2007**, *661*, 250.

[30] J. Cernicharo, A. M. Heras, A. G. G. M. Tielens, J. R. Pardo, F. Herpin, M. Guélin, and L. B. F. M. Waters, *Astrophys. J.* **200**1, *546*, L123.

[31] H. G. Arce, J. Santiago-García, J. K. Jørgensen, M. Tafalla and R. Bachiller, *Astrophys. J.* **2008**, *681*, L21.

[32] V. C. Geers, E. F. van Dishoeck, K. M. Pontoppidan, F. Lahuis, A. Crapsi, C. P. Dullemond and G. A. Blake, *Astron. Astrophys.* **2009**, *495*, 873.

[33] S. A. Sandford, J. Aléon , C. M. O'D. Alexander, T. Araki et al., *Science* **2006**, *314*, 1720.

[34] J. Kissel, R. Z. Sagdeev, J. L. Bertaux, V. N. Angarov et al., *Nature* **1986**, *321*, 280.

[35] F. Goesmann, H. Rosenbauer, J. H. Bredehöft, M. Cabane et al., **2015**, *349*, aab0689.

[36] D. T. Halfen, V. V. Ilyushin, and L. M. Ziurys, *Astrophys. J.* **2015**, *812*, L5.

[37] C. A. Griffith, P. Penteado, T. K. Greathouse, H. G. Roe and R. V. Yelle, **2005**, *629*, L 57.

[38] Ronald F. Elsner, G. Randall Gladstone, J. Hunter Waite, *Astrophys. J.* **2002**, *572*, 1077.

[39] R. Mauersberger, C. Henkel, C. M. Walmsley, L. J. Sage, and T. Wiklind, *Astron. Astrophys.* **1991**, *247*, 307.

[40] J. Bernard-Salas, E. Peeters, G. C. Sloan, J. Cami, S. Guiles, and J. R. Houck, **2009**, *652*, L29.

[41] F. C. Gillett, W. J. Forrest and K. M. Merrill, *Astrophys. J.* **1973**, *183*, 87.

[42] A. G. G. M. Tielens, S. Hony, C. van Kerckhoven and E. Peeters, *Proc. ESA Symp., The Universe as Seen by ISO*, **1999**, 579.

[43] K. Sellgren, *Spectrochim. Acta*, **2001**, *57*, 627.

[44] E. Peeters, S. Hony, C. Van Kerckhoven, A. G. G. M. Tielens, L. J. Allamandola, D. M. Hudgins and C. W. Bauschlicher, *Astron. Astrophys.* **2002**, *390*, 1089.

[45] A. Leger and J. L. Puget, *Astron. Astrophys.* **1984**, *137*, L5

[46] L. J. Allamandola, A. G. G. M. Tielens and J. R. Barker, *Astrophys. J.* **1985**, *290*, L25.

[47] A. P. Jones, W. W. Duley and D.A. Williams, *QJRAS* **1990**, *31*, 567.

[48] L. J. Allamandola, D. M. Hudgins and S.A. Sandford, *Astrophys. J.* **1999**, *511*, L115.

[49] L. J. Allamandola, D. M. Hudgins, Jr. C. W. Bauschlicher and S. R. Langhoff, *Astron. Astrophys.* **1999**, *352*, 659.

[50] K. I. Uchida, K. Sellgren and M. W. Werner, *Astrophys. J.* **1998**, *493*, L109.

[51] K. I. Uchida, K. Sellgren, M. W. Werner and M. L. Houdashelt, *Astrophys. J.* **2000**, *530*, 817.

[52] L. J. Allamandola, A. G. G. M. Tielens and J. R. Barker, *Astrophys. J. Suppl* **1989**, *71*, 733.

[53] A. J. Huneycutt, R. N. Casaes, B. J. McCall, C-Y Chung, Y-P Lee and R. J. Saykally, *Chem. Phys. Chem*, 2004, 5, 321.

[54] D. J. Cook , S. Schlemmer , N. Balucani , D. R. Wagner , J. A. Harrison , B. Steiner and R. J. Saykally, *J. Phys. Chem A* **1998**, *102*, 1465.

[55] K-H. Homann, *Angew. Chem. Int. Ed.* **1998**, *37*, 2434.

[56] H. Richter and J.B. Howard, *Phys. Chem. Chem. Phys.* **2002**, *4*, 2038.

[57] J.A. Miller and C. F. Melius, *Combust. Flame.* **1992**, *91*, 21.

[58] J.A. Miller and S. J Klippevstein, *J. Phys. Chem. A* **2003**, *107*, 7783.

[59] G. da Silva, J.W. Bozzelli, *J. Phys. Chem. A* **2009**, *113*, 12045.

[60] G. A. Olah, C. U. Pittman, R. Waack and M. Doran, *J. Am. Chem. Soc*. **1966**, *88*, 1488.

[61] D. B. Milligan , P. F. Wilson , C. G. Freeman , M. Mautner and M. J. McEwan, *J. Phys. Chem. A* **2002**, *106*, 9745.

[62] T. P. Snow, *Spectrochim. Acta A* **2001**, *57*, 615.

[63] P.J. Sarre, J.R. Miles, T.H. Kerr, S.J. Fossey and W.B. Sommerville, *Mon. Not. Royal. Astron. Soc.* **1995**, *277*, L41.

[64] P. Ehrenfreund and B. H. Foing, *Astron. Astrophys.* **1996**, *307*, L25.

[65] J. Krelowski and M. Schmidt, *Astrophys. J.* **1997**, *477*, 209.

[66] M. L. Heger, *Lick Obs. Bull.* **1922**, *10*, 146.

[67] P. W. Merrill, *Publ. Astron. Soc. Pac.* **1934**, *46*, 206.

[68] A. McKellar and H.L. Welsh, *Astron. J.* **1952**, *60*, 170.

[69] G.B. Herbig, *Astrophys. J.* **1963**, *137*, 200.

[70] J.M. Malville, *Astrophys. J.* **1964**, *139*, 198.

[71] R.D. Wolstencroft, J.G. Ireland, K. Nandy and H. Seddon, *Mon. Not. R. Astron. Soc.* **1969**, *144*, 245.

[72] P.G. Manning, *Nature* **1970**, *226*, 829.

[73] D.R. Huffman, *Astrophys. J.* **1970**, *161*, 1157.

[74] H. A. J. McIntyre and D.A. Williams, *Mon. Not. R. Astron. Soc.* **1970**, *148*, 53.

[75] W.W. Duley and W.R.M. Graham, *Astron. Nachrichten* **1971**, *293*, 33.

[76] F.M. Johnson, *Ann. Bull. NY Acad. Sci.* **1972**, *187*, 186.

[77] B. Donn and R.K. Khanna, *Astrophys. Space Sci.* **1981**, *68*, 19.

[78] A. Adamson, D.C.B. Whittet, *Mon. Not. R. Astron. Soc.***1991**, *252,* 234.

[79] J. Cami, P. Sonnentrucker and B.H. Foing, *Astron. Astrophys.* **1997**, *32*6, 822.

[80] G.B. Herbig, *Astrophys. J.* **1975**, *196* , 129.

[81] P. Jenniskens. http://leonid.arc.nasa.gov/DIBcatalog.html NASA **2009.**

[82] A.E. Douglas, *Nature* **1977**, *269*, 130.

[83] A. Danks and D.L. Lambert, *Mon. Not. R. Astron. Soc.* **1976**, *174*, 571.

[84] W.H. Smith, T.P. Snow, D.G. York, *Astrophys. J.* **1977**, *218*, 124.

[85] K. Campbell, M. Holz, D. Gerlich and J. P. Maier, *Nature* **2015**, *523*, 322.

[86] T. P. Snow, *Astrophys. J.* **2002**, *567*, 407.

[87] J. Huang and T. Oka, *Mol. Phys.* **2015**, *113*, 2159.

[88] J. Fulara, A. Nagy, I. Garkusha and J. P. Maier, *J. Chem. Phys*. **2010**, *133***,** 024304.

[89] J. Fulara, M. Grutter and J. P. Maier, *J. Phys. Chem. A.* **2007**, *111*, 11831.

Chapter 2
Matrix Isolation

METHODOLOGY

2

A fundamental challenge in probing interstellar molecules is that they are not stable in terrestrial environments. In the last decades, pulse radiolysis and flash photolysis techniques have been tried for *in situ* synthesis and characterization of such species.[1-3] The weakness of these techniques is that they are not species selective and hence not conclusive for structural assignments. In this context, the experimental approach involving isolation of mass-selected ions in solid neon and their subsequent neutralization, serves a pivotal role in the spectroscopic characterization of transient species.[4] After confinement of the molecules (ionic/neutral), spectroscopic analysis (IR, Raman, ESR, UV/Vis) is performed. Despite the emergence of several laser-based techniques, matrix isolation (MI) is still considered as a fundamental experiment in molecular spectroscopy. A spectroscopic survey on cryogenically solid sample was first attempted by Kamerlingh Onnes in Leiden. The emission of oxygen and nitrogen atoms was observed after energetic processing of impure solid nitrogen ices. Unfortunately, this work was not reported anywhere and never repeated. In the 1920s organic glasses were employed for the MI spectroscopy.[5] The idea of using rare gases for the purpose of isolating reactive molecules at low temperature was first introduced by Broida and Pimental in 1950s.[6-8] Rare gas atoms by freezing at a certain temperature lower to their sublimation point build crystals through *van der Waals* attraction.

MI experiments involve a combination of several technologies. One of the fundamental requirements is cryogenic temperatures for rapid freezing of guest and host species. MI technique was adopted worldwide after the advent of microrefrigerators. However, the second prerequisite is high/ultra high vacuum to avoid contamination of matrix by air. As the goal is to study reactive radicals and ions, therefore matrix should be free of impurities (O_2, OH etc). The third is the choice of ideal host material which must be chemically inert and possesses no spectroscopic interference in the experimental regions.

2.1 Cryogenic Matrices

A variety of molecules such as alcohols, haloalkanes, O_2, CO_2, CH_4, SF_6 were employed for matrix material.[1,5,9] Many of them have interfering infrared or electronic transition and they were not ideal chemically inert host. Thereafter, from the physical and chemical properties (**Table 2.1**), rare gases, and nitrogen are found to be the authentic matrix materials. Noble gases are extremely inert, which can be discerned by their ionization energy and polarization values given in **Table 2.1**. Such inertness allows isolating ionic species. Rare gas matrices are transparent from far IR to VUV region; the lower energy limit can be determined from the Debye energy cut-off, below which photons will excite the vibrations of atomic lattice (phonons) and the upper limit depends upon the energy gap between valence and conduction band of the noble gas atoms.

It is essential in matrix isolation experiments that during spectral survey matrix must be rigid that means should not permit diffusion of the guest. Deposition carried out at a temperature (Ne_{depo} : 6 K) which is 2/3 of the sublimation temperature (Ne_{sublim} : 9 K) of the host builds rigid matrix.[10]

Table 2.1: Solid-state properties of most ideal matrix materials.[11,12]

	Ne	**Ar**	**Kr**	**Xe**	**N_2**
Vander-Walls-radius (Å)	1.54	1.88	2.02	2.16	
Ionization energy (eV)	21.56	15.8	14.0	12.1	15.6
Polarization ($Å^3$)	0.39	1.63	2.46	4.02	1.76
Binding energy (eV/atom)	0.02	0.08	0.116	0.170	
Energy band gap (eV)	21.69	14.15	11.60	9.28	
Refractive index (λ=540 nm)	1.11	1.29	1.38	1.49	1.22
Melting point (K) at 1 atm	24.6	83.3	115.8	161.4	
Lattice constant (Å)	4.47	5.31	5.65	6.13	5.66
Sublimation temperature (K) at 10^{-6} mbar	9	31	42	58	34

2.1.1 Matrix Arrangements

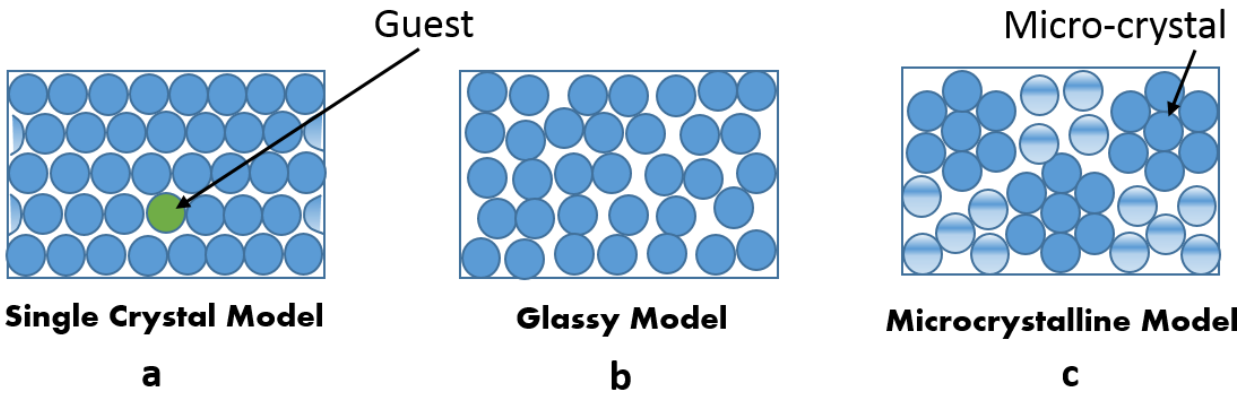

Figure 2.1: Plausible structures of the cryogenic matrices: a) single crystal model b) glassy model, c) microcrystalline model.

Gases are cryogenically solidified onto a substrate to form matrix. Three different models – single crystal, glassy and microcrystalline – have been proposed to describe the probable structure of the matrix in atomic or molecular level.

Single Crystal model: This is the simplest model which can be a starting point in analyzing matrix structure. The entire solid is considered as a uniform crystal in this model. The interstitial and substitutional (a site where a single matrix atom replaced by guest atom) sites can be clearly distinguished (**Figure 2.1a**).

It is very unlikely that a crystal produced by rapidly freezing of gas molecules at a higher pressure and temperature than the triple point will be of uniform structure. Moreover, at such low temperatures where diffusion of deposited atoms is not allowed, crystallization cannot produce single crystal structure.

Glassy Model: The random arrangement of host materials is considered in this model (**Figure 2.1b**). The density of the matrix in glassy arrangement will be lower than the close-packed single crystal model. Substitutional sites will vary in size and number of neighboring atoms. According to this model, one can compare the isolation to the trapping of a species in an infinitely viscous liquid. If this model would be true, then one should see broadened spectral features but vibrationally resolved spectra are observed in MI spectroscopy. Hence the glassy model is not correct.

Microcrystalline model: The most logically postulated one is the microcrystalline model. The whole matrix is considered as a combination of several small discrete microcrystals. The arrangement has been shown in **Figure 2.1c**. These microcrystals offer cages for the confinement of the guest species. In between these crystals, random arrangement of host exists which is called boundary. Segregation of trapped species from crystalline to boundary region in a rigid matrix is inconceivable. Therefore, two arrangements of host materials co-exist inside the matrix in absence of diffusion. As molecules are confined in different cages which are separated by boundary regions, therefore long-range interaction between guests can be ruled out which is prominent in spectral pattern of matrix isolated molecules.

The rare gases crystallize in the face-centered cubic structure. Each atom in the lattice is surrounded by 12 equidistant atoms and the symmetry of the site is O_h. A less stable packing, hexagonal arrangement, producing D_{3h} site can be possible. Though this D_{3h} hole is thermodynamically less stable compared to O_h but due to the rapid freezing some microcrystals carry D_{3h} sites; this is the origin of "Matrix site" effect (see below). The rearrangement of sites allowing diffusion can be done by increasing the matrix temperature, which is called annealing.[13]

2.1.2 Effect of Matrix on Spectroscopy

A shift of transition wavelength of a species in gas-phase from matrix spectrum is a common phenomenon (**Figure 2.2**). This observation implies a change in the energy gap between ground and absorbing state of the guest in matrix environment. Both blue- and redshifts have been detected although the latter one is more common.[14-16] The interaction between different electronic states of the isolated species with the matrix potentials (host cage) causes this spectral shift. The extent of wavelength displacement depends upon the size of the guest as well as on the size of the host. Host effect can be determined by recording spectrum of a same molecule in Ne, Ar, Kr, Xe matrices separately.

However, it is not so straightforward to infer the direction of the matrix-shift for a molecule. The blueshift in an electronic spectrum is evident when bonding electron is excited, because bond in upper state elongates and the repulsive interaction between molecule and matrix cage becomes more pronounced. The repulsive force increases the energy of the absorbing state more than the ground one and the energy gap becomes higher in comparison to gas-phase. When an electron is excited from non-bonding orbitals, a redshift is observed in the matrix. As it is stated before

matrix offers host cages of different energies (section 2.1.1). "Site structure" in pure electronic or vibronic bands recorded in cryogenic matrices is due to this isolation of guests in energetically

non-equivalents matrix environments.[13] Contribution from molecules confined in slightly different energy holes broadens the spectral bandwidth. The extent of broadening in comparison to gas-phase spectrum is shown in **Figure 2.2**.

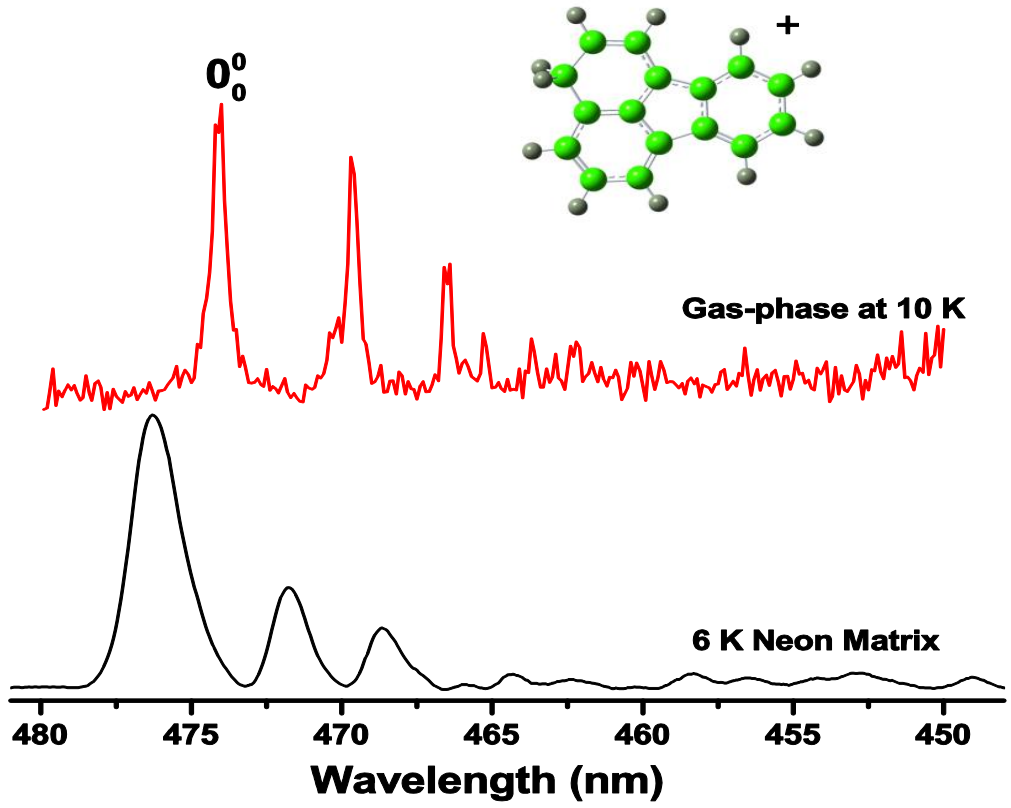

Figure 2.2: Electronic absorption spectra of γ-protonated fluoranthene (H^+-FT) recorded in a 6 K neon matrix (black trace) and in gas-phase at 10 K (red trace). The gas-phase spectrum has been recorded in 22-pole ion trap (courtesy to Ions Trap Lab).

2.1.3 Advantages in Spectral measurements

Experiments reported in this thesis (Part B & C) have been carried out in 6 K neon matrices. Although helium has the highest ionization energy (24.59 eV) indicating to be the most ideal host for ions but its melting point is extremely low 0.95 K which makes its use to be economically impractical. Neon is the next element of group 18 after helium and has 21.56 eV ionization energy. Neon forms rigid matrices at 5-6 K. In addition, neon matrix has highest transmission in optical domain which enables the detection of weak absorptions. These aspects illustrate why neon is the best matrix material over all rare gases.

The advantages of the MI technique are:

1) The host atoms have very weak *van der Waals* interaction in the lattice. Pairwise interaction energy is only 60 cm^{-1} which is far less than internal bond vibration of poly atomic guest molecules. Therefore, Born-Oppenheimer type separation between internal bond vibration of the isolated molecule and low-frequency lattice modes exists.[17]

2) At such a low temperature all molecules reside in the v = 0 level of the ground electronic state; therefore, complicacy due to the hot bands is absent in matrix spectra which facilitates the interpretation.

3) Electronic relaxations in solid matrix often pursue *via* complicated interelectronic cascades populating forbidden states which allows spectroscopic analysis of them.

4) Although "matrix-shift", the difference in wavelength between gas-phase and condensed-phase studies, is always evident but matrix investigation is a good starting point to provide a spectral range for the high resolution analysis. The gas-phase study initiated by the experiment in neon matrix is shown in **Figure 2.2**.

2.2 The apparatus:

The matrix set-up involves a combination of three major units — ion source, ion guide segment and matrix generation chamber. Cations and anions are produced inside a hot cathode discharge source *via* electron impact induced ionization of precursors. Then, ions are extracted from the source by three electrostatic lenses. Positive or negative voltage is applied on them depending on the polarity of the species of interest. Thereafter, the ion beam is injected into a quadrupole bender where neutrals are eliminated deflecting the ion beam by 90°. The ions of interest (*m/z*) have been selected in the quadrupole mass filter (QMS) and subsequently co-deposited with neon atoms onto the matrix substrate, a rhodium coated sapphire plate at 6 K. The substrate is mounted on an oxygen-free, high thermal-conductivity copper head cooled by closed-cycle helium refrigerator. The instrument is shown in **Figure 2.3**.

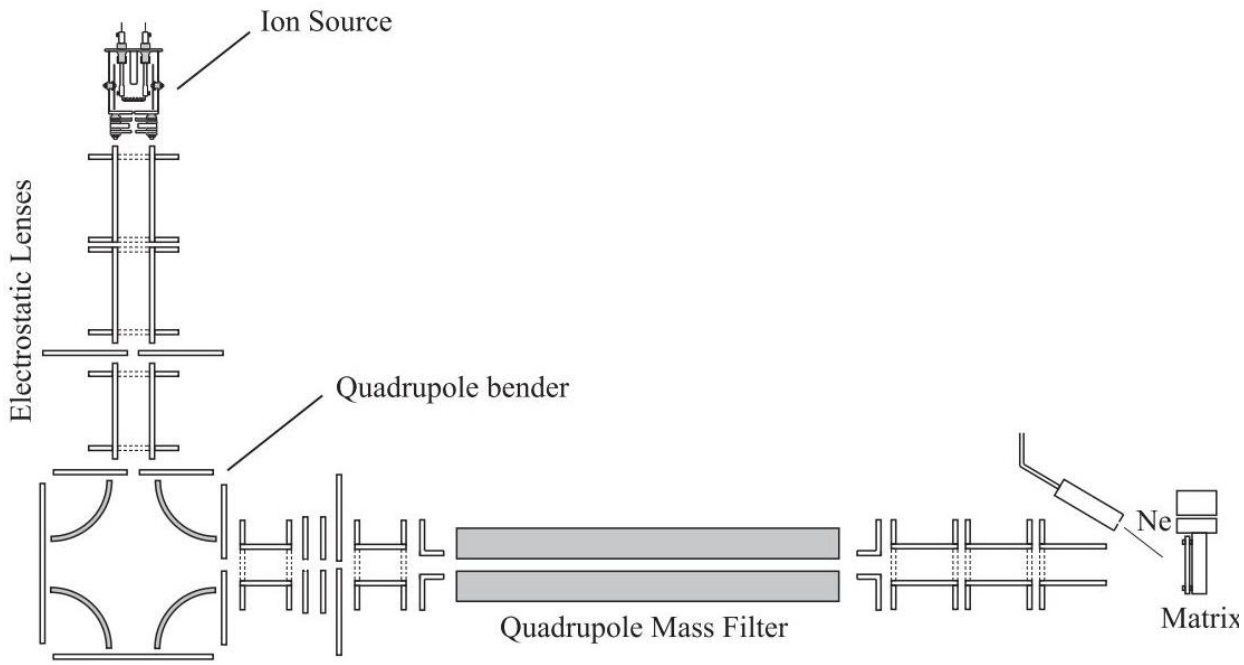

Figure 2.3: The matrix isolation set-up

The lowest temperature can be reached by this helium cryostat is ~ 4 K. A DC potential (0.3 A and 5 V) is applied to 25 Ω resistive heater cartridges to conduct the deposition at 6 K, a secure experimental temperature to prevent cracking of the neon crystal. Deposition at very low

temperature creates stress when the warmer region needs to contract more than the cooler surface and breaks the crystal. A polished aluminum radiation shield is used just over the cold head to prevent blackbody heating.[18]

The matrix is built with a controlled flow of neon. The typical pressure of neon inside the matrix chamber is kept around 2 x 10^{-6} mbar to generate a matrix of width around 100-150 μm in 4-5 hours. The volume of the matrix is 2 x 2 x 0.015 cm^3. The matrix growth is monitored by the intensity decay from a light emitting diode passing through the matrix. The substrate is floated, and from the deposited charge, the guest concentration in the matrix can be deduced. The deposited charge in 4-5 hours ranges from 1-100 μC depending on the stability of the mass-selected ion beam. The quality of the spectra in terms of signal-to-noise ratio depends on — if the oscillator strength of the experimental molecule is large then 2-10 μC is adequate for achieving good signal otherwise guest concentration needs to be high. Therefore, molecules with relatively low oscillator strengths are accumulated as long as possible and neon deposition rates are also kept comparatively slow.

2.2.1 Generation of Ionic Species:

The production of a continuous ion beam is crucial to achieve higher concentration of the guest (ions) in the matrix. A number of techniques are now available for the generation of ionic species**:** Laser photolysis, microwave discharge, ion sputtering, combustion, DC discharge and electron impact (EI) ionization.

The most simple, suitable and widely used in mass spectrometry is electron impact (EI) ionization technique. One advantage of EI is that minimal amount of precursor is consumed by the source to produce a continuous ion beam for hours. The typical pressure of precursor gas maintained in the source chamber is around 2 x 10^{-5} mbar. The precursor introduced inside the source is bombarded by electrons ejected from filament which causes ionization in following mechanism:

$$M + e^- \rightarrow M^+ + 2\ e^-$$ (cation formation)

The ionizing electron ejects a valence electron of the precursor molecule (M). The kinetic energy transferred from the ionizing electron to the M during the impact causes fragmentation of M^+ producing variety of other species. Electron impact induced chemistry produces exotic molecular systems which have immense importance in astrochemistry. The source is situated inside an

electromagnetic coil. By varying the magnetic field the ionization efficiency is controlled; the magnetic field monitors the mean free path of the electrons from filament. The types of ion source used in the set-up are discussed below.

Ion Source

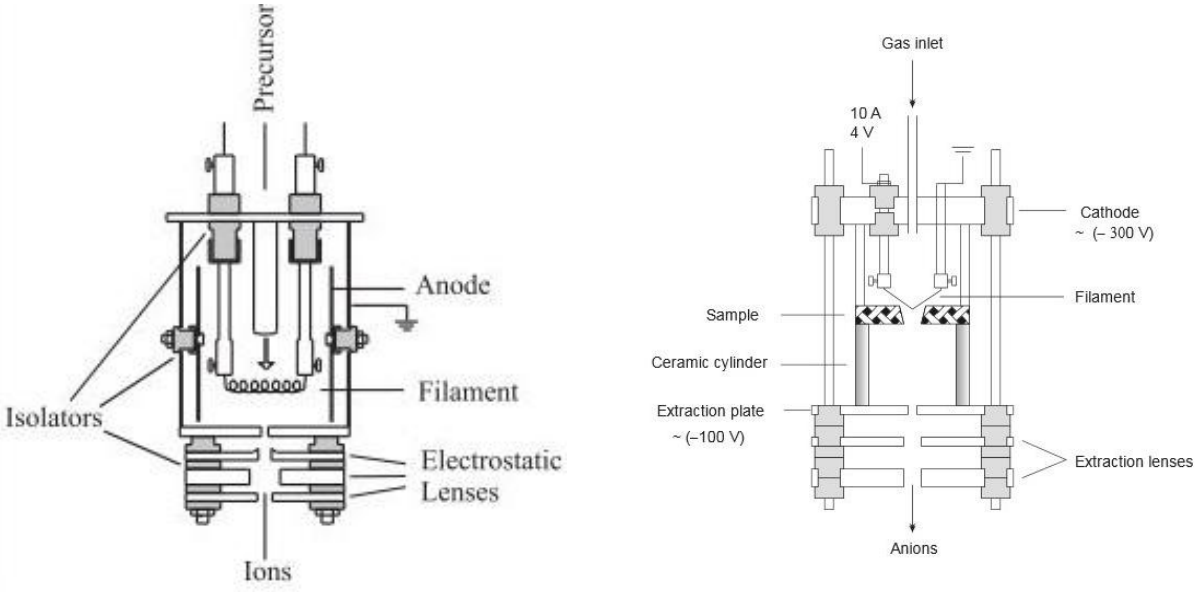

Figure 2.4: Schematic representation of electron impact ion sources for production of cations (left) and anions (*r*ight).

Cationic and anionic species both have been studied during this course of PhD. Two different electron impact ion sources have been employed for the production of cations and anions. Solid, liquid and gas samples can be used as precursor in these sources. The gaseous samples are easy to inject inside the source while liquids are kept in a bubbler and carried to the source by inert carrier gases. The solid samples are resistively-heated in an electrical oven attached to the ion source to vaporize; under vacuum solids sublimate easily. The diluted precursor by helium (normally 1:4) has been used to enhance the lifetime of the filament. The cation producing source is shown in **Figure 2.4** (left).

This source consists of two hollow cylinders made of stainless steel with outer diameters 3.5 and 4.5 cm. The smaller cylinder is situated inside the larger one and electrically isolated from each other by ceramics. The inner cylinder, set at a potential ~ 50 V, is used as the anode. The cathode is represented by the filament. Tungsten (W) and rhenium (Re) made wires have

been used for filament. Oxygen containing precursors react vigorously with tungsten and form WO_2 which shortens the lifetime of filament. Thus, rhenium were employed for these samples. Normally heated by 7-9 A current is enough to emit electrons from filament. After stabilizing the discharge current without any sample, the precursor gas is injected into the source. Production of species larger than the precursor in discharge are usually seen. For instance, naphthalene (*m/z*=128), triacetylene (*m/z*=74) cations are always present in the mass spectrum of diacetylene (HC_4H) sample. 2,4-hexadiyne (C_6H_6) shows efficient production of larger species particularly m/z=115, 141, 152, and 156 in cation source.[19]

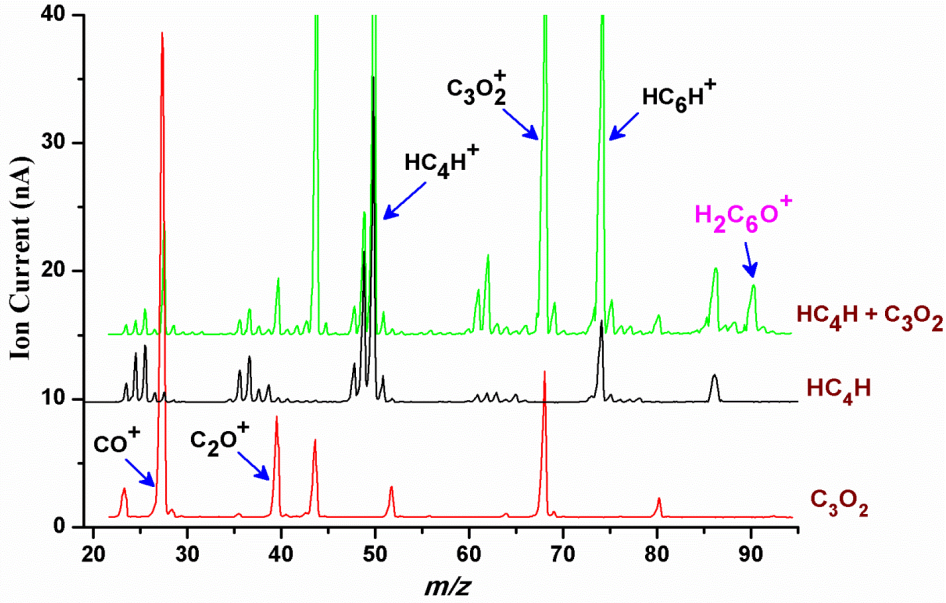

Figure 2.5: Mass spectra of pure C_3O_2 (red), pure HC_4H (black) and 1:1 mixture of C_3O_2 and HC_4H (green trace) recorded using discharge source. The ion-molecule reaction product $H_2C_6O^+$ (m/z=90) is in pink.[20]

Bi-component gas mixtures are very useful to generate a larger variety of species. The primary fragments of the individual molecules react in the plasma and produce exotic species. The production of $H_2C_6O^+$ (m/z=90) is an example of this. The m/z = 90 peak was not present either in the mass spectra of pure C_3O_2 or HC_4H while 1:1 mixture of C_3O_2 and HC_4H yielded the peak at mass 90 (**Figure 2.5**). The $H_2C_6O^+$ generated in the ion source *via* the ion-molecule reaction between C_2O ($C_3O_2^+ \rightarrow C_2O + CO^+$) and HC_4H^+. The formation of CO and C_2O unit is apparent in above Figure.

Anions were produced using the ion source shown in **Figure 2.4** (right). Filament mounnted on the cathode floats at a potential 150-200 V and similarly emits electrons after heating by 7-9 A of current. By monitoring the discharge between cathode and extracting plate (~100 V) one could regulate the degree of ionization. The diameter of the orifice on extraction plate is chosen smaller than that of cation producting source to prevent the interconnection among extracting electrodes through electron plasma.

Slow electrons are needed for the efficient formation of anions. The volume after the filament surrounded by ceramic cylinder is given for the slow sputtering of molecule by ejected elctrons from filament.

With these two sources it is possible to work for several hours, but after 4-5 hours of functioning the entire inner part is coated by soot and the source become too hot. These factors diminish the ion production efficiency.

Chemical Ionization (CI)

The chemical ionization (CI) is a relatively soft ionizing technique compared to EI. CI is more focused to study molecular ions. The fragmentation of precursors during EI can be avoided by employing CI. CI is carried out *via* transfer of proton, electrophilic addition, anion abstraction and charge exchange. In this dissertation, protonated polycyclic aromatics (H^+-PAHs) have been generated *via* proton transfer process.[21] The ethanol or toluene can be employed as protonating agent. *In situ* generated $EtOH_2^+$ or $C_7H_9^+$ by colliding with the neutral precursor tranfers proton.

$$PAH\ (accepter) + EtOH_2^+\ (donar) \rightarrow H^+\text{-}PAH + EtOH$$

Several aspects of CI technique are similar to EI and the protonation experiments have been done using same ion source with slight modification. The efficiency of phototransfer lies on the effective collisions between donar and acceptor. Therefore, small orifice of extracting plate has been used to achieve high pressure inside the soure. the production of $EtOH_2^+$ (m/z= 47) is apparent in **Figure 2.6** (inset). The generation of protonated fluorenone H^+-FL (m/z=181) is directly proportional to the strength of $EtOH_2^+$ peak.

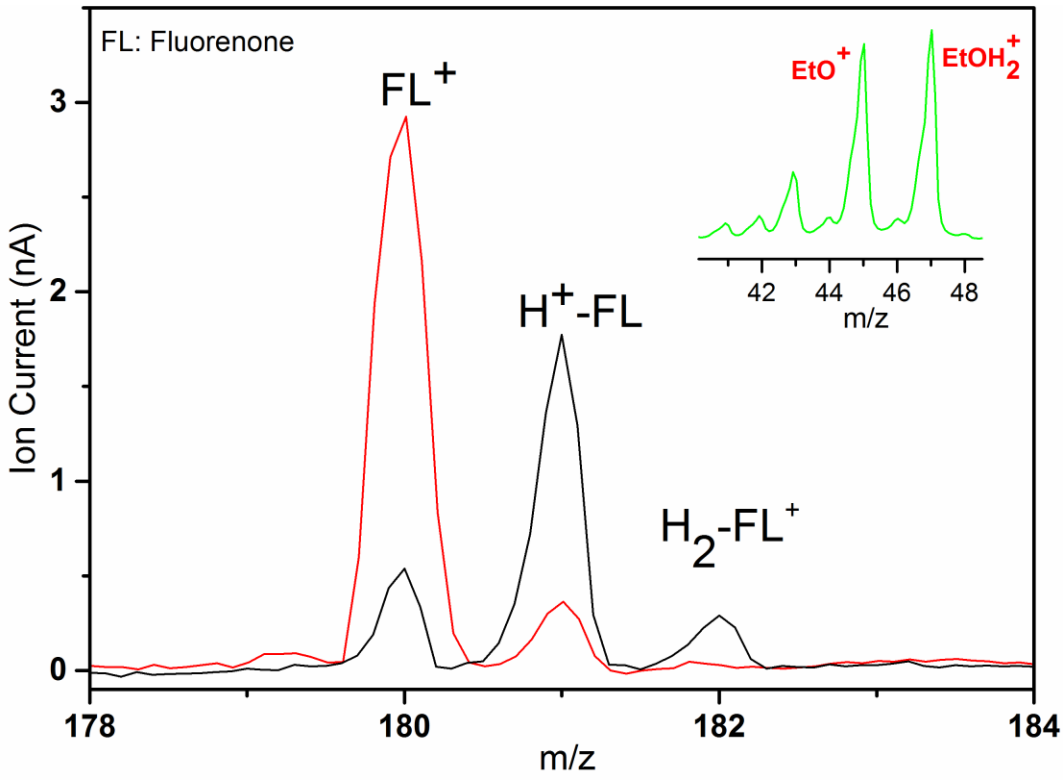

Figure 2.6: Formation of protonated fluorenone **H^+-FL** by chemical ionization technique. EtOH is used as the protonating agent.

This reactions are driven by the difference in photon affinity between the donar and the accepter. Dissociative protonation is occurred for the difference more than 100 kJ mol^{-1} due to high exothermicity of the reaction.[22]

2.2.2 Ion Guide

The ions after extracting from the source need to be guided otherwise they would be scattered due to the electric repulsion and velocity distribution. Electrostatic lenses are employed for the focusing of the ions. Most of lenses are cylindrical with 20 mm inner diameter (**Figure 2.7**). The disk-shaped ones with smaller apertures are used between chambers of different vacuums. Typical pressures inside segments of the instrument are − source chamber: 2 x 10^{-6} mbar; QMS chamber: 1 x 10^{-7} mbar; matrix chamber: 2 x 10^{-8} mbar. Metal grid has been used as a cylindrical lens in the source chamber to pump off the carrier gas and neutral impurities. Cylindrical grids generate similar potential field as the solid ones. Focusing occurs between the lenses while ions fly in constant potential inside the cylindrical electrodes. Detail discussion on focusing of ions can be found elsewhere.[23]

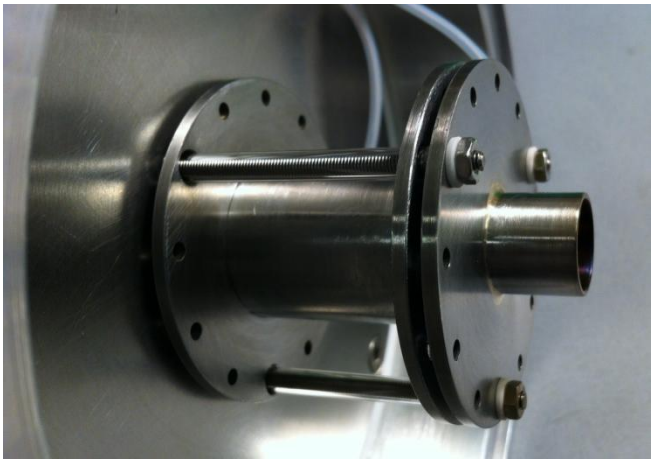

Cylindrical lens

Cylindrical lenses made of metal grids

Figure 2.7: Two different types of cylindrical electrostatic lenses

2.2.2.1 Quadruple Mass Filter

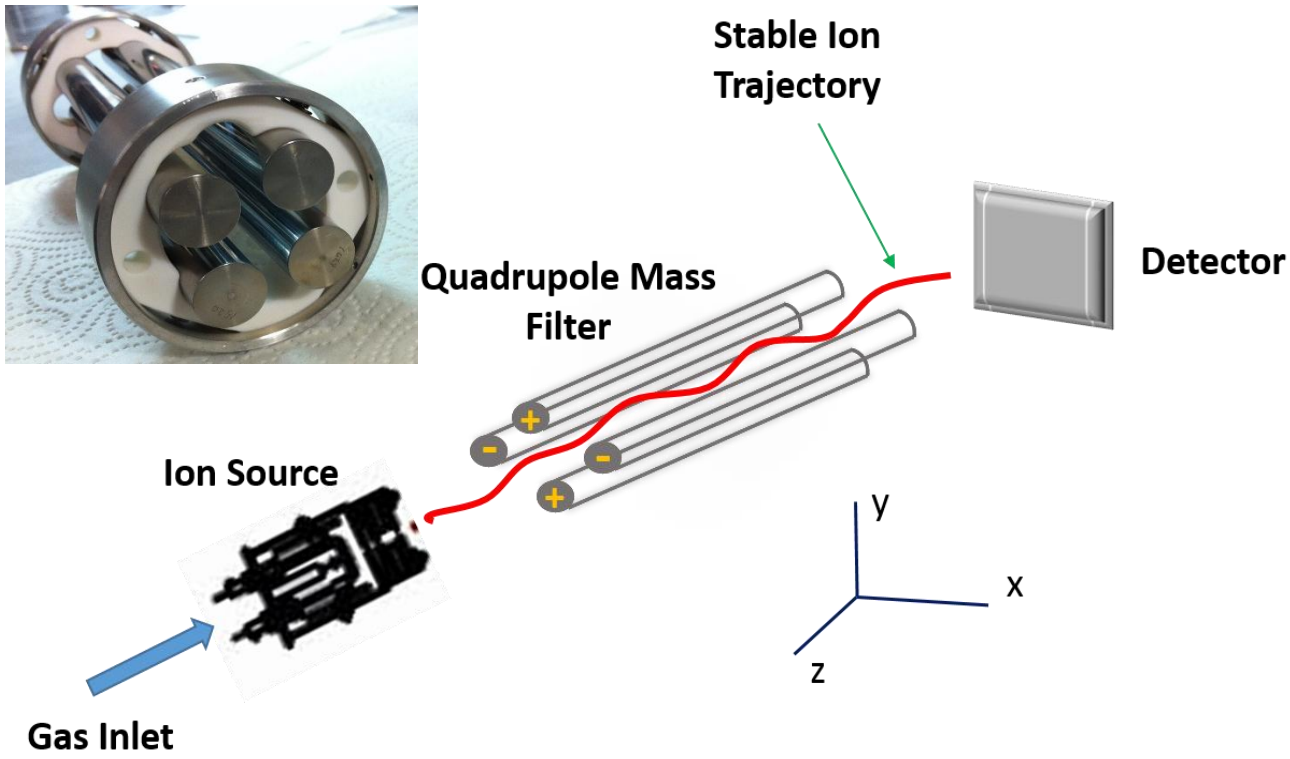

Figure 2.8: Schematic representation of a quadruple mass analyzer (QMS) set-up. The compact arrangement of rod electrodes is shown in inset.

The mass-selective deposition of species in matrix simplifies the spectral interpretation by expurgating the range of plausible absorbers. For instance, if multiple electronic systems are observed in MI spectroscopy after mass-selected deposition then they are likely transition of different isomers only.

Quadrupole mass filter (QMS) is currently in widespread use for mass spectrometry. It offers several advantages such as linear mass range, fast scanning ability, operating in continuous and pulse modes and high transmission. The QMS is comprised of four parallel metal rods as electrodes aligned symmetrically in a square array and compactly constituted on a teflon made frame (inset, **Figure 2.8**). Two opposite rods have an applied potential +(U+Vcos2πft) and the other pair has potential −(U+Vcos2πft). U is the DC voltage, and Vcos2πft is the radio-frequency

potential where V is the amplitude and *f* is the frequency. A constant potential (B) is applied to each rods. Hence, the total potential (φ) applied to the opposite filter electrodes is:

$$\varphi = B \pm (U + Vcos2\pi ft)$$

The principle of QMS is based on the control of ion trajectories by a set of dc current and radio-frequency (rf) voltages. Ions injected inside quadrupole experience an oscillating potential down the ways (Z-axis) and a certain combination of U and V transmits a definite mass-to charge ratio (m/z). Ions of other *m/z* ratio are thrown out by the quadrupole field. The stable ion trajectory is shown in **Figure 2.8** in red.

The mass spectra are recorded by monitoring the ion passing through the filter by changing the quadrupole field. There are two common settings: 1) varying the angular frequency ω (ω=2π*f*) and keeping U and V constant, 2) scanning U and V together maintaining constant U/V ratio at certain ω. The 2nd procedure has been followed in our experiment.

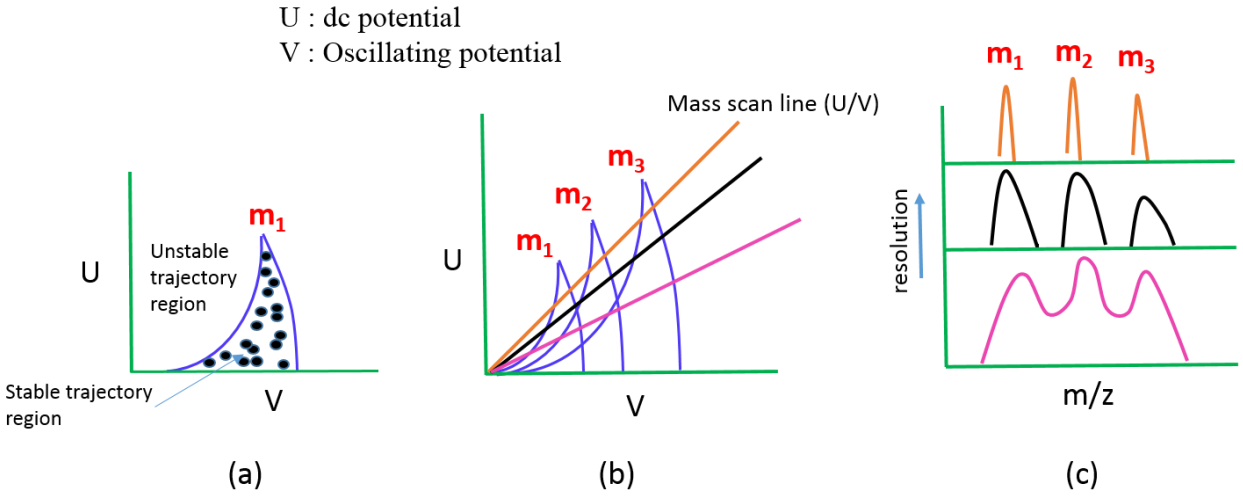

Figure 2.9: a) The stable and unstable trajectory region for a certain mass (m_1), **b)** the mass scan lines, simultaneous increase of U and V keeping U/V constant, c) effect of U/V ratio on the resolution of mass spectrum.

The mass resolution $\frac{m}{\Delta m}$ needs to be almost 1 a.m.u for selective deposition of the species of interest. The resolution and the mass range of QMS depend on the amplitude V and

frequency f of AC voltage, length of rod electrodes L, half distance r_o between two opposite electrodes and the initial kinetic energy $E_{kin,z}$ of ions along the propagating axis (Z).

Resolution ($\frac{m}{\Delta m}$) particularly lies on the number of rf cycles of ion within QMS and its kinetic energy along the propagating axis (Z).

$$\frac{m}{\Delta m} \propto \frac{mL^2 f^2}{E_{kin,z}}$$

The stable trajectory region of a certain ion of mass m_1 is shown in **Figure 2.9**. The mass scan line (U/V) monitors the resolution of the mass spectrum.

2.3 Spectroscopic Measurement

The isolated species at 6 K neon matrices have been characterized by electronic spectroscopy. The spectral survey is conducted with several 60-70 nm overlapping sections covering 270-1100 nm. Two wavelength specific light sources, xenon arc (250-390 nm) and halogen lamp (370-1100 nm), are used for spectral measurements. The schematic representation of detection system has been shown in **Figure 2.10**. Broadband light after passing through two quartz concave lenses are focused onto the entrance slit. The beam transverse through the 20 mm matrix in "wave guide" manner is focused on a bundle of optical fiber. Thereafter, the light is transferred to the spectrograph through the 2 meter (m) long optical fiber bundle. The spectrograph with a focal length 0.3 m, a resolution 0.1 nm and effective aperture *f*/4 (ANDOR Shmrock 303) is used. It is equipped with three gratings on a rotatable turret and two wavelength specific (open electrode: **OE**, 430-1100 nm and back illuminated **BU**, 220-430 nm) CCD cameras.

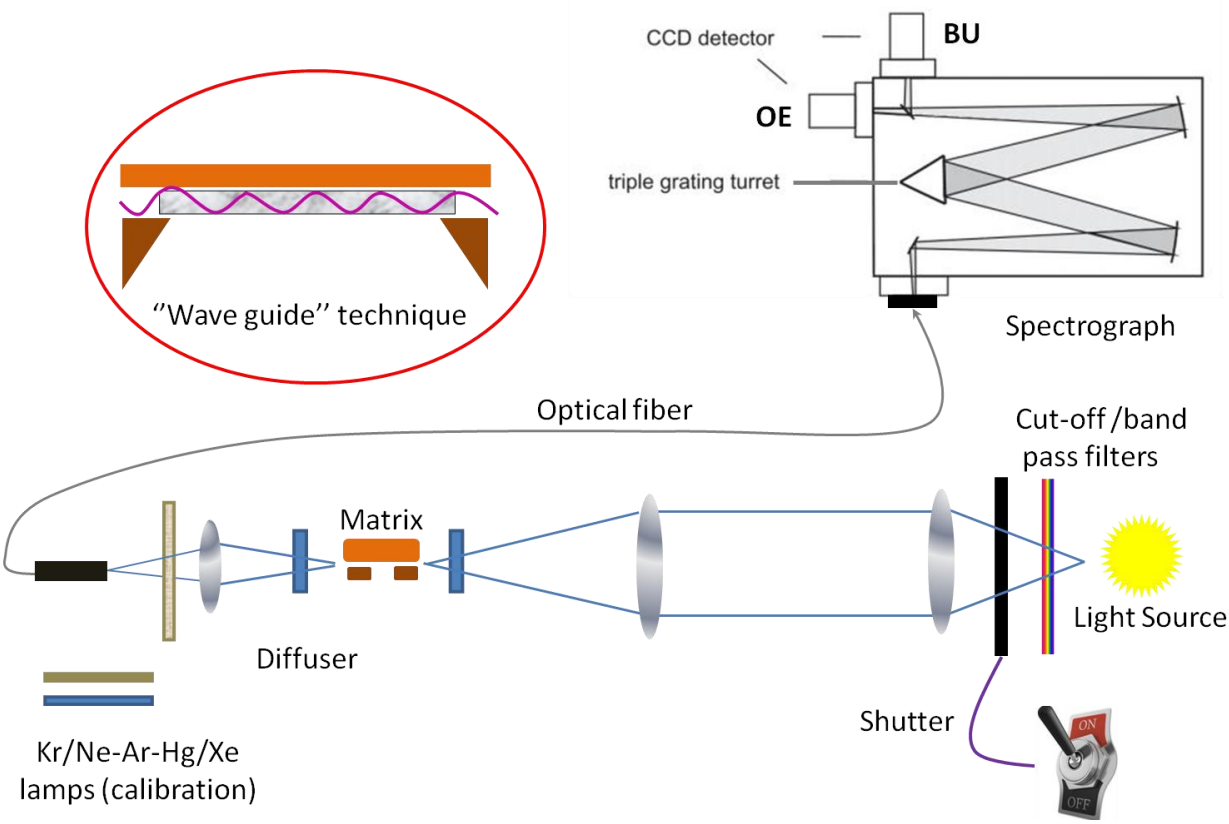

Figure 2.10: The layout of optical detection system with spectrograph. The passing of light through the matrix in "wave guide" fashion is shown inside a red circle.

As the white light without passing through monochromator is directly focused on the matrix, hence there is always an issue of photoconversion[24] of trapped species during measurement due to high intensity of incident light. Special cares are taken during spectral survey. The light intensities are reduced by using appropriate cut-off filters and also by choosing lowest possible exposure time of matrix during recording of spectra. A manual shutter is placed between light source and quartz lenses to turn off the light exposure as soon as possible after the completion of the measurement. Scans are always carried out form the red end (1100 nm) and continued to UV (270 nm). To know whether photoprocessing was taken place or not, the whole range has been repeated once again. Neon microcrystals at 6 K rigidly hold the guest molecules and only allow hydrogen- or proton-switching processes. Cis-trans photoisomerization is very unlikely.[24] The wavelength correction of electronic spectra has been done using pen-ray (Ne/Ar/Kr/Xe/Hg atomic line) lamps attached just beside the diffuser (**Figure 2.10**).

Fluorescence study

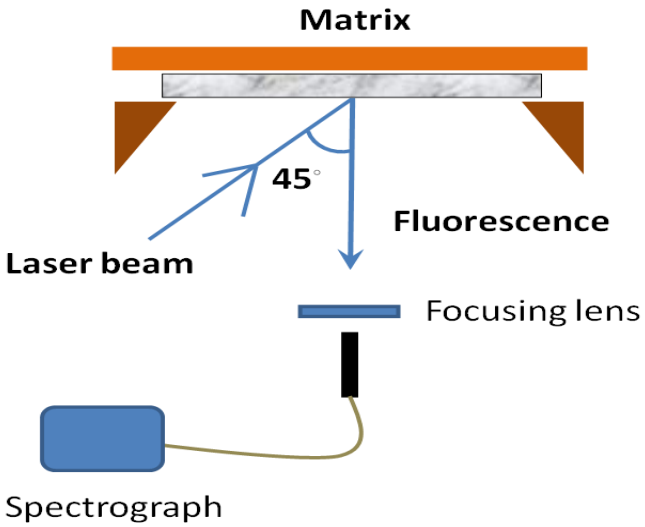

Figure 2.11: The set-up for an emission measurement.

The fluorescence has been recorded after exciting the isolated species by laser beam. Several isomers can co-exist in the matrix after mass-selected deposition of ions. In this context, laser induced fluorescence measurement plays a crucial role to discriminate the spectral contributions

from different structures. The matrix is illuminated at an incident angle 45° with a pulsed (20 Hz) Nd:YAG-pumped tunable OPO (EKSPLA NT 342/3/UVE) laser. This laser has bandwidth of 3-8 cm^{-1} with energies 2-30 mJ depending on spectral region. The coherent beam is guided by few irises and mirrors and finally projected onto the surface with 45° inclination. The fluorescence is collected perpendicular to the substrate surface. Laser beam only focuses onto a small section of the matrix, therefore, signal to noise ratio in emission spectra is normally lower than that of absorption spectra.

2.4. Experimental Tricks

A mixture of neon with chloromethane (CH_3Cl) in a ratio 1 : 30000 is used to trap cations. Impingement of ions with the metal walls of the instrument produces electrons and they neutralize the deposited cation. CH_3Cl (electron affinity ~ 3 eV) acts as the electron scavenger. It captures free electrons and dissociates to $CH_3^{\bullet}$ and Cl^-; Cl^- reduces the space charge of the matrix and facilitates to pursue deposition of cations for hours. Both $CH_3^{\bullet}$ and Cl^- possess no absorption in experimental detection range, 270-1100 nm.

The spectral survey is carried out after the deposition and thereafter, the matrix is exposed to UV photons (λ < 260 nm) for 17-25 minutes to distinguish the neutral and cationic absorptions. The UV light is generated from a high pressure mercury lamp. The irradiation causes photodetachment electrons from Cl^-. These electrons then recombine with trapped cations after migrating through the lattice and form neutrals. Therefore, the peak intensity of neutrals increase and the cationic bands diminish. The electron affinity of chloride is around 3.61 eV in gas-phase. Due to the matrix environment, the photodetatchment threshold of Cl^- is expected to be higher by ~0.5 eV compared to gas-phase. Therefore, one can expect 300 nm (4.1 eV) light to be enough for detachment of electron from Cl^-. Cut-off and bandpass filters are also chosen for irradiating specific band(s).

During deposition of anions no such scavenger to reduce the space charge of the matrix has been used. The ion current of anion drops almost 3-4 times after 5 minutes of deposition and this fall continues. Therefore, for a successful experiment with anion, the initial ion current of that particular m/z species must be very high, at least around 12-14 nA. To overcome

the repulsive space charge of matrix, anions are deposited with very high kinetics energies which also causes fragmentation of a portion of deposited species.

C_2^+ and N_2^+ (impurity) are the common species observed in experiments with cations, while with anions a large number of collisionally-induced fragments such as C_3, C_2, C_2^-, N_2^+, CNN, NCO, are generated.

- **List of common matrix impurities and their absorption wavelengths (nm)**

v' ← v"	0 ← 0	1 ← 0	2 ← 0	3 ← 0	4 ← 0
OH	309	283	262		
C_2	1020	886.7	780.7	688	232.3
C_2^+	505.8	470.3	439.8		
C_2^-	528	479	439		
N_2^+	397	364	336		
C_3	405.8				
CNN	420.8	407.2			
C_2O	854.7	727.8	634.9		
CO_2^+	288.5	277			
NCO	439	316			
CN	1098	918	791	695	

2.5 Quantum-Chemical Calculation

Due to excess energy, fragments formed *via* dissociative ionization of precursors in ion source isomerize to different structures. Absorption measurements after mass-selected deposition often reveal several electronic systems. Their different molecular origin is elucidated by band widths and vibrational profiles but exact structural assignments cannot be made. The relative population of isomers in the matrix depends upon their ground state stability, kinetics of the ion-molecule reaction processes happening inside the source and to some extent on the structure of the precursor. The precursor dependency on the structure of the ions only prevails under low electrical discharge otherwise in high discharge condition plasma chemistry always favors the most stable isomer. However, to pursue the structural assignment of the carriers, normally 15-20 plausible isomers of deposited species are envisaged and optimized with DFT and MP2 methods for equilibrium geometry.[25] B3LYP/M062X functional and cc-pV[D/T]Z basis sets are employed to describe the system.[26-29] Augmentated basis sets have been used for electron rich systems like anions. Harmonic frequencies for each structure are calculated to ensure the real minima rather some transition state. The most stable structure, global minimum, and the isomers within 100 kJ/mol in the potential energy surface are expected to form in the ion source. Ground-state optimization also renders the information about the location of charge in case of cations and anions.

The geometries obtained from DFT or MP2 optimization are used for the calculation of excitation energies of the isomers along with the oscillator strengths of the transitions. TD DFT, SAC-CI[30,31] and CASPT2[32] methods were employed for this. DFT, TD DFT, MP2, SAC-CI calculations were carried out using Gaussian09 program package.[33] The higher level calculations with CASPT2 (implemented in MOLCAS software[34]) are done by Dr. J. Fulara. TD DFT or SAC-CI produce very reliable value of excitation energies for closed shell species (singlet) while high level approach CASPT2 is needed for open shell ones. However, depending on the ground state stability and the agreement between the predicted and observed transition energies structural assignments are made. The comparison between vibrational progression bands and the calculated harmonic frequencies supports the assignment.

BIBLIOGRAPHY

[1] T. Bally, Z. Zhu, J. Wirz, M. Fülscher and J.-Y. Hasegawa, *J. Chem. Soc., Perkin Trans. 2* **2000**, 2311.

[2] P. Costa and W. Sander, *J. Phys. Org. Chem.* **2015**, ***28***, 71.

[3] P. Costa, I. Trosien, M. Fernandez-Oliva, E. Sanchez-Garcia and W. Sander, *Angew. Chem. Int. Ed.* **2015**, *54*, 2656.

[4] A. Chakraborty, J. Fulara and J. P. Maier, *Angew. Chem. Int. Ed.* **2015**, *55*, 228.

[5] G. N. Lewis and D. Lipkin, *J. Am. Chem. Soc.***1942**, *64*, 2801.

[6] E. Whittle, D. A. Dows and G. C. Pimentel, *J. Chem. Phys.* **1954**, *22*, 1943.

[7] E. D. Becker and G. C. Pimentel, *J. Chem. Phys.* **1956**, *25*, 224.

[8] I. Norman and G. Porter, *Nature (London)* **1954**, *174*, 58.

[9] C. Sandorfy, *Can. J. Chem.* **1965**, *10*, 85.

[10] B. Meyer, *Low Temperature Spectroscopy*, American Elsevier Publishing Company, New York, **1971**.

[11] A. Bondi, *J. Phys. Chem.* **1964**, *68*, 441.

[12] W. Schulze and D. M. Kolb, **J. Chem. Soc., Faraday Trans. 2 1974**, **70**, 1098.

[13] S. Cradock and A. J. Hinchcliffe, Matrix isolation. Cambridge University Press. **2011**.

[14] J. P. Maier, J. Phys. Chem. A **1998**, 102, 3462.

[15] L. N. Zack and J. P. Maier, *Chem. Soc. Rev.* **2014**, *43*, 4602.

[16] C. A. Rice, F.-X. Hardy, O. Gause and J. P. Maier, Astrophys. J. **2015**, *812*, L4.

[17] K. Rebane, *Chem. Phys.* 1994, *189*, 139.

[18] R. Loudon, The Quantum Theory of Light, Chapter 1 *Cambridge University Press*. **2000**.

[19] A. Nagy, J. Fulara and J. P. Maier, *J. Am. Chem. Soc.***2011**, *133*, 19796.

[20] A. Chakraborty, J. Fulara and J. P. Maier, *J. Phys. Chem. A* **2015**, *119*, 50.

[21] I. Garkusha, PhD thesis **2012.** http://edoc.unibas.ch/33430/1/Diss_Roth_Garkusha.pdf

[22] D. B. Milligan , P. F. Wilson , C. G. Freeman , M. Mautner and M. J. McEwan, *J. Phys. Chem. A* **2002**, *106*, 9745.

[23] A. Batalov. PhD thesis **2006**. http://edoc.unibas.ch/421/1/DissB_7531.pdf

[24] J. Fulara, A. Nagy, K.l Filipkowski, V. S. Thimmakondu, J. F. Stanton and J. P. Maier *J. Phys. Chem. A* **2013**, *117*, 13605.

[25] C. Møller and M. S. Plesset, *Phys. Rev.* **1934**, *46*, 618.

[26] A.D. Becke, Phys. Rev. A **1988**, *38*, 3098.

[27] C. Lee, W. Yang and R.G. Parr, *Phys. Rev. B* **1988**, *37*, 785.

[28] T.H. Dunning, *J. Chem. Phys*. **1989**, *90*, 1007.

[29] Y. Zhao and D. G. Truhlar, *Theor. Chem. Acc.* **2008**, *120*, 215.

[31] H. Nakatsuji, K. Hirao, *J. Chem. Phys.* **1978**, *68*, 2053.

[31] H. Nakatsuji, *Chem. Phys. Lett.* **1979**, *67*, 329.

[32] J. Finley, P. Malmqvist, B. O. Roos, and L. Serrano-Andrés, *Chem. Phys. Lett.* **1998**, *288*, 299.

[33] M. J. Frisch, G. W. Trucks, H. B. Schlegel, G. E. Scuseria, et al. *Gaussian, Inc., Wallingford CT*, **2009**.

[34] F. Aquilante, L. De Vico, N. Ferré, G. Ghigo, et al. *Comp. Chem.* **2010**, *31*, 224.

PART-B

Results

Chapter 3

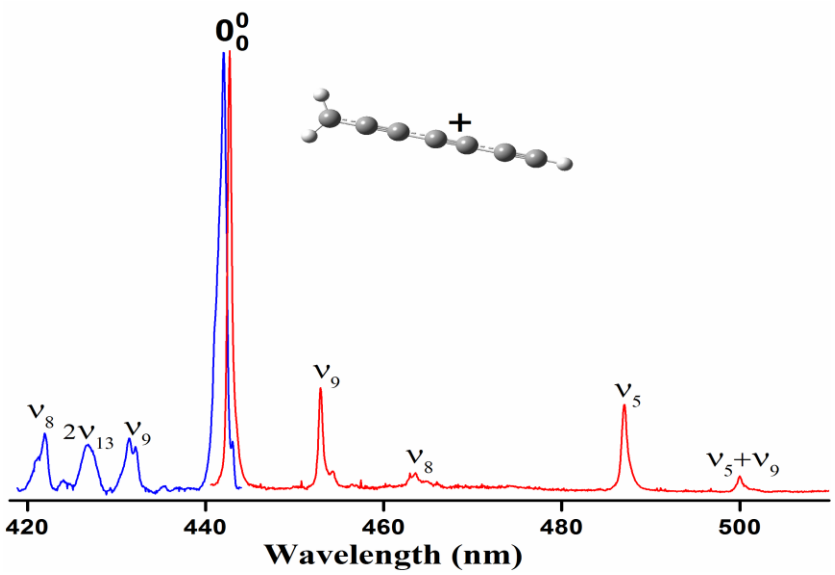
0_0^0
ν_8
$2\nu_{13}$
ν_9
ν_9
ν_8
ν_5
$\nu_5+\nu_9$
420
440
460
480
500
Wavelength (nm)

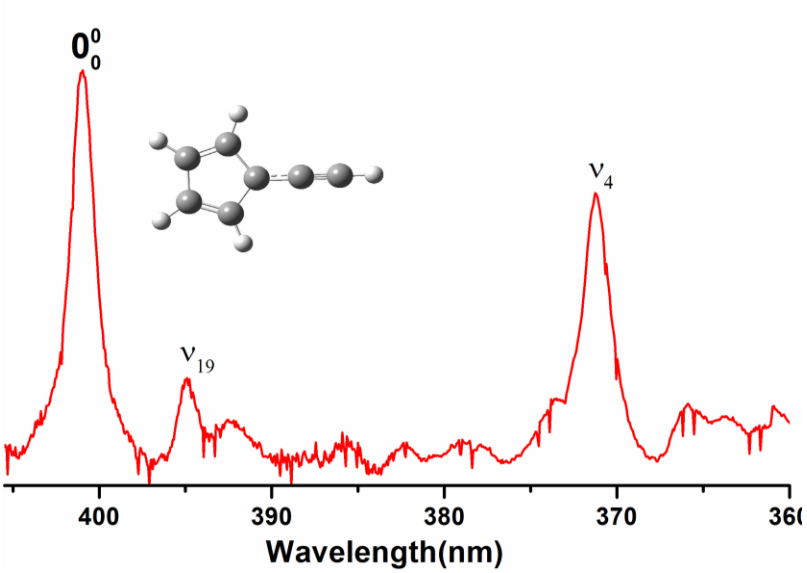
0_0^0
ν_{19}
ν_4
400
390
380
370
Wavelength(nm)

ELECTRONIC TRANSITIONS OF C_7H_n (n=3-5) CATIONS AND RADICALS

3

Mass selective deposition of $C_7H_3^+$ (m/z=87) into solid neon has revealed the **1** $^1A_1 \leftarrow X\ ^1A_1$ electronic absorption system of hepta-1,2,3,4,5,6-hexaenylium **B**$^+$ $[H_2CCCCCCCH]^+$ with origin band at 441.3 nm, **1** $^1A' \leftarrow X\ ^1A'$ transition of 1-ethynyl-2,4-pentadiynylium **C**$^+$ $[HCCCHCCCCH]^+$ starting at 414.6 nm and the **1** $^1A_1 \leftarrow X\ ^1A_1$ one of 1,3-butadiynyl-cyclopropenylium **A**$^+$ $[HCCCCC<(CH=CH)]^+$ with onset at 322.2 nm. Vibrationally resolved fluorescence was recorded for isomer **B**$^+$ upon laser excitation of the absorption bands in the **1** $^1A_1 \leftarrow$ **X** $^1A_1$ electronic system. After neutralization of the cations in the matrix four absorption systems of the C_7H_3 radicals starting at 530.3, 479.4, 482.3 and 302.5 nm were detected. These are identified as the **1** $^2A' \leftarrow X\ ^2A'$ and **2** $^2A' \leftarrow X\ ^2A'$ electronic transitions of 2-(buta-1,3-diynyl)cycloprop-2yl-1-1ylidene **E** $[HCCCCC<(C=CH_2)]$, **1** $^2B_1 \leftarrow X\ ^2B_1$ of 1,2,3,4,5,6-heptahexaenyl **B** and **3** $^2B_1 \leftarrow X\ ^2B_1$ of 3-buta-1,3-diynyl-cyclopropenyl **A**, respectively.

Absorptions commencing at 602.6 nm are detected following deposition of mass-selected $C_7H_4^+$ (m/z=88) in a 6 K neon matrix produced from a 1:1 mixture of diacetylene and propyne in an ion source. The strongest band at 602.6 nm, and a weaker one at 421.1 nm, are assigned to the **1** $^2E \leftarrow X\ ^2E$ and **2** $^2E \leftarrow X\ ^2E$ electronic transitions of methyltriacetylene cation ($CH_3CCCCCCH^+$), based on mass-selection, spectroscopic analysis of the vibrational structure and the calculated excitation energies. Structured fluorescence is detected in the 600-760 nm range upon laser excitation of absorption bands of $CH_3CCCCCCH^+$.

Fulvenallenyl radical (HCC-cyc-C_5H_4) has been produced in 6 K neon matrices after mass selective deposition of $C_7H_5^-$ and $C_7H_5^+$ generated from organic precursors in a hot cathode ion source. Absorptions commencing at 401.3 nm are detected following photodetachment of electrons from the deposited $C_7H_5^-$ and also by neutralization of $C_7H_5^+$ in the matrix. The absorption system is assigned to the **1** $^2B_1 \leftarrow X\ ^2B_1$ electronic transition of fulvenallenyl radical on the basis of calculated vertical excitation energies. The vibrational progression bands concur with the structure of fulvenallenyl radical. Fulvenallenyl anion and the radical are the global minimum of the potential energy surface of $C_7H_5^-$ and C_7H_5, respectively.

3.1 INTRODUCTION

Several classes of unsaturated species including polycyclic aromatics are produced during combustion of hydrocarbons in an oxygen deficient environment, as established by gas chromatography and molecular beam mass spectrometry (MBMS).[1-5] However, this production of larger aromatics during the pyrolysis of small hydrocarbons is still a mystery. It is conceived that resonance stabilized organic radicals, having high thermal stability and resistance to oxidation in flames, could be the precursors and chain propagators in this mass growth process. Theoretical kinetics and MBMS emphasize on $C_{2n+1}H_3$ class of molecules.[5-9] The recombination mechanism of propargyl radical, C_3H_3, was considered as one of the key processes for larger aromatics formation.[10-12] The generation of benzene was detected in a self-reaction of propargyl radical in high-pressure shock tube experiments.[13] But the further experimental evidences were not conclusive to establish its role in the generation of higher aromatics in sooting environments. In this context, the higher carbon chain analogue, $C_7H_3^{+/0}$, presents an intriguing subject for spectroscopic exploration, and moreover the identification of the electronic absorptions of various isomers will enable their *in situ* monitoring in soot formation. There is only circumstantial experimental and computational understanding on C_7H_3 species; gas-phase electronic spectrum of a C_7H_3 radical by resonant two-color-two-photon-ionization (R2C2PI) technique is reported.[14]

Fulvenallenyl radical (C_7H_5) **FA** has drawn attention as one of the key intermediate in polycyclic aromatics formation in sooting environment ever since its generation in a toluene pyrolysis has been established by comparing the theoretical and experimental ionization energies.[15] **FA** is considered as a very stable radical because of its conjugated propargyl and cyclopentadienyl sub-units. The formation of C_7H_5 in electrical discharge from acetylene, allene, diacetylene, cyclopentadiene, benzene and toluene is established by mass spectrometry. Computational models suggest low energy pathways for polycyclic aromatic hydrocarbons (PAHs) formation by the self-assembly of **FA** radicals or via addition of diacetylene to fulvenallenyl.[16]

Interstellar clouds contain a rich collection of exotic molecular systems because of very low density and temperature.[17a] A C_7H_n species, methyltriacetylene (C_7H_4), has already been identified towards TMC-1.[17b] The broad mid-infrared emission features detected in space have

been attributed to vibrational transitions of PAHs.[18] Interstellar origin of these aromatics is still unknown. It is considered that PAHs are formed at high temperatures (≥ 4800 K) in the outflow of post-AGB stars where chemistry is similar to the terrestrial combustion systems.[19] Therefore, one could envisage the existence of resonance stabilized C_7H_n species in the interstellar medium. So, this class of longer chain unsaturated radicals and cations carry significant interest in terrestrial combustion processes and astrochemistry, and their spectroscopic knowledge is needed. The $C_7H_n^+$ and C_7H_n species are also relevant in the planetary atmosphere of Saturn's moon Titan.[20]

This chapter focuses on the electronic characterization of $C_7H_n^{+/0}$ (n=3-5) species isolated in neon matrices at 6 K. $C_7H_n^+$ or $C_7H_n^-$ ions are produced in two different ion sources, then mass-selected and co-deposited with neon onto cold substrate and subsequently neutralized. On the basis of the electronic excitation energies obtained by CASPT2 calculations after ground-state optimization of the possible isomers, the structural assignments of the absorbers have been made.

3.2 PRODUCTION OF IONS

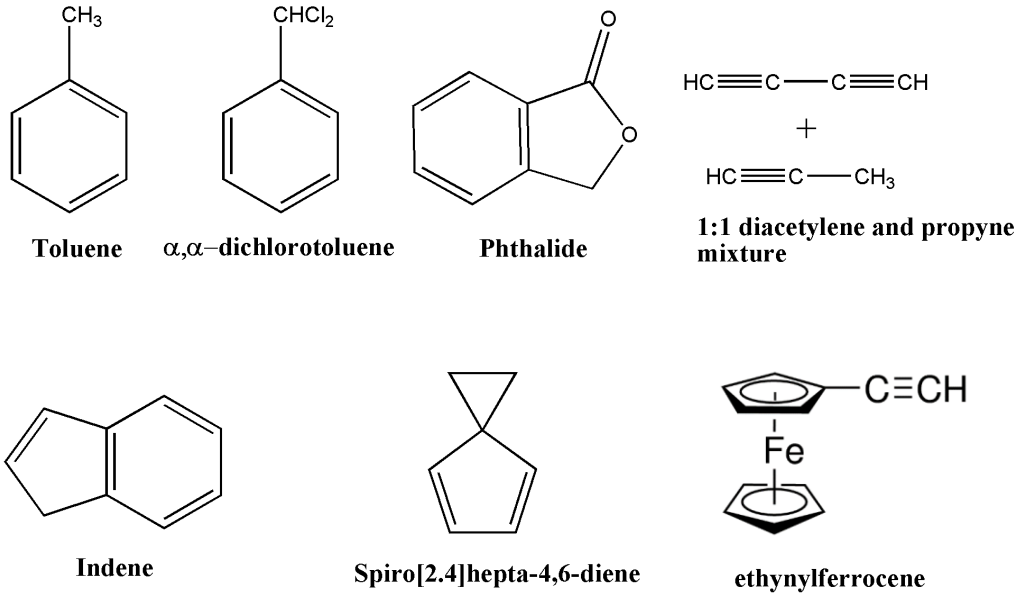

Chart 3.1: The precursors used for the generation of $C_7H_n^{+/-}$ ions

The C_7H_n cations and anions were produced from several organic molecules *via* dissociative ionization in discharge sources.[21] Toluene was used as a precursor of $C_7H_3^-$ and $C_7H_5^-$. $C_7H_3^+$ was produced from indene and 1:1 mixture of diacetylene and propyne. $C_7H_4^+$ and $C_7H_5^+$ were generated also from this 1:1 mixture of diacetylene and propyne. Alongside toluene, α,α-dichlorotoluene, phthalide, spiro[2.4]hepta-4,6-diene, ethynylferrocene have been employed for the production of $C_7H_5^+$. 1:1 mixture of diacetylene and propyne and indene are the rich sources for $C_7H_n^+$ ions and m/z=89, $C_7H_5^+$, is the strongest peak after the parent ions in the mass spectra. Structures of all these precursors are shown in **Chart 3.1**.

3.3 RESULTS AND DISCUSSIONS

3.3.1 $C_7H_3^+$:

3.3.1.1: Absorption

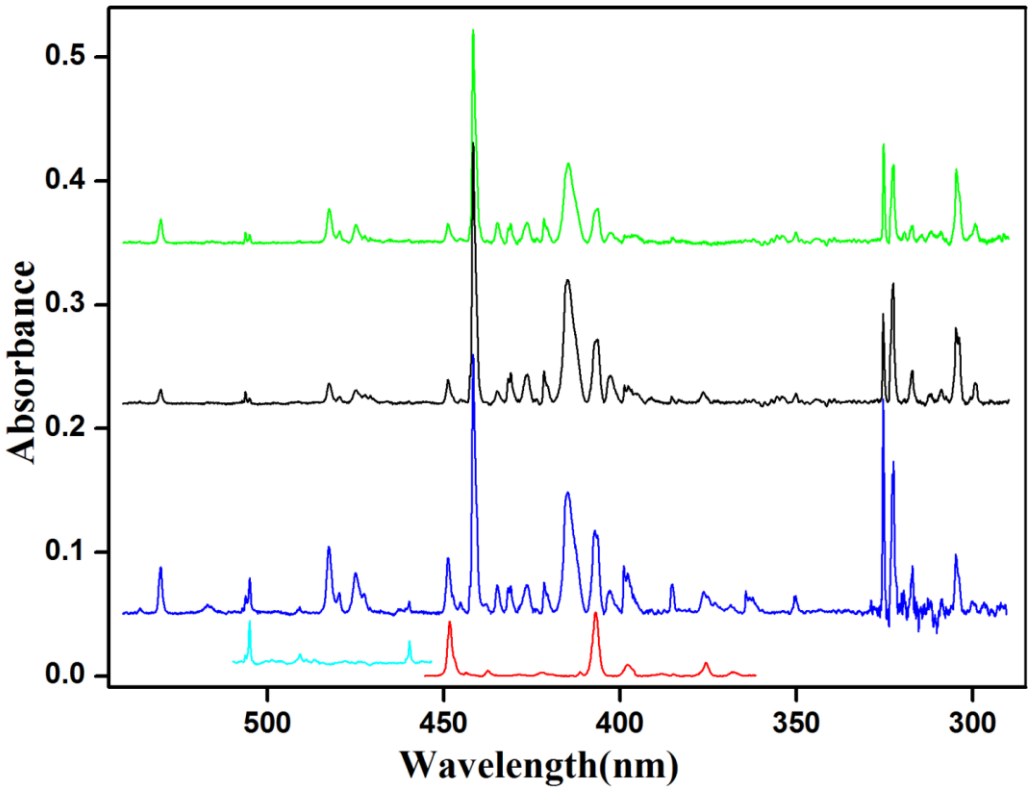

Figure 3.1: Electronic absorption spectra recorded in neon matrix after mass-selected deposition of $C_7H_3^+$ (black) and after 30 min irradiation by λ < 260 nm photons (green). The spectrum obtained after deposition of high kinetic energy (~90 eV) $C_7H_3^+$ is in blue. The transitions of *l* -HC_7H^+ (red) and *l* -HC_7H (light blue) were identified in earlier studies.[22,23]

Strong absorptions are recorded in the 300−450 nm range (**Figure 3.1**) along with some weaker ones between 470 and 540 nm after mass-selected deposition of $C_7H_3^+$ in a neon matrix containing trace of CH_3Cl (1 : 30000). The strongest as well as very sharp peak is seen at 441.3 nm, and a relatively broader absorption at 414.6 nm (**Figure 3.1,** black trace). In addition, an electronic system with onset at 322.2 nm is apparent. To distinguish absorptions of the cations from neutrals, the matrix was exposed to λ < 260 nm photons from a medium pressure mercury lamp. The Cl^- anions generated from CH_3Cl during deposition (see **Chapter 2**, section 2.4) release electrons which recombine with $C_7H_3^+$ producing neutral species. The intensity of the absorption systems commencing at 441.3, 414.6 and 322.2 nm decreased while the bands around 325, 530.3 and 482.3 nm became stronger after irradiation (**Figure 3.1,** green traces). A

moderately intense band with doublet structure is present in the spectrum around 305 nm. One component of this decreases and other increases upon irradiation due to the superposition of a cationic and a neutral absorption. The peaks which diminish are of $C_7H_3^+$ isomers while those gain intensity correspond to C_7H_3 neutrals. The two weak bands at 448 and 407 nm (**Figure 3.1,** black trace) that diminish after irradiation are due to *l*-HC_7H^+, a polyacetylene cation,[22] formed by collisionally-induced fragmentation of $C_7H_3^+$ during growth of the matrix.

To distinguish absorptions of the primary isomers from the collision-induced ones, $C_7H_3^+$ with 90 eV kinetic energy was deposited. The spectrum obtained (**Figure 3.1,** blue trace) is compared with the one recorded with 50 eV kinetic energy. The spectra have been normalized to the intensity of the strongest band at 441.3 nm. As expected the absorptions of the *l*-HC_7H^+ fragment are much stronger with 90 eV deposition energy. The bands of neutral species which gained intensity upon UV irradiation are stronger in this blue trace. Additionally, a moderately intense system at 505 nm appeared. It is identical with the electronic spectrum of *l*-HC_7H obtained previously[23] as shown in the light blue trace of **Figure 3.1**

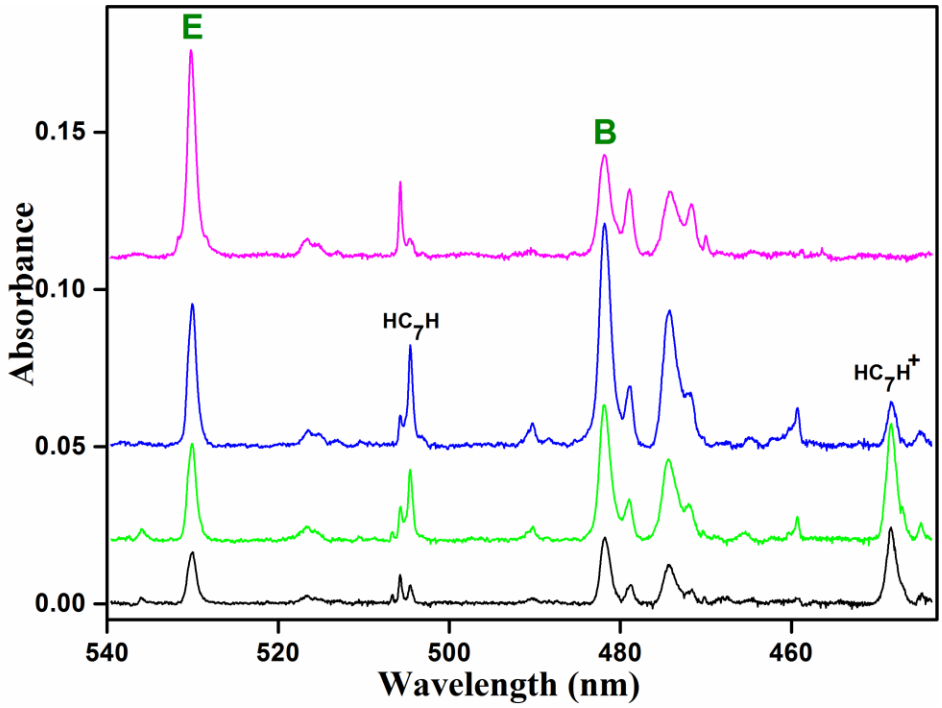

Figure 3.2: A section of the absorption spectra recorded: after deposition of $C_7H_3^+$ with ~50 eV deposition energy (black), after 30 min irradiation by a medium pressure mercury lamp λ < 260 nm (green), after deposition of $C_7H_3^+$ cations with kinetic energy ~90 eV (blue) and after depositing $C_7H_3^-$ followed by irradiation (pink).

Figure 3.2 is a close up of the region where the differences in the spectra recorded with kinetic energies of 50 and 90 eV are pronounced. Apart from the absorptions of *l*-HC_7H^+, two absorptions of neutral C_7H_3 species with onsets at 530.3 and 482.3 nm are observed. The intensities of these absorptions are much stronger in the spectrum obtained by mass selected deposition of $C_7H_3^-$ anions followed by irradiation (pink trace). The relative intensities of the 530.3 and 482.3 nm systems vary with deposition energy and also upon irradiation, which suggests that these bands belong to two C_7H_3 isomers. The origin of the 530.3 nm system lies close to the absorption onset (528.3 nm) of 2-(buta-1,3-diynyl)cycloprop-2yl-1-1ylidene radical (isomer **E** in **Chart 3.2**) recorded in gas-phase[14] and the pattern of the vibrational progression is similar. The enhancement of the relative concentration of isomer **E** in the matrix with higher kinetic energy deposition, as well as in $C_7H_3^-$ anion deposition at even higher kinetic energy ~150 eV, elucidates that **E** is produced as a secondary product during matrix growth. The primary ions should have a similar structure as **E**, a cyclic three-membered carbon ring with a butynyl group C_4H attached. Stronger absorption of *l*-HC_7H^+ seen in the spectra obtained with higher than 50 eV deposition energy indicates that the other primary $C_7H_3^+$ absorbers have open chain structure, from which the removal of a hydrogen atom easily produce *l*-HC_7H^+ in the matrix. Though the identification of the absorptions from secondary products of $C_7H_3^+$ produced under higher kinetic energy conditions provides a hint about the structure of the primary absorber cations, but this information is not sufficient to assign specific $C_7H_3^+$ isomers. Theoretical studies on the stability of different isomers of $C_7H_3^+$ and the corresponding neutrals as well as excitation energies of these species are needed and have been carried out (*vide infra*). All absorption wavelengths are given in **Table 3.1**.

3.3.1.2: Fluorescence

All the intense absorption bands seen in **Figure 3.1** were excited with a laser for fluorescence measurement after depositing $C_7H_3^+$ with neon. The concentration of the CH_3Cl scavenger was kept lower (1: 50000) to have enough concentration of cations as well as neutrals in the matrix. The neutral systems at 530.3 and 482.3 nm do not fluoresce. However, a structured emission system was detected, commencing at 442.7 nm and extending to 514 nm, after laser excitation of the sharp band at 441.3 nm (**Figure 3.3**). The same fluorescence spectrum, though less intense, was obtained after the laser excitation of the weak absorptions lying 558, 809 and 1087 cm^{-1} above the 441.3 nm peak and it confirms that these bands belong to the 441 nm electronic system. Origin of the fluorescence and absorption overlap at 442.4 nm which is the zero-phonon line (ZPL) of the two spectra. The wavelengths of the fluorescence bands are collected in **Table 3.2**. No fluorescence was detected upon excitation of the 414.6, 322.2, 325 and 303 nm bands.

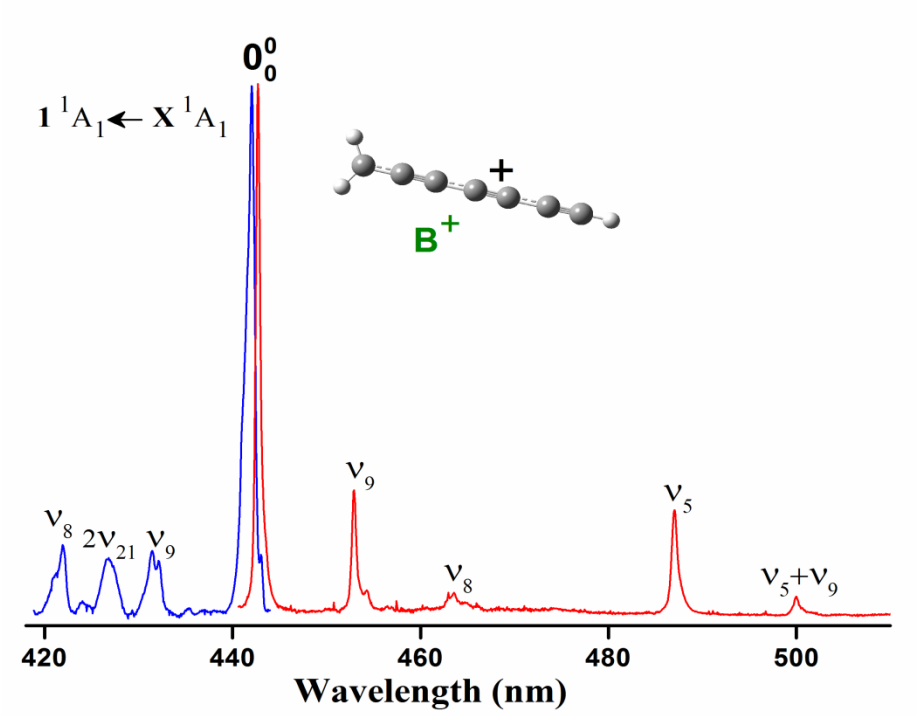

Figure 3.3: Electronic absorption (blue trace) and fluorescence (red trace) spectra of isomer $\mathbf{B}^+$ recorded in a 6 K neon matrix. The fluorescence was recoded by exciting the ν_9 absorption band of the **1** $^1A_1 \leftarrow X\ ^1A_1$ system.

Table 3.1: Absorption band maxima (±0.1 nm) in the electronic transitions of $C_7H_3^+$ and C_7H_3 isomers in neon matrices.[30] The assignment is based on the calculated harmonic frequencies of the totally symmetric vibrations given in the footnote. Structural assignments are discussed in section 3.3.1.3.

λ (nm)	ν (cm^{-1})	Δν (cm^{-1})	Assignment	
A^+				
322.2	31037	0	0_0^0	**1** $^1A_1 \leftarrow X\ ^1A_1$
316.8	31566	529	ν_9	
303.2	32982	1945	ν_4	
298.5	33501	2464	$\nu_9 + \nu_4$	
B^+				
441.3	22660	0	0_0^0	**1** $^1A_1 \leftarrow X\ ^1A_1$
430.9	23218	558	ν_9	
426.1	23469	809	$2\nu_{21}$	
421.2	23747	1087	ν_8	
B				
482.3	20734	0	0_0^0	**1** $^2B_1 \leftarrow X\ ^2B_1$
474.6	21070	337	$2\nu_{15}$	
C^+				
414.6	24120	0	0_0^0	**1** $^1A' \leftarrow X\ ^1A'$
406.6	24592	462	ν_{14}	
402.5	24845	725	ν_{10}	
E				
530.3	18857	0	0_0^0	**1** $^2A' \leftarrow X\ ^2A'$
516.8	19350	493	ν_{14}	
515.5	19399	542	ν_{13}	
504.8	19810	953	ν_9	
479.4	20859	0	0_0^0	**2** $^2A' \leftarrow X\ ^2A'$
472.2	21177	318	ν_{15}	

Totally-symmetric vibrations (cm^{-1}) of the identified species calculated at the DFT /cc-pVDZ level:
A^+ (a_1)**:** $\nu_1 - \nu_9$: 3451, 3314, 2378, 2098, 1739, 1425, 1114, 929, 538;
B^+ (a_1)**:** $\nu_1 - \nu_9$: 3442, 3157, 2543, 2245, 2088, 1532, 1431, 1049, 545;
B (a_1)**:** $\nu_1 - \nu_9$: 3669, 3239, 3021, 2711, 2247, 1472, 1083, 1008, 537;
C^+ (a')**:** $\nu_1 - \nu_{17}$: 3440, 3435, 3164, 2495, 2199, 2115, 1471, 1260, 1068, 776, 710, 685, 507, 472, 267, 179, 65;
E (a')**:** $\nu_1 - \nu_{16}$: 3647, 3045, 2955, 2553, 1621, 1353, 1217, 1098, 952, 947, 801, 744, 587, 508, 269, 109.

Table 3.2: Fluorescence band maxima (±0.1 nm) of the **1** $^1A_1 \rightarrow X\ ^1A_1$ electronic transition of isomer $\mathbf{B}^+$ trapped in a neon matrix at 6 K.[30] The assignment is based on the calculated harmonic vibrational frequencies given in the footnote of Table 3.1.

λ (nm)	ν (cm^{-1})	Δν (cm^{-1})	Assignment	
442.7	22589	0	0_0^0	**1** $^1A_1 \rightarrow X\ ^1A_1$
452.9	22080	509	ν_9	
463.6	21570	1019	ν_8	
487.0	20534	2055	ν_5	
500.0	20000	2589	$\nu_9 + \nu_5$	
513.5	19474	3115	ν_2	

3.3.1.3 Computations: comparison with experiment

Geometry optimization of nine plausible $C_7H_3^+$ isomer and their corresponding neutrals (**Chart 3.2**) was carried out with DFT using B3LYP functional and the cc-pVDZ basis set. Harmonic vibrational frequencies in the ground state were calculated to check whether the structures are real minima on the potential energy surface (PES) or not. The DFT optimized co-ordinates have been used further for the excitation energy calculation.

Chart 3.2: Structures of the nine most stable isomers of $C_7H_3^+$. The relative ground state energies (kJ mol^{-1}) of the cations are given in black; neutrals in blue and anions in red.

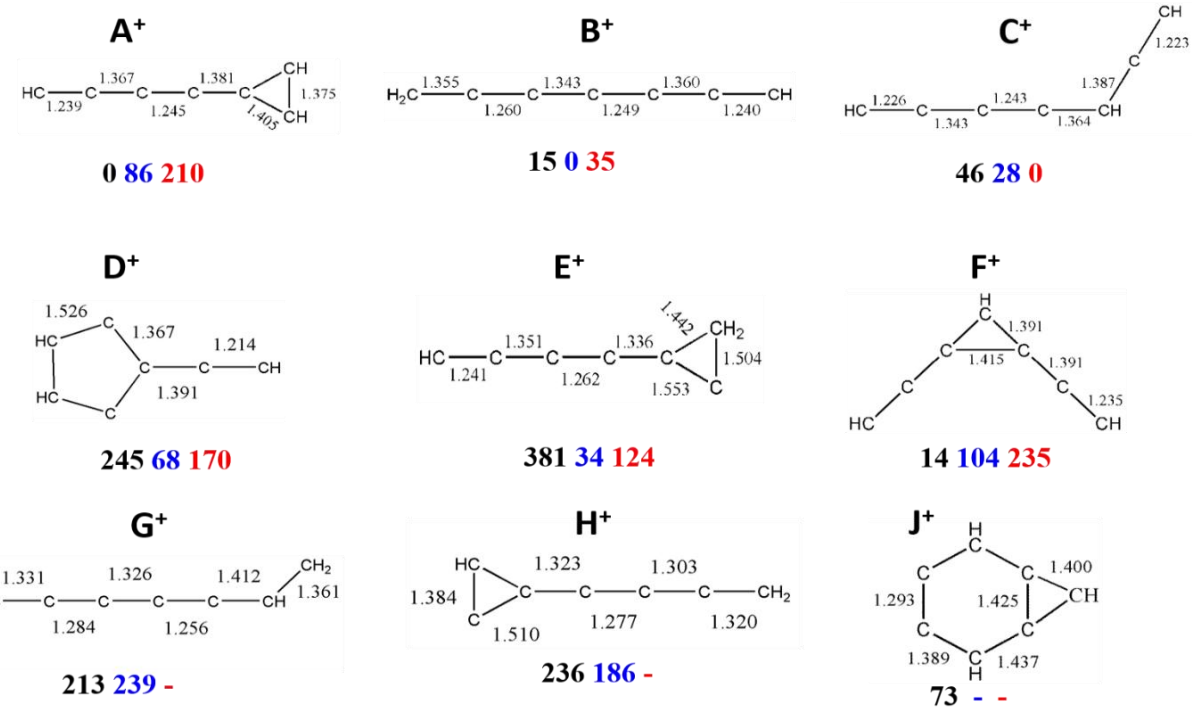

The vertical excitation energies were calculated using a second order multiconfigurational perturbation theory (CASPT2) implemented in the Molcas program package. 13 electrons partitioned in 13 orbitals formed the active space and six roots were calculated for the irreducible representation of each species. The vertical excitation energies obtained are given in **Table 3.3** and compared with the origin band positions in the spectra of $C_7H_3^+$ and C_7H_3 in neon matrices. The results for the five lowest energy structures, $\mathbf{A}^+$, $\mathbf{B}^+$, $\mathbf{C}^+$, $\mathbf{F}^+$, $\mathbf{J}^+$ and for isomer **E** (responsible for the 528.8 nm electronic system identified in a gas–phase study[14]), are discussed below in next paragraphs. The structures of the **A**, **B**, **C**, **D, E, F, G, H** and **J** are presented in **Chart 3.2** together with the ground state energies calculated for the cationic, anionic and neutral forms. The bond lengths for the cations, calculated with the DFT method, are shown. The global minimum on the $C_7H_3^+$ PES is isomer $\mathbf{A}^+$, a three - membered carbon ring fused with the linear C_4H chain. The second lowest energy structure $\mathbf{F}^+$ has the same three - member carbon ring motif but with two ethynyl groups attached. The next in energy isomer $\mathbf{J}^+$ - fused three and six carbon rings – is located 40 kJ/mol above $\mathbf{A}^+$ according to DFT calculation. Isomers $\mathbf{B}^+$ and $\mathbf{C}^+$ are almost isoenergetic and lie 61 and 69 kJ/mol above $\mathbf{A}^+$. Cation $\mathbf{E}^+$ lies 452 kJ/mol above $\mathbf{A}^+$. However $\mathbf{E}^+$ is also under consideration because the electronic transition of neutral **E** is observed in the present studies. The most stable structure of neutral C_7H_3 is **J**.

Table 3.3: Electronic excitation energies E_{cal} (eV) and oscillator strength (*f*) of the dipole allowed electronic transitions for $C_7H_3^+$ and C_7H_3 isomers calculated by the MS CASPT2 method and comparison to the experimental observations E_{exp}.[30] [not observed = n.o.]

	Transitions	E_{cal}	f	E_{exp}
$\mathbf{A}^+$	**1** $^1A_1 \leftarrow X\ ^1A_1$	**4.13**	*0.401*	3.85
	2 $^1A_1 \leftarrow$	5.99	*0.012*	
A	**1** $^2A_2 \leftarrow X\ ^2B_1$	1.72	*0.000*	
	3 $^2B_1 \leftarrow$	4.76	*0.133*	4.09
$\mathbf{B}^+$	**1** $^1A_1 \leftarrow X\ ^1A_1$	**2.99**	*0.334*	2.81
	2 $^1A_1 \leftarrow$	3.95	*0.020*	
	3 $^1A_1 \leftarrow$	4.21	*0.000*	
	4 $^1A_1 \leftarrow$	5.53	*0.010*	
B	**1** $^2B_1 \leftarrow X\ ^2B_1$	**2.46**	*0.002*	2.57
	2 $^2B_1 \leftarrow$	5.73	*0.001*	

C$^+$	**1** ^{1}A' ← X ^{1}A'	**3.13**	*0.641*	2.99
	2 ^{1}A' ←	4.17	*0.030*	
	3 ^{1}A' ←	4.73	*0.001*	
	4^1 A' ←	5.19	*0.040*	
C	**1** ^{2}A" ← X ^{2}A"	3.21	*0.030*	n.o.
	2 ^{2}A" ←	4.42	*0.010*	
	3 ^{2}A"←	5.08	*0.008*	
	4 ^{2}A"←	5.57	*0.020*	
D$^+$	**1** $^1A_1$ ←X $^1A_1$	5.11	*0.017*	n.o.
	2 $^1A_1$ ←	5.90	*0.011*	
D	**2** $^2B_1$ ←X $^2A_2$	2.49	*0.002*	n.o.
	4 $^2B_1$ ←	4.87	*0.026*	
	1 $^2A_2$ ←	3.28	*0.003*	
E$^+$	**1** ^{1}A'← X ^{1}A'	0.68	*0.000*	n.o.
	2 ^{1}A'←	2.94	*0.030*	
	3 ^{1}A'←	3.10	*0.172*	
	4 ^{1}A'←	3.26	*0.030*	
E	**1** ^{2}A'← X ^{2}A'	**2.28**	*0.010*	2.34
	2 ^{2}A' ←	**2.56**	*0.002*	2.58
	3 ^{2}A'←	3.43	*0.001*	
	4 ^{2}A' ←	3.86	*0.005*	
	5 ^{2}A' ←	5.30	*0.020*	
F$^+$	**1** $^1A_1$ ← X $^1A_1$	5.46	*0.132*	n.o.
	2 $^1A_1$ ←	6.15	*0.012*	
F	**1** $^2B_1$ ← X $^2A_2$	1.15	*0.031*	n.o
	2 $^2B_1$ ←	4.44	*0.040*	
	3 $^2B_1$ ←	5.67	*0.192*	
G$^+$	**1** ^{1}A' ← X ^{1}A'	2.60	*0.004*	n.o.
	2 ^{1}A' ←	2.69	*0.155*	n.o.
	3 ^{1}A' ←	4.31	*0.348*	
G	**1** ^{2}A ← X ^{2}A	4.54	*0.002*	n.o.
H$^+$	**1** ^{1}A' ← X ^{1}A'	2.59	*0.133*	n.o.
	2 ^{1}A' ←	4.15	*0.292*	
	3 ^{1}A' ←	4.33	*0.024*	
	4 ^{1}A' ←	5.48	*0.359*	
H	**1** ^{2}A ← X ^{2}A	3.59	*0.002*	n.o.

	2 $^2A \leftarrow$	4.17	*0.005*	
$\mathbf{J^+}$	**1** $^1B_2 \leftarrow X\ ^1A_1$	4.30	*0.064*	n.o.
	1 $^1B_2 \leftarrow$	5.80	*0.003*	
	1 $^1A_1 \leftarrow$	5.29	*0.013*	
	2 $^1A_1 \leftarrow$	5.89	*0.110*	
J	**1** $^2B_1 \leftarrow X\ ^2B_1$	3.36	*0.055*	n.o.
	2 $^2B_1 \leftarrow$	4.84	*0.074*	
	3 $^2B_1 \leftarrow$	6.42	*0.190*	
	3 $^2A_2 \leftarrow$	3.30	*0.021*	
	4 $^2B_1 \leftarrow$	5.25	*0.063*	

Isomers $\mathbf{A^+}$, A

The ground-state of two lowest energy $C_7H_3^+$ isomers, $\mathbf{A^+}$ and $\mathbf{F^+}$, has X $^1A_1$ symmetry. For both of them, the MS CASPT2 calculations predict two dipole-allowed electronic transitions to the **1** $^1A_1$ and **2** $^1A_1$ states below 6.5 eV (**Table 3.3**). The first **1** $^1A_1$ electronic state of $\mathbf{A^+}$ and $\mathbf{F^+}$ lies at 4.13 and 5.46 eV above the X $^1A_1$, with oscillator strengths (*f*) 0.401 and 0.132, respectively. The second **2** $^1A_1 \leftarrow$ X $^1A_1$ absorption around 6 eV is two orders of magnitude weaker in intensity compared to the first one. These results are consistent with earlier CASSCF and MRCI calculations on cyclic $C_3H_3^+$ which predict a electronic transition around 8 eV.[24] Substitution of two hydrogen atoms in c-$C_3H_3^+$ with two ethynyl groups ($\mathbf{F^+}$) shifts this **2** $^1A_1 \leftarrow$ X $^1A_1$ transition to 5.46 eV. A much lower energy 4.13 eV was predicted for $\mathbf{A^+}$ where one hydrogen atom of c-$C_3H_3^+$ is replaced with a butynyl group, because the electrons are delocalized over a larger distance.

c-$C_3H_3^+$, produced from cyclic and acyclic precursors, has been studied in neon matrices. Electronic transition of c-$C_3H_3^+$ is beyond the experimental detection range (270-1100 nm) but its presence in the matrix was identified by infrared measurements.[24] Hence, one can expect that $\mathbf{A^+}$ and $\mathbf{F^+}$ are also formed in the present experiments and trapped in the neon matrix, as the conditions were similar to those for c-$C_3H_3^+$. $\mathbf{F^+}$ with electronic transition around 5.46 eV, could not be observed as this is also beyond the measurement range.

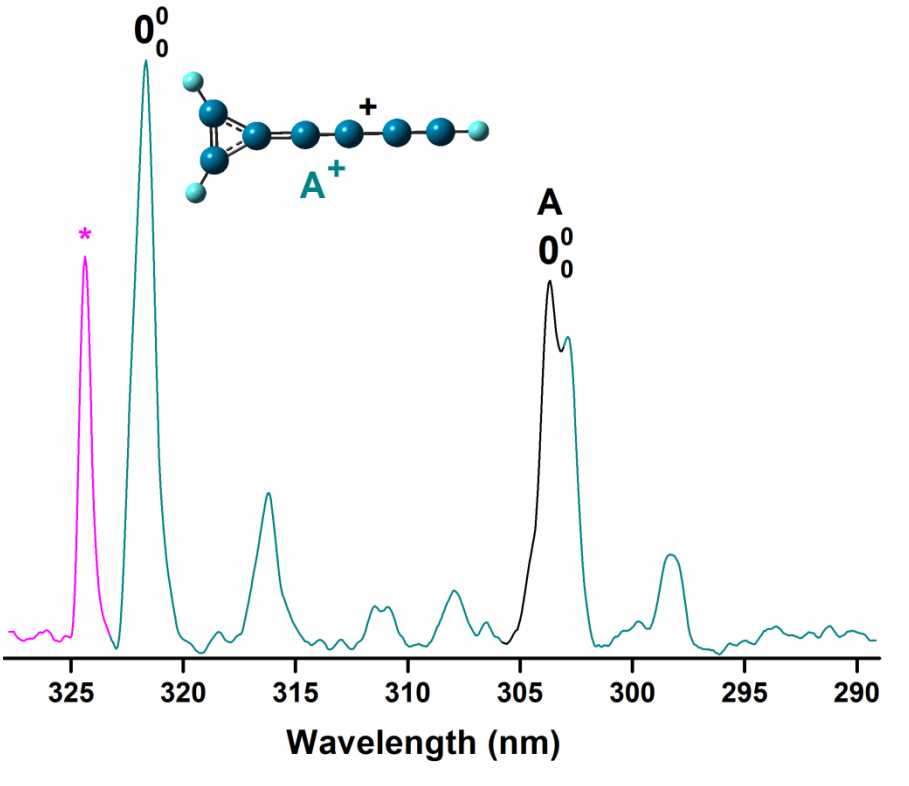

Figure 3.4: The UV part of the absorption spectrum recorded after mass selective deposition of *m/z* = 87 ($C_7H_3^+$) cations. The absorptions of $\mathbf{A}^+$ (light blue), **A** (black) are indicated. The peak in pink denoted by asterisk cannot be assigned from the calculated excitation energies.

$\mathbf{A}^+$ has the strong **1** $^1A_1 \leftarrow$ X $^1A_1$ (f = 0.40) transition at lower energy (4.13 eV; 300 nm), close to the 322.3 nm absorption system. In this region, MS-CASPT2 calculations predict also a moderately intense **1** $^1B_2 \leftarrow$ X $^1A_1$ transition (f=0.064, 4.30 eV) for isomer $\mathbf{J}^+$. As the oscillator strength of the electronic transition of $\mathbf{J}^+$ is an order of magnitude smaller than the **1** $^1A_1 \leftarrow$ X $^1A_1$ transition of $\mathbf{A}^+$, therefore, the 322.3 nm absorption system is assigned to the **1** $^1A_1 \leftarrow$ X $^1A_1$ transition of $\mathbf{A}^+$.

Isomer $\mathbf{A}^+$ is likely a progenitor of neutral **E** in the higher kinetic energy deposition experiments, because these two species have the same carbon skeleton (three membered carbon ring with C_4H chain) and differ only in the position of two hydrogen atoms; $\mathbf{A}^+$, during hard landing on the matrix surface, possesses enough internal energy to rearrange the two hydrogen atoms.

The section of the electronic spectrum, where the absorptions of $\mathbf{A}^+$ are present, is shown in **Figure 3.4**. Three vibrational bands located 529, 1945 and 2464 cm^{-1} above the origin belong to this system and correspond to the excitation of the ν_9, ν_4 modes and their combinations. Harmonic vibrational frequencies in the ground state of $\mathbf{A}^+$ calculated with DFT method are 538 and 2098 cm^{-1}. The wavelengths of the band maxima of $\mathbf{A}^+$ and the assignment are given in **Table 3.1**.

A transition of neutral species is apparent at 303 nm in **Figure 3.4**. Calculations predict a strong **3** $^2B_1 \leftarrow$ X $^2B_1$ (f = 0.13) transition of **A** at 4.76 eV. Relatively much weaker electronic transitions of other higher energy isomers predicted in this region are not considered and the absorption at 303 nm (4.09 eV) is assigned to the **3** $^2B_1 \leftarrow$ **X** $^2B_1$ transition of species **A**.

Isomers B^+, B and C^+

The 390–460 nm section of the electronic spectrum measured after mass-selected deposition of m/z = 87 cations (**Figure 3.5**) shows two absorption systems starting at 441.3 nm (2.81 eV) and 414.6 nm (2.99 eV) belonging to two $C_7H_3^+$ isomers. Only four isomers, $\mathbf{B}^+$, $\mathbf{C}^+$, $\mathbf{G}^+$ and $\mathbf{H}^+$ possess strong electronic transitions in this region. The $\mathbf{G}^+$ and $\mathbf{H}^+$ have been excluded because they have even stronger transitions around 300 nm, contrary to the experimental observation. Isomers $\mathbf{B}^+$ and $\mathbf{C}^+$ are open chain structure (**Chart 3.2**) and are good candidates for the 441 and 414 nm systems. Both cations, after removal of one hydrogen atom, can readily produce the l-HC_7H^+ fragment ion as observed in the higher kinetic energy studies.

The calculations predict a strong **1** $^1A_1 \leftarrow$ X $^1A_1$ transition (f = 0.33) at 2.99 eV and a two orders of magnitude weaker one at 3.95 eV for $\mathbf{B}^+$; the first excited **1** $^1A'$ state for $\mathbf{C}^+$ is 3.13 eV above the X $^1A'$ state (f = 0.64). Three other electronic transitions of $\mathbf{C}^+$ lie in 4.2 – 5.2 eV, however the oscillator strengths are two orders of magnitude smaller than to the **1** $^1A'$ state. The energy of the **1** $^1A_1 \leftarrow$ X $^1A_1$ transition of $\mathbf{B}^+$ matches with the onset at 441.3 nm (2.81 eV) of the strongest absorption system. Also the origin of the second system at 414.6 nm (2.99 eV) correlates well with the energy of the **1** $^1A' \leftarrow$ X $^1A'$ transition of $\mathbf{C}^+$. Therefore, the absorptions in the spectrum shown in **Figure 3.5** are assigned to the **1** $^1A_1 \leftarrow$ X $^1A_1$ of $\mathbf{B}^+$ and **1** $^1A' \leftarrow$ X $^1A'$ transitions of $\mathbf{C}^+$, respectively. $\mathbf{B}^+$ is a hydrogenated form of l-HC_7H^+. In case of triacetylene cation HC_6H^+, addition of one hydrogen shifts the origin band from 604.2 nm (HC_6H^+) to

378.6 nm ($HC_6H_2^+$).[25,26] Similarly the absorption of $\mathbf{B}^+$ at 441.3 nm is shifted ~160 nm to the blue in comparison to HC_7H^+ (599.8 nm).[22]

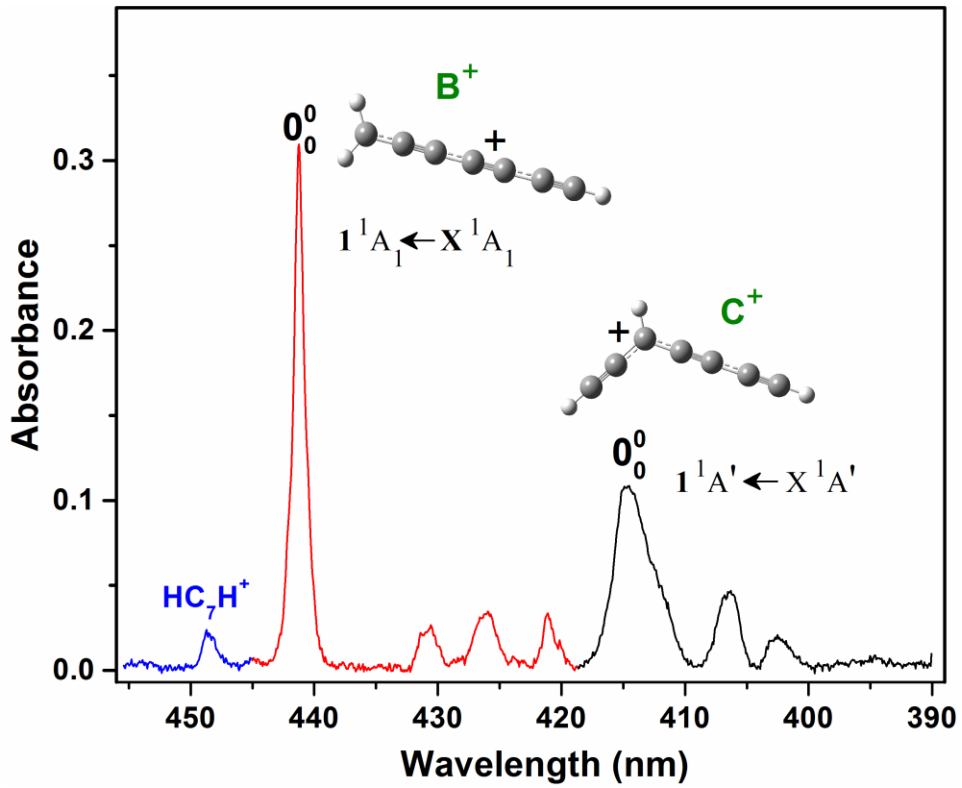

Figure 3.5: Visible portion of the absorption spectrum showing two electronic systems of the $\mathbf{B}^+$ (red) and $\mathbf{C}^+$ (black) isomers of $C_7H_3^+$ obtained after mass selected deposition of *m/z* = 87 cations in a neon matrix.

The vibrational bands present in the absorption and fluorescence spectra of $\mathbf{B}^+$ are assigned on the basis of calculated ground-state harmonic frequencies of $\mathbf{B}^+$ (**Table 3.1** & **3.2**). Four totally symmetric a_1 modes: ν_9, ν_8, ν_5 and ν_2 are active in the fluorescence spectrum of $\mathbf{B}^+$ and only the two former vibrations in the absorption. There is an absorption peak between the ν_9 and ν_8 bands at 809 cm^{-1} above the origin which belongs to $\mathbf{B}^+$ because the fluorescence starting at ~442 nm was detected by exciting the peak. This band arises from the excitation of two quanta of the ν_{21} (b_2) mode. In the spectrum of $\mathbf{C}^+$ two absorption peaks located 462 and 725 cm^{-1} above the origin 414.6 nm are apparent. The first one is hidden under the absorption of *l*-HC_7H^+. They are attributed to ν_{14} and ν_{10} mode excitations by comparison with the 472 and 776 cm^{-1} calculated ground state vibrational frequencies of $\mathbf{C}^+$.

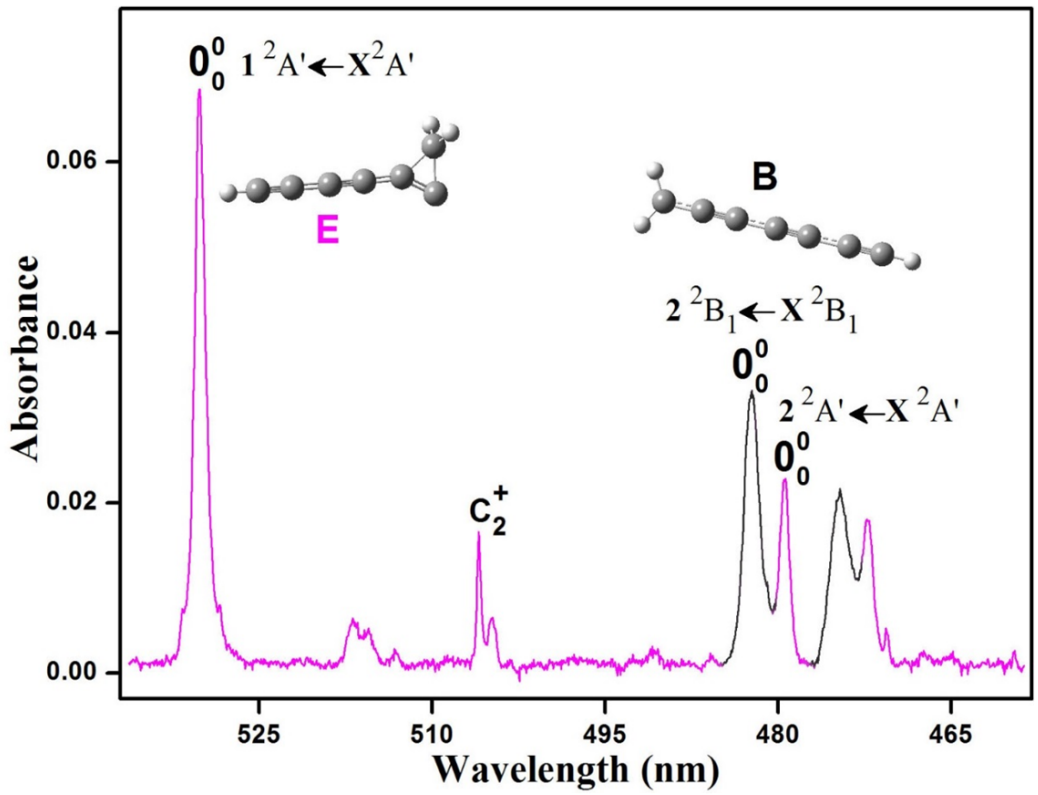

Figure 3.6: Visible section of the absorption spectrum showing the electronic systems of the **B (**black**)** and **E** (pink) isomers of C_7H_3. The spectrum was measured after a mass–selective deposition of $C_7H_3^-$ (*m/z* = 87) anion.

As the electronic transitions of $\mathbf{B}^+$ and $\mathbf{C}^+$ are detected, one can expect that **B** and **C** should also be present. A good candidate for either of these species is the absorption system starting at 482.3 nm (2.57 eV) which gains in intensity upon UV irradiation (**Figure 3.6**). The calculations predict a weak (*f* = 0.002) **1** $^2B_1 \leftarrow X\,^2B_1$ transition for **B** at 2.46 eV, the **1** $^2A'' \leftarrow X\,^2A''$ transition of **C** at 3.21 eV with oscillator strength 0.03. Due to a better match of the calculated excitation energy with the observations, the electronic system commencing at 482.3 nm is assigned to the **1** $^2B_1 \leftarrow X\,^2B_1$ transition of **B**.

Isomer E

The absorption at 530.3 nm shown in **Figure 3.6** belongs to isomer **E** identified in the gas phase studies at 528.8 nm and assigned to the origin band of the **1** $^2A' \leftarrow$ **X** $^2A'$ transition.[14] Some unassigned bands around 481 and 474 nm were also reported there. The 479.4 nm absorption system in the neon matrix behaves in a similar fashion to that of 530.3 nm upon irradiation. The calculations predict two transitions **1** $^2A' \leftarrow X\,^2A'$ and **2** $^2A' \leftarrow X\,^2A'$ at 2.28 and 2.56 eV, with

oscillator strength 0.010 and 0.002. The computed energies and the intensities agree with the onsets at 530.3 nm (2.34 eV) and 479.5 nm (2.58 eV). Three absorption bands located 493, 542 and 953 cm^{-1} above the origin of the first electronic system are attributed to the excitation of the ν_{14}, ν_{13} and ν_9 modes.

3.3.2 $C_7H_4^+$: Methyltriacetylene cation

The absorption spectrum recorded after deposition of $C_7H_4^+$ in a neon matrix containing a small admixture of CH_3Cl is shown as the blue trace of **Figure 3.7**. A strong absorption at 602.6 nm dominates the spectrum and several weaker features are present and extend up to 400 nm. All the bands diminished after irradiation of the matrix with a medium pressure mercury lamp (λ < 260 nm), suggesting their ionic nature (red trace, **Figure 3.7**). The stronger absorption at 441 nm do not belong to the 603 nm system, because this is still present after UV bleaching whereas the strongest 602.6 nm band is barely seen.

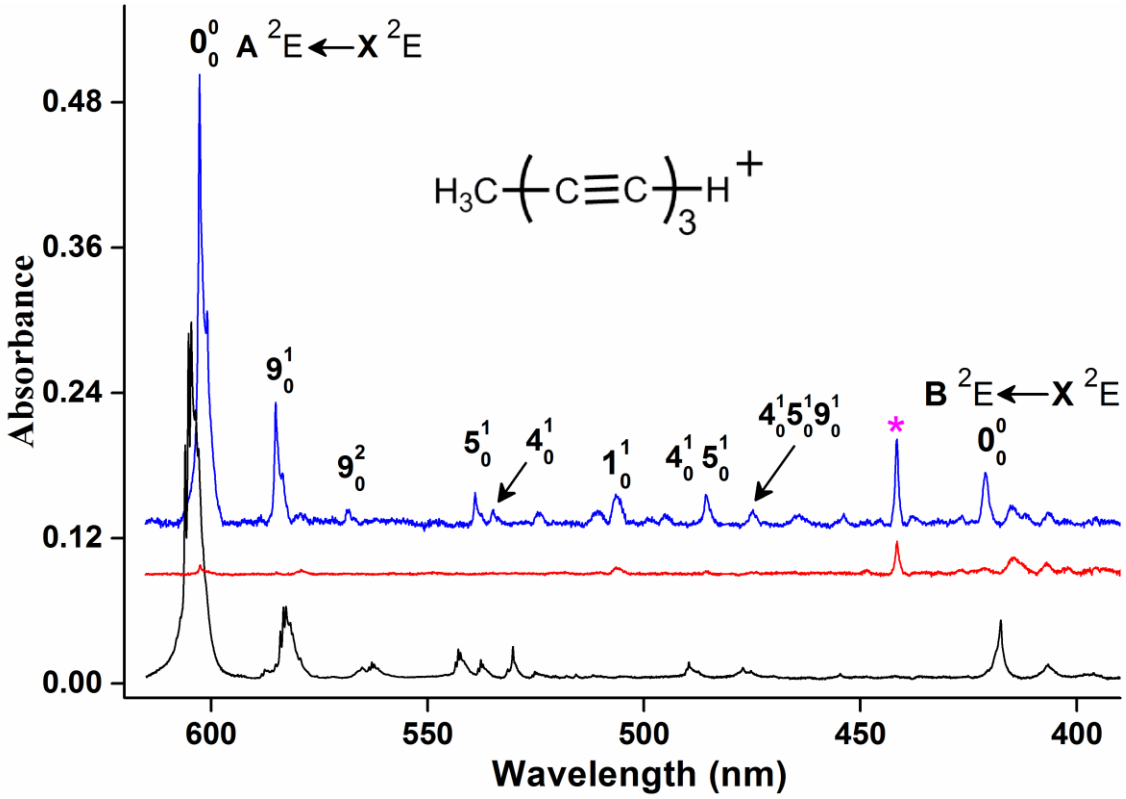

Figure 3.7: Electronic absorption spectra recorded after deposition of mass-selected $C_7H_4^+$ (blue trace) in a 6 K neon matrix and after 25 min irradiation with λ < 260 nm photons (red trace). The black trace is the $\mathbf{A}^2\Pi_g \leftarrow X^2\Pi_u$ absorption spectrum of triacetylene cation. The band denoted by * is the absorption of the $C_7H_3^+$ fragment ($\mathbf{B}^+$).

The origin at 602.6 nm lies close to the onset of the $\mathbf{A}\ ^2\Pi_g \leftarrow X\ ^2\Pi_u$ electronic transition of triacetylene cation HC_6H^+ at 604.6 nm in neon matrix,[27] shown as the black trace in **Figure**

3.7. The spectral patterns of $C_7H_4^+$ and HC_6H^+ are similar. The correspondence of the spectra of $C_7H_4^+$ and HC_6H^+ suggests that the 602.6 nm absorption system is of methyl substituted triacetylene cation ($CH_3C_6H^+$). The origin band in the absorption of $C_7H_4^+$ is shifted ~ 2.0 nm to the blue with respect to HC_6H^+. Effect of methyl substitution has also been studied on some related molecules in the gas phase.[28]

Table 3.4: Electronic excitation energies E_{cal} (eV) and oscillator strength (f) of the dipole-allowed electronic transitions for methyltriacetylene cation calculated by the CASPT2 method and comparison to the experiment E_{exp} (eV).[31]

Ground state	E_{cal}	f	E_{exp}	Excited states
X ^{2}E (C_{3V})	**2.21**	*0.065*	2.06	**1** ^{2}E
	3.34	*0.025*	2.96	**2** ^{2}E
	3.58	*0.000*		**3** ^{2}E
	4.30	*0.024*		**5** ^{2}E
	5.07	*0.000*		**6** ^{2}E

Vertical excitation energies of $CH_3C_6H^+$ were calculated using CASPT2 with C_s symmetry. Two electronic transitions are predicted from the X ^{2}A' ground-state to the **1** ^{2}A' and **2** ^{2}A' excited states below 4 eV with vertical excitation energies of 2.21 and 3.34 eV, and *f* values 0.065 and 0.025, respectively (**Table 3.4**). These energies agree with the observed two electronic transitions at 602.6 nm (2.06 eV) and 421.1 nm (2.94 eV) indicating $CH_3C_6H^+$ as the carrier of these absorptions. The ^{2}A' state correlates with ^{2}E in C_{3v} symmetry then the two observed band systems (**Figure 3.7**) are assigned to the **A** ^{2}E ← X ^{2}E and **B** ^{2}E ← X ^{2}E electronic transitions.

The wavelengths of the band maxima and vibrational frequencies derived from the absorption spectrum of $CH_3C_6H^+$ are collected in **Table 3.5**. The first vibrational transition lies 496 cm^{-1} above the origin, 0_0^0, and the next one is its overtone. DFT/B3LYP calculations of the harmonic frequencies in the ground-state of $CH_3C_6H^+$ predict the lowest energy ν_9 vibration (a_1) at 539 cm^{-1}. The vibrational bands of $CH_3C_6H^+$ lie 1958 and 2100 cm^{-1} above the origin are assigned, according to the calculated vibrational frequencies, to ν_5 (a_1) and ν_4 (a_1), respectively. The ν_3 and ν_2 vibrations of HC_6H^+ and ν_5 and ν_4 of $CH_3C_6H^+$ are similar in nature and their frequencies are not significantly affected by the methyl substituent.[25]

In the spectrum of HC_6H^+ between 425–525 nm, only two weak features, combinations $\nu_2 + \nu_3$ and $\nu_2 + \nu_3 + \nu_4$ are apparent. In contrast, in the absorption of methyltriacetylene cation several bands are in this region The narrow feature marked with asterisk in **Figure 3.7** is the absorption of $\mathbf{B}^+$ isomer of $C_7H_3^+$. A moderately intense band is present around 417 nm (black trace, **Figure 3.7**) which is the onset of the next electronic transition $\mathbf{B}\ ^2\Pi_g \leftarrow X\ ^2\Pi_u$ of HC_6H^+.[25] A corresponding feature is also seen in the absorption of $CH_3C_6H^+$ at 421.1 nm.

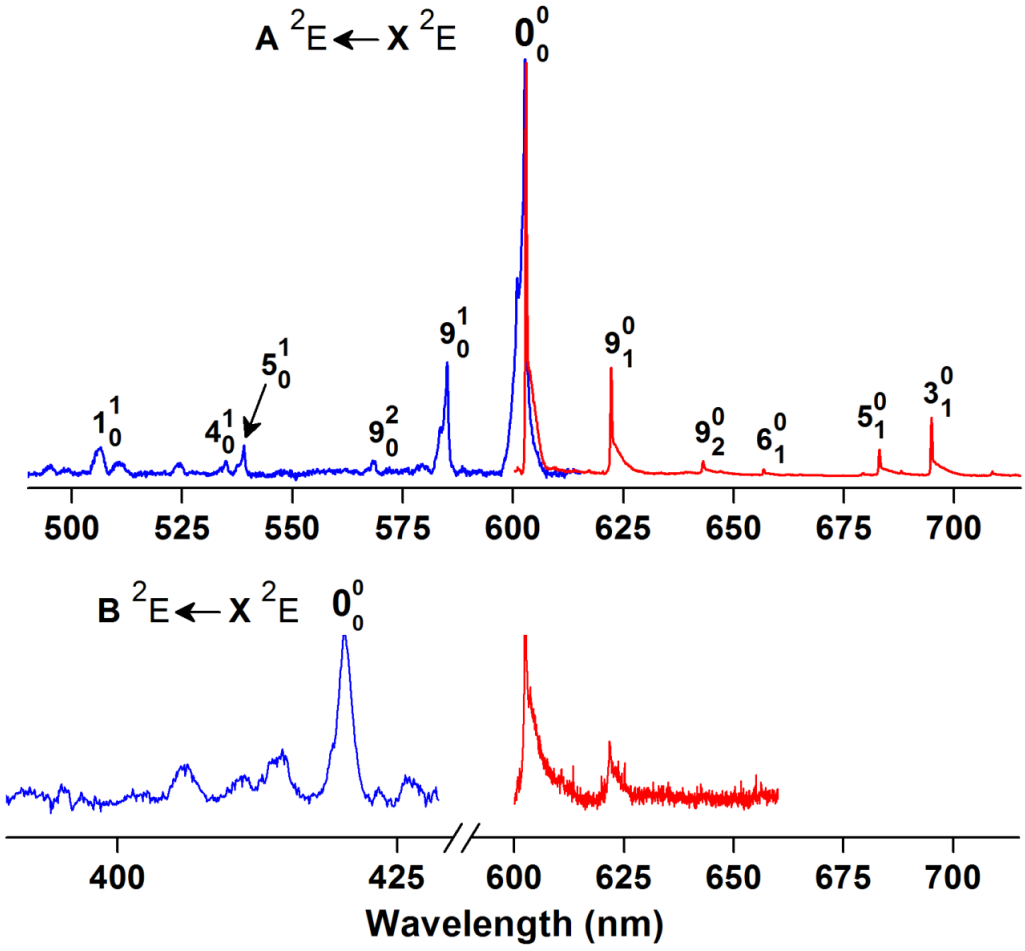

Figure 3.8: Electronic absorption (blue) and fluorescence (red) spectra of methyltriacetylene cation recorded in a 6 K neon matrix. Fluorescence was detected following laser excitation of the 0_0^0 band of the $\mathbf{A}\ ^2E \leftarrow X\ ^2E$ and $\mathbf{B}\ ^2E \leftarrow X\ ^2E$ transitions. The resulting spectra are shown in upper and lower traces, respectively. Vibrational assignment is based on the calculated harmonic frequencies of the totally symmetric vibrations.

A pulsed laser was tuned to the 602.6 nm wavelength, the **A** ^{2}E ← X ^{2}E absorption origin of $CH_3C_6H^+$. The emission in the origin band region was also recorded when the laser matched the wavelength of the first vibrational band at 585.1 nm. Fluorescence commences around 600 nm and extends up to 760 nm. The resulting spectrum is shown in **Figure 3.8**, together with the absorption to emphasize their similar appearance. The wavelengths of the fluorescence maxima and wavenumbers of the vibrations derived from the spectrum are given in **Table 3.6**. The assignment is based on the calculated harmonic vibrational frequencies included in the footnote of **Table 3.5**. Apart from these, ν_6 and its overtone, and combination with ν_9, are active in the X ^{2}E ground state.

Weak fluorescence around 600 nm, shown in bottom panel of **Figure 3.8**, was detected when the laser was tuned to the 421.1 nm absorption band. This confirms that the transition also originates from methyltriacetylene cation.

Table 3.5: Absorption band maxima (±0.1nm) in the **A** ^{2}E ← X ^{2}E and **B** ^{2}E ← X ^{2}E electronic transitions of methyltriacetylene cation in 6 K neon matrices.[31] The assignment is based on the calculated harmonic frequencies of the totally symmetric vibrations, given in the footnote.

λ (nm)	ν (cm^{-1})	Δν (cm^{-1})	Assignment	
602.6	16595	0	0_0^0	**A** ^{2}E ← **X** ^{2}E
585.1	17091	496	9_0^1	
568.4	17593	998	9_0^2	
539.0	18553	1958	5_0^1	
534.9	18695	2100	4_0^1	
524.2	19077	2482	$4_0^1 9_0^1$	
506.5	19743	3148	1_0^1	
485.6	20593	3998	$4_0^1 5_0^1$	
474.8	21061	4467	$4_0^1 5_0^1 9_0^1$	
453.8	22036	5441	$1_0^1 5_0^1 9_0^1$	
421.1	23748	0	0_0^0	**B** ^{2}E ← **X** ^{2}E

Totally-symmetric a_1 vibrations of $CH_3C_6H^+$ (C_{3v}) calculated with DFT using the B3LYP functional and the cc-pVDZ basis set. $\nu_1 - \nu_9$: 3274, 2883, 2192, 2153, 2007, 1349, 1294, 938, 517 cm^{-1}.

Table 3.6: Fluorescence band maxima (±0.1nm) of methyltriacetylene cation in 6 K neon matrices and assignment based on the calculated vibrational frequencies.[31]

λ (nm)	ν (cm^{-1})	Δν (cm^{-1})	Assignment	
602.9	16586	0	0_0^0	**A** ^{2}E → **X** ^{2}E
622.3	16069	517	9_1^0	
643.2	15547	1039	9_2^0	
657.0	15221	1365	6_1^0	
679.3	14721	1865	$6_1^0 9_1^0$	
683.0	14641	1945	5_1^0	
688.0	14535	2051	4_1^0	
694.9	14391	2195	3_1^0	
708.6	14112	2473	$5_1^0 9_1^0$	
720.8	13873	2713	6_2^0	
735.2	13601	2984	$5_1^0 9_2^0$	
748.6	13358	3228	1_1^0	
766.8	13041	3545	$3_1^0 6_1^0$	

3.3.3 C_7H_5: Fulvenallenyl Radical

Transient radicals are generated in the matrix in two steps: **1)** mass-selected anions or cations are co-deposited with neon at 6 K, **2)** trapped ions are irradiated by UV photons to produce the radicals via photodetachment of electrons from anions or recombination of electrons with the cations. To choose the right experimental approach and conditions for the production of Fulvenallenyl Radical **FA**, potential energy surfaces (PES) of neutrals, anions and cations of C_7H_5 have been calculated with the DFT method using the M06-2X functional and the cc-pVTZ basis set; aug-cc-pVDZ has been used for the anions. The justification of ground-state optimization is to infer the relative stability of cation $\mathbf{FA}^+$ and anion $\mathbf{FA}^-$ with respect to other isomers (**Chart 3.3**). It was found that **FA** and $\mathbf{FA}^-$ are the global minimum on the PES among twenty two plausible structures (**Chart 3.4**). $\mathbf{FA}^-$ is more stable by 157 kJ mol^{-1} relative to next isomer $\mathbf{B1}^-$, which suggests that the $C_7H_5^-$ ion beam produced from a discharge source predominantly contains $\mathbf{FA}^-$ and therefore the best approach for **FA** generation in a neon matrix would be the deposition of $C_7H_5^-$ followed by UV irradiation. Structural change of species trapped in neon matrices during the photodetatchment of electrons is unlikely because neon micro-crystals rigidly hold the guest molecules (see **Chapter 2**).

Chart 3.3: Structures and relative ground state energies in kJ mol^{-1} of the five most stable isomers of C_7H_5; the energies of anions are given in red; neutrals in blue and cations in black.

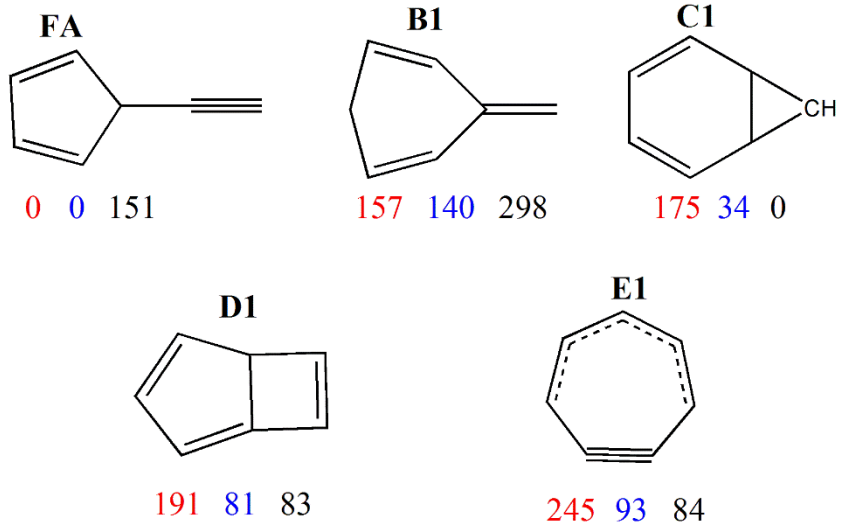

$C_7H_5^-$ was produced from toluene in a hot cathode discharge source. The *m/z*=89 anions after mass-selection were deposited with excess of neon onto a substrate held at 6 K. The

A $^1\Pi_u \leftarrow X\ ^1\Sigma_g^+$ electronic transition[29] of C_3 at 405.0 nm and **B** $^2\Sigma_u^+ \leftarrow X\ ^2\Sigma_g^+$ of N_2^+ at 398 nm were only detected after deposition of $C_7H_5^-$ (black trace, **Figure 3.9**). C_3 is the collisionally-induced fragment of $C_7H_5^-$ due to high kinetic energy deposition. N_2^+ is formed by collisionally-induced ionization of N_2 impurity in the matrix and acts as a counter ion balancing the negative charge.

An absorption system starting at 401.3 nm appeared after irradiating the matrix by $\lambda <$ 260 nm photons (**Figure 3.9**, red trace). It comprises absorption bands at 401.3, 395.5, 371.7 and 346.3 nm (**Table 3.7**). The bands of C_3 remained intact while those of N_2^+ vanished because of recombination with free electrons detached from the anions. The same rate of intensity increment for these four bands upon UV exposure and their similar relative peak intensities from different precursors indicate that they are of one neutral absorber. It means that the 401 nm electronic absorption system originates from neutral C_7H_5 produced *in situ* in solid neon by detachment of electron from trapped $C_7H_5^-$. The fulvenallenyl radical **FA** should be the carrier according to the calculated ground-state stability.

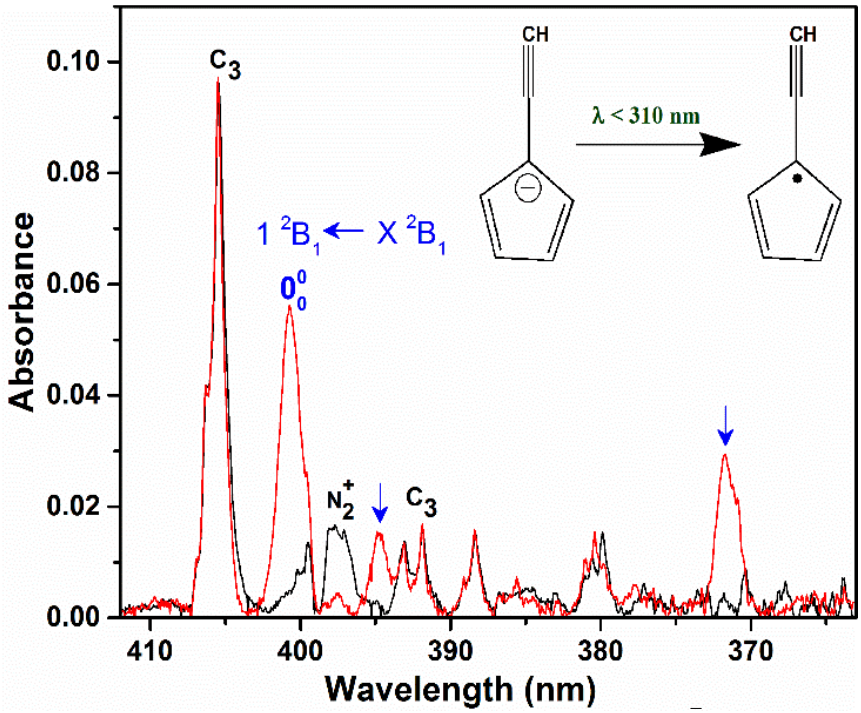

Figure 3.9: Absorption spectrum recorded after deposition of $C_7H_5^-$ in solid neon (black trace) and after irradiation with $250 < \lambda < 310$ nm photons (red trace). Bands appeared (blue arrows) after photodetachment of electrons from $C_7H_5^-$ are the absorptions of fulvenallenyl radical. The origin of **1** $^2B_1 \leftarrow X\ ^2B_1$ transition lies at 401.3 nm.

Table 3.7: Band maxima (±0.1nm) of the **1** $^2B_1 \leftarrow X\ ^2B_1$ absorption system of the fulvenallenyl radical in a 6 K neon matrix.[32] The assignment is based on the ground state vibrational frequencies of the normal modes calculated at the DFT/M06-2X/cc-pVTZ level and given in the footnote.

λ (nm)	$\tilde{\nu}$ (cm^{-1})	$\Delta\tilde{\nu}$ (cm^{-1})	Assignment	
401.3	24919	0	0_0^0	**1** $^2B_1 \leftarrow X\ ^2B_1$
395.5	25284	365	ν_{19}	
371.7	26903	1984	ν_4	
346.3	28877	3958	$2\nu_4$	

a_1; $\nu_1 - \nu_{11}$: 3467, 3271, 3250, 2138, 1531, 1421, 1309, 1087, 1008, 922, 561; **a_2**; $\nu_{12} - \nu_{14}$: 955, 747, 534; **b_1**; $\nu_{15} - \nu_{20}$: 933, 780, 681, 652, 409, 148

For the structural assignment excitation energies (and oscillator strengths) of the five most stables isomers of C_7H_5 and their anions were calculated with the MS(5)-CASPT2 method. The results are presented in **Table 3.8**. Three structures: **FA, B1** and **C1** possess moderately intense transitions at 3.21, 3.11 and 3.45 eV, respectively, close to the origin at 401.3 nm (3.09 eV). The isomers **E1** and **D1** can be excluded from further consideration because the predicted excitation energies are in disagreement with the 401 nm absorption (**Table 3.8**). The matrix was irradiated with varied photon wavelengths and revealed that the electron detachment threshold for the absorber of the 401 nm system is around 310 nm. According to the MS-CASPT2 calculations **FA**$^-$ and **B1**$^-$ possess transitions at 4.39 eV (282 nm) and 4.14 eV (299 nm), respectively, which are larger than the electron detachment energy.

Table 3.8: Excitation energies in eV and oscillator strengths (italics) of anions, neutrals and cations of C_7H_5 given in Chart 3.3 calculated with the MS(5)-CASPT2 method using coordinates from the DFT/M06-2X calculations.[32]

FA$^-$			**FA**			**FA$^+$**		
X $^1A_1$	0.00		X $^2B_1$	0.00		X $^1A_1$	0.00	
1 $^1A_1$	4.39	*0.180*	1 $^2B_1$	3.21	*0.033*	1 $^1A_1$	2.96	*0.001*
2 $^1A_1$	4.77	*0.182*	2 $^2B_1$	4.66	*0.005*	2 $^1A_1$	4.10	*0.480*
3 $^1A_1$	5.79	*0.010*	3 $^2B_1$	5.41	*0.150*	3 $^1A_1$	5.39	*0.007*
1 $^1B_2$	4.69	*0.120*	2 $^2A_2$	5.60	*0.002*	1 $^1B_2$	0.97	*0.004*
1 $^1B_2$	4.98	*0.040*						
B1$^-$			**B1**			**B1$^+$**		
X $^1A_1$	0.00		X $^2B_1$	0.00		X $^1A_1$	0.00	
1 $^1A_1$	4.14	*0.370*	1 $^2B_1$	3.11	*0.027*	1 $^1A_1$	4.20	*0.130*
2 $^1A_1$	4.73	*0.130*	2 $^2B_1$	5.20	*0.025*	2 $^1A_1$	4.46	*0.018*
3 $^1A_1$	5.59	*0.011*	2 $^2A_1$	5.64	*0.001*	3 $^1A_1$	4.89	*0.054*
1 $^1B_2$	4.88	*0.097*	1 $^2A_2$	1.62	*0.000*	1 $^1B_1$	0.95	*0.001*
2 $^1B_2$	5.27	*0.054*	2 $^2A_2$	4.94	*0.020*	3 $^1B_1$	4.93	*0.004*
3 $^1B_2$	5.60	*0.010*	3 $^2A_2$	5.87	*0.003*	2 $^1B_2$	5.12	*0.001*
C1$^-$			**C1**			**C1$^+$**		
X $^1A'$	0.00		X $^2B_1$	0.00		X $^1A_1$	0.00	
1 $^1A'$	1.67	*0.001*	1 $^2B_1$	3.45	*0.018*	1 $^1A_1$	5.44	*0.006*
3 $^1A'$	2.33	*0.009*	2 $^2B_1$	4.64	*0.032*	1 $^1B_1$	4.79	*0.001*
4 $^1A'$	4.77	*0.013*	3 $^2B_1$	4.83	*0.005*	1 $^1B_2$	4.51	*0.063*
5 $^1A'$	5.42	*0.001*	1 $^2A_1$	4.50	*0.000*			
			1 $^2A_2$	2.16	*0.004*			
			2 $^2A_2$	3.37	*0.020*			
			3 $^2A_2$	5.69	*0.000*			
D1$^-$			**D1**			**D1$^+$**		
X $^1A'$	0.00		X $^2B_1$	0.00		X $^1A_1$	0.00	
1 $^1A'$	2.03	*0.003*	1 $^2B_1$	3.60	*0.000*	1 $^1A_1$	4.02	0.000
2 $^1A'$	2.20	*0.007*	2 $^2B_1$	4.17	*0.002*	2 $^1A_1$	5.90	*0.390*
3 $^1A'$	2.79	*0.002*	3 $^2B_1$	4.52	*0.033*	1 $^1B_1$	4.67	*0.002*
4 $^1A'$	3.32	*0.013*	1 $^2A_1$	4.71	*0.001*	1 $^1B_2$	2.90	*0.003*
5 $^1A'$	3.78	*0.006*	2 $^2A_2$	2.38	*0.000*	2 $^1B_2$	5.66	*0.110*
			3 $^2A_2$	5.47	*0.003*			
			4 $^2A_2$	5.65	*0.001*			
E1$^-$			**E1**			**E1$^+$**		
X $^1A_1$	0.00		X $^2B_1$	0.00		X $^1A_1$	0.00	
1 $^1A_1$	2.50	*0.005*	1 $^2B_1$	4.02	*0.013*	1 $^1A_1$	4.82	*0.037*
2 $^1A_1$	3.18	*0.025*	2 $^2B_1$	5.04	*0.010*	1 $^1B_1$	3.80	*0.001*
3 $^1A_1$	4.01	*0.001*	1 $^2A_1$	4.60	*0.001*	1 $^1B_2$	4.80	*0.022*
1 $^1B_1$	5.21	*0.028*	1 $^2A_2$	1.08	*0.001*	2 $^1B_2$	5.86	*0.280*
1 $^1B_2$	1.19	*0.028*	2 $^2A_2$	4.43	*0.031*			
4 $^1B_2$	5.42	*0.120*	1 $^2A_2$	5.26	*0.000*			

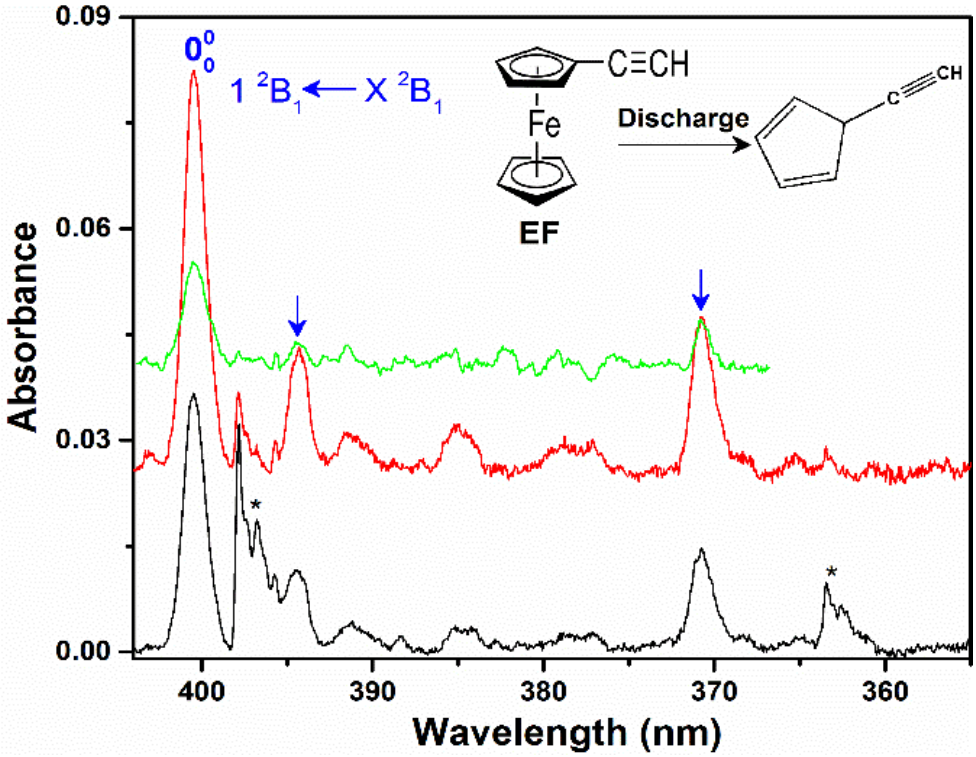

Figure 3.10: Absorption spectrum recorded after deposition of $C_7H_5^+$ produced from 1,1-dichlorotoluene in a hot cathode source (black trace) and after irradiation by $\lambda <$ 260 nm photons (red trace). The green trace was measured after deposition of $C_7H_5^+$ produced from ethynylferrocene **EF** in pure neon followed by the neutralization. The absorptions belonging to the **1** $^2B_1 \leftarrow X\ ^2B_1$ transition of fulvenallenyl radical are denoted by blue arrows. The bands due to N_2^+ are marked by asterisks.

Unlike **FA** and **FA**$^-$, the cation **FA**$^+$ is the fifth stable isomer on the PES of $C_7H_5^+$ lying 151 kJ/mol above the global minimum **C1**$^+$. Vertical excitation energies of the five cations **FA**$^+$, **B1**$^+$, **C1**$^+$, **D1**$^+$ and **E1**$^+$ were calculated with the CASPT2 method (**Table 3.8**). This predicts that detectable electronic transitions of **C1**$^+$, **D1**$^+$ and **E1**$^+$ lie in UV, beyond the range of detection (270-1100 nm). The transitions of **FA**$^+$ and **B1**$^+$ lie at the edge of the experimental measurement range. Structure **B1**$^+$ is ~300 kJ/mol above **C1**$^+$ and excluded from consideration. Therefore, to investigate whether the fulvenallenyl radical can be generated in the matrix via deposition of $C_7H_5^+$, mass-selected deposition was carried out from several precursors (**Chart 3.1**) with neon contaminated by CH_3Cl in a ratio 1 : 30000. The spectrum recorded after deposition of the *m/z*=89 cations from 1,1 dichlorotoluene is shown in **Figure 3.10**, black trace, and after irradiation of matrix with UV photons ($\lambda <$ 260 nm) in the red trace. The 401 nm absorption system is dominant. The absorptions of neutral C_7H_5 gain in intensity after UV irradiation. The

401 nm system is also detected following deposition of $C_7H_5^+$ generated from toluene, indene, mixtures of diacetylene and propyne, and phthalide.

According to the calculations **FA**$^+$ has a strong (f = 0.48) **2** $^1A_1 \leftarrow$ X $^1A_1$ electronic transition around 4.10 eV (302 nm). However no absorption was detected in this region. One can argue that the carrier of the 401 nm system is **C1** as it also possesses the **1** $^2B_1 \leftarrow$ X $^2B_1$ transition at 3.45 eV and **C1**$^+$ has absorption beyond the detection range. Consequently, ethynylferrocene **EF** (**Chart 3.1**) was used for the generation of $C_7H_5^+$ and the *m/z*=89 ions were deposited with neon without electron scavenger. In a pure neon matrix, concentration of neutrals dominates. Due to the absence of scavenger, electrons released from the nearby metal surface of the matrix by impingement of cations, neutralize trapped cations. **EF** comprises one molecular sub-unit, that of **FA**. $C_7H_5^+$ was produced from the **EF** precursor in a mild discharge to avoid plasma chemistry. The spectrum obtained is shown as the green trace in **Figure 3.10**. The one-to-one correspondence of the peaks with those assigned to fullvenallenyl radical confirms the carrier.

Two vibrational modes of 365 and 1984 cm^{-1} frequency and an overtone 3958 cm^{-1} above the 401.3 nm origin are observed in the spectrum of **FA**. The 1984 cm^{-1} value is typical for a C≡C stretching vibration and confirms the assignment of the 401 nm system to **FA** because the C≡C bond is only present in this radical among most stable structures of C_7H_5 shown in **Chart 3.3**. Absorption system is the **1** $^2B_1 \leftarrow$ X $^2B_1$ electronic transition of **FA** according to MS(5)-CASPT2 calculations. The vibrational modes are assigned on the basis of calculated (DFT/M06-2X/cc-pVTZ) harmonic frequencies in the **1** $^2B_1$ state (**Table 3.7**).

Chart 3.4: The structures and the ground state energies of anions (**bold**), neutrals and cations (*italics*) of C_7H_5 above the most stable structure calculated at the DFT/M06-2X level using the aug-cc-pVDZ basis set for anions and cc-pVTZ for the neutrals and cations.

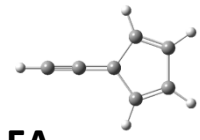

FA

0.00 0.00 *151.2*

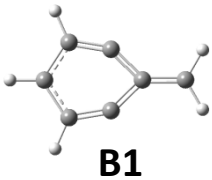

B1

157.4 139.7 *298.1*

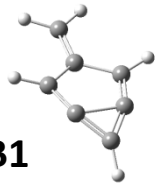

SB1

200.5 139.6 *255.7*

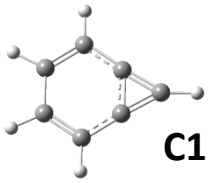

C1

175.2 33.6 *0.00*

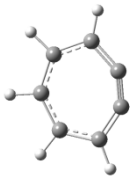

E1

244,7 93.4 *84.2*

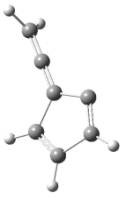

F1

214.3 143.9 *303.3*

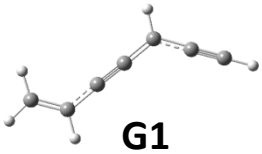

G1

198.8 133.6 *221.6*

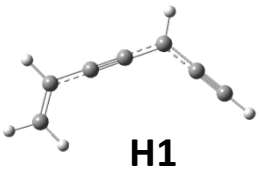

H1

199.5 133.3 *221.4*

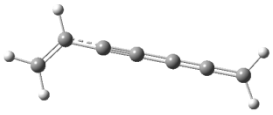

I1

192.8 121.9 *208.4*

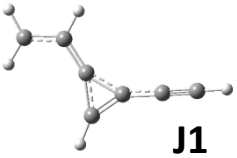

J1

234.5 232.4 *148.3*

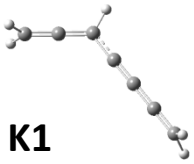

K1

296.1 183.1 *228.9*

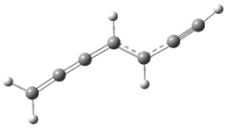

L1

200.6 133.*8* *216.1*

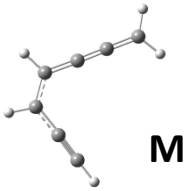

M1

209.2 136.3 *222.7*

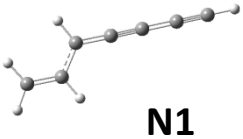

N1

183.2 114.4 *202.2*

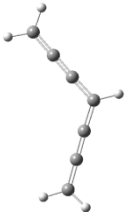

P1

156.7 *228.9*

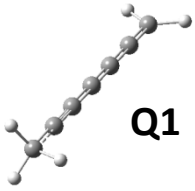

Q1

264.8 151.7 *207.0*

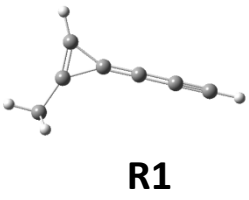

R1

400.3 256.5 *273.9*

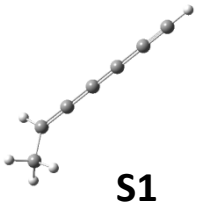

S1

256.3 172.9 *252.3*

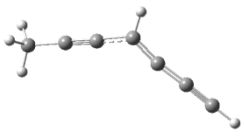

T1

286.2 200.6 *313.4*

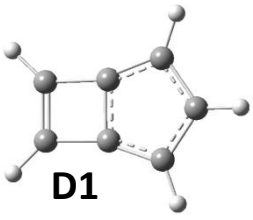

D1

191.3 80.*8* *83.0*

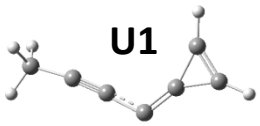

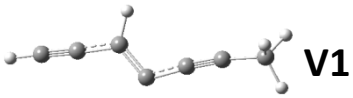

420.1 264.9 *256.1*

290.5 195.7 *273.4*

3.4 CONCLUDING REMARKS

The open chain isomers **B**$^+$ and **C**$^+$, and **A**$^+$ with a three membered carbon ring are identified in the neon matrix after mass-selected deposition of $C_7H_3^+$. Cation **B**$^+$ exhibits vibrationally structured fluorescence following excitation into the absorption bands of the **1** $^1A_1 \leftarrow X\ ^1A_1$ system. No fluorescence was detected for the isomers **A**$^+$ and **C**$^+$. Weak absorptions of neutral C_7H_3 isomers are also present which gain in intensity upon photobleaching of the cations. Intensity increment for the absorptions of the neutrals and *l*-HC_7H^+ is observed after deposition of $C_7H_3^+$ at ~90 eV, a higher kinetic energy. This indicates that fragmentation of $C_7H_3^+$ with ~90 eV deposition energy is mild and only one hydrogen atom is removed. Enhancement of the absorptions of **E** in higher kinetic energy experiments suggest that besides the fragmentation, rearrangement of hydrogen atoms takes place upon collisional impact of $C_7H_3^+$ with the neon surface. **E** is a secondary product as the **E**$^+$ lies 450 kJ/mol above of the lowest energy isomer **A**$^+$, and is unlikely to be formed in the source.

Unsaturated longer chain hydrocarbons have always been of interest in astronomy because of their intense absorption in visible domain. They can be carriers of DIBs. The detection of methyltriacetylene towards dense cloud has appealed for the existence of its ions in ISM. Electronic characterization of fulvenallenyl radical **FA** was a long-standing goal in combustion chemistry because such highly stable radicals could serve a vital role in the formation of PAHs. **FA** can also be expected in carbon-rich extraterrestrial clouds. Therefore, present studies on methyltriacetyene cation and **FA** radical in neon matrix are a starting point of their astrophysical findings.

BIBLIOGRAPHY

[1] K-H. Homann, *Angew. Chem. Int. Ed.* **1998**, *37*, 2434.

[2] C. S. McEnally, L. D. Pfefferle, B. Atakan and K. Kohse-Hoinghaus, *Prog. Energy Combust. Sci.* **2006**, *32*, 247.

[3] K. Kohse-Hoinghaus, B. Atakan, A. Lampprecht, G. G. Alatorre, M. Kamplus, T. Kasper and N-N. Liu, *Phys. Chem. Chem. Phys.* **2002**, *4*, 2056.

[4] J. Appel, H. Bockhorn and M. Frenklach, *Combust. Flame* **2000**, *121*, 122.

[5] J. Vandooren and V. Detilleux, *J. Phys. Chem. A.* **2009**, *113*, 10913.

[6] N. Hansen, T. Kasper, S. J. Klippenstein, P.R.Westmoreland, M.E. Law, C.A. Taatjes,

K. Kohse-Hoinghaus, J. Wang and T.A. Cool, *J. Phys. Chem. A.* **2007**, *111*, 4081.

[7] G. Da Silva and W. J. Bozzelli, *J. Phys. Chem. A.* **2009**, *113*, 12045.

[8] G. da Silva and J. A. Trevitt, *Phys. Chem. Chem. Phys*. **2011**, *13*, 8940.

[9] G. da Silva, J. A. Trevitt, M. Steinbauer and P. Hemberger, *Chem. Phys. Lett*. **2011**, *517*, 144.

[10] H. Richter and J.B. Howard, *Phys. Chem. Chem. Phys.* **2002**, *4*, 2038.

[11] J.A. Miller and C. F. Melius, *Combust. Flame.* **1992**, *91*, 21.

[12] J.A. Miller and S. J Klippevstein, *J. Phys. Chem. A* **2003**, *107*, 7783.

[13] W. Tang, R. S. Tranter and K. Brezinsky, *J. Phys. Chem. A* **2006,** *110*, 2165.

[14] H. Ding, T. Pino, F. Güthe and J. P. Maier, *J. Am. Chem. Soc.* **2003**, *125*, 14626.

[15] T. Zhang, L. Zhang, X. Hong, K. Zhang, F. Qi, C. K. Law, T. Ye, P.Zhao, Y.Chen, *Comb. Flame* **2009**,*156*, 2071.

[16] G. da Silva, J.W. Bozzelli, *J. Phys. Chem. A* **2009**, *113*, 12045.

[17] a) M. C. McCarthy, M. J. Travers, A. Kovacs, C. A. Gottlieb and P. Thaddeus, *J. Astrophys. Suppl. Ser.* **1997**, *113***,** 105.

b) A. R. Remijan, J. M. Hollis, L. E. Snyder, P. R. Jewell, and F. J. Lovas, *Astrophys. J.* **2006**, *643*, L37.

[18] A. G. G. M. Tielens, *Annu. Rev. Astron. Astrophys.* **2008**, *46*, 289.

[19] J. R. Barkar, L. J. Allamandola, A.G.G.M. Tielens, *Astrophys. J.* **198**7, *315*, L61.

[20] V. G. Kunde, A. C. Aikin, R. A. Hanel, D. E. Jennings, W. C. Maguire and R. E. Samuelson, *Nature* **1981**, *292*, 686.

[21] A. Nagy, I. Garkusha, J. Fulara and J. P. Maier, *Phys. Chem. Chem. Phys*. **2013**, *15*, 19091.

[22] J. Fulara, A. Nagy, I. Garkusha and J. P. Maier, *J. Chem. Phys*. **2010**, *133***,** 024304.

[23] J. Fulara, P. Freivogel, D.Forney and J. P. Maier, *J. Chem. Phys*. **1995**, *103*, 8805.

[24] M. Wyss, E. Riaplov and J. P. Maier, *J. Chem. Phys.* **2001**, *114*, 10355.

[25] J. Fulara, M. Grutter and J. P. Maier, *J. Phys. Chem. A.* **2007**, *111*, 11831.

[26] A. Batalov, J. Fulara, I. Snitko and J. P. Maier, *J. Phys. Chem. A.* **2006**, *110*, 10404.

[27] P. Freivogel, J. Fulara, D. Lessen, D. Forney and J. P. Maier, *Chem. Phys.* **1994**, *189*, 335.

[28] T. W. Schmidt, H. Ding, A. E. Boguslavskiy, T. Pino and J. P. Maier, *J. Phys. Chem. A* **2003**, *107*, 6550.

[29] M. Tulej, J. Fulara, A. Sobolewski, M. Jungen and J. P. Maier, *J. Chem. Phys.* **2000**, *112*, 3747.

[30] A. Chakraborty, J. Fulara, R. Dietsche and J. P. Maier, *Phys. Chem. Chem. Phys.* **2014**, *16*, 7023.

[31] A. Chakraborty, J. Fulara and J. P. Maier, *Aust. J. Chem.* **2013**, *67*, 416.

[32] A. Chakraborty, J. Fulara and J. P. Maier, *Angew. Chem. Int. Ed.* **2016**, *55*, 228.

Chapter 4

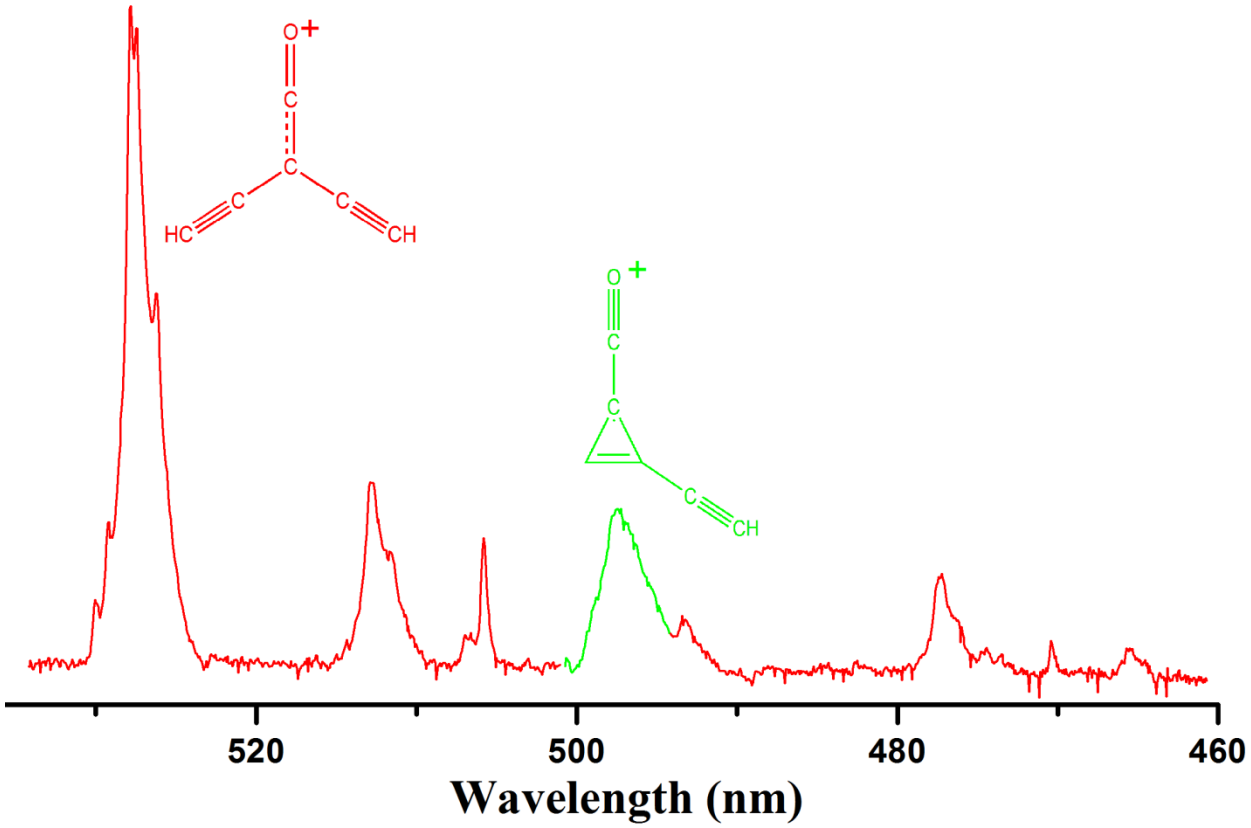

4 ELECTRONIC CHARACTERIZATION OF OXYGEN CONTAINING HYDROCARBON CATIONS: ION-MOLECULE REACTION PRODUCT

Three absorption systems with origin at 354, 497 and 528 nm are detected after mass-selected deposition of $H_2C_6O^+$ (m/z=90) in a 6 K neon matrix. The ions have been formed by the reaction of C_2O with HC_4H^+ in a 1 : 1 mixture of C_3O_2 and diacetylene in a hot cathode source, or by dissociative ionization of tetrabromocyclohexadienone. The absorption systems at 497 and 354 nm are assigned to the **1** ^{2}A" ← X ^{2}A" and **2** ^{2}A" ← X ^{2}A" electronic transition of isomer **B**$^+$, (2-ethynylcycloallyl)methanone cation and the 528 nm one to the **1** $^2A_2$ ← X $^2B_1$ of **F**$^+$, 2-ethynylbut-3-yn-1-enone-1-ylide, on the basis of calculated excitation energies with CASPT2.

Vibrationally resolved electronic absorption spectrum of 2,4,6-heptatriynal cation (*l*-HC_7O^+) has been recorded in a 6 K neon matrix after mass-selected deposition of m/z=101 species produced from the 1,2,3,4,5-benzenepentacarboxylic acid in the ion source. The band system originated at 278 nm is assigned to the **2** $^1\Sigma^+$ ← X $^1\Sigma^+$ transition of *l*-HC_7O^+ on the basis of theoretical calculations. Vibrational analysis supports the structural assignment.

An electronic system originating at 417.0 nm has been recorded after mass-selected deposition of m/z=80 ($C_4O_2^+$) cation produced from C_3O_2 in electrical discharge. On the basis of ground-state stability and excitation energy calculation, the 417 nm absorption system is attributed to the **1** $^2\Pi_u$ ← X $^2\Pi_g$ electronic transition of 1,2,3-butatriene-1,4-dione-2-ylium (*l*-OC_4O^+).

4.1 INTRODUCTION

Carbon and oxygen are the most common elements in the interstellar medium (ISM) after hydrogen and helium. Therefore, it is pertinent that CO is the most abundant heteroatomic molecule in space with a cosmic abundance 10^{-4} relative to H_2. Approximately one third of the complex molecules (atomicity $n \geq 6$) detected in the ISM are comprised of carbon, oxygen and hydrogen, which exemplifies the richness of their chemistry in space. Smaller carbon oxides CO^+, C_2O, C_3O, HCO^+, HC_2O, have also been identified in galactic environments like protostars, planetary nebulae and dark clouds.[1-5]

$C_{2n}H^-$ (n=2-4) have been identified in space by radio-astronomy.[6-8] It is found that these unsaturated hydrocarbon anions have higher abundance in dense clouds. To explain this observation, kinetic models have been developed. Gas-grain model indicates that due to the depletion of oxygen atoms onto dust in denser medium, $C_{2n}H^-$ species dominantly form.[9] This model also studied the reactions of these anions in an oxygen dominated environment to determine the probable cosmic abundance of polycarbon chain oxides, C_6O, C_7O, HC_6O and HC_7O. Denser clouds have a lower H-abundance compared to hot corino or young stellar objects which should favor the formation of oxygen containing unsaturated hydrocarbons or pure carbon chain oxides.

The ways to produce oxygen containing species in the interstellar medium (ISM) could be either radiative association of atomic oxygen with hydrocarbons or ion molecule reaction.[10] An example of this is the cyclopropenone c-H_2C_3O which has been detected in Sagittarius B2(N),[11] a region where cyclopropenylidene c-C_3H_2 was identified previously. In this context, reactions of some astrochemically relevant ions such as C_4H^+, $C_4H_2^+$, $C_4H_3^+$, C_5H^+, C_6H^+ with CO and O_2 were studied by the selected-ion flow tube technique. All of these species reacted with CO produced mono-oxygenated hydrocarbon cations.[12]

To date, a number of carbon chain monoxides have been characterized in the laboratory via infrared (C_2O, C_3O, C_4O, $C_{13}O$),[13-18] ESR (C_2O, C_4O, C_6O),[19,20] and electronic ($C_2O^{0/-}$, C_4O^-, $C_7O^{+/0}$) spectroscopy.[21-24] Microwave spectra of HCO^+ and HC_nO (n=5-7) are only reported.[25,26] In Chapter 4, electronic absorptions of $H_2C_6O^+$, HC_7O^+ and $C_4O_2^+$ species in a 6 K neon matrix are reported. The structural assignments have been made on the basis of calculated excitation energies with CASPT2 method.

4.2. PRODUCTION OF OXYGEN BEARING CATIONS

4.2.1 $H_2C_6O^+$ and $C_4O_2^+$

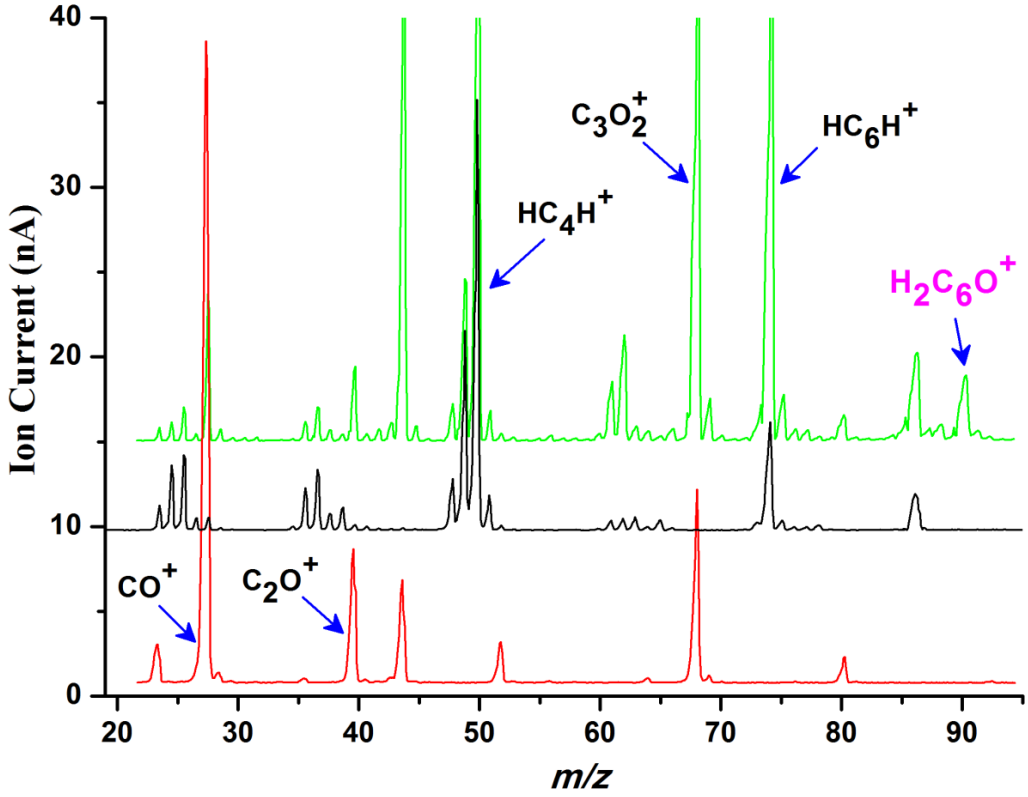

Figure 4.1: Mass spectra of C_3O_2 (red), HC_4H (black) and 1:1 mixture of C_3O_2 and HC_4H (green). The $H_2C_6O^+$ (m/z = 90) peak appeared upon mixing C_3O_2 and HC_4H.

A 1:1 mixture of carbon suboxide C_3O_2 and diacetylene HC_4H diluted with helium was used to produce $H_2C_6O^+$ in a hot cathode discharge source. Pure C_3O_2 or HC_4H does not yield the *m/z*=90 peak in the mass spectrum but it appears in their mixture (**Figure 4.1**, green trace). The C_2O^+ and CO^+ fragment ions are present in the mass spectrum of C_3O_2 (red trace) and in the mixture with HC_4H. $H_2C_6O^+$ can be formed in the source by insertion of the C_2O^+ fragment into HC_4H, or C_2O into HC_4H^+. As HC_6H^+ is present in the mass spectrum of diacetylene, as well as in the mixture with carbon suboxide, formation of $H_2C_6O^+$ could also proceed *via* reaction of CO/CO^+ with HC_6H^+/HC_6H. However, the latter pathway is excluded because the *m/z*=90 cation was not observed with a CO/HC_4H mixture under similar condition whereas the mass peak of HC_6H^+ was intense. It was found that the intensity of the mass peaks of C_2O^+ and $H_2C_6O^+$ ions

are correlated, suggesting that the formation of $H_2C_6O^+$ depends on the production of C_2O^+. $H_2C_6O^+$ was also produced from a vapor of 2, 4, 4, 6-tetrabromo-2,5-cyclohexadienone (TBrC).

The production $C_4O_2^+$ (m/z=80) is apparent in the mass spectrum of pure C_3O_2 (**Figure 4.1**, red trace). It is possibly formed in the source *via* the ion-molecule reaction between C_2O^+ and C_2O. Pressure of precursor gas mixture in the source was kept quite high ($9x10^{-5}$ mbar) for the efficient generation of $C_4O_2^+$.

4.2.2 HC_7O^+

The precursor, 1,2,3,4,5-benzenepentacarboxylic acid, is solid at room temperature, therefore it was resistively-heated in an oven to vaporize and carried to the source by Helium. HC_7O^+ has been generated in source via dissociative ionization of the precursor molecule.

4.3 RESULTS AND DISCUSSIONS

4.3.1 $H_2C_6O^+$

Moderately intense absorptions are detected in the 320─530 nm region (**Figure 4.2**, upper traces) after trapping of mass-selected $H_2C_6O^+$ in solid neon. Two types of bands, which differ in width, are apparent in the spectrum. The narrower features start around 528, 362 and 329 nm and broader ones at ~ 497 and ~ 354 nm. The 362 and 329 nm absorptions are **2** $^2\Pi_g \leftarrow X\ ^2\Pi_u$ and **3** $^2\Pi_g \leftarrow X\ ^2\Pi_u$ transitions of *l*-HC_5H^+.[27] These have been measured in an earlier study and are shown in the red trace of **Figure 4.3** with the absorptions detected after deposition of $H_2C_6O^+$ in black. The traces are scaled to the intensity of the 362 nm band. The HC_5H^+ cation is produced in the matrix as a result of collisionally-induced fragmentation of $H_2C_6O^+$ during deposition.

The matrix was exposed for 20 min to UV light ($\lambda < 260$ nm) resulting in the detachment of electrons from Cl^- and neutralization of trapped cations. The spectrum obtained is shown as the lower traces **Figure 4.2**. The absorptions starting at 528, 497 and 354 nm almost disappeared whereas the ones of HC_5H^+ slightly reduced. The HC_5H^+ bands behave in a regular way upon UV irradiation – the intensity noticeably decreases after irradiation. In this present

experiment, very little decrement of the HC_5H^+ bands after UV exposure indicates that photofragmentation of $H_2C_6O^+$ is contributing to these 362 and 329 nm absorptions. No new peaks appeared after UV irradiation. $H_2C_6O^+$ ions were also deposited in a pure neon matrix but only a weak absorption at 528 nm was detected. In the absence of scavenger CH_3Cl, free electrons in the matrix neutralized most of the deposited $H_2C_6O^+$ ions. However, the behavior of the absorption features in **Figure 4.2** under exposure to UV light indicates that they belong to photo-unstable isomer/s of $H_2C_6O^+$.

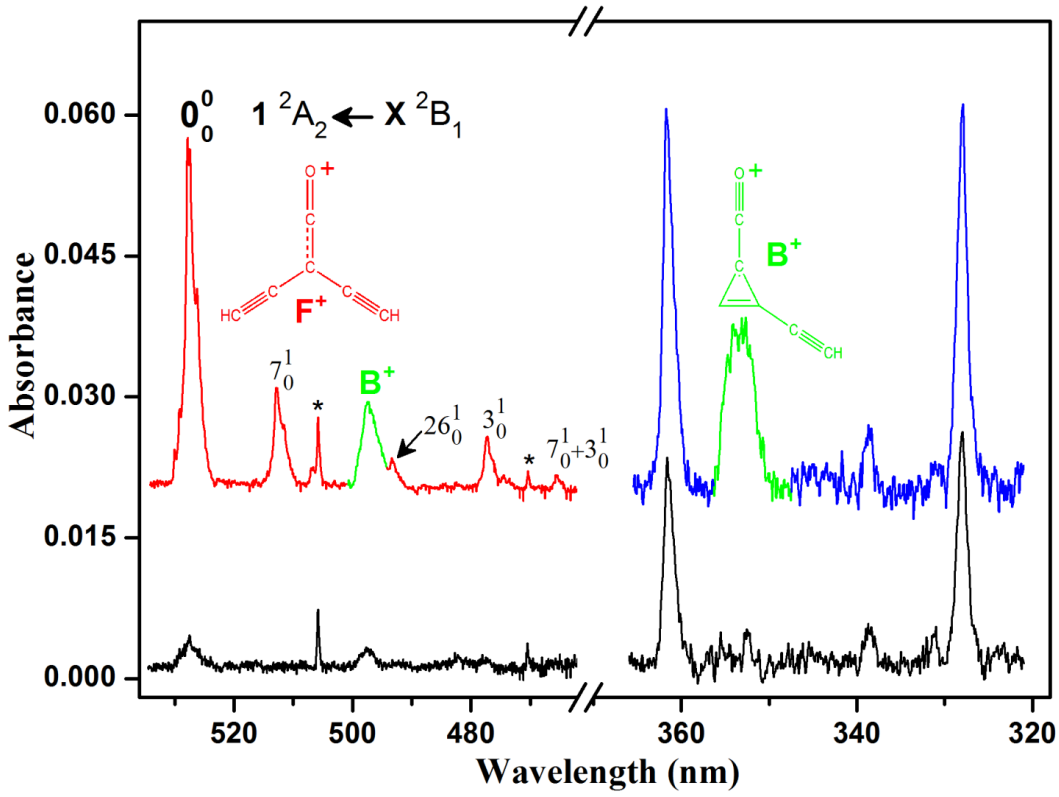

Figure 4.2.: Electronic absorption spectra recorded after deposition of $H_2C_6O^+$ produced from a 1:1 mixture of C_3O_2 and diacetylene (upper traces) and after 20 minute irradiation with $\lambda < 260$ nm photons (lower traces). Bands denoted by * belong to C_2^+.

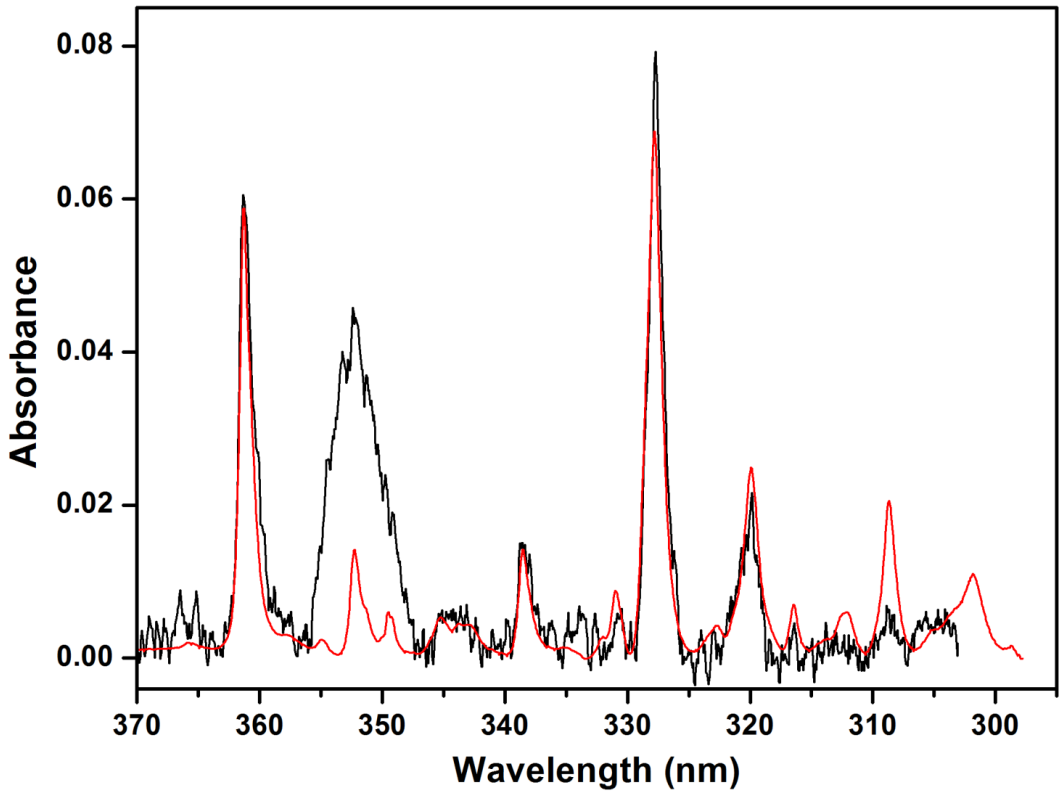

Figure 4.3: Electronic absorption spectra recorded after deposition of $H_2C_6O^+$ generated from a 1:1 mixture of C_3O_2 and diacetylene (black), and after deposition of HC_5H^+ produced from diacetylene (red, in another experiment). The spectrum of HC_5H^+ is normalized to the intensity of the 362 nm band.

$H_2C_6O^+$ was also produced from precursor TBrC and deposited in neon. The spectrum obtained shows two broader features starting at 497 and 354 nm and a weak absorption at 528 nm (**Figure 4.4**, red trace). The signal-to-noise ratio is relatively low compared to the **Figure 4.2** because the accumulated charge in this experiment was not very high. However, after irradiation (260-390 nm) the 497 and 354 nm absorptions diminish substantially implying that they belong to the same $H_2C_6O^+$ isomer. The decay of the absorptions under such irradiation conditions is due to photo–instability of the cation, as neutralization is not efficient at these wavelengths.

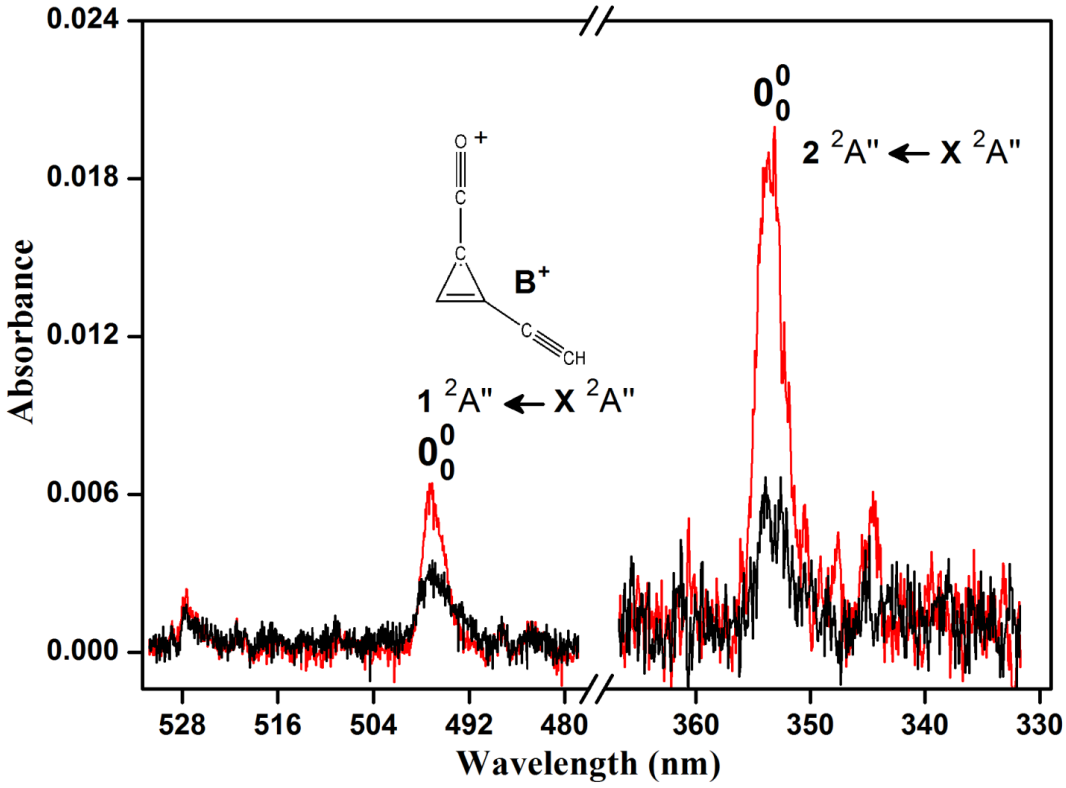

Figure 4.4: Electronic absorption spectrum of $H_2C_6O^+$ obtained after deposition of *m/z* = 90 ions produced from 2, 4, 4, 6-tetrabromo-2,5-cyclohexadienone (TBrC) – red, and after 20 minute irradiation with 250 - 390 nm photons – black.

Use of different precursors for the production of $H_2C_6O^+$ established that two isomers contribute to the spectra (**Figures 2 – 4**). One has a weak transition in the visible (2.49 eV; 497 nm) and a much stronger in the UV (3.51 eV; 354 nm). The second cation is characterized by the strong transition in the visible (2.35 eV; 528 nm) with resolved vibrational structure.

Chart 4.1: Structures and relative ground state energies (kJ mol^{-1}) of H_2C_6O cations (**bold**) and neutrals (*italic*), calculated with the DFT method and cc-pVTZ basis set. Bond lengths (Å) correspond to the optimized cation geometries.

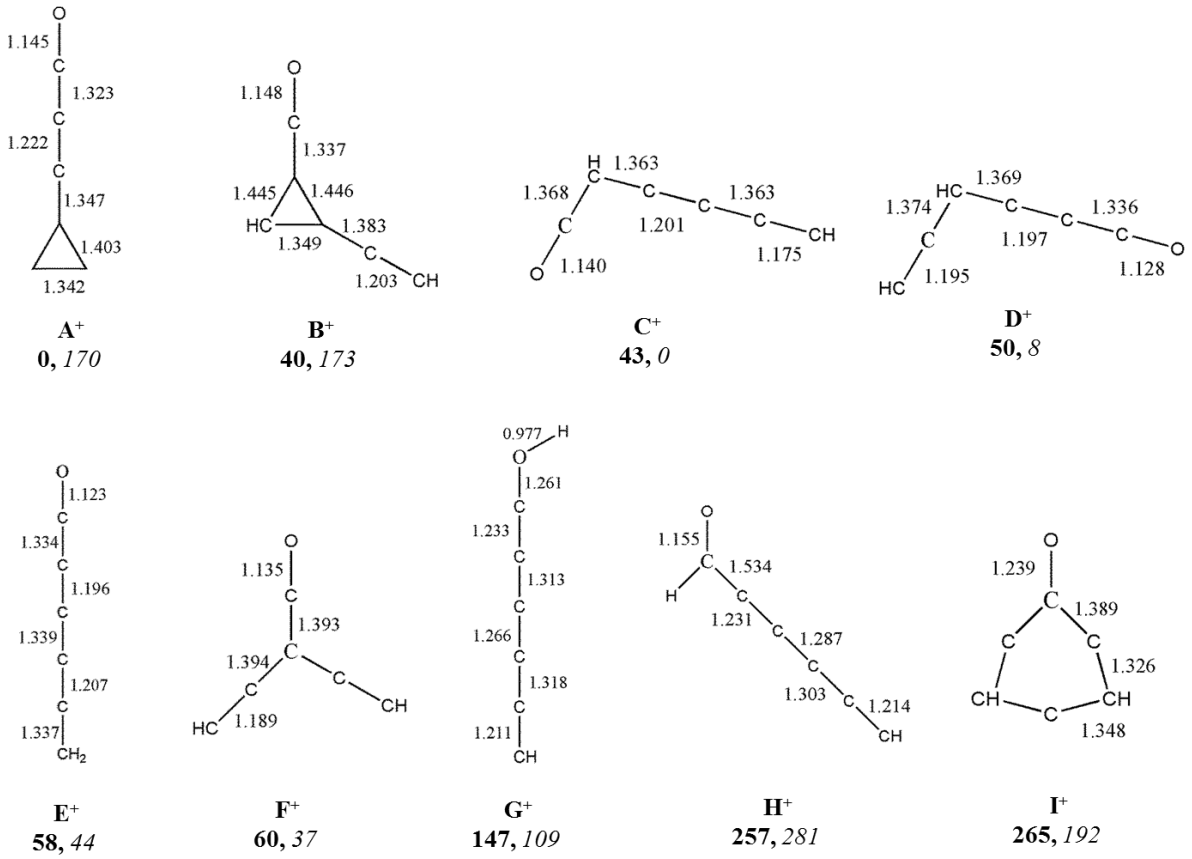

Vertical excitation energies of nine most stable $H_2C_6O^+$ isomers (**Chart 4.1**) were calculated with MS-CASPT2 to assign the observed absorptions to specific molecules. The results for the candidates are collected in **Table 4.1**. Among these only structures $\mathbf{B}^+$ and $\mathbf{D}^+$ can be responsible for the two absorptions at 497 and 354 nm. The calculations predict a moderately intense transition with energy 2.68 (f =0.024) and 2.60 eV (f=0.040) and about a ten times stronger transition at 3.68 and 3.67 eV for $\mathbf{B}^+$ and $\mathbf{D}^+$, respectively. The oscillator strengths are in accord with the intensities of the 497 and 354 nm systems. The vertical excitation energies overestimate the onsets of the observed systems by ~ 0.2 eV; calculated adiabatic values should match better with the experimental ones. As $\mathbf{D}^+$ lies only slightly higher in energy than $\mathbf{B}^+$, it cannot be ruled out from consideration as the carrier.

In contrast to isomers **B**$^+$ and **D**$^+$, the carrier of the 528 nm system should possess only a single strong transition around 2.35 eV. Apart from isomers **B**$^+$ and **D**$^+$ four others: **C**$^+$**, E**$^+$, **F**$^+$ and **G**$^+$ have transitions in this region. The first electronic system of **E**$^+$ at 2.45 eV is weak (f = 0.006) and two stronger ones (f = 0.02 and 0.065) are predicted in the 3.1-3.3 eV range, in contrast to the observation. The first electronic transition of **G**$^+$ is calculated at 2.26 eV with f = 0.085 and the next one at 3.22 eV (f = 0.045). **G**$^+$ cannot be the carrier because its UV transition is not seen. Isomer **C**$^+$ is also eliminated from consideration: although the **1** ^{2}A" ← X ^{2}A" electronic transition at 2.51 eV is very strong (f = 0.2) but an equally intense band at 3.92 eV is predicted, contrary to the experiment.

Table 4.1: Excitation energies E_{cal} (eV) and oscillator strengths (f) of $H_2C_6O^+$ isomers calculated by the MS-CASPT2 method and comparison with the observations (E_{obs}).[33]

Species	Transitions	E_{cal}	f	E_{obs}
A$^+$ (C_{2V})	**1** $^2B_1$ ← X $^2B_1$	3.70	*0.02*	
	3 $^2B_1$ ←	4.81	*0.00*	
	4 $^2B_1$ ←	5.27	*0.02*	
	5 $^2B_1$ ←	5.77	*0.01*	
B$^+$ (C_S)	**1** $^2A"$ ← X $^2A"$	**2.68**	*0.02*	2.49
	2 $^2A"$ ←	**3.68**	*0.20*	3.51
	3 $^2A"$ ←	5.32	*0.10*	
	4 $^2A"$ ←	5.73	*0.06*	
C$^+$ (C_S)	**1** $^2A"$ ← X $^2A"$	2.51	*0.19*	
	2 $^2A"$ ←	3.92	*0.17*	
	3 $^2A"$ ←	4.08	*0.03*	
	4 $^2A"$ ←	4.47	*0.15*	
D$^+$ (C_S)	**1** $^2A"$ ← X $^2A"$	2.60	*0.04*	
	2 $^2A"$ ←	3.67	*0.49*	
	3 $^2A"$ ←	4.16	*0.01*	
	4 $^2A"$ ←	4.44	*0.00*	
	5 $^2A"$ ←	4.70	*0.02*	
E$^+$ (C_{2V})	**1** $^2B_1$ ← X $^2B_2$	2.45	*0.01*	
	2 $^2B_1$ ←	3.08	*0.02*	
	3 $^2B_1$ ←	3.32	*0.07*	
	4 $^2B_1$ ←	4.36	*0.02*	
	5 $^2B_1$ ←	5.36	*0.00*	

F$^+$ (C_{2V})	**1** $^2A_2 \leftarrow X\ ^2B_1$	**2.38**	*0.11*	2.35
	2 $^2A_2 \leftarrow$	5.58	*0.05*	
	1 $^2B_1 \leftarrow$	4.26	*0.00*	
	2 $^2B_1 \leftarrow$	5.30	*0.27*	
	2 $^2B_1 \leftarrow$	5.90	*0.01*	
G$^+$ (C_S)	**1** $^2A'' \leftarrow X\ ^2A''$	2.26	*0.09*	
	2 $^2A'' \leftarrow$	3.22	*0.05*	
	3 $^2A'' \leftarrow$	3.74	*0.00*	
	4 $^2A'' \leftarrow$	4.64	0.03	
H$^+$ (C_S)	**2** $^2A'' \leftarrow X\ ^2A''$	3.15	*0.00*	
	3 $^2A'' \leftarrow$	3.39	*0.02*	
	4 $^2A'' \leftarrow$	3.88	*0.03*	
	5 $^2A'' \leftarrow$	4.35	*0.00*	
I$^+$ (C_{2V})	**1** $^2B_1 \leftarrow X\ ^2B_1$	3.46	*0.01*	
	2 $^2B_1 \leftarrow$	3.92	*0.46*	
	3 $^2B_1 \leftarrow$	4.26	*0.02*	

Isomer **F**$^+$ fulfils the criteria for being the carrier of 528 nm system. A strong transition at 2.38 eV (f=0.11) close to the observation (2.35 eV) and a weak UV absorption (5.58 eV) beyond the experimental detection range were predicted by theory. Moreover, **F**$^+$ during depositing with ~50 eV kinetic energy on solid neon can fragment to produce *l*-HC_5H^+ and CO which was previously inferred from spectral behaviors. Therefore the 528 nm system is assigned to the **1** $^2A_2 \leftarrow X\ ^2B_1$ transition of **F**$^+$. A well resolved vibrational structure is apparent in the spectrum and results from the excitation of the ν_7, ν_6 and ν_3 vibrational modes and their combinations. The assignment is based on the harmonic frequencies calculated for the ground state of **F**$^+$ with the DFT method using the B3LYP /cc-pVTZ level of theory (**Table 5.2**).

Table 4.2: Absorption band maxima (±0.1nm) of electronic transitions of $H_2C_6O^+$ isomers $\mathbf{B}^+$ and $\mathbf{F}^+$ in 6 K neon matrices and assignment based on MS-CASPT2 calculations.[33] The vibrational interpretation of the $\mathbf{F}^+$ spectrum is based on the calculated ground–state harmonic frequencies (footnote).

Species	λ (nm)	ν (cm^{-1})	Δν (cm^{-1})	Assignment	
$\mathbf{F}^+$	527.6	18954	0	0_0^0	$\mathbf{1}\ ^2A_2 \leftarrow \mathbf{X}\ ^2B_1$
	512.8	19501	547	ν_7	
	493.1	20280	1326	$2\nu_6$	
	476.9	20969	2015	ν_3	
	465.0	21505	2551	$\nu_3 + \nu_7$	
$\mathbf{B}^+$	497.3	20109	0	0_0^0	$\mathbf{1}\ ^2A'' \leftarrow \mathbf{X}\ ^2A''$
	353.6	28281	0	0_0^0	$\mathbf{2}\ ^2A'' \leftarrow \mathbf{X}\ ^2A''$

Totally-symmetric vibrations (a_1) of $\mathbf{F}^+$ calculated with DFT/B3LYP/cc-pVTZ: ν_1 to ν_7; 3412, 2276, 2169, 1198, 754, 669, 543, 121 cm^{-1}.

The reactants which lead to the formation of $H_2C_6O^+$ are C_2O and HC_4H^+, and/or C_2O^+ with HC_4H, as both cations were observed in the mass spectrum of the precursor (**Figure 4.1**). The ionization potential (IP) of diacetylene is 10.17 eV,[28] but the experimental value for C_2O is unknown. Therefore the IPs of HC_4H and C_2O were calculated using the CCSD(T) method for the geometry optimized at the CCSD level leading to 10.08 eV for HC_4H and 10.81 eV for C_2O. Hence, the most probable way of $H_2C_6O^+$ production is the reaction of C_2O with HC_4H^+. The reactions of C_2O^+ with diacetylene, as well as C_2O with HC_4H^+, are exothermic. The calculated enthalpy of the reaction between C_2O with HC_4H^+ is 539 kJ/mol at the MP2/cc-pVTZ level of theory. C_2O in the $^3\Sigma^-$ ground state is a reactive biradical with two electrons on the terminal -carbon atom. C_2O attacks the electrophilic center of HC_4H^+ which is located on the middle carbon atoms.

In the case of the reaction C_2O^+ with HC_4H, a charge-exchange is likely the first step. C_2O^+ in the $^2\Pi$ ground state possesses an unpaired electron on the terminal carbon atom and reacts as a radical. The preferred site of reaction of C_2O^+ with diacetylene is on the electronegative carbon atom adjacent to the terminal hydrogens.

On the basis of the calculated vertical excitation energies and the oscillator strengths (**Table 4.1**) as well as the ground state stabilities (**Chart 4.1**) of $\mathbf{B}^+$ and $\mathbf{D}^+$, one cannot firmly

deduce the carrier for the 497 and 354 nm absorptions. However, the structure of $\mathbf{B}^+$ produced *via* dissociative ionization of TBrC is analogous to that of the $C_6H_4^+$ isomer: three carbon–member ring with aliphatic chain ($\mathbf{T}^+$) generated from 1,2-dibromobenzene under similar discharge condition.[29] MS-CASPT2 calculation predicts strong electronic transition (f=0.2) at 4.45 eV (280 nm) for neutral **D** which was not observed (See **Table 4.3**). Thus, the 497 and 354 nm systems are assigned to the **1** ^{2}A" ← X ^{2}A" and **2** ^{2}A" ← X ^{2}A" electronic transitions of $\mathbf{B}^+$.

As the neutral counterparts of $H_2C_6O^+$ were not observed after photobleaching or in pure neon, then, either they do not have any electronic transitions in the 250-1100 nm detection range or are extremely weak. The excitation energies of the neutral counterparts of the observed cations calculated with MS-CASPT2 explain why neutral absorptions systems were not seen. The results are collected in **Table 4.3**. They all possess strongest transitions in the UV, beyond the experimental detection range.

Table 4.3. Electronic excitation energies E_{cal} (eV) and oscillator strengths (f) of some selected H_2C_6O neutral isomers calculated by the MS-CASPT2 method.[33]

Species	Transitions	E_{cal}	f
F (C_{2V})	**1** $^1A_1$ ← X $^1A_1$	5.67	*0.17*
	2 $^1A_1$ ←	6.61	*0.36*
	1 $^1B_2$ ←	7.13	*0.16*
B (C_1)	**1** ^{1}A ← X ^{1}A	2.59	*0.00*
	2 ^{1}A ←	3.43	*0.04*
	3 ^{1}A ←	5.21	*0.00*
	4 ^{1}A ←	5.47	*0.00*
	5 ^{1}A ←	6.27	*0.03*
D (C_S)	**1** ^{1}A' ← X ^{1}A'	4.45	0.20
	2 ^{1}A' ←	5.32	0.01
	3 ^{1}A' ←	5.48	0.04

4.3.2 HC_7O^+ : $2\ ^1\Sigma^+ \leftarrow X\ ^1\Sigma^+$ TRANSITION

Spectral measurements carried out after the mass-selected deposition of HC_7O^+ cation produced from 1,2,3,4,5-benzenepentacarboxylic acid reveal moderately intense absorptions in UV (black trace, **Figure 4.5**). The descending peak intensities towards the blue with a regular spacing indicates that these belong to one electronic system originating at 278.0 nm. To identify whether the absorber is cationic or neutral, the matrix was irradiated by $\lambda < 260$ nm photons for 17 minutes. The decrement of all bands at a similar rate conveys that only one HC_7O^+ isomer is responsible for these absorptions (red trace, **Figure 4.5**). No new peak appeared after irradiation.

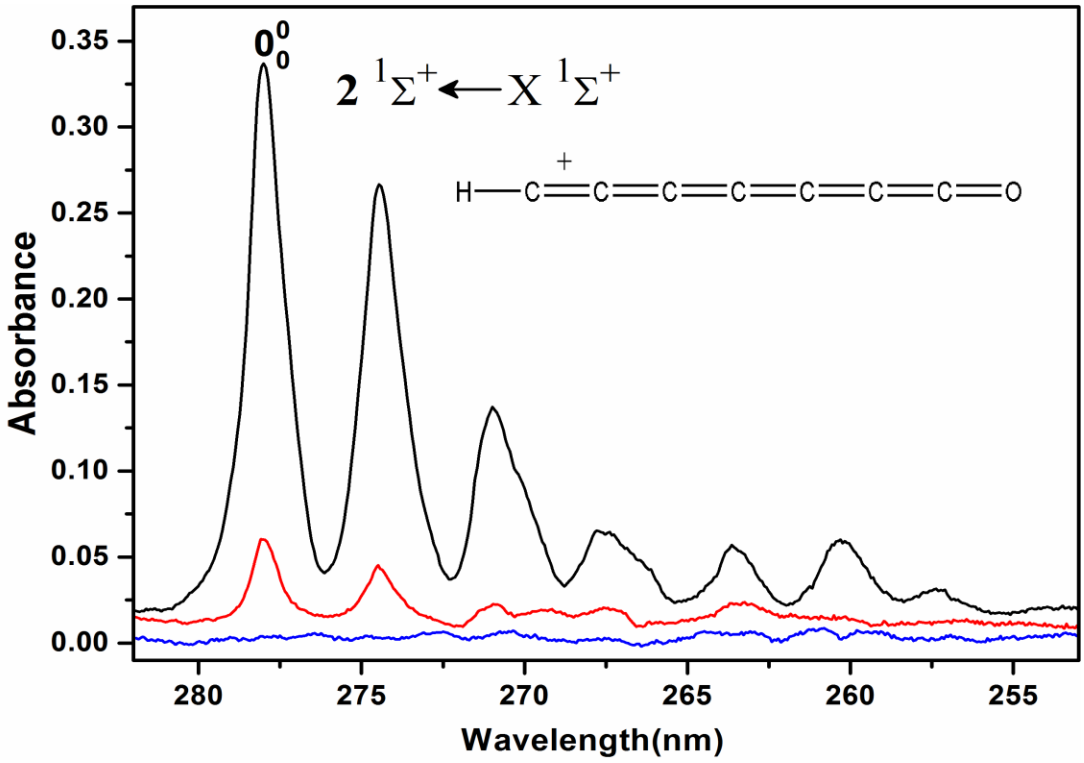

Figure 4.5: Electronic absorption spectrum recorded in 6 K neon matrix after deposition of m/z = 101 cations produced from 1,2,3,4,5-benzenepentacarboxylic acid (black) and after irradiation by photons below 260 nm (red). The blue trace was recorded after deposition in pure neon.

Previous studies with oxygenated hydrocarbon cations have shown that this class of species has a tendency to lose CO upon UV irradiation. Photodissociation of $H_2C_6O^+$ and $H_2C_7O^+$ yielding HC_5H^+ and HC_6H^+, respectively, have been observed in neon matrices. Hence,

the intensity decrease of the 278 nm system could be due to the photofragmentation of the carrier, although absorption of C_6H^+ was not detected. In another experiment, HC_7O^+ was deposited in a pure neon matrix to confirm the ionic character of the carrier (blue trace, **Figure 4.5**). No absorption was detection which establishes that the species is a cation. Due to the absence of the scavenger (CH_3Cl), free electrons in the matrix generated by the impingement of defocused ions with the metal walls readily neutralize the deposited cations. As a consequence, cationic bands are barely seen in pure neon matrices.

Chart 4.2: Structure and relative ground state energies (kJ mol^{-1}) of the HC_7O^+ cations (bold) and neutrals (italic) calculated with DFT using M062X/cc-pVTZ theory.

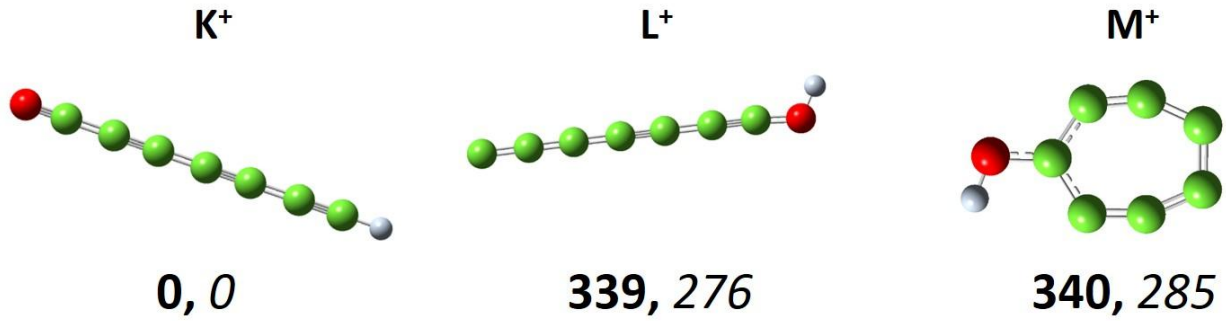

In order to assign the 278 nm electronic system to a specific HC_7O^+ structure, three plausible isomers $\mathbf{K}^+$, $\mathbf{L}^+$ and $\mathbf{M}^+$ were optimized with DFT using cc-pVTZ basis set and M062X functional (**Chart 4.2**). The isomer $\mathbf{K}^+$ is the most stable and the $\mathbf{L}^+$ and $\mathbf{M}^+$ lie 340 kJ mol^{-1} to higher energy, which indicates that the generation of $\mathbf{L}^+$ and $\mathbf{M}^+$ in the ion source is very unlikely. Thus, vertical excitation energy was only calculated for $\mathbf{K}^+$. MS(6)-CASPT2 was employed to predict the excited state energies using the DFT optimized ground-state coordinate (**Table 4.4**). Calculation gives the strongest transition of $\mathbf{K}^+$ to the **2** $^1\Sigma^+$ state at 4.89 eV, in agreement with the experimental observation at 278 nm (4.46 eV). The next transition to the **3** $^1\Sigma^+$ state is almost 75 times weaker. Therefore, the absorption at 278 nm is the **2** $^1\Sigma^+ \leftarrow$ X $^1\Sigma^+$ transition of $\mathbf{K}^+$**.** The calculated excited state energies for **K** explain why no absorption of neutral was observed after irradiation of the matrix; **K** possesses an allowed transition **7** $^2\Pi \leftarrow$ X $^2\Pi$ at 5.36 eV, beyond the experimental measurement range (250-1100 nm).

Table 4.4: Vertical excitation energies (eV) and oscillator strengths (f) of isomer $\mathbf{K}^+$ and **K** calculated at the MS(6)-CASPT2/cc-pVTZ level. The experimental value is in bold.

Species	State	Energy	f	Exp.
K^+	X $^1\Sigma^+$	0.00		
	1 $^1\Sigma^+$	3.25	*0.00*	
	2 $^1\Sigma^+$	4.89	*1.13*	**4.46**
	3 $^1\Sigma^+$	5.22	*0.02*	
K	X $^2\Pi$	0.00		
	1 $^2\Pi$	2.73	*0.001*	
	2 $^2\Pi$	3.09	*0.001*	
	7 $^2\Pi$	5.36	*0.02*	

Several vibrational excitations are seen in the **2** $^1\Sigma^+ \leftarrow$ X $^1\Sigma^+$ system (**Figure 4.5**). The active vibrational modes are identified by comparison to the totally symmetric (σ^+) harmonic frequencies in the **2** $^1\Sigma^+$ electronic state calculated with TD DFT/cc-pVTZ/M062X. The peaks apparent 464, 927, 1927 cm^{-1} blue of the origin are assigned to the ν_8, ν_7 and ν_5 modes while those located at 1398 and 2446 cm^{-1} are probably due to the combinations $\nu_7+\nu_8$ and $\nu_5+\nu_8$, respectively. The vibrational frequencies are consistent with the linear HC_7O^+ structure.

Table 4.5. Electronic absorption band maxima ($\pm$0.1nm) of *l*-HC_7O^+ in a 6 K neon matrix and the assignment is based on the calculated totally-symmetric harmonic frequencies at **2** $^1\Sigma^+$ state listed in the footnote.

λ (nm)	ν (cm^{-1})	Δν (cm^{-1})		Assignment
278.0	35971	0	0_0^0	**2** $^1\Sigma^+ \leftarrow$ X $^1\Sigma^+$
274.5	36435	464	ν_8	
271.0	36900	929	ν_7	
267.6	37369	1398	ν_6 / $\nu_7+\nu_8$	
263.6	37936	1965	ν_5	
260.3	38417	2446	$\nu_5+\nu_8$	

$\nu_1 - \nu_8$ (σ^+): 3428, 2430, 2307, 2273, 2149, 1412, 972, 491.

4.3.3 $C_4O_2^+$: $1\,^2\Pi_u \leftarrow X\,^2\Pi_g$ TRANSITION

The electronic absorption spectrum recorded after mass-selected deposition of $C_4O_2^+$ (m/z=80) in solid neon shows a number of transitions in 370 – 420 nm region (**Figure 4.6**, red trace). As stated for $H_2C_6O^+$ and HC_7O^+, the matrix was irradiated by λ < 260 nm photons (black trace) to identify whether the carrier(s) of these bands is ionic or neutral. Intensity decreases proportionally across all bands. This implies that one $C_4O_2^+$ isomer is responsible for these transitions. Multiplet band profile was observed for the 417.0 nm origin band, which occurred due to the isolation of the absorbers in energetically not equivalent matrix sites. Every two adjacent peaks are separated by 150-170 cm^{-1}, indicating a Franck-Condon active bending mode in the excited state (**Figure 4.6**).

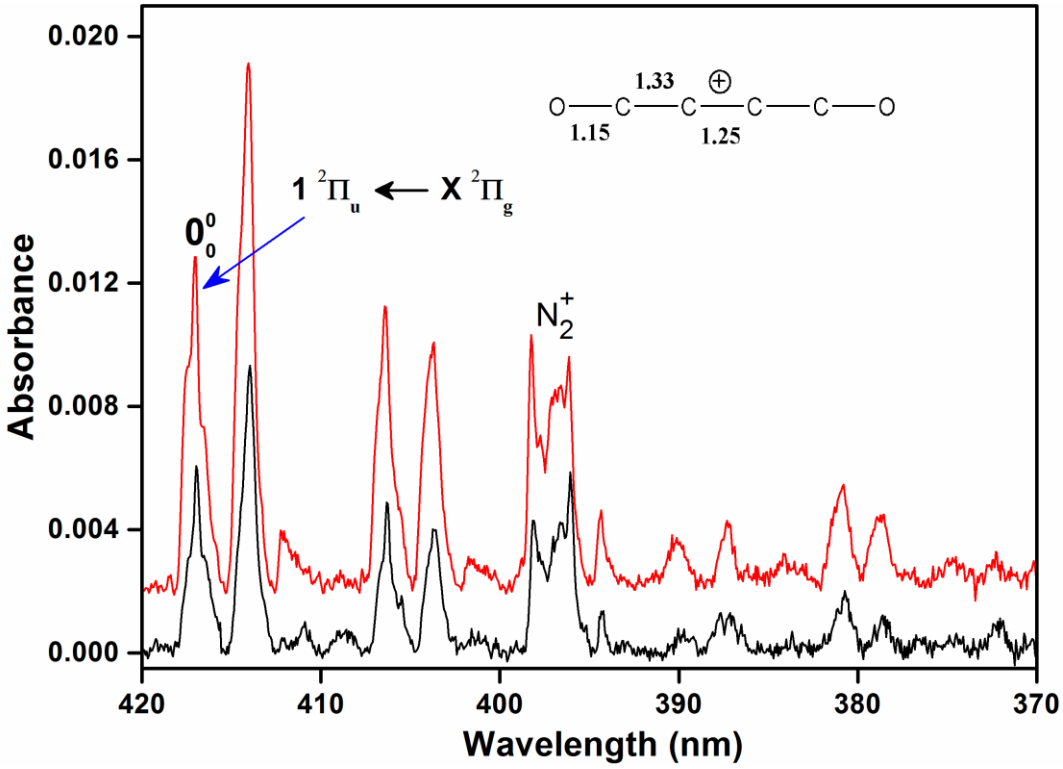

Figure 4.6: Electronic absorption spectrum recorded in a 6 K neon matrix after mass-selected deposition of $C_4O_2^+$ (red trace) and after 17 minutes UV irradiation (λ < 260 nm) of the matrix (black trace). Bond lengths (Å) of *l*-OC_4O^+ correspond to the optimized geometry at M062X/cc-pVTZ/DFT level.

The $C_4O_2^+$ cation was most likely generated in the source by an ion-molecule reaction between C_2O^+ and C_2O. Therefore, the preliminary guess was: the linear OC_4O^+ structure is the carrier of 417 nm system. The other plausible isomers are highly unstable compared to this linear one and unlikely to form in a hot cathode discharge source.

Table 4.6. Electronic excitation energies E_{cal} (eV) and oscillator strength (*f*) of the dipole-allowed electronic transitions of *l*-OC_4O^+ calculated by the MS CASPT2 method and compared with the experimental value E_{exp}.

Species	Transitions	E_{cal}	*f*	E_{exp}
l-OC_4O^+	**1** $^2\Pi_u \leftarrow X\ ^2\Pi_g$	3.19	*0.004*	2.97
	2 $^2\Pi_u \leftarrow$	3.24	*0.000*	
	3 $^2\Pi_u \leftarrow$	3.78	*0.000*	
	5 $^2\Pi_u \leftarrow$	4.04	*0.001*	

Vertical excitation energies were calculated for *l*-OC_4O^+ to assist the structural assignment of 417 nm system (**Table 4.6**). The ground-state geometry was optimized first with DFT/ M062X/cc-pVTZ level and that co-ordinate was used for the excitation energy calculation with MS CASPT2 methods. According to calculation, *l*-OC_4O^+ possesses a detectable transition **1** $^2\Pi_u \leftarrow X\ ^2\Pi_g$ at 3.19 eV (*f*=0.004) which agrees with the observation at 2.97 eV (417 nm). Vibrational bands to the blue of the origin are assigned on the basis of excited state frequencies calculated with CIS/cc-pVTZ level (**Table 4.7**). This CIS method has unveiled a change of geometry in excited state to C_{2h} from $D_{\infty h}$ (**Figure 4.7**).

Table 4.7. Electronic absorption band maxima (±0.1 nm) of *l*-OC_4O^+ in a 6 K neon matrix. The assignment is based on the calculated ground state vibrations (cm^{-1}), given in the footnote.

λ (nm)	ν (cm^{-1})	Δν (cm^{-1})	Assignment	
417.0	23979	0	0_0^0	**1** $^2\Pi_u \leftarrow X\ ^2\Pi_g$
414.0	24152	173	ν_{12}	
406.4	24606	627	ν_4	
403.8	24768	789	$\nu_4 + \nu_{12}$	
390.1	25634	1655	ν_2	
387.3	25820	1841	$\nu_2 + \nu_{12}$	
380.8	26259	2280	ν_1	
378.7	26405	2426	$\nu_1 + \nu_{12}$	

ν_1- ν_5 (a_g): 2492, 1805, 857, 597, 286 cm^{-1}; ν_6 (b_g): 497 cm^{-1}; ν_7- ν_8 (a_u): 727, 129 cm^{-1}; ν_9- ν_{12} (b_u): 2799, 1599, 1136, 140 cm^{-1}.

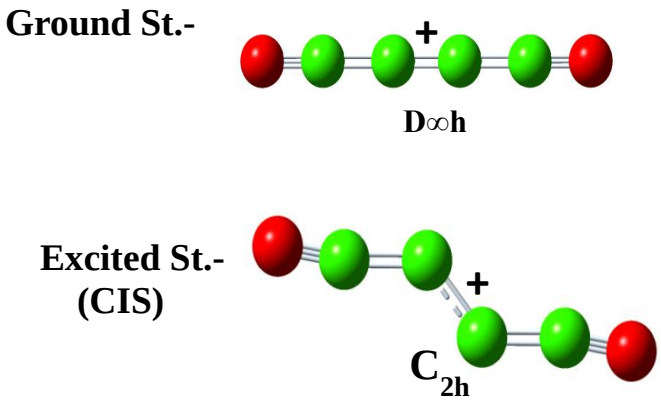

Figure 4.7: Geometry change of *l*-OC_4O^+ in the excited state **1** $^2\Pi_u$ (^{2}Ag), computed with CIS method using cc-pVTZ basis set.

4.4 CONCLUSION

Two isomers of $H_2C_6O^+$ (2-ethynylcycloallyl)methanone cation $\mathbf{B}^+$ and 2-ethynylbut-3-yn-1-enone-1-ylide, $\mathbf{F}^+$ were produced in a hot cathode discharge source from a mixture of carbon suboxide C_3O_2 and diacetylene HC_4H. The reactions between C_2O and HC_4H^+, or C_2O^+ and HC_4H, are exothermic. They should be considered in the astrophysical models as a way of incorporation of oxygen into the hydrocarbon moieties. The $\mathbf{B}^+$ and $\mathbf{F}^+$ isomers were found unstable under 260─390 nm photon exposure.

The 2,4,6-heptatriynal cation HC_7O^+ is isoelectronic to cyanotriacetylene HC_7N[30] identified in space. The intense rotation transitions of cyanopolyynes have been observed in the dense clouds due to the large-dipole moments. In case of 2,4,6-heptatriynal cation this is calculated to be 1.5 D, suitable for the interstellar identification via millimeter-wave technique. As oxygen is as abundant as nitrogen in the ISM, one can expect the existence of $HC_7O^{+/0}$ species. Ion-molecule reactions driven by cosmic rays are used to discuss the chemistry in the dense clouds,[31] therefore, insertion of O^+ into C_7H or the reaction between C_6H and CO^+ can yield HC_7O^+. These possible reactants CO^+, C_6H, C_7H have been identified in such environments.[32] Production of polycarbon chain oxides in interstellar clouds is a challenging issue in astrochemical research. The spectrum

reported for the *l*-OC_4O^+ can be a starting point for the gas-phase analysis and the astrophysical findings.

Moreover, oxygenated hydrocarbons and their ions are likely reactive intermediates in combustion, and the present spectroscopic data provide the means to monitor them in situ *via* their electronic absorptions.

BIBLIOGRAPHY

[1] W. Klemperer, *Nature* **1970**, *227*, 1230.

[2] M. Agúndez, J. Cernicharo, and M. Guélin, *Astron. Astrophys.* **2015**, *577*, L5.

[3] M. Ohishi, S.-I. Ishikawa, C. Yamada, H. Kanamori, W. M. Irvine, R. D. Brown, P. D. Godfrey, N. Kaifu and H. Suzuki, *Astrophys. J.* **1985**, *290*, L65.

[4] W. B. Latter, C. K. Walker and P. R. Maloney, *Astrophys. J.* **1993,** *419*, L97.

[5] H. E. Matthews, W. M. Irvine, P. Friberg, R.D. Brown and P. D. Godfrey, *Nature* **1987**, *310*, 125.

[6] N. Sakai, T. Sakai and S. Yamamoto, *Astrophys. J.* **2008,** *673*, L71.

[7] N. Sakai, T. Sakai, Y. Osamura and S. Yamamoto, *Astrophys. J.* **2007**, *667*, L65.

[8] S. Brünken, H. Gupta, C. A. Gottlieb, M. C. McCarthy and P. Thaddeus, *Astrophys. J.* **2007,** *664*, L43.

[9] M. A. Cordiner and S. B. Charnley, *Astrophys. J.* **2012,** *749*, 120.

[10] T. P. Snow and V. M. Bierbaum, *Annu. Rev. Anal. Chem.* **2008**. *1*, 229.

[11] J. M. Hollis, A. J. Remijan, P. R. Jewell and F. J. Lovas, *Astrophys. J.* **2006**, *642*, 933.

[12] N. G. Adams, D. Smith, K. Giles and E. Herbst, *Astron*. *Astrophys*. **1989**, *220*, 269.

[13] M. E. Jacox, D.E. Milligan, N.G. Moll, and W.E. Thompson, *J. Chem. Phys*. **1965**, *43*, 3734.

[14] R.D. Brown, D.E. Pullin, E. H. N. Rice and M. Rodler, *J. Am. Chem. Soc.* **1985,** *107*, 7877.

[15] G. Maier, H. P. Reisenauer, U. Schafer and H. Balli, *Angew*. *Chem.* **1988,** *100*, 590.

[16] G. Maier, H. P. Reisenauer and A. Ulrich, *Tetrahedron Lett.* **1991**, *32*, 4469.

[17] D. Strelnikov, R. Reusch, and W. Kratschmer, *J. Mol. Spec.* **2007,** *243*, 189.

[18] P. Botschwina and H. P. Reisenauer, *Chem. Phys. Lett.* **1991,** *183*, 217.

[19] G. R. Smith and W. Weltner, *J. Chem. Phys.* **1975**, *62*, 4592.

[20] R. J. Van Zee, G.R. Smith and W. Weltner, *J. Am. Chem. Soc.* **1988**, *110*, 609.

[21] C. Devillers and D. A. Ramsay, *Can. J. Phys.* **1971,** *49*, 2839.

[22] J. Fulara, M. Grutter, M. Wyss and J. P. Maier, *J. Phys. Chem. A* **1998**, *102*, 3459.

[23] E. Riaplov, M. Wyss, N.M. Lakin and J.P. Maier, *J. Phys. Chem. A* **2001**, *105*, 4894.

[24] S. M. E. Joseph, J. Fulara, I. Garkusha and J. P. Maier, *Mol. Phys.* **2013**, *111*, 1977.

[25] R. C. Woods, T. A. Dixon, R. J. Saykally and P. G. Szanto, *Phys. Rev. Lett.* **1975**, *35*, 1269.

[26] S. Mohamed , M.C. McCarthy , A.L. Cooksy , C. Hinton and P. Thaddeus, *J. Chem. Phys.* **2005**, *123*, 234301.

[27] J. Fulara, A. Nagy, I. Garkusha and J. P. Maier, *J. Chem. Phys.* **2010**, *133*, 024304.

[28] G. Bieri, A. Schmelzer, L. Asbrink and M. Jonsson, *Chem. Phys.* **1980**, *49*, 213.

[29] J. Fulara. A. Nagy, K. Filipkowski, V. S. Thimmakondu, J. F. Stanton, J. P. Maier, *J. Phys. Chem. A* **2013**, *117*, 13605.

[30] G. Winnewisser and C. M. Walmsley, *Astron. Astrophys.* **1978,** *70*, L37.

[31] E. Herbst and E. F. van Dishoeck, *Annu. Rev. Astron. Astrophys.* **2009**, *47*, 427.

[32] M. Agúndez and V. Wakelam, *Chem. Rev.* **2013**, *113*, 8710.

[33] A. Chakraborty, J. Fulara and J.P.Maier, *J. Phys. Chem. A* **2015**, *119*, 50.

Chapter 5

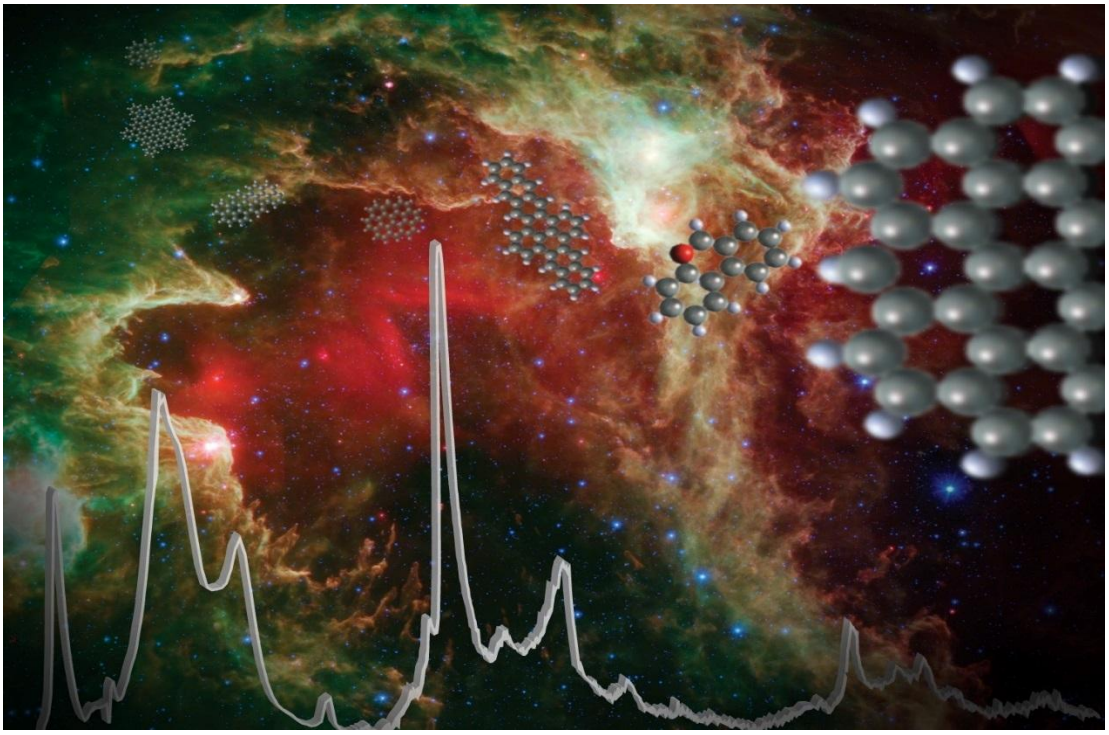

SPECTROSCOPY OF PROTONATED POLYCYCLIC AROMATICS

5

Four electronic systems starting at 759.5, 559.3, 476.3, and 385.5 nm are detected in a 6 K neon matrix following deposition of mass-selected protonated fluoranthene (m/z = 203) produced from reactions of neutral vapour and ethanol in a hot-cathode ion source. Two different isomers are identified as the carriers of these absorprion systems after irradiation of the matrix by $\lambda < 260$ nm photons. The 559.5, 476.3 and 385.5 nm systems are assigned to **4, 3, 2** $^1A' \leftarrow X\ ^1A'$ transitions of isomer γ-protonated fluoranthene $\mathbf{E}^+$ on the basis of theoretical predictions. The 759.5 nm systems is the **2** $^1A_1 \leftarrow X\ ^1A_1$ absorption of isomer $\mathbf{C}^+$, α- protonated fluoranthene.

The electronic transitions of 9-fluorenone $\mathbf{FL}^+$ and 2,3,6,7-dibenzotropone $\mathbf{DBT}^+$ cations are also detected in 6 K neon matrices following the mass-selective deposition. The absorptions at 649.2 and 472.2 nm are assigned to the **2** $^2B_1 \leftarrow X\ ^2A_2$ $\mathbf{FL}^+$ and **2** $^2A' \leftarrow X\ ^2A'$ $\mathbf{DBT}^+$ electronic transitions. Absorption spectra of protonated 9-fluorenone $\mathbf{H}^+$**-FL** and 2,3,6,7-dibenzotropone $\mathbf{H}^+$**-DBT** have also been measured. Ethanol was employed as the protonating agent. Vibrationally resolved absorptions commencing at 423.3 nm of **H–**$\mathbf{FL}^+$ and two band systems of **H–**$\mathbf{DBT}^+$ with origins at 502.4 and 371.5 nm are assigned to the **2** $^1A' \leftarrow X\ ^1A'$ electronic transition of 9-hydroxy-fluorenyl cation and **1** $^1A \leftarrow X\ ^1A$, **2** $^1A \leftarrow X\ ^1A$ of 2,3,6,7-dibenzocycloheptenol cation. The assignments are based on vertical excitation energies calculations with TD DFT, SAC-CI and MS-CASPT2 methods.

5.1 INTRODUCTION

A significant portion of carbon in interstellar medium is supposed to be in the form of polycyclic aromatic hydrocarbons (PAHs). The broad infrared emission features detected from galactic and extragalactic objects, the unidentified infrared emission bands (UIR), are universally assigned to vibrational transitions of PAHs and their ions.[1-6] In dense molecular clouds or disks of young stellar objects where temperatures are low 10-20 K, PAHs are believed to be condensed on interstellar grains as a part of molecular ices, containing mainly water. Grain surface is conceived as an important site for prebiotic chemistry. Therefore, investigation on the chemistry of PAHs in cosmic ice analogues upon ultra-violet radiation has become a topic in astrochemistry, and several experiments were carried out by varying the temperature, size of aromatics and using different molecular ices (e.g. H_2O, O_2, CO_2, HCN, NH_3).[7-12] The results demonstrate that solid -phase light driven chemistry modifies the organics and even creates new systems. In the case of H_2O mantels, formation of ketones and alcohols of the corresponding PAHs is predominent.[8,10]

As closed shell PAHs generally have the strongest absorption more to the UV region, their radical cations (PAH^+s) and isoelectronic protonated analogues (H-PAH^+s) became a subject for spectroscopy and quantum chemistry;[13] it has unveiled that most of the H^+-PAHs and PAH^+s have strongest transition in the visible. Significance of protonated PAHs as the carrier of UIRs and DIBs has been discussed in **Chapter 1** (section 1.5). We are now at the golden age of observational astronomy, *Spitzer* and ISO have already created a huge database and JWST, E-ELT missions are around the corner, therefore, a significant amount of laboratory characterization of PAHs, H^+-PAHs and their derivatives will be needed in near future. Matrix-isolation approach has proven to be suited to study both positive and negative ions.[14-16] Molecular spectroscopic characterization of neon/argon matrix-isolated PAHs and their ions produced by *in situ* photoionisation have been carried out.[17] Mass-selected deposition of charged PAHs in 6 K solid-neon has also been very successful.[18] Such data are also of general interest as ionized PAHs are considered to be reaction intermediates in combustion.[19]

So far, spectroscopic analysis has been focused on one class of PAHs bearing six-membered rings and having absorption in the IR and visible.[20,21] The recent identification of C_{60}^+ in the ISM[21] suggests the existence of polycyclic species containing both five- and six membered

rings together. Hence, electronic and IR spectra are required for the latter sort of molecules. In this context, electronic characterization of protonated fluoranthene (**H^+-FT**), having both five- and six membered rings, has been carried out.

Oxygenated analogs of PAHs have not been much studied except for few photoelectron spectra.[22] Oxygen containing PAHs (O-PAHs) could be present in astronomical environments as incorporation of oxygen is apparent from the UV photolysis of PAHs in solid H_2O.[8] Aromatic ketones have been reported in meteorites.[23-25] In addition to the possible astrophysical importance, O-PAHs are also detected in the soot of woods and organic oils.[26,27]

In this chapter the electronic absorption spectra of two O-PAH$^+$s, 9-fluorenone **FL^+** and 2,3,6,7-dibenzotropone **DBT^+** cations and their corresponding protonated species **H-FL^+** and **H-DBT^+** are reported. The assignment of the transitions is made on the basis of ground-state stability and calculated excitation energies.

5.2 PRODUCTION OF PROTONATED AROMATICS

The proton transfer technique is an energetically soft approach applied in mass spectrometry. The solid precursor, fluoranthene **FT**, 9-fluorenone **FL** and 2,3,6,7-dibenzotropone **DBT** were heated in an oven and carried to the source by ethanol EtOH vapor which served as the protonating agent. The structures of the precursors are shown in **Chart 5.1.**

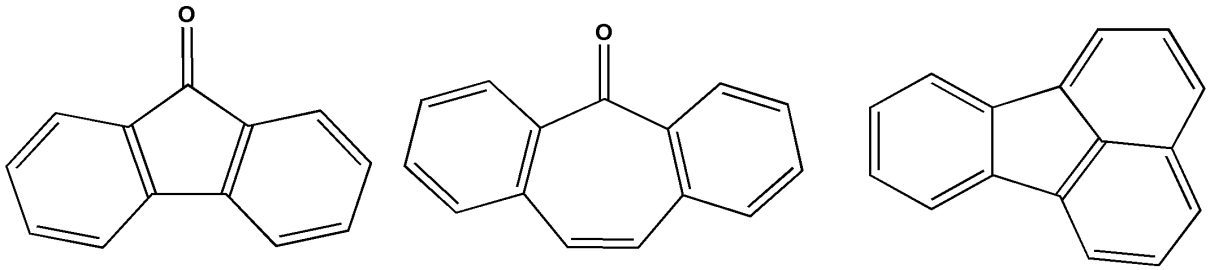

9-fluorenone (FL)
m/z=180

2,3,6,7-dibenzotropone (DBT)
m/z=206

Fluoranthene
m/z=202

Chart 5.1: Structure of the precursor molecules

The protonated PAHs are produced in the source *in situ via* $EtOH_2^+$ (protonated EtOH). It has been previously demonstrated that high pressure of EtOH vapor in the source favors the formation of $EtOH_2^+$ and as a consequence the production of protonated PAH (**Chapter 2**).

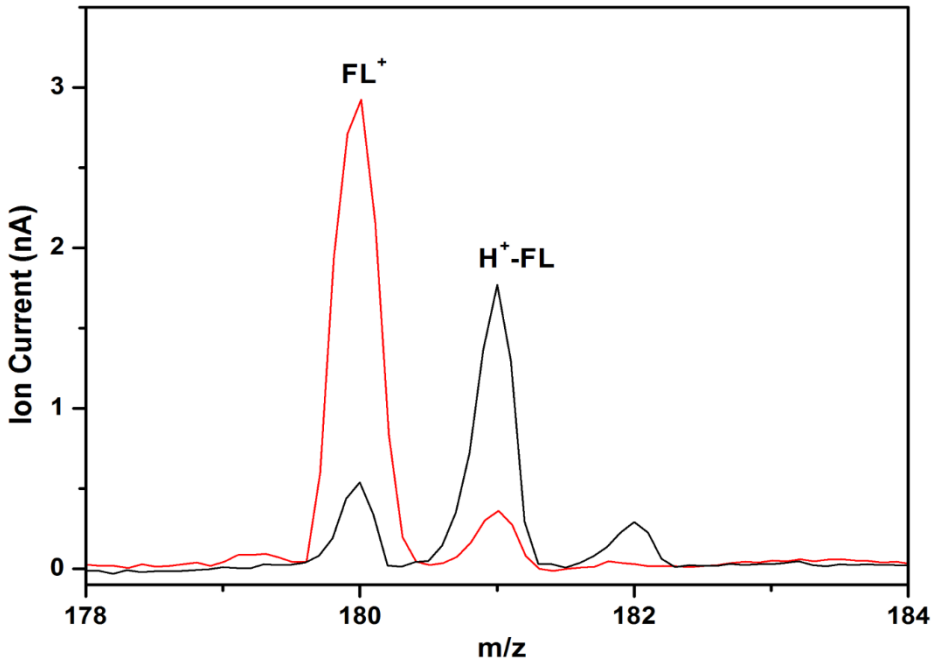

Figure 5.1: Section of the mass spectrum of 9-fluorenone **FL** vapor (red) and in the presence of ethanol (black) in the hot cathode discharge source.

In vapor of pure O-PAHs, the molecular ion M^+ (m/z=180) had the highest intensity in the mass spectrum while the M^++1 signal grew with EtOH presence (**Figure 5.1**). Electronic spectra are recorded normally after accumulation of at least 10-15 μC of cations in matrix.

5.3 COMPUTATION

There are five non-equivalent protonation sites in **FT** (**Chart 5.2**). Ground state geometry optimization of these five isomers $\mathbf{A}^+$–$\mathbf{E}^+$ of $\mathbf{H}^+$**-FT** was carried out with DFT/B3LYP/cc-pVTZ theory. Four other isomers, except $\mathbf{D}^+$, lie energetically within 22 kJ mol^{-1} of each other, and $\mathbf{E}^+$ is the global minimum on the potential energy surface of $\mathbf{H}^+$**-FT**. Vertical excitation energies and oscillator strengths of $\mathbf{H}^+$**-FT** isomers were calculated at the equilibrium coordinates obtained from B3LYP/cc-pVTZ computations. Symmetry Adapted Cluster/Configuration Interaction (SAC-CI) method was employed with the Gaussian09 software using the cc-pVTZ basis set with 350 orbitals at an energy < 3.3 Hartree.

9–fluorenone **FL** and 2,3,6,7-dibenzotropone **DBT** have five and six non-equivalent protonation sites respectively. Computational data are needed for the determination of the most

stable protonation site as well as for the assignment of the carriers of the absorptions. Ground state optimization of the plausible protonated isomers of **H-FL**$^+$ and **H-DBT**$^+$ was carried out with the DFT method using a cc-pVDZ basis set and the hybrid B3LYP functional in the Gaussian 09 programme. Relative ground state energies for the **H-FL**$^+$ isomers [**A1**$^+$**–E1**$^+$] are listed in **Chart 5.3**. Isomer **A1**$^+$, proton attached to the oxygen atom, is found to be the most stable and **C1**$^+$ is next, 75 kJ/mol^{-1} to higher energy. A similar tendency is observed for **H-DBT**$^+$; among the six **F**$^+$**–K**$^+$ isomers, **F**$^+$ obtained by protonating the oxygen atom of **DBT**, is found as the global minimum. The next stable one **H**$^+$ is found 102 kJ/mol higher in energy (**Chart 5.3**). Therefore the most stable structures: **A1**$^+$ and **F**$^+$, designated as **H-FL**$^+$ and **H-DBT**$^+$, were selected for excitation energy calculations.

The coordinates of **FL**$^+$, **H-FL**$^+$, **DBT**$^+$, **H-DBT**$^+$ and their neutral counterparts were optimized with the DFT method using the correlation consistent (cc-VTZ) basis set and the M06-2X functional. These coordinates were used for the calculations of vertical excitation energies. A real minimum was found for **DBT**$^+$ in C_S symmetry, which lies 2.0 kJ/mol below the C_{2V} structure. Nevertheless the C_{2V} geometry was also used for the excitation energies calculations.

Vertical excitation energies were calculated with (TD) DFT, SAC-CI, and MS-CASPT2 methods. In the SAC-CI calculations the cc-pVDZ basis set was used and about 200 orbitals with an energy < 3 Hartree were exploited. In CASPT2 an active space was constructed from twelve electrons distributed over twelve orbitals (12,12) in the case of singlets and (11,12) for doublets with the exception of **H-DBT**$^+$ where the active space was reduced to (10,10).

Chart 5.2: Structure and relative ground-state energies (kJ mol^{-1}) of the **H$^+$-FT** isomers calculated with the B3LYP/cc-pVTZ level of theory. The detected isomers are highlighted by red.

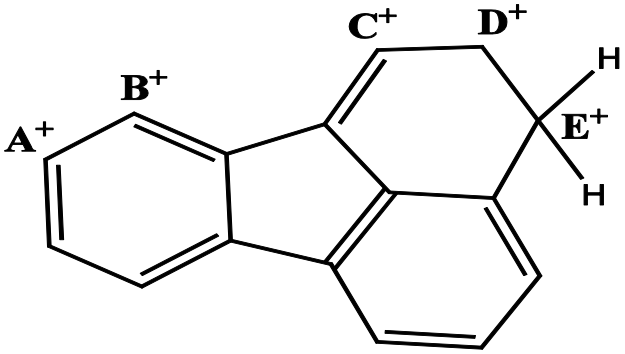

Protonated-fluoranthene (H$^+$-FT)

A$^+$	**5**
B$^+$	**20**
C$^+$	**22**
D$^+$	**40**
E$^+$	**0**

Chart 5.3: Structure and relative ground state energies (kJ mol^{-1}) of the **H-FL$^+$** and **H-DBT$^+$** isomers, calculated with DFT using the cc-pVDZ basis set and the B3LYP hybrid functional.

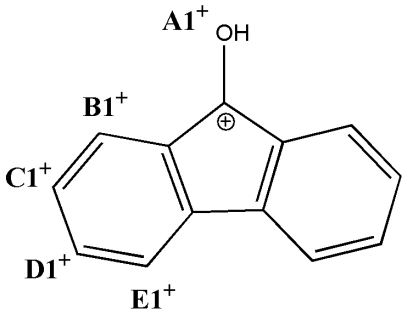

Protonated 9-fluorenone (H$^+$-FL)

A1$^+$	**0**
B1$^+$	**129**
C1$^+$	**75**
D1$^+$	**121**
E1$^+$	**92**

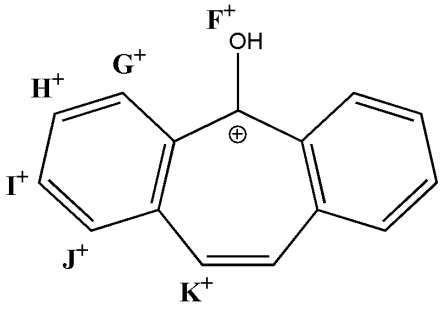

Protonated 2.3,6,7-dibenzotropone (H$^+$-DBT)

F$^+$	**0**
G$^+$	**142**
H$^+$	**102**
I$^+$	**120**
J$^+$	**106**
K$^+$	**119**

5.4 RESULTS AND DISCUSSIONS

5.4.1 Protonated Fluoranthene (H^+-FT):

Mass-selected deposition of m/z=203 (**H^+-FT**) cation reveals a number of moderately strong absorption systems in visible and UV regions (red trace of **Figure 5.2, 5.3**). Three dominant origin bands followed by similar vibrational progressions are observed at 559.3, 476.3 and 385.5 nm (**Figure 5.2**) where the one at 476 nm is the strongest. Another vibrationally resolved system is apparent at 759.5 (**Figure 5.3**). A small percentage of deposited cations recombine with electrons in the matrix and thus there is always a contribution of neutrals in the spectra recorded after deposition. The matrix was then exposed to $\lambda < 260$ nm photons to distinguish the cationic and neutral absorptions.

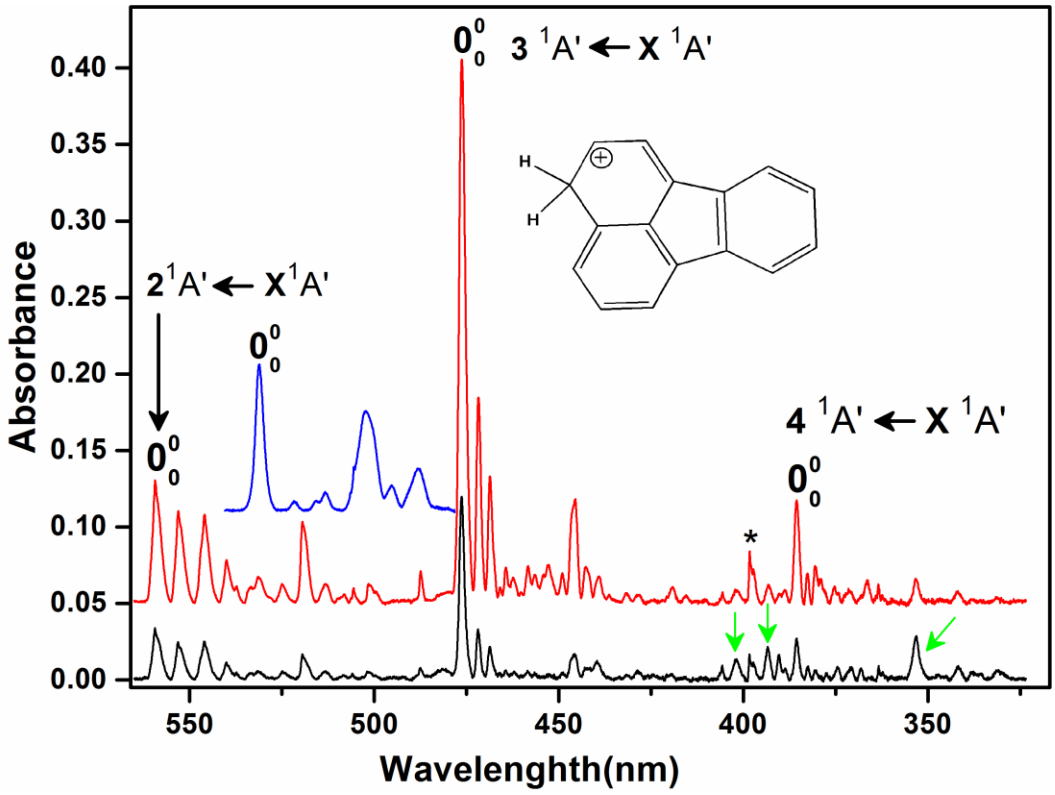

Figure 5.2: Electronic absorption spectra recorded after depositing *m/z* = 203 cations produced by protonation of fluoranthene in the source using ethanol (red trace), and after irradiation of the matrix with $\lambda < 260$ nm photons (black trace). The electronic absorption spectrum of fluoranthene cation ($C_{16}H_{10}^+$) is shown as blue trace. The origins of neutral absorptions are denoted by green arrows; that of N_2^+ is marked (*).

After irradiation cationic bands diminish while peaks of neutrals increase. The band intensities of all the three intense systems at 559, 476 and 385 nm noticeably decreased (**Figure 5.2**, black trace). The other absorption system at 759 nm also has a reduced band strength after irradiation (**Figure 5.3**, black trace). On the other hand, peaks at 401.9 393.3, and 353.2 nm gained intensity (green arrows in **Figure 5.2**). The 401.9, 393.3 and 353.2 nm features lie among the vibrational progressions of the 476 and 385 nm absorption systems. The decrement of intensity indicates that the systems at 559, 476, 385 and 759 nm are cationic in nature while the carrier(s) of the 401.9, 393, and 353 nm ones is neutral. No new peak appeared after irradiation.

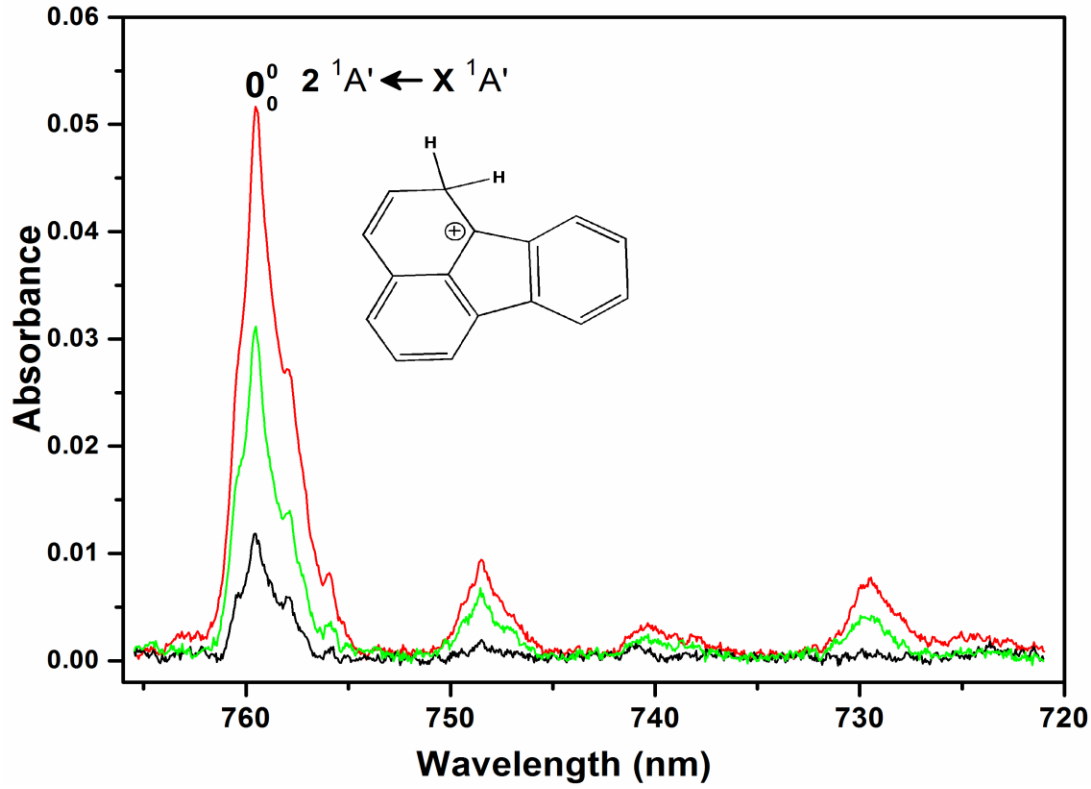

Figure 5.3: Electronic absorption spectra recorded after depositing *m/z* = 203 cations produced by the protonation of fluoranthene in the source using ethanol (red trace), after irradiation of the matrix in the 285–300 nm range (green trace) and exposure with photons below 260 nm (black trace).

In previous studies of H^+-PAHs in neon matrices, absorption from precursor cations were detected after mass-selected deposition of the corresponding protonated species.[28] The reasons were: 1) collisionally induced H loss during deposition 2) ^{13}C isotopologues with the same mass as the protonated species. Hence, in separate experiment, mass-selected deposition **FT$^+$**

(m/z=202) was carried out. The absorption spectrum is shown in the blue trace of **Figure 5.2**, and the origin of the **3** ^{2}A" ← X ^{2}A" electronic transition of **FT$^+$** lies at 531.1 nm. The band maxima and assignments are listed in **Table 5.1**. The peaks which belong of **FT$^+$** do not coincide with any absorption in the deposition of **H$^+$-FT**, which implies that all cationic bands in **Figure 5.2** and **5.2** are of the **H$^+$-FT** species.

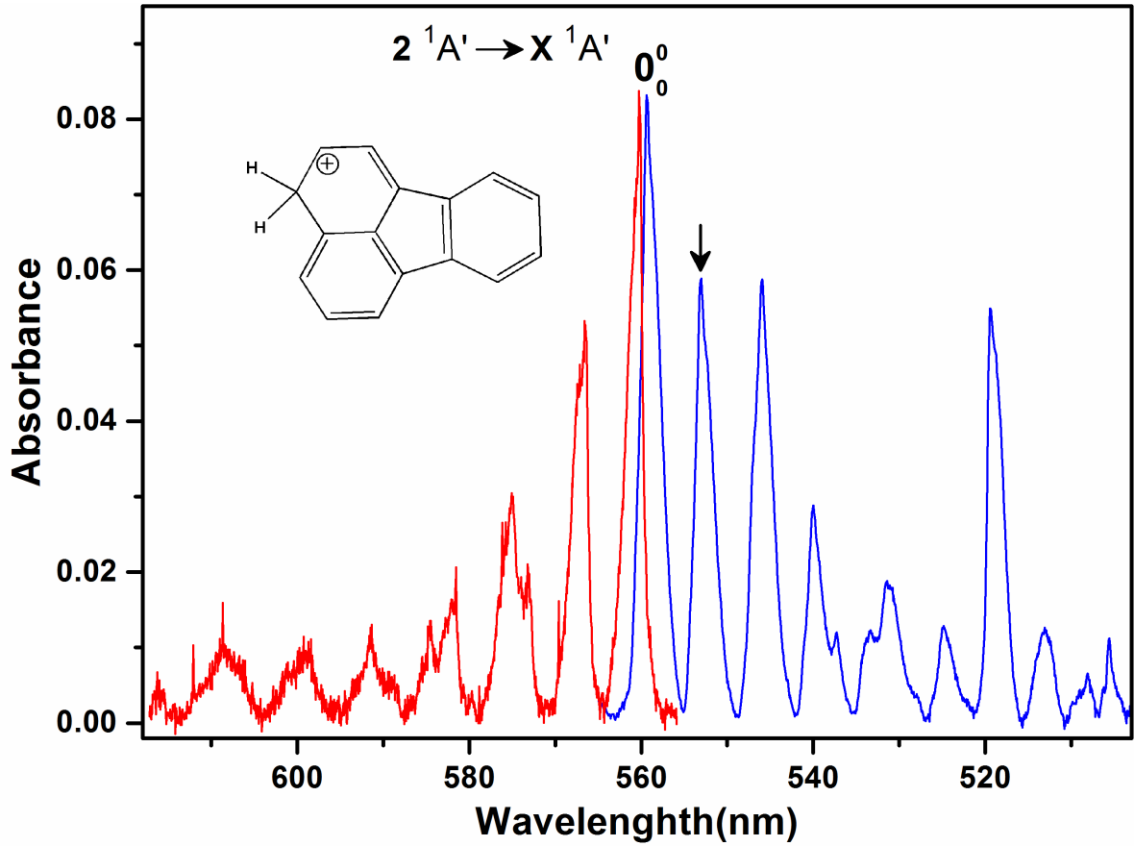

Figure 5.4: Electronic absorption (blue) and fluorescence (red) spectra recorded after depositing *m/z*=203 cations in neon matrices at 6 K. Emission was measured after exciting the ν_{50} absorption band of the **2** ^{1}A' ← X ^{1}A' electronic system (arrow).

The decrement rate of the bands upon UV exposure suggests that the 559, 476 and 385 nm systems are of one **H$^+$-FT** isomer and the 759 nm of another. Fluorescence measurements were carried out. The same spectrum (**Figure 5.4**, red trace) was obtained by exciting the three absorption origins at 559, 476 and 385 nm and their vibrational progression bands. On the other hand, no fluorescence was detected by exciting the bands of 759 nm system which affirms the previous speculation that this absorption is of another **H$^+$-FT** isomers.

SAC-CI calculation for the vertical excitation energies of the five most stable isomer of **H^+-FT**, **A^+**, **B^+**, **C^+**, **D^+** and **E^+** were carried for the structural assignments. Isomer **C^+** gives the best correspondence for the 759 nm (1.63 eV) system. SAC-CI predicts only one intense **2** ^{1}A' ← X ^{1}A' transition at 1.84 eV (*f*=0.19) for **C^+** in the 260-1100 nm region in agreement with the experimental observation (**Table 5.3**). The next equally intense absorption **4** ^{1}A' ← X ^{1}A' of **C^+** is predicted at 4.41 eV, at the edge of the experimental detection range and additionally, the absorption below 270-280 nm would be difficult to observe due to Rayleigh scattering. Hence, the 759 nm absorption system is attributed to isomer **C^+**. Transitions to the vibrationally excited levels in the **2** ^{1}A' electronic state are seen 193, 341 and 547 cm^{-1} blue to the 759.5 nm origin peak. These vibrations are assigned on the basis of totally symmetric ground state values of **C^+** calculated with DFT (**Table 5.1**).

As deduced above, the other three cationic bands are due to one isomer of **H^+-FT**. SAC-CI predicts intense transitions **4, 3, 2** ^{1}A' ← X ^{1}A' at 2.25 eV (*f*=0.17), 2.99 eV (*f*=0.19) and 3.41 eV (*f*=0.16), respectively, for the most stable isomer **E^+**. **B^+** also has three electronic transitions at 2.08 eV (*f*=0.20), 2.53 eV (*f*=0.13) and 3.57 eV (*f*=0.26). The excitation energies for both **B^+** and **E^+** agree well with experimental result but the most intense transition of **B^+** is predicted at 3.57 eV contradictory to the observation. Calculated oscillator strengths of **E^+** are consistent with observed relative intensities, and **E^+** is the global minimum. **B^+** is less stable by 20 kJ mol^{-1} relative to **E^+**.

In further experiment, the matrix was exposed to different energy photons to probe the stability of these two protonated isomers. Light in the 285-300 nm range removes the hydrogen from isomer **C^+** and as a consequence 759 nm band system losses in intensity (green trace, **Figure 5.3**). The 559 nm system must also decrease in intensity if the carrier would be the **B^+**; **B^+** and **C^+** are energetically similar (**Chart 5.2**). But the 559 nm system was found to be very stable upon exposure of this 285-300 nm photons which supports the assignment of the **E^+** as the carrier. Thus, **E^+** is assigned as the carrier of the three absorption systems at 559 (2.21 eV), 476 (2.60 eV) and 385 nm (3.22eV). Vibrational assignments are made (**Table 5.1**) on the basis of totally symmetric ground-state frequencies of **E^+** calculated with DFT.

Vibrationally resolved **2** ^{1}A' → X ^{1}A' fluorescence spectrum was recorded after laser excitation of the absorption wavelengths of **E^+** isomer. The bands obtained by the emission from v = 0 level of **2** ^{1}A' electronic state to vibrational levels of X ^{1}A' are seen at 208, 451, 666, 745,

945, 1162 and 1414 cm^{-1} red to the 560.2 nm origin. They are assigned as ν_{50}, ν_{48}, ν_{43}, ν_{42}, ν_{39}, ν_{32} and ν_{20} totally symmetric (a_1) vibrations in the X ^{1}A' state on the basis of calculated ground-state frequencies of $\mathbf{E}^+$ (**Table 5.2**). All of these modes are also apparent in the absorption spectra. The zero phonon line of the origin band is at 559.9 nm. Absorption signal results from all deposited cations as the light is collected after propagating through whole matrix while fluorescence is recorded by exciting the trapped molecules present in a portion of the matrix. Hence, the signal-to-noise is reduced in fluorescence spectrum.

The weak absorptions of neutrals were detected at 401.9, 393.3 and 353.2 nm. The relative intensity change upon UV irradiation, suggesting that these bands are of one carrier. According to SAC-CI calculation, **E** has the strongest transition at 3.45 eV in agreement with the experimentally found most intense neutral band at 353 nm (**Table 5.3**). SAC-CI is not a satisfactory method for prediction of excitation energies of such large open shell molecules. As the three absorptions are not of a **FT** photofragment, no distinct features were seen at these wavelengths after irradiation of $\mathbf{FT}^+$. Thus, 401.9, 393.3, and 353.2 nm systems are assigned to neutral **E**.

Table 5.1: Absorption band maxima (±0.1nm) of electronic transitions of protonated fluoranthene (H^+-FT) cations, their neutrals (H-FT) and fluoranthene cation (FT^+) in 6 K neon matrices. The assignment is based on the vibrational frequencies of the normal modes listed in the footnote of Table 5.2.

λ (nm)	ν (cm^{-1})	Δν (cm^{-1})	Assignment	
E^+				
559.3	17879	0	0_0^0	**2** A' ← X A'
553	18083	204	ν_{50}	
545.9	18318	439	ν_{48}	
540	18519	640	ν_{43}	
537.3	18612	733	ν_{42}	
533.4	18748	869	ν_{40}	
531.4	18818	939	ν_{39}	
524.9	19051	1172	ν_{32}	
519.4	19253	1374	ν_{22}	
513.1	19489	1610	ν_{14}	
508.1	19681	1802	$\nu_{22}+\nu_{48}$	
501.3	19948	2069	$\nu_{22}+\nu_{42}$	
487.4	20517	2638	–	
476.3	20995	0	0_0^0	**3** A' ← X A'
471.8	21195	200	ν_{50}	
468.7	21336	341	ν_{49}	
465.9	21464	469	ν_{48}	
464.4	21533	538	ν_{46}	
462.4	21626	631	ν_{43}	
458.4	21815	820	ν_{40}	
456.5	21906	911	ν_{39}	
452.8	22085	1090	ν_{35}	
449	22272	1277	ν_{27}	
445.7	22437	1442	ν_{20}	
442.5	22599	1604	ν_{14}	
439	22779	1784	$\nu_{20}+\nu_{49}$	
419.1	23861	2866	$2\nu_{20}$	
385.5	25940	0	0_0^0	**4** A' ← X A'
382.6	26137	197	ν_{50}	
380.5	26281	341	ν_{49}	
375.1	26660	720	ν_{42}	
366.3	27300	1360	ν_{23}	

λ (nm)	ν (cm^{-1})	Δν (cm^{-1})	Assignment	
C^+				
759.5	13167	0	0_0^0	**2** ^{1}A' ← X ^{1}A'
748.5	13360	193	ν_{50}	
740.3	13508	341	ν_{49}	
729.2	13714	547	ν_{46}	
H-FT				
401.9	24882	0	0_0^0	
393.3	25426	544		
353.2	28313	3431		
FT^+ ($C_{16}H_{10}^+$)				
531.1	18829	0	0_0^0	**3** ^{2}A" ← X ^{1}A"
521.6	19172	343	ν_{48}	
515.8	19387	558	ν_{44}	
513.3	19482	653	ν_{42}	
502.3	19908	1079	ν_{34}	
495.4	20186	1357	ν_{23}	
488.1	20488	1559	ν_{14}	

Table 5.2: Fluorescence band maxima (±0.1nm) of protonated fluoranthene (H-FT^+) cation, E^+ in 6 K neon matrices. The assignment is based on the vibrational frequencies of the normal modes listed in the footnote of table 1.

λ (nm)	ν (cm^{-1})	Δν (cm^{-1})	Assignment	
560.2	17876	0	0_0^0	**2** A' → X A'
566.8	17674	208	ν_{50}	
574.7	17416	451	ν_{48}	
581.9	17203	666	ν_{43}	
584.6	17129	745	ν_{42}	
591.5	16932	945	ν_{39}	
599.2	16711	1162	ν_{32}	
608.4	16450	1414	ν_{20}	

E^+ a′ (C_S); $\nu_1 - \nu_{50}$:3208, 3204, 3202, 3199, 3194, 3190, 3185, 3184, 3179, 2982, 1658, 1641, 1633, 1616, 1566, 1549, 1507, 1501, 1473, 1458, 1420, 1394, 1373, 1363, 1340, 1322, 1296, 1260, 1223, 1208, 1200, 1184, 1160, 1106, 1101, 1050, 1041, 990, 949, 887, 807, 767, 674, 614, 566, 555, 482, 462, 349, 208.

C^+ a′ (C_S); $\nu_1 - \nu_{50}$ :: 3210, 3205, 3201, 3199, 3198, 3189, 3187, 3186, 3184,2984, 1654, 1643, 1636, 1622, 1582,1531, 1507, 1495, 1458, 1443, 1435, 1406, 1390,1343, 1329, 1313, 1284, 1251, 1242, 1209, 1209, 1182, 1136, 1109, 1084, 1042, 1039,986, 943, 896, 794, 769, 674, 618, 563, 548, 489,461, 349, 205.

Table 5.3: Vertical excitation energies and oscillator strengths (f) of protonated fluoranthene cations (**H^+-FT**) and hydrofluoranthene radicals (**H-FT**) calculated with SAC-CI using cc-pVTZ basis and the internal coordinates from B3LYP/cc-pVTZ level of theory. Experimentally observed transitions are in bold.

Protonated fluoranthenes (H^+-FT)			Hydro fluoranthene radicals (H-FT)		
Ext. State Sym.	E_{ex} (ev)	f	Ext. State Sym.	E_{ex} (ev)	f
A^+ X 'A, Cs			C X "A, Cs		
A'	1.82	0.104	A"	2.02	0.007
A'	2.39	0.043	A"	2.85	0.009
A'	3.02	0.237	A"	3.95	0.005
A'	3.92	0.211	A"	4.45	0.008
A'	4.19	0.180	A"	5.28	0.009
A'	4.38	0.034			
			E X "A, Cs		
B^+ X 'A, Cs			A"	2.33	0.005
A'	1.91	0.014	A"	3.45	0.017
A'	2.08	0.204	A"	3.52	0.010
A'	2.53	0.136	A"	4.40	0.014
A'	3.57	0.264	A"	5.20	0.007
A'	3.94	0.020			
A'	4.17	0.079			
C^+ X 'A, Cs					
A'	1.10	0.002			
A'	**1.84**	**0.186**			
A'	3.0	0.062			
A'	4.04	0.075			
A'	4.41	0.185			
A'	5.07	0.538			
D^+ X 'A, Cs					
A'	1.52	0.035			
A'	1.86	0.013			
A'	3.13	0.029			
A'	3.48	0.043			
A'	3.99	0.000			
A'	4.44	0.299			
E^+ X 'A, Cs					
A'	0.99	0.001			
A'	**2.25**	**0.177**			
A'	**2.99**	**0.184**			
A'	**3.41**	**0.169**			
A'	4.60	0.502			
A'	5.12	0.321			

5.4.2 9–fluorenone cation (FL^+) and protonated 9–fluorenone (H^+-FL)

Spectra recorded after mass–selected deposition of the 9-fluorenone **FL^+** cation with neon including a trace of CH_3Cl shows four moderately intense absorption features in the 580-660 nm range. The strongest band is apparent at 649.2 nm and three weaker ones lying 211, 419 and 1463 cm^{-1} to higher energy (**Figure 5.5**, red trace). Thereafter, the matrix was exposed to $\lambda <$ 260 nm photons. The same rate of decrement of band intensities after irradiation (black trace) indicates that all of them belong to one 649 nm system and the carrier is cationic (**Table 5.4**). No new bands appeared after irradiation suggesting that neutral 9-fluorenone **FL** has absorptions beyond the detection range. The strongest transition of **FL** has been detected around 245 nm in solvents.[29,30]

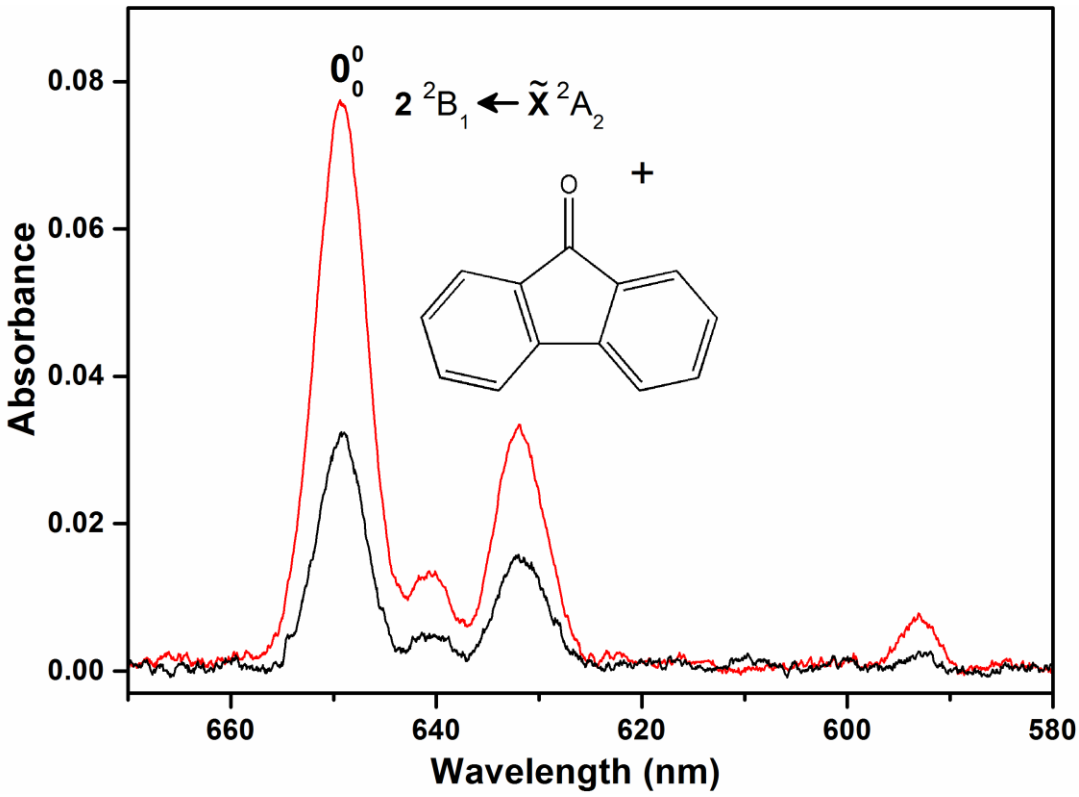

Figure 5.5: Electronic absorption spectrum recorded after deposition of 9-fluorenone cation **FL^+** into a neon matrix (red trace) and after neutralization of the cations with UV photons $\lambda <$ 260 nm (black trace).

Table 5.4: Absorption band maxima (±0.1nm) of electronic transitions of 9-fluorenone cation **FL**$^+$ and protonated fluorenone **H**$^+$**-FL** in 6 K neon matrices and assignment based on the vibrational frequencies of the normal modes listed in the footnote.[33]

λ (nm)	ν (cm^{-1})	Δν (cm^{-1})	Assignment	
FL$^+$				
649.2	15404	0	0_0^0	**2** $^2B_1 \leftarrow X\ ^2A_2$
640.4	15615	211	ν_{21}	
632.0	15823	419	ν_{20}	
592.9	16866	1463	ν_9	
H$^+$**-FL**				
423.3	23624	0	0_0^0	**2** $^1A' \leftarrow X\ ^1A'$
419.2	23855	231	ν_{43}	
416.2	24027	403	ν_{41}	
413.8	24166	542	ν_{39}	
409.5	24420	796	ν_{35}	
406.7	24588	964	ν_{33}	
404.6	24716	1092	ν_{30}	
402.7	24832	1208	ν_{24} or ν_{25}	
399.8	25013	1389	ν_{20}	
393.2	25432	1808	$\nu_{20}+\nu_{41}$	
391.4	25549	1925	$\nu_{20}+\nu_{39}$	

FL$^+$ (C_{2v}); (a_1) ν_1– ν_{21}: 3227, 3225, 3214, 3201, 1899, 1680, 1594, 1525, 1465, 1420, 1357, 1253, 1189, 1169, 1113, 1028, 783, 720, 557, 415, 200

H$^+$**-FL** (C_S); (a') ν_1– ν_{43}: 3759, 3242, 3235, 3213, 3212, 3205, 3201, 3200, 3172, 1671,1681,1690, 1667, 1601, 1530, 1526, 1495, 1494, 1439, 1392, 1326, 1323, 1290, 1229, 1209, 1204, 1197, 1178, 1122, 1113, 1056, 1053, 1029, 921, 786, 743, 638, 623, 560, 508, 423, 275, 208.

FL has been previously studied by photoelectron (PE) spectroscopy.[31] The PE spectrum reveals a triplet structure at 0.86, 0.99 and 1.18 eV and a distinct band at 1.91 eV above the ground state of **FL**$^+$. Vertical excitation energies of **FL**$^+$ were calculated (**Table 5.5**) with TD DFT, SAC-CI and MS(5)-CASPT2 (11,12) methods to assign the detected electronic absorptions in the current matrix experiment. All three methods predict low-lying electronic states **1** $^2A_2$, **1** $^2B_1$, **1** $^2B_2$ above the X $^2A_2$ ground-state with energies close to the derived ones by PE study. A strong electronic transition with oscillator strength f =0.15 - 0.30, to the **2** $^2B_1$ state with energy 2.10 - 2.35 eV agrees well with the observation at 649 nm (1.91 eV); the band 1.91 eV above the ground state of the ion seen in PE spectrum corresponds to this **2** $^2B_1 \leftarrow X\ ^2A_2$ transition. The TD DFT and CASPT2 calculations predict also a strong **3** $^2B_1 \leftarrow X\ ^2A_2$ transition between 3.1 - 3.4

eV which has not been observed experimentally. TD DFT and CASPT2 likely overestimated the *f* values.

Table 5.5: Electronic states, vertical excitation energies (eV) and oscillator strengths (italics) of 9-fluorenone cation and protonated 9-fluorenone calculated with TD DFT/M06-2X/cc-pVTZ, SAC-CI/ cc-pVDZ and MS(5)-CASPT2/cc-pVTZ using coordinates from DFT M06-2X/cc-pVTZ.[33]

State	TD DFT		SAC-CI		CASPT2	
FL$^+$ C_{2v}						
X $^2A_2$	0.00		0.00		0.00	
1 $^2A_2$	1.51	*0.001*	1.53	*0.001*	1.26	*0.002*
1 $^2B_1$	1.68	*0.0004*	1.63	*0.002*	1.43	*0.001*
2 $^2B_1$	2.09	*0.18*	2.34	*0.320*	2.14	*0.150*
3 $^2B_1$	3.36*	*0.084*	4.73	*0.003*	3.12	*0.260*
4 $^2B_1$	4.52	*0.014*	6.26	*0.120*	4.21	*0.000*
1 $^2B_2$	1.65	*0.0000*	1.20	*0.000*	1.48	*0.000*
H-FL$^+$ C_s						
X $^1A'$	0.00		0.00		0.00	
1 $^1A'$	2.19	*0.003*	1.54	*0.001*	2.00	*0.021*
2 $^1A'$	3.55	*0.23*	2.93	*0.220*	3.26	*0.230*
3 $^1A'$	4.24	*0.003*	3.75	*0.002*	3.94	*0.004*
4 $^1A'$	4.89	*0.17*	4.54	*0.200*	4.61	*0.008*
5 $^1A'$	5.49	*0.88*	5.14	*0.930*	4.77	*0.085*

*Spin contaminated state $<S^2>$=0.9 instead 0.75. The active space in the CASPT calculations was (11,12) for **FL**$^+$ and (12, 12) in case of **H-FL**$^+$.

The three vibrational bands apparent in the spectrum are due to excitation of the ν_{21}, ν_{20} and ν_9 totally symmetric modes in the **2** $^2B_1$ excited electronic state of **FL**$^+$. The assignment given in **Table 5.4** is based on the ground state frequencies calculated at the DFT/M06-2X/ cc-pVTZ level.

The absorption spectrum recorded after a mass-selective deposition of protonated fluorenone **H-FL**$^+$, m/z=181, shows an intense band at 423.3 nm with several weaker peaks between 390 - 420 nm (red trace, **Figure 5.6**). The double headed features separated by 20-25 cm^{-1} are evident for most of the peaks. This is due to trapping of the species at energetically non-equivalent neon sites. Thereafter, the matrix was exposed to $\lambda < 260$ nm photons. All the absorption bands diminished at the same rate upon irradiation (black trace, **Figure 5.6**). This indicates that these absorptions belong to one electronic system with origin at 423.3 nm and the carrier is cationic. No new peaks appeared after irradiation.

The absorptions recorded after depositing **HFL**$^+$ do not coincide with any band of **FL**$^+$**.** The contribution of ^{13}C isotopologue of **FL** to **H**$^+$**-FL** (m/z=181) ion current was negligible with higher pressure of ethanol in the source (black trace, **Figure 5.1**).

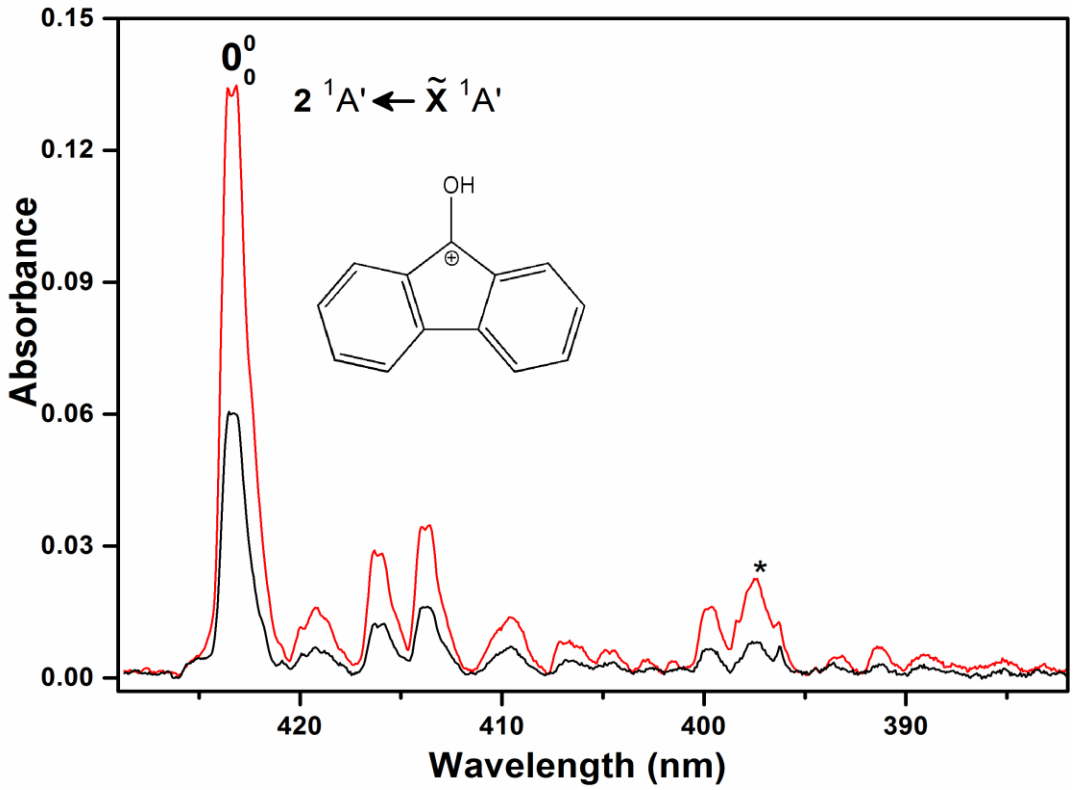

Figure 5.6: Electronic absorption spectra recorded after deposition of m/z=181 cations produced by the proton transfer reaction of $EtOH_2^+$ with 9-fluorenone in the source (red trace) and after irradiation of the matrix by $\lambda < 260$ nm photons (black trace). Asterisk marks the band of **H-FL**$^+$.

Calculations of the ground state energies of five plausible isomers of protonated fluorenone (**Chart 5.3**) indicate that structure **A**$^+$ is by far the most stable and expected to be the carrier of the 423 nm absorption system. Calculated vertical excitation energies of **A**$^+$ with TDDFT, SAC-CI and MS(6)-CASPT2(12,12) (**Table 5.5**) predict a strong **2** ^{1}A′← X ^{1}A′ electronic transition at 3.55, 2.93 and 3.26 eV respectively, and two other with energy ~4.5 and ~5.5 eV beyond the experimental detection range. Therefore the 423 nm (2.92 eV) system is assigned to the **2** ^{1}A′← X ^{1}A′ transition of **A**$^+$, fluorenone protonated on the oxygen. The resolved vibrational structure apparent in the 423 nm system of **H-FL**$^+$ is due to excitation of a number of modes in the **2** ^{1}A′ state. The assignment in **Table 5.4** is based on the calculated ground state harmonic frequencies of **H-FL**$^+$.

Table 5.6: Vertical excitation energies (eV) and oscillator strengths (italics) of **H-FL** and **H-DBT** calculated with TD DFT and SAC-CI methods.[33]

State	TD DFT		SAC-CI	
H-FL	0.00		0.00	
X ^{2}A"	2.44	*0.000*	2.47	*0.001*
1 ^{2}A"	2.89	*0.008*	3.80	*0.110*
2 ^{2}A"	3.42	*0.001*	4.29	*0.031*
3 ^{2}A"			4.83	*0.043*
H-DBT				
X ^{2}A			0.00	
1 ^{2}A	1.61	0.003	3.63	*0.035*
2 ^{2}A	3.03	0.056	4.08	*0.072*
3 ^{2}A	3.45	0.026	4.66	*0.005*
4 ^{2}A			4.86	*0.002*

After release of electrons into the matrix by UV irradiation, neutral **HFL** was not observed. The TD DFT and SAC-CI methods predict a much weaker transition for **HFL** compared to **HFL^+** (**Table 5.6**). As the neutrals are formed in the matrix by electron recombination in some percentage of the cations, the detection of a transition with such a low oscillator strength is not expected. Photofragmentation of the cation could also be another reason.

5.4.3 Dibenzotropone cation (DBT^+) and protonated dibenzotropone (H^+DBT)

Mass-selected **DBT^+** (*m/z*=206) was deposited with neon containing a trace of CH_3Cl as scavenger. Two absorption systems were observed commencing at 472.2 nm and 896.4 nm (**Figure 5.7**, red trace). The 472 nm system decreased upon UV irradiation (black trace, right section) while the 896 nm one gained in intensity (black trace, left section). Thus, the former belongs to a cation, most likely **DBT^+**, whereas the latter behaves in a way typical of a molecular fragment. The 896 nm absorption system is that of phenanthrene cation **PH^+**; the spectrum of the mass-selected **PH^+** is shown in green trace of **Figure 5.7**. Thus, **DBT^+** fragments to **PH^+** and CO during deposition. **DBT^+** is also photochemically unstable as it produced **PH^+** upon UV irradiation. Release of CO from trapped ketones in a neon matrix upon UV exposure has been observed previously in **Chapter 4** (section 4.3.1).

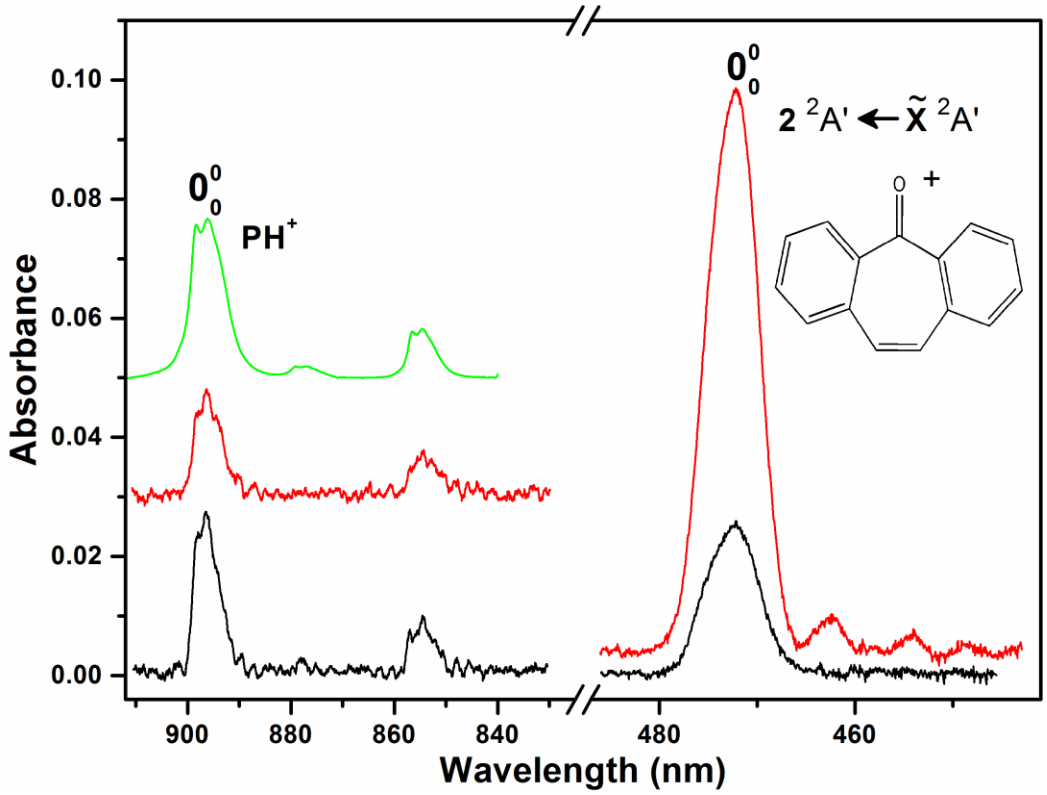

Figure 5.6: Electronic absorption spectra recorded after deposition of 2,3,6,7-dibenzotropone **DBT**$^+$ into a neon matrix (red trace) and after photobleaching with UV photons, $\lambda <$ 260 nm (black trace). Green trace shows the spectrum obtained after deposition of phenanthrene cation **PH**$^+$.

DBT has been studied by photoelectron (PE) spectroscopy and semiempirical calculations indicated that the ground state of **DBT**$^+$ has $^2B_1$ symmetry.[22] In the PE spectrum, a band lying at 2.64 eV above the ground state of the cation is present. This energy is close to the 472 nm (2.63 eV) system observed in a neon matrix after deposition of **DBT**$^+$. Optimization of the ground state geometry revealed that the cation as well as neutral molecule have a saddle point at C_{2v} symmetry and a real minimum at C_s. Nevertheless the C_{2v} coordinates were used for the vertical excitation energy calculations. TD DFT, SAC-CI and MS(5)-CASPT2, all predict a strong **2** $^2A_2 \leftarrow$ X $^2B_1$ transition with energy 1.86 -2.03 eV (f= 0.12-0.26). As no absorption was detected in the near infrared region, the calculated vertical energy and/or the oscillator strength of the **2** $^2A_2 \leftarrow$ X $^2B_1$ transition are overestimated.

The TD DFT, CASPT2 and SAC-CI indicate a moderately intense **2** $^2B_1 \leftarrow$ X $^2B_1$ transition with energy 3.15, 3.13 and 3.52 eV (**Table 5.8**), respectively; the two former methods

also gives an even stronger $3\,^2A_2 \leftarrow X\,^2B_1$ transition at 3.26 and 2.95 eV. The **3** $^2A_2$ state of **DBT**$^+$ can only be accessed from the ground state of **DBT** *via* a two photon process, therefore the state obtained at 2.64 eV by the PE study does not correspond to **3** $^2A_2$. Hence, the band present in PE spectrum of **DBT** at 2.64 eV corresponds to the $2\,^2B_1$ state of the cation and the absorption starting at 472 nm (2.63 eV) belongs to the **2** $^2B_1 \leftarrow X\,^2B_1$ electronic transition of **DBT**$^+$. The CASPT2 calculations provides the best estimate of the energy of this transition, overestimate by 0.5 eV. Vertical excitation energies calculated with the coordinates optimized at C_s symmetry give similar results (**Table 5.8**). As the **DBT**$^+$ is not planar the 472 nm system is assigned to the **2** $^2A' \leftarrow X\,^2A'$ electronic transition (corresponding to $2\,^2B_1 \leftarrow X\,^2B_1$ in higher symmetry).

Table 5.7: Absorption band maxima (±0.1nm) of electronic transitions of 2,3,6,7-dibenzotropone cation **DBT**$^+$ and protonated dibenzotropone **H-DBT**$^+$ in 6 K neon matrices and assignment based on the vibrational frequencies of the normal modes listed in the footnote.[33]

λ (nm)	ν (cm^{-1})	Δν (cm^{-1})		Assignment
DBT$^+$				
472.2	21177	0	0_0^0	**2** $^2A' \leftarrow \tilde{X}\,^2A'$
462.5	21622	445	ν_{31}	
454.1	22022	845	ν_{23} or ν_{24}	
H-DBT$^+$				
502.4	19904	0	0_0^0	**1** $^1A \leftarrow \tilde{X}\,^1A$
493.3	20272	368	ν_{67}	
474.3	21084	1180	ν_{33} or ν_{34}	
470.3	21263	1359	ν_{25}	
466.0	21459	1555	ν_{16} or ν_{17}	
371.5	26918	0	0_0^0	**2** $^1A \leftarrow \tilde{X}\,^1A$
358.1	27925	1007	ν_{43}	
353.6	28281	1363	ν_{25}	

DBT$^+$ (C_S); ν_1-ν_{37} (a'): 3237, 3224, 3214, 3212, 3200, 1791, 1660, 1621, 1592, 1533, 1468, 1406, 1352, 1273, 1206, 1195, 1190, 1124, 1076, 1059, 1029, 953, 887, 838, 819, 792, 682, 674, 589, 511, 468, 400, 318, 253, 209, 125, 44.

H$^+$**-DBT** (C_1); ν_1-ν_{75}: 3810, 3248, 3228, 3218, 3218, 3211, 3208, 3203, 3199, 3193, 3189, 1700, 1679, 1674, 1614, 1598, 1548, 1533, 1529, 1495, 1480, 1447, 1437, 1407, 1392, 1318, 1230, 1282, 1264, 1235, 1219, 1215, 1207, 1191, 1169, 1141, 1095, 1082, 1062, 1056, 1048, 1030, 1016, 941, 936, 920, 877, 862, 841, 832, 799, 782, 757, 735, 697, 687, 625, 604, 587, 579, 555, 516, 497, 478, 422, 413, 384, 331, 324, 270, 218, 195, 138, 80, 50.

The electronic spectrum of **DBT^+** is simple and consists of a strong origin band at 472.2 nm and two weaker vibrational bands lying 445, 845 cm^{-1} to the blue. The assignment is based on the calculated ground state frequencies (**Table 5.7**).

Two electronic systems starting at 502.3 and 371.5 nm were detected after mass-selected deposition of the *m/z*=207, **H-DBT^+** cations (red trace, **Figure 5.8**). Resolved vibrational structure is apparent for both electronic systems. Exposition of the matrix to $\lambda < 260$ nm photons caused a decrease in intensity for all the bands (black trace) implying cationic carrier. The rate of decrement suggests that the 502.3 and 371.5 nm absorption systems are of same **H-DBT^+** isomer.

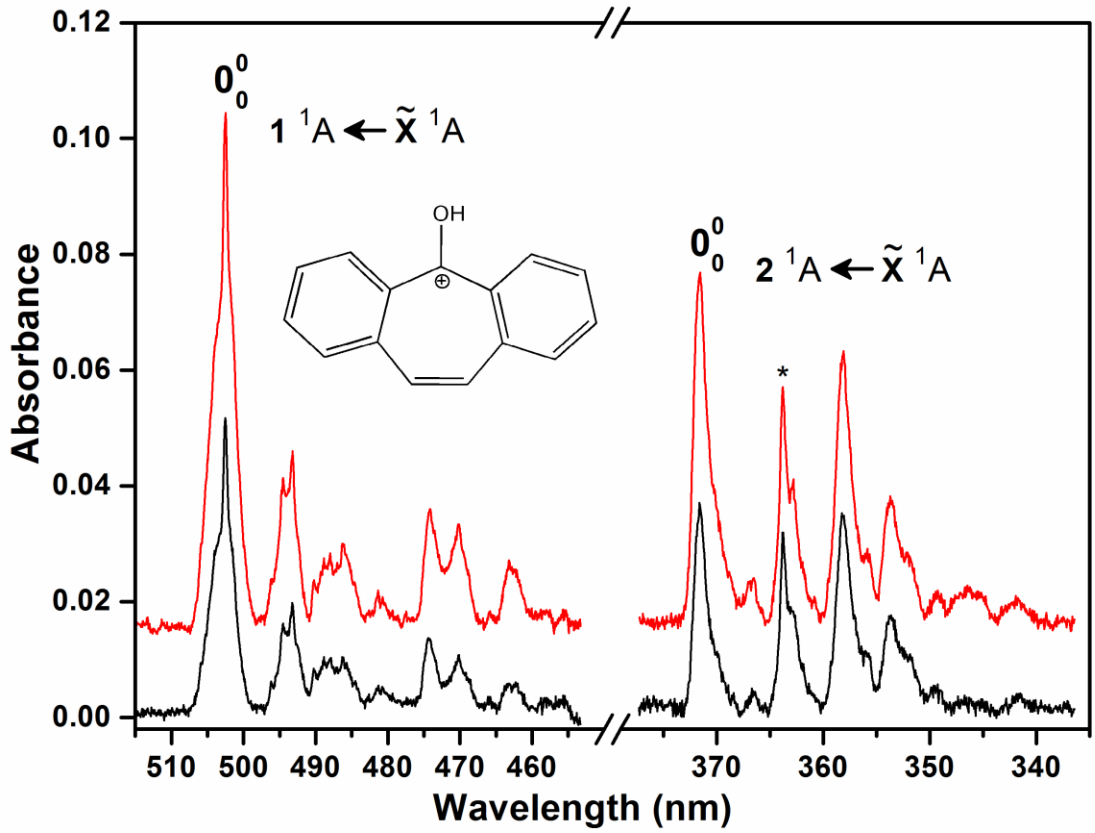

Figure 5.8: Electronic absorption spectra recorded after depositing m/z=207 cations produced by protonation of 2,3,6,7-dibenzotropone in the source using ethanol (red trace), and after irradiation of the matrix by $\lambda < 260$ nm photons (black trace).

As in the case of **H^+-FL**, protonation on the oxygen site gives the most stable isomer, **F^+** of **H^+-DBT** which is believed to be absorber. TD DFT and CASPT2 predict two ^{1}A electronic states below 4 eV, whereas SAC-CI three (**Table 5.8**). The two former methods locate a moderately intense lowest energy **1** ^{1}A ← X ^{1}A transition around 3 eV, while the later at 2.23 eV, comparable with 502 nm (2.47 eV) system. The TD DFT and CASPT2 calculations

overestimate the observed value by ~ 0.5 eV. The 502 nm system is assigned to the **1** ^{1}A ← X ^{1}A transition of **H-DBT**$^+$. According to TD DFT the transition to the **2** ^{1}A state is expected around 3.76 eV with f= 0.005, next is at 4.28 eV with f = 0.21. SAC-CI and CASPT2 give the **2** ^{1}A ← X ^{1}A transition at 3.29 eV (f=0.032) and 3.84 eV (f=0.14) respectively, which can be compared with 3.34 eV (371.5 nm) in the spectrum.

Table 5.8: Electronic states, vertical excitation energies (eV) and oscillator strengths (italics) of 2,3,6,7-dibenzotropone cation **DBT**$^+$ and protonated dibenzotropone **H-DBT**$^+$ calculated at the TD DFT/M06-2X/cc-pVTZ, SAC-CI/cc-pVDZ and MS(5)-CASPT2/cc-pVDZ level using coordinates from DFT M06-2X/cc-pVTZ.[33]

State	TD DFT		SAC-CI		CASPT2	
DBT$^+$ C_{2v}						
$\tilde{X}$ $^2B_1$	0.00		0.00		0.00	
1 $^2B_1$	1.65	*0.0013*	1.64	0.002	1.47	*0.001*
2 $^2B_1$	3.15	*0.033*	3.52	0.075	3.13	*0.017*
1 $^2A_2$	1.79	*0.0066*	1.82	*0.002*	1.53	*0.025*
2 $^2A_2$	1.86	*0.13*	2.03	*0.260*	1.92	*0.120*
3 $^2A_2$	3.26	*0.32*	5.13	*0.000*	2.95	*0.550*
1 $^2B_2$	1.77	*0.0000*	1.62	*0.000*	1.48	*0.000*
DBT$^+$ C_s						
$\tilde{X}$ $^2A'$	0.00		0.00		0.00	
1 $^2A'$	1.74	*0.0017*	1.72	*0.002*	1.50	*0.002*
2 $^2A'$	3.15	*0.038*	3.51	*0.072*	3.09	*0.013*
3 $^2A'$	4.02	*0.0002*	4.85	*0.007*	4.12	*0.020*
4 $^2A'$	4.30	*0.0014*	5.46	*0.001*	4.41	*0.005*
1 $^2A''$	1.53	*0.081*	1.40	*0.005*	1.40	*0.003*
2 $^2A''$	1.95	*0.065*	1.85	*0.034*	1.70	*0.280*
3 $^2A''$	3.34	*0.31*	2.07	*0.220*	3.28	*0.510*
4 $^2A''$	3.82	*0.0084*	4.76	*0.000*	4.19	*0.000*
5 $^2A''$	3.97	*0.0038*	5.15	*0.001*	4.73	*0.003*
6 $^2A''$	4.99	*0.0009*	5.28	*0.000*	5.04	*0.003*
H-DBT$^+$ C_1						
$\tilde{X}$ ^{1}A	0.00		0.00		0.00	
1 ^{1}A	3.06	*0.058*	2.23	*0.059*	3.01	*0.084*
2 ^{1}A	3.76	*0.005*	3.29	*0.032*	3.84	*0.140*
3 ^{1}A	4.28	*0.21*	3.67	*0.096*	4.41	*0.180*
4 ^{1}A	4.82	*1.13*	4.45	*1.430*	4.80	*1.170*
5 ^{1}A	4.88	*0.13*	4.57	*0.016*	5.05	*0.140*
6 ^{1}A	5.23	*0.055*	4.86	*0.047*	5.45	*0.003*

The active space used in CASPT2 calculations was (11,11) for **DBT**$^+$ and (10,10) for **H-DBT**$^+$.

Though no new bands were detected after neutralization of the trapped cations, the expected electronic transitions of **F** were calculated (**Table 5.6**). SAC-CI predicts two electronic

transitions at 3.63 and 4.08 eV with an intensity similar as for **H-DBT**$^{+}$. If the oscillator strengths are correct the neutral should also be detected, in contrast to the observation. Protofragmentation of the cations could be the reason for the lack of detection of **F**.

5.5 CONCLUDING REMARKS

The measurement of the gas-phase electronic spectrum of protonated fluoranthene was motivated by the confirmation of C_{60}^{+} as the carrier of two DIBs at λ963.27 and λ957.75. Other observations at 942.85 and 936.59 nm in the astronomical and laboratory spectra has given validity to this claim that gas-phase C_{60}^{+} is responsible for the absorptions with in HD 183143 along this line-of-sight.[21,32] One can speculate about how a complex molecular ion with 60 carbon atoms can be produced within such a harsh environment and have a column density on the order of 10^{13} cm^{-2}. However, if skeleton structures are available for a basis, the formation of C_{60} and C_{60}^{+} may increase the abundance of these carbonaceous species, while that of sub-units are depleted. In view of the astrophysical relevance, protonated fluoranthene could be considered as a building block of fullerene production in the ISM. The origin band maximum of the **2** ^{1}A' ← X ^{1}A' system lies at 559.3 nm and the strongest electronic transition **3** ^{1}A' ← X ^{1}A' is detected at 476.3 nm.

The studied O-PAH class of molecules are astrobiologically interesting as they have been found in lipids, vitamins, pigment and are involved in electron transport. Aromatic ketones are also present in plants, fungi, lichens. Identification of 9-fluorenone in Murchison meteorite suggests that such aromatic ketones can be present on cosmic ices; ice photolysis in astronomical environments is believed to be the leading chemical process for the formation of the oxidized PAHs. They may also be found in the gas-phase because complex organics detected in the ISM are thought to be formed in cold grain surfaces and thereafter delivered into gas-phase through ablation by shock waves or heating from stars/supernova. This work provides spectroscopic data on the protonated fluoranthene and O-PAHs systems in inert neon matrices at 6 K and is a starting point for their gas-phase studies and astrophysical findings.

BIBLIOGRAPHY

[1] L. J. Allamandola, D.J. Hudgins and S.A. Sandford, *Astrophys. J.* **1999,** *511*, L115.

[2] L. J. Allamandola, S.A. Sandford, and B. Wopenka, *Science* **1987,** *237*, 56.

[3] M. K. Crawford, A. G. G. M. Tielens, L. J.Allamandola, *Astrophys. J.* **1985**, *293*, L45.

[4] T. Onaka, I. Yamamura, T. Tanabe, T. L. Roellig and L. Yuen, *PASJ* **1996**, *48*, L59.

[5] J. Kahanpää, K. Mattila, K. Lehtinen, C. Leinert and D. Lemke, *Astron. & Astrophys.* **2003**, *405*, 999.

[6] I. Sakon, T. Onaka, D. Ishihara, T. Ootsubo, I.Yamamura, T. Tanabé, and T. L. Roellig, *Astrophys. J.* **2004**, *609*, 203.

[7] M. P. Bernstein, J. E. Elsila, J. P. Dworkin, S. A. Sandford, L. J. Allamandola and R. N. Zare, *Astrophys. J.* **2002**, *576*, 1115.

[8] S. F. M. Ashbourn, J. E. Elsila, J. P. Dworkin, M. P. Bernstein, S. A. Sandford and L. J. Allamandola, *Meteorit. Planet. Sci*. **2007**, *42*, 2035.

[9] E. E. Hardegree-Ullman, M. S. Gudipati, A. C. A. Boogert, H. Lignell, L. J. Allamandola, K. R. Stapelfeldt and M. Werner, *Astrophys. J.* **2014**, *784*, 172.

[10] M. P. Bernstein, S. A. Sandford, L. J. Allamandola, J. S. Gillette, S. J. Clemett and R. N. Zare, *Science* **1999**, *283*, 1135.

[11] M. P. Bernstein, S. A. Sandford, A. L. Mattioda and L. J. Allamandola, *Astrophys. J*. **2007**, *664*, 1264.

[12] J. Bouwman, H. M. Cuppen, A. Bakker, L. J. Allamandola and H. Linnartz, *Astron. Astrophys.* **2010**, *511*, A33.

[13] P. J. Sarre, *J. Mol. Spectrosc*. **2006**, *238*, 1.

[14] M. E. Jacox, *Chem. Soc. Rev.* **2002**, *31*, 108.

[15] A. Nagy, I. Garkusha, J. Fulara and J. P. Maier, *Phys. Chem. Chem. Phys.* **2013**, *15*, 19091.

[16] R. Wester, *J. Phys. Chem. B* **2009**, *42*, 154001.

[17] M. E. Jacox, *Res. Chem. Intermediat.* **1978**, *2*, 1.

[18] J. P. Maier, *J. Phys. Chem. A* **1998**, *102*, 3462.

[19] A. B. Fialkov, *Prog. Energy Combust. Sci.* **1997**, *23*, 399.

[20] R. G. Harvey, *American Chemical Society:Washington, D.C.*, **1985**.

[21] E. K. Campbell, M. Holz, D. Gerlich and J. P. Maier, *Nature* **2015**, *523*, 322.

[22] M. Allan, E. Heilbronner and E. Kloster-Jensen, *J. Elec. Spec.* **1975**, *6*, 181.

[23] B. P. Balise, B. S. Middleditch and J. Oro, *Org. Geochem.* **1987**, *5*, 211.

[24] R.V Krishnamurthy, J. R. Cronin, S. Pizzarello and G. U. Yuen, *Geochim. Cosmochim. Acta* **1992**, *56*, 4045.

[25] G. D. Cody and C. M. Alexander, *Geochim. Cosmochim. Acta* **2005**, *69*, 1085.

[26] A. L. Knecht , B. C. Goodale , L. Truong, M. T. Simonich, A. J. Swanson, M. M. Matzke, K. A. Anderson, K. M. Waters and R. L. Tanguay, *YTAAP* **2013**, *271*, 266.

[27] J. Konig, E. Balfanz, W. Funcke and T. Romanowsk, *Anal. Chem.* **1983**, *55*, 599.

[28] I. Garkusha, J. Fulara, P. J. Sarre and J. P. Maier, *J. Phys. Chem. A* **2011**, *115*, 10972.

[29] A. I. Adeogun, N. W. Odozi, N. O. Obiegbedi and O. S. Bello, *African J. Biotech.* **2008**, *7*, 2736.

[30] K. K. Ding and C. P. Pan, *Crystallography Reports* **2013**, *58*, 604.

[31] G. Centineo, I. Fragala, G. Bruno and S. Spampinato, *J. Mol. Struct.* **1978**, *44*, 203.

[32] G. A. H. Walker, D. A. Bohlender, J. P. Maier and E. K. Campbell, *Astrophys. J.* **2015**, *12*, L8.

[33] A. Chakraborty, J. Fulara and J. P. Maier, *J. Chem. Phys.* **2015**, *143*, 084312.

Chapter 6

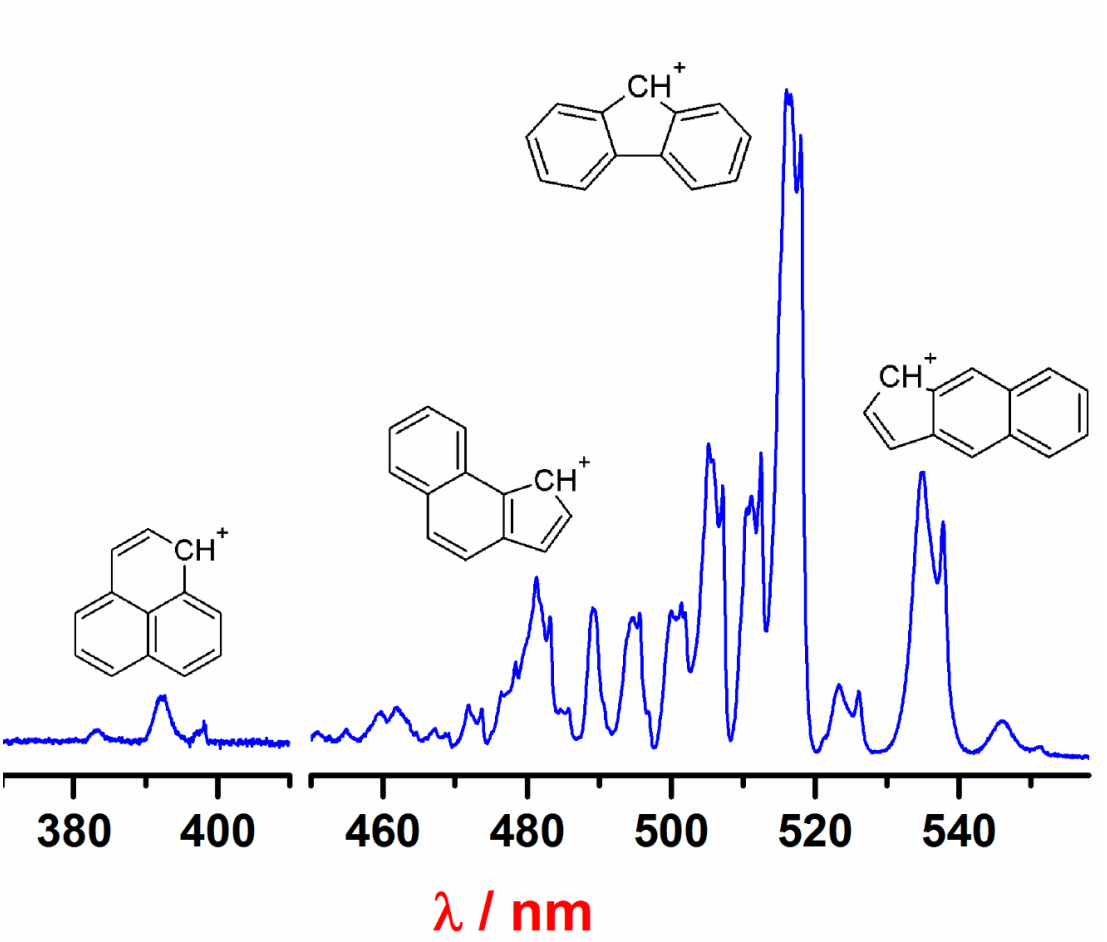

ABSORPTION OF ORGANIC REACTION INTERMEDIATES: PRODUCED IN ELECTRICAL DISCHARGE

6

Three vibrationally resolved absorption systems commencing at 538, 518 and 392 nm have been detected in a 6 K neon matrix after mass-selected deposition of $C_{13}H_9^+$ (m/z = 165) produced from fluorene in a hot cathode discharge ion source. Benz[f]indenylium (**BfI$^+$:** 538 nm**),** fluorenylium (**FL9$^+$:** 518 nm) and phenalenylium (**PHL$^+$:** 392 nm) cation are the absorbers. Two electronic systems of neutral species at 490 and 546 nm are apparent after irradiation of the matrix by $\lambda < 260$ nm photons and assigned to **FL9** and **BfI** radicals, respectively. The strongest peak at 518 nm is the origin of the **2** $^1B_2 \leftarrow X\ ^1A_1$ absorption of **FL9$^+$** and 490 nm is the origin of **2** $^2A_2 \leftarrow X\ ^2B_1$ transition of **FL9**. The systems commencing at 538 nm 546 nm are assigned to the **1** $^1A_1 \leftarrow X\ ^1A_1$ and **1** $^2A_2 \leftarrow X\ ^2A_2$ transitions of **BfI$^+$** and **BfI**. The 392 nm system is the **1** $^1E' \leftarrow X\ ^1A_1'$ transition of **PHL$^+$**. The electronic spectra of $C_{13}H_9^{+/0}$ are assigned on basis of vertical excitation energies calculated with SAC-CI and MS-CASPT2 methods. The vibrational analysis supports the structural assignments.

6.1 INTRODUCTION

The spectroscopic investigation of fluorenylium **FL9**$^+$, a text book example of an anti-aromatic carbenium ion, has been a standing goal in physical organic chemistry. Some information has been obtained on **FL9**$^+$ *via* photolysis of 9-hydroxyfluorene (**9-OH-FL**) in a H_2O/CH_3OH solution. A broad transient absorption identified around 515 nm was assigned to **FL9**$^+$,[1,2] in agreement with previous studies such as photolysis of **9-OH-FL** within metal zeolites,[3] and 9-diazafluorene (**9-DAFL**) in CH_3OH.[4] Recently, investigation of photochemical products of **9-DAFL** in amorphous water ice in the infrared and optical domain confirmed that the broad absorption at 515 nm originates from **FL9**$^+$.[5]

FL9$^-$ anion was the focus of gas-phase photoelectron studies which provided vibrational frequencies in the ground and the first excited state of neutral **FL9**.[6,7] This radical produced by electron bombardment and UV photolysis of fluorene trapped in solid argon has also been studied by infrared, Raman and UV/visible spectroscopies.[8,9] The bands observed in the vibrational spectra were attributed to specific modes of **FL9** on the basis of calculated ground-state frequencies. Electronic absorptions apparent in an argon matrix starting at 494.6 nm were assigned to the **1** $^2A_2 \leftarrow X\ ^2B_2$ system of **FL9**.[9]

Spectroscopic knowledge of another reactive intermediate, phenalenylium **PHL**$^+$, is almost unexplored. A weak absorption obtained after γ-radiolysis of 7,7a-dihydro-6b H-cycloprop[a]acenaphth-yleneothere in a freon matrix was tentatively assigned to **PHL**$^+$.[10] NMR studies have established its D_{3h} structure.[11] The corresponding neutral, phenalenyl radical **PHL**, is a resonance-stabilized species with a doublet ground-state. In solutions **PHL** dimerizes spontaneously forming σ and π associates. **PHL** has been characterized in frozen n-pentane by an emission feature[12] and in the gas-phase by resonant ionization spectroscopy.[13]

Despite these studies, structured optical spectra of **FL9**$^+$ and **PHL**$^+$ have not been obtained. It is achieved in the present work; electronic spectra of **PHL**$^+$, **FL9**$^+$, **BfI**$^+$ and the corresponding radicals have been recorded *via* mass-selected $C_{13}H_9^+$ deposition into a 6 K neon matrix.

6.2 PRODUCTION OF $C_{13}H_9^+$

Fluorene and a mixture of naphthalene and propyne have been used as precursors for the production of $C_{13}H_9^+$ species. H abstraction by the ionization of fluorene generated the mass 165. The same species was generated via the electron impact induced chemistry in a mixture of naphthalene and propyne.

6.3 RESULTS AND DISCUSSIONS

Electronic absorption spectra measured after mass–selected deposition of $m/z = 165$ cations in solid neon are shown in **Figure 6.1**, blue trace. The spectra obtained after irradiation of the matrix with $\lambda < 260$ nm photons are in red. A small amount 0.003% of CH_3Cl was added to neon; CH_3Cl reduces the space charge and suppresses neutralization of the cations during matrix growth. All absorptions in the blue trace except the two at 490 and 546 nm diminished upon exposure to UV photons. This suggests a cationic nature of the carrier(s). The relative decrement of band intensities establishes the presence of three electronic systems with distinct vibrational progressions starting at 537.8, 518.2 and 392.4 nm (**Table 6.1**). The strongest absorption is at 518 nm. These absorption systems are due to three isomers of $C_{13}H_9^+$.

A multiplet band profiles are seen for the 537.8, 518.2 nm systems. In case of the 538 nm absorptions, these doublets, one narrower and other component broader, are separated by 101 cm^{-1}. The bands of the 518 nm system are triplets spaced by *ca.* 50 and 25 cm^{-1}. These features correspond to molecules trapped at energetically different matrix sites.

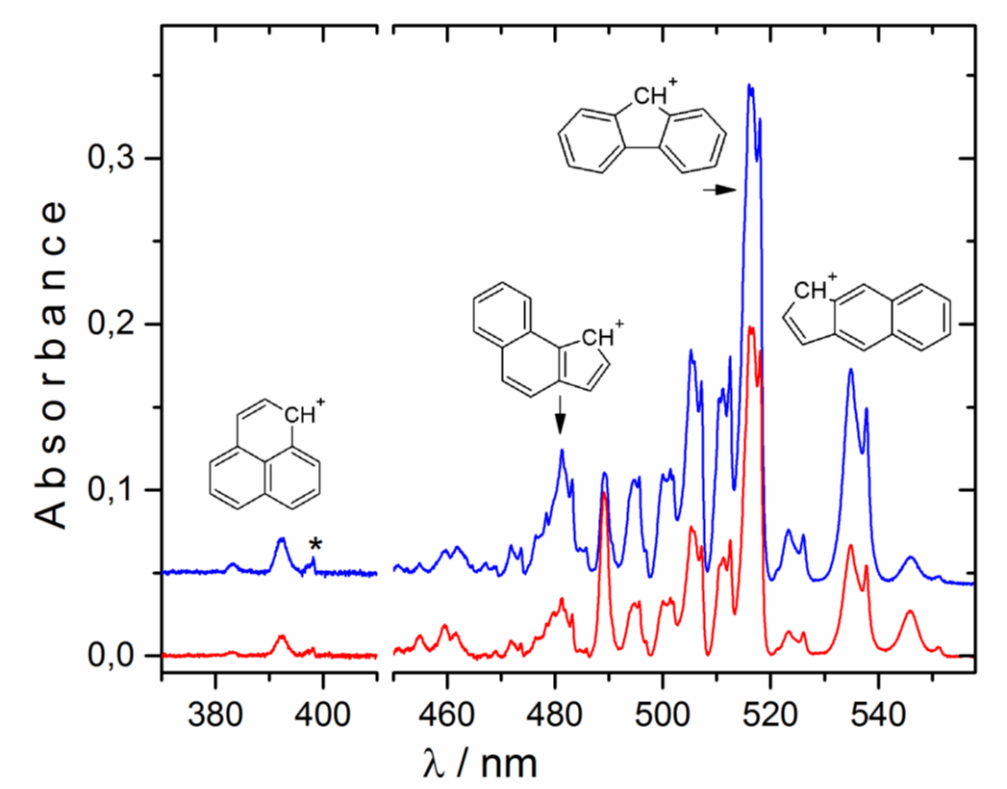

Figure 6.1: Electronic absorption spectra in a 6 K neon matrix recorded after mass-selected deposition of $C_{13}H_9^+$ cations produced from fluorene in a hot cathode discharge source (blue trace) and after irradiation with $\lambda < 260$ nm photons (red trace). Transition of N_2^+ is denoted by asterisk.

The $C_{13}H_9^+$ ion was then produced in the source from a mixture of naphthalene and propyne. The spectra obtained after deposition are shown in the blue trace of **Figure 6.2** and after irradiation of the matrix ($\lambda < 260$ nm) in red. All the electronic systems detected previously are evident, however, a difference in relative intensities to that in **Figure 6.1** experiment is apparent. The 392 and 518 nm bands are comparable using the naphthalene–propyne precursor, but from fluorene the 392 nm band is almost 15 times weaker than the 518 nm one. This implies that the 392 nm absorption is due to another structure of $C_{13}H_9^+$ and the mixture of naphthalene and propyne favors the formation of this isomer.

A broad feature at 515 nm obtained *via* photolysis of 9-diazafluorene in amorphous water ice was assigned to the absorption of **FL9**$^+$,[5] close to the 518 nm system detected in the present studies. The 518 nm system is the most intense absorption observed after deposition of $C_{13}H_9^+$ ions produced from fluorene and hence one can propose **FL9**$^+$ as the carrier of the 518 nm system. However, there are two other cationic origins at 538 and 392 nm and to make the structural assignment, theoretical calculations for plausible isomers of $C_{13}H_9^+$ have been carried out.

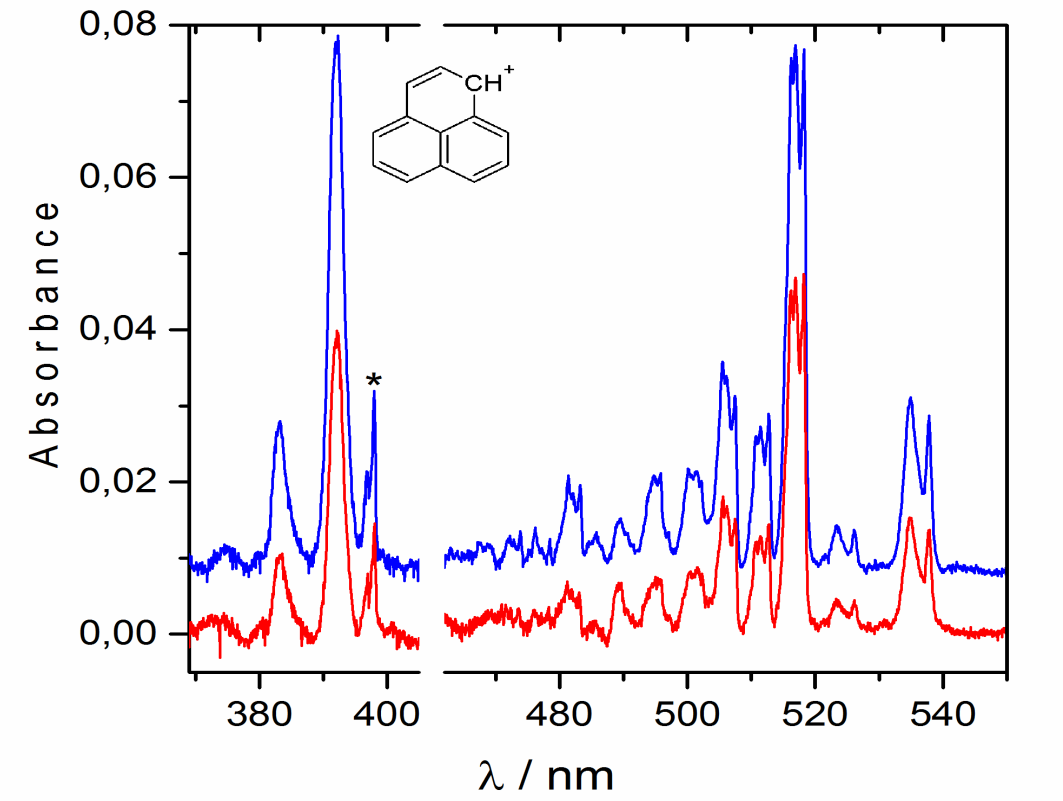

Figure 6.2: Electronic absorption spectra in a 6 K neon matrix recorded after mass-selected deposition of $C_{13}H_9^+$ cations produced from a mixture of naphthalene and propyne in a hot cathode discharge source (blue trace) and after irradiation with $\lambda < 260$ nm photons (red trace). Absorption of N_2^+ is denoted by asterisk.

Five isomers produced by the removal of non-equivalent hydrogens from of fluorene, **PHL**$^+$ and two benzindenyl cations **BeI**$^+$, and **BfI**$^+$ and a biphenyl like structure with one phenyl replaced with tropene were considered for the ground state optimization. Calculations were performed with the DFT method using the M06-2X functional and the cc-pVTZ basis set. These revealed that **PHL**$^+$ is the global minimum and **FL9**$^+$ lies 114 kJ/mol above it. **BeI**$^+$ and **BfI**$^+$ are less stable relative to **PHL**$^+$ by 130 and 181 kJ/mol, respectively. Other

isomers are higher energy structures by ~ 250 and 300 kJ/mol, and unlikely to be formed in the source. Structures and the relative ground-state energies of four most stable isomers are shown in **Chart 6.1**.

Chart 6.1. Names, acronyms (bold) and relative ground state energies (in kJ/mol) of four most stable isomers of $C_{13}H_9^+$ and neutral analogues (italics) calculated with DFT using the M06-2X functional and the cc-pVTZ basis set.[14]

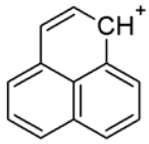

Phenalenylium

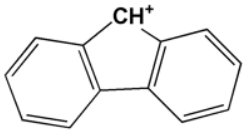

Fluorenylium

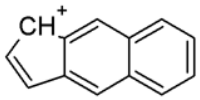

Benz[f]indenylium

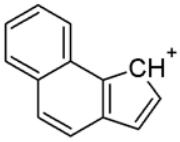

Benz[e]indenylium

PHL 0.0 *0.0*	**FL9** 113.9 *58.0*	**BfI** 129.5 *81.3*	**BeI** 181.3 *92.6*

Vertical electronic excitation energies of the four lowest energy $C_{13}H_9^+$ isomers have been calculated with symmetry adapted cluster configuration interaction (SAC-CI) and multistate multi-configurational second-order perturbation (MS-CASPT2) methods using the equilibrium coordinates obtained from the DFT optimization.

Table 6.1: Vertical excitation energies (eV) of the strongest transitions of cationic and neutral isomers of $C_{13}H_9$ calculated with the SAC-CI and MS-CASPT2 methods using coordinates obtained from the DFT/M06-2X/cc-pVTZ calculations.[14] [n.o. – not observed]

Species	Transitions	SAC-CI	CASPT2	Exp.
FL9$^+$	**2** $^1B_2 \leftarrow X\ ^1A_1$	2.34 *0.27*	2.50 *0.31*	2.39
BfI$^+$	**1** $^1A_1 \leftarrow X\ ^1A_1$	2.35 *0.26*	2.59 *0.28*	2.31
BeI$^+$	**2** $^1A' \leftarrow X\ ^1A'$	2.01 *0.12*	2.65 *0.15*	2.58
PHL$^+$	**1** $^1E' \leftarrow X^1A_1'$	*3.17 0.26*	*3.49 0.23*	3.16
FL9	**2** $^2A_2 \leftarrow X\ ^2B_1$	3.27 *0.14*	2.82 *0.011*	2.53
BfI	**1** $^2A_2 \leftarrow X\ ^2A_2$	2.92 *0.16*	2.52 *0.039*	2.27
BeI	**2** $^2A'' \leftarrow X\ ^2A''$	*2.96 0.067*	2.67 *0.010*	n.o.
	3 $^2A'' \leftarrow X\ ^2A''$	3.77 *0.048*	3.19 *0.008*	n.o.

FL9$^+$, **BeI**$^+$ and **BfI**$^+$ possess strong electronic transitions (**Table 6.1**) in the visible close to the 518 and 538 nm systems. Based on the calculations the 518 nm system is the **2** $^1B_2 \leftarrow X\ ^1A_1$ transition of **FL9**$^+$. Several vibrational features are apparent in the spectra (**Table 6.2**) and assigned with reference to the ground-state frequencies calculated with DFT.

Vibrational frequencies of **FL9**$^+$ derived from the spectrum are close to the ones observed in the ground-state of **FL9** in the photoelectron spectrum of the anion.[7]

The excitation energy calculations (**Table 6.1**) show that both **BeI**$^+$ and **BfI**$^+$ are possible candidates for the 538 nm absorption system. As **BeI**$^+$ is ~50 kJ/mol less stable than **BfI**$^+$, the 538 nm system is assigned to the **1** $^1A_1 \leftarrow X\ ^1A_1$ electronic transition of **BfI**$^+$. A weak and broad band is seen around 481 nm (**Figure 6.1**, blue trace). The 1389 and 1592 cm^{-1} vibrational progressions of **FL9**$^+$ overlap in this region, though they are not responsible for the broadness of the 481 nm band. This system is most likely an electronic transition of another isomer of $C_{13}H_9^+$. **BeI**$^+$ can be the carrier as calculations predict its most intense (f = 0.15) absorption around 465 nm (**Table 6.1**).

Table 6.2: Wavelengths of the absorption peaks (±0.1 nm) in the electronic spectra of cationic and neutral isomers of $C_{13}H_9$ trapped in 6 K neon matrices and their assignment. In the footnote are given calculated vibrational frequencies in the ground state.[14]

λ/nm	$\tilde{\nu}$/cm^{-1}	$\Delta\tilde{\nu}$/cm^{-1}	assignment	
9FL$^+$				
518.2	19298	0	0_0^0	**2** $^1B_2 \leftarrow X\ ^1A_1$
512.8	19501	203	21_0^1	
507.4	19708	410	20_0^1	
502.3	19908	610	19_0^1	
495.9	20165	867	17_0^1	
486.0	20576	1278	12_0^1	
483.4	20687	1389	10_0^1	
478.7	20890	1592	7_0^1	
474.0	21097	1799	$7_0^1 21_0^1$	
469.1	21317	2019	$7_0^1 20_0^1$	
451.3	22158	2860	$7_0^1 12_0^1$	
9FL				
489.5	20429	0	0_0^0	**2** $^2A_2 \leftarrow X\ ^2B_1$

484.4	20644	215	21_0^1	
479.6	20851	422	20_0^1	
474.7	21066	637	19_0^1	
472.3	21173	744	18_0^1	
469.8	21286	857	17_0^1	
461.8	21654	1225	12_0^1	
459.9	21744	1315	11_0^1	
455.2	21968	1539	8_0^1	

BfI$^+$

537.8	18594	0	0_0^0	**1** $^1A_1 \leftarrow X\ ^1A_1$
526.2	19004	410	21_0^1	
501.8	19928	1334	11_0^1	
4972	20113	1519	8_0^1	

BfI

546.3	18305	0	0_0^0	**1** $^2A_2 \leftarrow X\ ^2A_2$
534.0	18727	422	21_0^1	
507.3	19712	1407	10_0^1	
505.0	19802	1497	8_0^1	

BeI$^+$

481.0	20790	0	0_0^0	**2** $^1A' \leftarrow X\ ^1A'$

PHL$^+$

392.4	25484	0	0_0^0	**1** $^1E' \leftarrow X\ ^1A_1'$
383.4	26082	598	5_0^1	

9FL$^+$ a_1; ν_1- ν_{21}: 3238, 3228, 3224, 3212,3197, 1692, 1653, 1554,1501, 1443,1329,1312, 1210, 1202, 1121, 1045, 887, 753, 656, 426, 217
9FL a_1; ν_1- ν_{21}: 3225, 3213, 3202, 3195, 3179, 1664, 1639, 1526, 1476, 1389, 1324, 1275, 1221, 1176, 1127, 1051, 890, 760, 655, 429, 213
BfI$^+$ a_1; ν_1- ν_{21}: 3257, 3236, 3221, 3193, 3190, 1695, 1630, 1540, 1496, 1452, 1353, 1276, 1220, 1195, 1101, 1076, 879, 817, 755, 618, 422,
BfI a_1; ν_1- ν_{21}: 3247, 3223, 3207, 3177, 3175, 1659, 1571, 1493, 1485, 1424, 1389, 1244, 1194, 1172, 1089, 1061, 874, 821 , 761, 624 ,424; **PHL$^+$** a_1'; ν_1- ν_5: 3195, 1587, 1132, 793, 639.

The calculated vertical excitation energies (**Table 6.1**) establish that the strong absorption at 392 nm obtained from a naphthalene-propyne mixture is that of phenalenyl cation **PHL**$^+$ (**Figure 6.2**). SAC-CI and CASPT2 predict a strong **1** ^{1}E' ← X ^{1}A$_1$' electronic transition at 3.17 and 3.49 eV, respectively, in agreement with the observation at 3.16 eV (392 nm). The **PHL**$^+$ spectrum consists of one weak vibrational band 598 cm^{-1} blue of the origin, the excitation of the ν_5 totally symmetric vibration in the **1** ^{1}E' state.

Although the gas-phase investigation of **PHL** reported an electronic absorption at ~510 nm,[13] no neutral band observed around this wavelength in the present study. This implies that the oscillator strength of the visible transition of **PHL** is much weaker than the **1** ^{1}E'←X^{1}A$_1$' one of **PHL**$^+$.

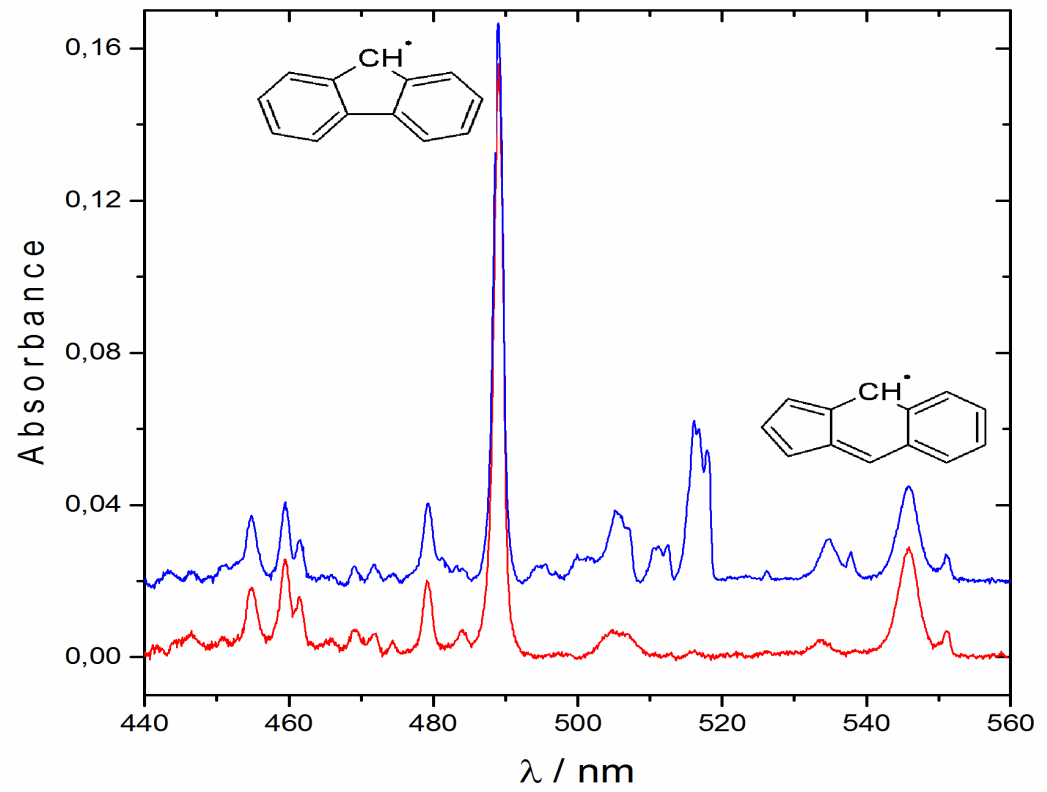

Figure 6.3: Electronic absorption spectrum measured after mass-selected deposition of $C_{13}H_9^+$ from fluorene in a pure neon matrix at 6 K is the blue trace. The red trace was obtained after irradiation with $\lambda < 260$ nm photons.

$C_{13}H_9^+$ ions produced from fluorene were also deposited in a pure neon matrix. The spectrum recorded after the deposition is shown in **Figure 6.3** (blue trace) and after UV irradiation of the matrix in red. Two absorption systems of neutral $C_{13}H_9$ commencing at 546 and 490 nm dominate the spectrum. The absence of scavenger in the matrix enhances neutralization

of cations, hence signals of the neutrals dominate. One can presume that the strongest absorption in **Figure 6.3** with onset at 490 nm originates from **FL9**, because $\mathbf{FL9}^+$ is predominately produced from the fluorene precursor. The wavelength of the origin peak of **FL9** in a neon matrix is close to the previously observed 494.6 nm band in UV photolysis of fluorene in an argon matrix.[8,9] The SAC-CI and CASPT2 calculations predict intense **2** $^2A_2 \leftarrow X\ ^2B_1$ electronic transition at 3.27 and 2.87 eV (**Tables 6.1**) which can be compared with 2.53 eV (489.5 nm) derived from **Figure 6.3**. The peaks in this system are the result of the excitation of vibrational modes in the **2** $^2A_2$ state (**Table 6.2**).

The weaker 546 nm electronic system is assigned to the radical **BfI**, the corresponding cation is second most stable structure after $\mathbf{FL9}^+$ according to calculation. The SAC-CI and CASPT2 calculations overestimate the **1** $^2A_2 \leftarrow X\ ^2A_2$ excitation energy of **BfI** by 0.65 and 0.25 eV, respectively (**Table 6.1**).

6.4 Concluding Remarks

Mass–selection in combination with quantum chemical calculations allowed an unambiguous characterization of $C_{13}H_9^{0/+}$ species. In situ detection of intermediates helps to understand the plausible pathway of chemical reactions and with this concern, the presented data may enable the identification of the transient $C_{13}H_9^{0/+}$ organics *via* their electronic spectra. This electronic characterization in 6 K neon matrices is the starting point for gas-phase spectroscopy.

BIBLIOGRAPHY

[1] S. L. Mecklenburg and E. F. Hilinski, *J. Am. Chem. Soc.* **1989**, *111*, 5471.

[2] R. A. McClelland, N. Mathivanan and S. Steenken, *J. Am. Chem. Soc.* **1990**, *112*, 4857.

[3] M. A. O'Neill, F. L. Cozens and N. P. Schepp, *Tetrahedron* **2000**, *56*, 6969.

[4] J. Wang, J. Kubicki, E. F. Hilinski, S. L. Mecklenburg, T. L. Gustafson and M. S. Platz, *J. Am. Chem. Soc.* **2007**, *129*, 13683.

[5] P. Costa, I. Trosien, M. Fernandez-Oliva, E. Sanchez-Garcia and W. Sander, *Angew. Chem. Int. Ed.* **2015**, *54*, 2656.

[6] B. Römer, Gordon A. Janaway and J. I. Brauman, *J. Am. Chem. Soc.* **1997,** *119,* 2249.

[7] J. B. Kim, M. L. Weichman, T. I. Yacovitch, C. Shih and D. M. Neumark, *J. Chem. Phys.* **2013**, *139,* 104301.

[8] J. Szczepanski, J. Banisaukas, M. Vala, S. Hirata, R. J. Bartlett and M. Head-Gordon, *J. Phys. Chem. A* **2002,** *106,* 63.

[9] J. Szczepanski, J. Banisaukas, M. Vala, S. Hirata and W. R. Wiley, *J. Phys. Chem. A* **2002,** *106,* 6935.

[10] T. Bally, Z. Zhu, J. Wirz, M. Fülscher and J.-Y. Hasegawa *J. Chem. Soc*., *Perkin Trans. 2* **2000**, 2311.

[11] D. Small, S. V. Rosokha, J. K. Kochi and M. Head-Gordon, *J. Phys. Chem. A* **2005,** *109,* 11261.

[12] W. P. Cofino , S. M. van Dam , D. A. Kamminga , G.Ph. Hoornweg, C. Gooijer , C. MacLean and N. H. Velthorst, *Mol. Phys.* **1984**, *51*, 537.

[13] G. D. O'Connor, T. P. Troy, D. A. Roberts, N. Chalyavi, B. Fückel, M. J. Crossley, K. Nauta, J. F. Stanton and T. W. Schmidt, *J. Am. Chem. Soc.* **2011**, *133*, 14554.

[14] J. Fulara, A. Chakraborty and J. P. Maier, *Angew. Chem. Int. Ed.* **2016**, *55*, 3424.

Part-C
Appendix

SIDE PROJECTS: ELECTRONIC ABSORPTIONS OF C_5H_n (*n=1,3*) CATIONS AND RADICALS

I. C_5H^+ : $1\,^1\Pi \leftarrow X\,^1\Sigma^+$ TRANSITION

Organic species with high carbon to hydrogen ratio are very important in terrestrial and extraterrestrial chemistry.[1-3] Such systems possess unique structural flexibility providing many isomers of almost similarly ground-state energy. Two cations of C5 family, C_5H^+ and $C_5H_3^+$, have drawn attention after the detection of C_5H IRC +10216 and TMC-1 and the identification of $C_5H_3^+$ in the coma of Halley's comet.[4-6] These acyclic organics are also important in the hydrocarbon-rich atmosphere of Titan.[7]

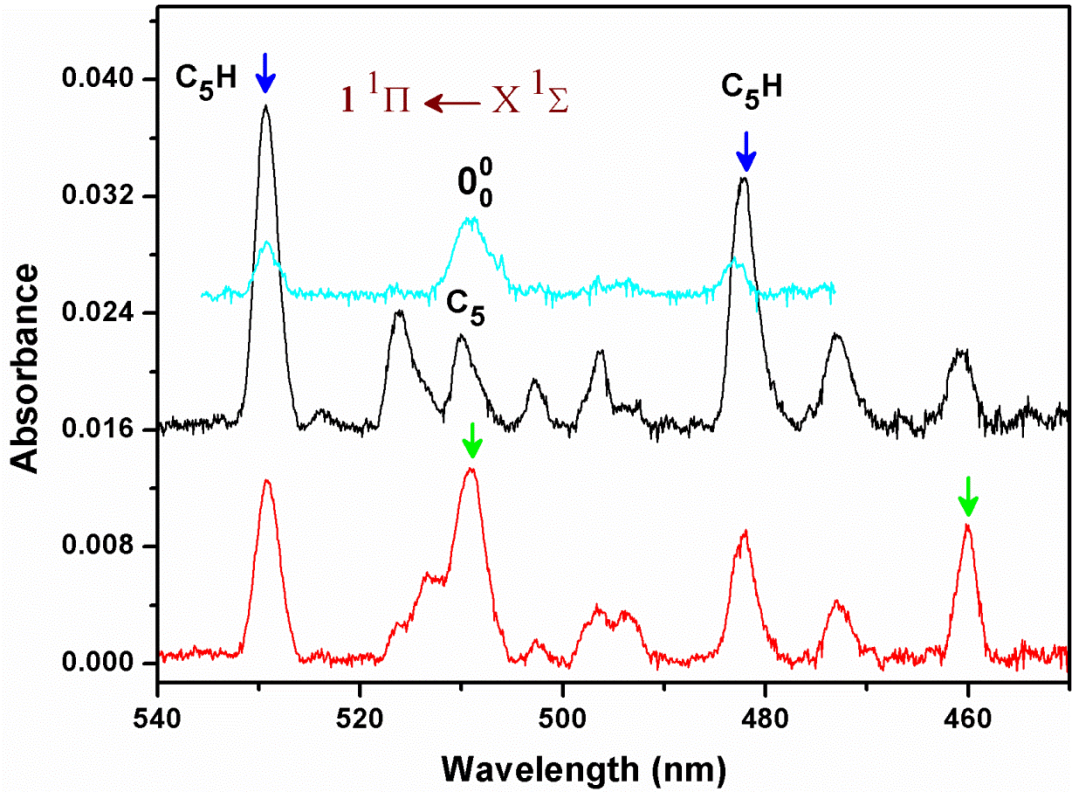

Figure I : Electronic absorption spectrum recorded after mass-selected deposition C_5H^+ produced from pentabromophenol (red trace) and after irradiation of the matrix by below 260 nm photons (black trace). The spectrum obtained after the deposition of the same species from ethynylcyclopropane is shown in light blue. The transitions of collisionally-induced fragment C_5 and the neutral counterpart of the deposited cation C_5H are assigned. The absorptions of C_5H^+ are denoted by green arrows.

Moderately intense absorptions in 450-540 nm region were recorded after mass-selected deposition of C_5H^+ (m/z=61) in solid neon produced from pentabromophenol (**Figure I, red trace**). The most prominent bands are located at 529.2, 509, 482.1 and 460.1 nm. The contribution of neutral counterpart of the deposited cation in the spectrum recorded after deposition is commonly seen in matrix experiments. Therefore, to distinguish cationic and neutral absorptions, the matrix was irradiated by $\lambda < 260$ nm photons from a high pressure mercury lamp. The justification for the UV irradiation has been thoroughly discussed in **Chapter 2** and **3**. Except these two at 509 and 460.1 nm all other band intensities increased after UV exposure (black trace). It clearly indicates that 509 and 460 nm ones are the absorption of C_5H^+ species. The rate of intensity increment for 529.2, 482.1 nm bands and the other weaker ones apparent in between 470-520 nm establishes that they are of one neutral C_5H species. The gas-phase electronic spectrum of *l*-C_5H species has already been recorded by two-color two-photon ionization technique (R2P2CI).[8] R2P2CI analysis shows two equally intense transition of *l*-C_5H at 532.2 and 485.2 nm which are comparable to 529.2 and 482.1 nm bands seen in this present study. Wavelengths are 3 nm blueshifted for both of these bands in matrix spectrum.

The relative intensity decrement for two cationic bands at 509.0 and 460.1 nm indicates that they are of one C_5H^+ isomer. An overlapping absorption of C_5 to 509 band was seen after the irradiation. The C_5 is the collisionally-induced fragment generated in the matrix during deposition of C_5H^+. Therefore, to get rid of complicacy arisen from the fragmentation, C_5H^+ has been deposited from ethynylcyclopropane, a more convenient precursor for the production of m/z=61 species. The kinetic energy of deposition was kept slightly lower around 45 eV (previous deposition was carried out at 50-52 eV). The result of lowering the deposition energy can be seen in **Figure I**, light blue trace. No absorption of C_5 was observed and the 509.0 nm one is dominant in the spectrum. As the absorptions of *l*-C_5H are apparent, therefore, *l*-C_5H^+ is inferred as the carrier of these two cationic bands at 509 and 460.1 nm. The high level MRD-CI study predicts a **1** $^1\Pi \leftarrow X\ ^1\Sigma^+$ electronic transition at energy 2.52 eV with oscillator strength (*f*) around 0.007.[9] The predicted energy is in agreement with experimental observation at 509.0 nm (2.44 eV). Thus, the 509 nm band is attributed to the **1** $^1\Pi \leftarrow X\ ^1\Sigma^+$ transition of *l*-C_5H^+ and the peak at 406.1 nm, 2032 nm blue to the origin, is due to excitation of C≡C stretching mode at **1** $^1\Pi$ state.

BIBLIOGRAPHY

[1] K-H. Homann, *Angew. Chem. Int. Ed.* **1998**, *37*, 2434.

[2] C. S. McEnally, L. D. Pfefferle, B. Atakan and K. Kohse-Hoinghaus, *Prog. Energy Combust. Sci.* **2006**, *32*, 247.

[3] K. Kohse-Hoinghaus, B. Atakan, A. Lampprecht, G. G. Alatorre, M. Kamplus, T. Kasper and N-N. Liu, *Phys. Chem. Chem. Phys.* **2002**, *4*, 2056.

[4] J. Cernicharo, C. Kahane, J. Gómez-González and M. Guélin, *Astron. Astrophys.* **1986**, *164*, L1.

[5] J. Cernicharo, M. Guélin and C. M. Walmsley, *Astron. Astrophys.* **1987**, *172*, L5.

[6] A. Korth, , F. R. Krueger, D. A. Mendis and D. L. Mitchell, Asteroids, comets, meteors III, Proceedings of a meeting: Uppsala Universitet **1990**, 373.

[7] M. G. Trainer, A. A. Pavlov † , H. L. DeWitt , J. L. Jimenez , C. P. McKay , O. B. Toon and M. A. Tolbert, PNAS **2006**, *103*, 18035**.**

[8] H. Ding, T. Pino, F. Gu ¨the, and J. P. Maier, *J. Chem. Phys.* **2002**, *117*, 8362.

[9] J. Haubrich, M. Mühlhaüser and S. D. Peyerimhoff, *J. Mol. Struct.* **2003**, *623*, 335.

II: Electronic Absorption of $C_5H_3^+$ and C_5H_3 Species

THE JOURNAL OF PHYSICAL CHEMISTRY A

Article

pubs.acs.org/JPCA

Electronic Transitions of $C_5H_3^+$ and C_5H_3: Neon Matrix and CASPT2 Studies

Jan Fulara, Arghya Chakraborty, Adam Nagy, Karol Filipkowski, and John P. Maier*

Department of Chemistry, University of Basel, Klingelbergstrasse 80, CH-4056 Basel, Switzerland

ABSTRACT: Two absorption systems of $C_5H_3^+$ starting at 350 and 345 nm were detected following mass-selective deposition of m/e = 63 ions in a 6 K neon matrix. These are assigned to the **1** $^1A_1 \leftarrow$ X $^1A_1$ electronic transition of 1,2,3,4-pentatetraenylium $H_2CCCCCH^+$ (isomer $\mathbf{B}^+$) and **1** $^1B_2 \leftarrow$ X $^1A_1$ of penta-1,4-diyne-3-ylium $HCCCHCCH^+$ ($\mathbf{C}^+$). The absorptions of neutral C_5H_3 isomers with onsets at 434.5, 398.3, 369.0, and 267.3 nm are also detected. The first two systems are assigned to the **1** $^2B_1 \leftarrow$ X $^2B_1$ and **1** $^2A_2 \leftarrow$ X $^2B_1$ transitions of isomer **B** and **C**, respectively, and the latter two to ethynylcyclopropenyl (**A**) and 3-vinylidenecyclo-prop-1-enyl (**D**) radicals. The structural assignments are based on the adiabatic excitation energies calculated with the MS-CASPT2 method. A vibrational analysis of the electronic spectra, based on the calculated harmonic frequencies, supports this.

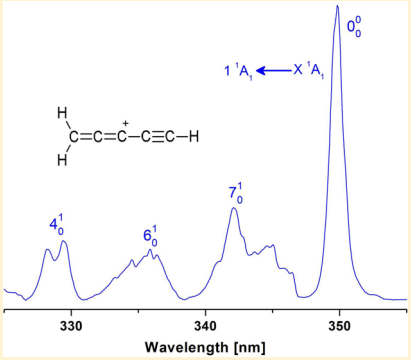

INTRODUCTION

Unsaturated organic radicals and ions are important transients in terrestrial environments such as plasmas and combustions of hydrocarbons under oxygen-deficient conditions.[1−3] They are also abundant in the interstellar medium (ISM)[4] and postulated to play a role in the hydrocarbon-rich atmosphere of Titan.[5,6] Neutral and ionic C_5H_3 are just one example among these. Furthermore, the $C_5H_3^+$ cation has been detected in the coma of comet Halley using mass spectrometry.[7]

C_5H_3 and $C_5H_3^+$ species were hitherto studied in the laboratory only by a mass spectrometric technique.[8,9,11] Unimolecular fragmentation of 1,3-pentadiyne in the A ^2E electronic state, leading to $C_5H_3^+$, was observed using a photoelectron−photoion coincidence method. The breakdown curves obtained for deuteroisotopologues of the precursor suggested that two isomers, $H_2CCCCCH^+$ and H_3CCCCC^+, were formed.[10] Different structures of $C_5H_3^+$ were deduced from reactivity studies with diacetylene.[11] Twenty five isomers of $C_5H_3^+$ have been investigated with ab initio methods to evaluate the plausible structures involved in a high-energy dissociation channel of benzene leading to $C_5H_3^+$ and CH_3 products.[12]

The formation of C_5H_3 radicals in the reaction of carbon atoms/vinylacetylene,[13] C_2/allene,[14] and C_3 with ethylene[15] in crossed molecular beams has been studied. Two isomers, 2,4-pentadiynyl-1 (structure **B**) and 1,4-pentadiynyl-3 (**C**) radicals, were identified, and the mass spectrum of the former was reported.[15] The **B** and **C** isomers of C_5H_3 were also detected in fuel-rich benzene/oxygen flames by mass analysis using synchrotron radiation for photoionization.[16,17]

The electronic spectra of some $C_{2n+1}H_3$ (n = 3−6) radicals have been obtained in the gas phase by the two-photon ionization technique.[18,19] However, no firm conclusion concerning the structure of these species was drawn, except for C_7H_3, where the 2-(buta-1,3-diynyl)cycloprop-2-yl-1ylidiene radical was identified.[18] The electronic absorption spectra of several C_7H_3 and $C_7H_3^+$ isomers have been detected in 6 K neon matrixes.[20] $C_3H_3^+$ and $C_7H_3^+$ are the only species with the general formula $C_{2n+1}H_3^+$ for which the electronic transitions are known.[20,21] In this contribution, electronic absorption spectra of several C_5H_3 and $C_5H_3^+$ molecules are presented and assigned to specific isomers on the basis of adiabatic excitation energies calculated with the CASPT2 method. The spectroscopic data derived will serve as a basis for gas-phase studies and their in situ monitoring in reactive environments.

EXPERIMENTAL SECTION

Several acyclic and cyclic molecules were used for production of the C_5H_3 cations. These precursors were methyldiacetylene, a mixture of acetylene with allene, phenylacetylene, indene, and cyclopropylacetylene, all premixed with helium buffer gas. Various neutrals and ions were formed in a hot cathode ion source. Cations were extracted, deflected by 90° to remove the uncharged species, and guided to a quadrupole mass filter (QMF). After passing the QMF, a beam of several nA of $C_5H_3^+$ was attained with mass resolution less than ±1 u. The largest current of m/z = 63 cations was obtained using methyldiacetylene. Mass-selected $C_5H_3^+$ ions were co-deposited with neon onto a rhodium-coated sapphire plate held at 6 K, forming an approximately 150 μm thick matrix over 3−5 h. A small amount of CH_3Cl was added to neon (ratio roughly about 1:30000−50000) to balance the charge. CH_3Cl is an

Special Issue: Markku Rasanen Festschrift

Received: July 4, 2014
Revised: August 29, 2014
Published: September 2, 2014

dx.doi.org/10.1021/jp506706f | J. Phys. Chem. A 2015, 119, 2338−2343

electron scavenger and traps free electrons ejected from the metal surface by impinging cations.

After growth of the matrix, electronic absorption spectra were measured in the 250−1100 nm range. A single-beam homemade spectrometer consisting of a light source (halogen and high-pressure xenon lamps), the matrix as the probe, a spectrograph, and a CCD camera, was used. Broad-band radiation was guided through the matrix, parallel to the substrate surface, and focused on a bundle of quartz fibers to illuminate the grating of a 0.3 m spectrograph. Absorption spectra were recorded with two wavelength-specific CCD cameras in several overlapping sections of 60−70 nm. Cations embedded in solid neon were neutralized with UV photons to enhance the absorptions of neutrals.

RESULTS AND DISCUSSION

Experimental Observations. The electronic spectrum obtained after deposition of mass-selected $C_5H_3^+$ cations in a 6 K neon matrix containing traces of CH_3Cl reveals strong absorptions commencing at 350 nm and weaker ones in the 250−450 nm range (blue trace, Figure 1). The strongest system

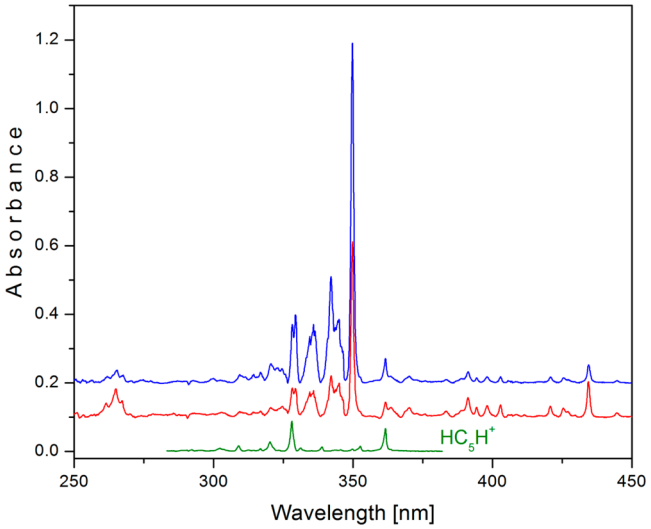

Figure 1. Overview of the electronic absorption spectra of the $C_5H_3^+/C_5H_3$ species measured after deposition of m/z = 63 cations (blue) and after neutralization of cations (red) in a 6 K neon matrix. Cations were generated in the source from methyldiacetylene. The green trace shows the spectrum of HC_5H^+ recorded previously.[22]

diminishes upon exposure of the matrix to UV radiation (> 260 nm), whereas the weak bands in the 250−450 nm region, except for the ones at 362 and 328 nm, gain intensity (red trace, Figure 1). The latter, which behave upon irradiation as the strong system, have already been identified[21] as the origin bands of the **2** $^2\Pi_g \leftarrow X\ ^2\Pi_u$ and **3** $^2\Pi_g \leftarrow X\ ^2\Pi_u$ electronic transitions of linear HC_5H^+. The absorption spectrum of HC_5H^+, scaled to the intensity of the 362 nm band in the blue trace, is shown in the bottom trace in Figure 1. HC_5H^+ is present as a result of collisionally induced fragmentation of $C_5H_3^+$ while impinging onto solid neon.

Absorptions, which diminished upon UV irradiation, originate from the $C_5H_3^+$ cations or their fragments; those that gained intensity belong to neutrals. UV photons detach electrons from Cl^- produced from the CH_3Cl electron scavenger during growth of the matrix. These migrate in solid neon and cause neutralization of cations and thus a decrease of their absorptions, whereas the ones of neutrals increase.

A close-up of the region where the absorptions of cations were detected is shown in Figure 2. The blue trace is redrawn

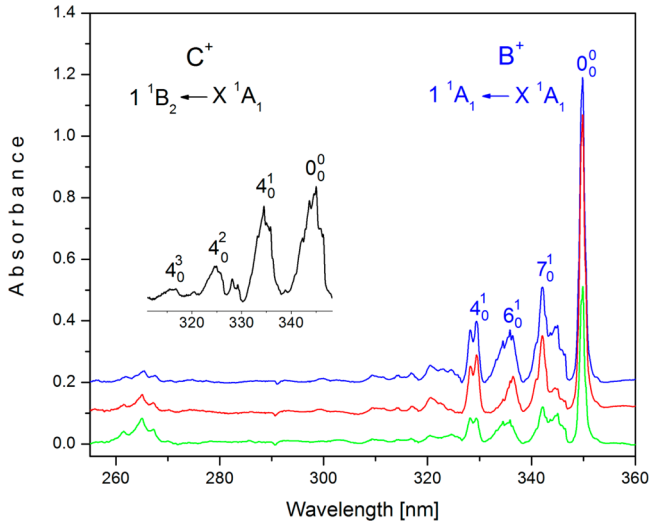

Figure 2. Absorption spectra in the UV of isomers $\mathbf{B}^+$ and $\mathbf{C}^+$ of $C_5H_3^+$ recorded in a 6 K neon matrix following deposition of m/z = 63 cations (blue), irradiation of the matrix with photons in the 260−390 nm range (red), and after subsequent irradiation with a medium-pressure mercury lamp (green). The inset shows the spectrum of $\mathbf{C}^+$ obtained by subtracting the red trace from the blue one after scaling to the intensity of the 350 nm band.

from Figure 1. The red and green traces were obtained after irradiation of the matrix with 260−390 nm photons of a high-pressure xenon lamp and subsequently with a more intense and shorter-wavelength radiation from a medium-pressure mercury lamp. Two absorption systems can be distinguished. The system starting at 350 nm remained with comparable intensity after the first irradiation, whereas the one at 345 nm was eliminated. The second irradiation caused attenuation of the 350 nm system. The two overlapping absorptions originate from two isomers of $C_5H_3^+$. A clean spectrum of the 345 nm system is shown in the inset of Figure 2 and was obtained by subtracting the red trace from the blue one after scaling to the intensity of the 350 nm band.

Irradiation with 260−390 nm photons caused a slight increase of the absorptions of neutrals in the visible region and a much larger change of the 267 nm system. More pronounced changes due to neutral C_5H_3 were observed after exposure to UV photons from a medium-pressure mercury lamp, which causes neutralization of cations. The electronic spectra of neutral C_5H_3 measured after this bleaching are presented in Figures 3 and 4. They are compared with the spectra recorded after deposition of the $C_5H_3^+$ cations.

In the visible region (Figure 3), absorption bands overlap, and the one at 434.5 nm dominates. The number of spectral features and their irregular pattern suggest that they originate from more than one species. In the UV, a medium-intensity system of neutral C_5H_3 commencing at 267 nm is apparent (left panel in Figure 4). A much weaker band at around 369 nm is due to absorbing neutrals present (red trace in Figure 1). This feature became stronger when cyclopropylacetylene was used for the production of $C_5H_3^+$ cations (right panel in

dx.doi.org/10.1021/jp506706f | J. Phys. Chem. A 2015, 119, 2338−2343

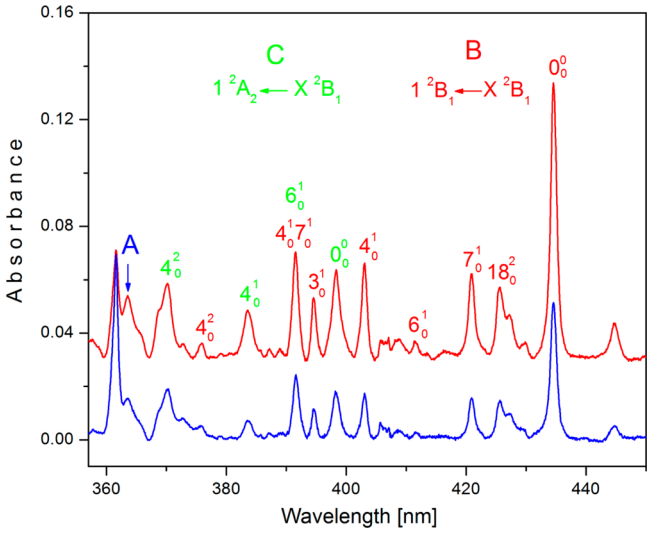

Figure 3. Visible section of the absorption spectra of the **B** and **C** isomers of C_5H_3 measured after deposition of $C_5H_3^+$ generated from methyldiacetylene (blue) and after neutralization of the cations (red).

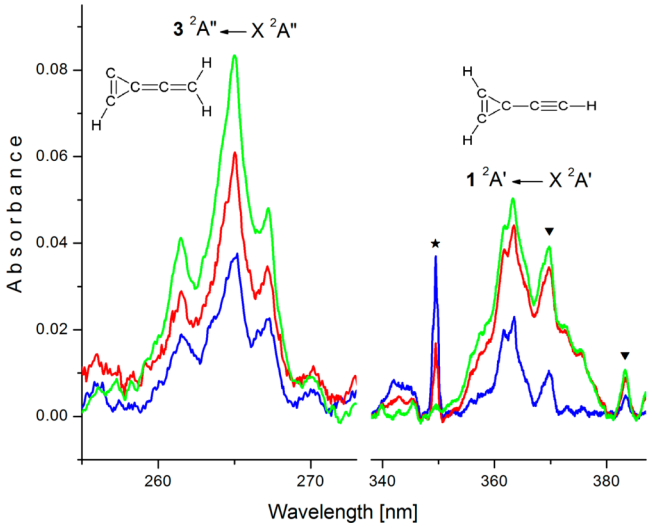

Figure 4. Absorption systems of the **A** and **D** isomers of C_5H_3 in a neon matrix. Blue traces were recorded after deposition of the cations produced from cyclopropylacetylene and methyldiacetylene, respectively. Red traces were obtained after irradiation with 260−390 nm photons. The green ones were measured after complete neutralization of cations.

Figure 4). The intensity of this band may be overestimated as the baseline may contain an undulating light background.

Use of cyclopropylacetylene as a precursor of $C_5H_3^+$ suggests that the neutral responsible for the 369 nm system retains the structure of the parent cation—an ethynyl group attached to a three-membered carbon ring. Though a number of precursors were used for generation of the $C_5H_3^+$ cations, no firm conclusion concerning their structure and of the C_5H_3 neutrals responsible for the observed absorptions could be drawn, except for the carrier of the 369 nm feature.

One can speculate on the structure of the $C_5H_3/C_5H_3^+$ species by comparing the spectra obtained with the ones of $C_7H_3/C_7H_3^+$, measured previously under similar conditions.[19] A strong, sharp absorption was detected at 441.3 nm for isomer $H_2CCCCCCCH^+$, and a weaker, broader one commencing at 414.6 nm for $HCCCHCCCCH^+$. The spectra of $C_5H_3^+$ and $C_7H_3^+$ look similar. The strongest narrow absorption lies at 350 nm, and weaker, broader ones of the other isomer are at shorter wavelengths, with an onset at 345 nm (Table 1). In view of these similarities, it is assumed that the 350 and 345 nm systems originate from similar isomers as those for $C_7H_3^+$: $H_2CCCCCH^+$ and $HCCCHCCH^+$, respectively. These belong to two homologous series, and hence the onset of the electronic transition of the smaller member lies at a shorter wavelength. The wavelength difference for the origin band of $H_2CCCCCCCH^+$ and $H_2CCCCCH^+$ is ~90 nm, close to that observed for the structurally similar series of the unsaturated hydrocarbon chain cations $HC_{2n+1}H^+$ and $H_2C_{2n}H^+$.[22,23]

Table 1. Band Maxima (±0.1 nm) and Assignment of Electronic Absorption Spectra of $C_5H_3^+$ and C_5H_3 Isomers in 6 K Neon Matrixes[a]

species	λ/nm	$\tilde{\nu}$/cm^{-1}	$\Delta\tilde{\nu}$	assignment
B$^+$	349.7	28596	0	0_0^0 **1** $^1A_1 \leftarrow X\ ^1A_1$
	342.2	29233	637	ν_7
	336.3	29735	1139	ν_6
	329.6	30349	1753	ν_4
C$^+$	345.1	28977	0	0_0^0 **1** $^1B_2 \leftarrow X\ ^1A_1$
	334.4	29904	927	ν_4
	324.9	30779	1802	$2\nu_4$
	315.8	31666	2689	$3\nu_4$
B	444.7	22487	−528	**1** $^2B_2 \leftarrow X\ ^2B_1$
	434.5	23015	0	0_0^0 **1** $^2B_1 \leftarrow X\ ^2B_1$
	427.3	23403	388	$2\nu_{12}$
	425.6	23496	481	$2\nu_{18}$
	420.9	23759	744	ν_7
	411.5	24301	1286	ν_6
	408.6	24474	1459	$2\nu_7$
	407.0	24570	1555	ν_5
	403.1	24808	1793	ν_4
	394.6	25342	2327	ν_3
	391.5	25543	2528	$\nu_7 + \nu_4$
	376.1	26589	3574	$2\nu_4$
C	398.3	25107	0	0_0^0 **1** $^2A_2 \leftarrow X\ ^2B_1$
	391.5	25543	436	ν_6
	388.9	25714	607	ν_5
	383.7	26062	955	ν_4
	370.4	26998	1891	$2\nu_4$
A	369.0	27100	0	0_0^0 **1** $^2A' \leftarrow X\ ^2A'$
D	267.3	37411	0	0_0^0 **3** $^2A'' \leftarrow X\ ^2A''$
	265.4	37679	268	ν_{12}
	261.9	38183	772	ν_{10}

[a]Frequencies of the totally symmetric vibrations (cm^{-1}) of $C_5H_3^+$ and C_5H_3 isomers were calculated with the CASPT2 method. Harmonic frequencies of the totally symmetric vibrations (cm^{-1}) of $C_5H_3^+$ and C_5H_3 isomers were calculated with the CASPT2 method. Lower-symmetry vibrations (italic), due to the program limitations, were calculated at the CAS level. **B**$^+$; **1** $^1A_1$; a1: 703, 1072, 1446, 1786, 2066, 3167, 3402; X $^1A_1$; b1: *142, 311, 607, 760, 1201*; b2: *143, 258, 468, 623, 1063*, 3375. **B**; **1** $^2B_1$; a1: 727, 1233, 1523, 1796, 2462, 3213, 3491; X; b1: *55, 173, 402. 483, 599, 689*; a2: *343*. **C**$^+$; **1** $^1B_2$; a1: 115, 519, 570, 994, 2139, 3240, 3413; b2: *350, 816, 1098, 1352, 2657, 3575*; a2: *308, 833*. **C**; **1** $^2A_2$; a1: 101, 397, 581, 988, 2040, 3245, 3502; b2: *72, 269, 504, 950, 1385, 1954, 3475*; a2: *61, 356*. **D**; X $^2A''$; a1: 205, 615, 707, 955, 980, 1082, 1292, 1414, 1727, 2227, 3164, 3294.

dx.doi.org/10.1021/jp506706f | J. Phys. Chem. A 2015, 119, 2338−2343

In recent studies[20] on $C_7H_3^+$, two neutral isomers have absorptions in the visible region. The onset of the **2** $^2B_1 \leftarrow X\ ^2B_1$ electronic transition of $H_2CCCCCCCH$ lies at 480 nm. As the strongest absorption of C_5H_3 is at 434.5 nm, it could be isomer $H_2CCCCCH$. To confirm this, excitation energies of cations and neutrals of C_5H_3 have been calculated.

Computations: Comparison with Experiment. The most plausible isomers of C_5H_3, shown in Chart 1, were chosen for ab initio calculations. The ground-state energy was obtained with the second-order Möller−Plesset perturbation method using the Gaussian 09 program suite.[24] The correlation-consistent (cc-pVDZ) basis set was used for carbon and hydrogen atoms. After geometry optimization, harmonic vibrational frequencies were calculated for the species to confirm whether the structure has a real energy minimum. The most stable structure among the eight $C_5H_3^+$ cations is isomer $\mathbf{A}^+$, ethynylcyclopropenylium. The two isomers $\mathbf{B}^+$ (1,2,3,4-pentatetraenylium) and $\mathbf{C}^+$ (penta-1,4-diyne-3-ylium), the next in energy, lie about 80 kJ/mol above $\mathbf{A}^+$. In the case of neutrals, the most stable is structure **C**, followed by **B**, **F**, and **A**.

Chart 1. Structure and Relative Ground-State Energy (kJ/mol) of Cations (bold) and Neutral Isomers (italic) of C_5H_3 Calculated with the MP2 Method Using the cc-pVDZ Basis Set

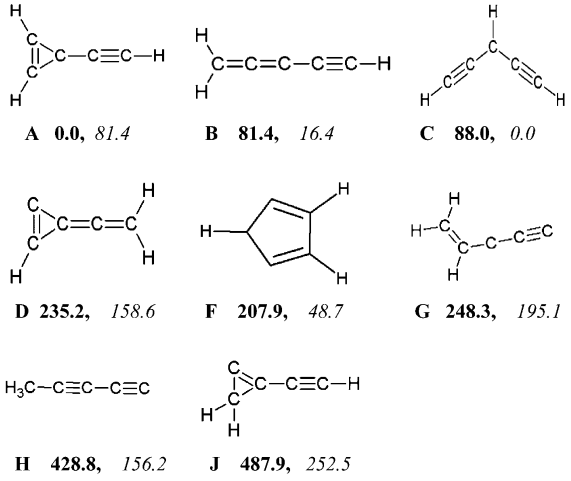

One can expect that the three lowest-energy isomers of $C_5H_3^+$ will be the main contributors to the observed absorptions. Weaker features can originate from the other ($\mathbf{D}^+$, $\mathbf{F}^+$, $\mathbf{G}^+$) cations. The important factors that affect the detection of the species via absorption are, apart from a sufficient concentration, the oscillator strength and the wavelength where the electronic transition occurs. In this study, the latter is limited to the 250−1100 nm range.

Vertical electronic excitation energies were calculated with a multireference second-order perturbation theory (CASPT2) using the MOLCAS program package.[25,26] The ground-state geometry optimized at the MP2 level was used. An active space was built from 12 electrons distributed on 12 orbitals in the case of the cations and 13 electrons on 13 orbitals for neutral C_5H_3. The orbitals were optimized for the average energy of six electronic states (multistate (MS)-CASPT2). The obtained excitation energies of the seven $C_5H_3^+$ cations together with the oscillator strengths and symmetries of the electronic states are collected in Table 2. The highest-energy isomer $\mathbf{J}^+$ was omitted from the calculations because during geometry optimization (MP2 level and C_s symmetry), a saddle point was reached. At lower symmetry, the cation rearranged to structure $\mathbf{B}^+$.

Table 2. Vertical, Adiabatic Excitation Energies (eV) and Oscillator Strengths of $C_5H_3^+$ Isomers Calculated with MS-CASPT2 (12,12) and the Absorptions in Neon Matrixes

species	transition	vert.	ad.	f	experiment
$\mathbf{A}^+$	**1** $^1A_1 \leftarrow X\ ^1A_1$	5.42	5.18	0.28	
	1 $^1B_1 \leftarrow$	5.61		0.002	
$\mathbf{B}^+$	**1** $^1A_1 \leftarrow X\ ^1A_1$	3.71	3.59	0.25	3.55
	2 $^1A_1 \leftarrow$	4.59		0.043	
	3 $^1A_1 \leftarrow$	4.96		0.006	
$\mathbf{C}^+$	**1** $^1B_2 \leftarrow X\ ^1A_1$	3.65	3.65	0.36	3.58
	1 $^1A_1 \leftarrow$	4.95		0.022	
$\mathbf{D}^+$	**1** $^1A' \leftarrow X\ ^1A'$	3.60	2.62	0.078	
	2 $^1A' \leftarrow$	5.68	4.93	0.46	
	1 $^1A'' \leftarrow$	2.68		0.001	
	3 $^1A'' \leftarrow$	5.86		0.020	
$\mathbf{F}^+$	**2** $^1A_1 \leftarrow X\ ^1A_1$	4.98		0.013	
	1 $^1B_1 \leftarrow$	5.44		0.002	
	2 $^1B_1 \leftarrow$	5.76		0.011	
	2 $^1B_2 \leftarrow$	5.65		0.008	
$\mathbf{G}^+$	**1** $^1A' \leftarrow X\ ^1A'$	3.06		0.008	
	2 $^1A' \leftarrow$	3.56	3.45	0.093	
	4 $^1A' \leftarrow$	5.22		0.11	
	2 $^1A'' \leftarrow$	3.03		0.010	
	5 $^1A'' \leftarrow$	5.92		0.012	
$\mathbf{H}^+$	**4** $^3A' \leftarrow X\ ^3A'$	3.76	3.70	0.024	
	6 $^3A' \leftarrow$	4.79		0.002	
	7 $^3A'' \leftarrow$	4.87		0.003	
	8 $^3A'' \leftarrow$	5.27		0.011	

The best candidates for the absorptions of $C_5H_3^+$ shown in Figure 2 are isomers $\mathbf{B}^+$ and $\mathbf{C}^+$. They possess strong electronic transitions at 3.71 and 3.65 eV with oscillator strengths of f = 0.25 and 0.36, respectively, close to the onsets of the 350 (3.55 eV) and 345 nm (3.58 eV) systems of $C_5H_3^+$. Calculations predict a strong f = 0.28 **1** $^1A_1 \leftarrow X\ ^1A_1$ electronic transition at around 5.42 eV for the global-minimum structure $\mathbf{A}^+$, far from the observation. The three higher-energy $C_5H_3^+$cations ($\mathbf{D}^+$, $\mathbf{G}^+$, $\mathbf{H}^+$) possess electronic transitions close to the observed systems; however, their oscillator strengths are much smaller than those of $\mathbf{B}^+$ and $\mathbf{C}^+$.

The calculations of the excitation energies were refined for the structures with transitions close to the observations. The geometries of the selected isomers were optimized in the ground and excited electronic states. The MS-CASPT2 method was used with a somewhat smaller active space (10 electrons, 10 orbitals) and the energy averaged over four electronic states. A reduction of the active space and a number of electronic states used has a minor effect on the vertical excitation energies calculated under such conditions, for example, changes from 3.71 eV for the larger space (Table 2) to 3.77 eV at the smaller one for the **1** $^1A_1$ state of $\mathbf{B}^+$.

The adiabatic excitation energies of the cations are compared with the experimental ones in Table 2. The 3.59 eV value of the **1** $^1A_1 \leftarrow X\ ^1A_1$ transition of $\mathbf{B}^+$ agrees with the 350 nm (3.55 eV) system of $C_5H_3^+$, to which it is assigned. Adiabatic and experimental energies are in good agreement for structure $\mathbf{C}^+$, 3.65 and 3.58 eV. Consequently, the 345 nm system is attributed to the **1** $^1B_2 \leftarrow X\ ^1A_1$ transition of $\mathbf{C}^+$. Corroboration comes from the vibrational analysis of the absorption systems. This is based on the calculated harmonic vibrational frequencies

dx.doi.org/10.1021/jp506706f | J. Phys. Chem. A 2015, 119, 2338−2343

(footnote Table 1) of $\mathbf{B}^+$ and $\mathbf{C}^+$ in the **1** $^1A_1$ and **1** $^1B_2$ excited states.

Because at least three absorption systems of neutral C_5H_3 starting at 434.5, 369.0, and 267.3 nm were detected in the neon matrix following the deposition and photobleaching of the m/z = 63 cations, electronic excitation energies of C_5H_3 were calculated. The results for the eight neutrals shown in Chart 1, obtained by MS-CASPT2, are compared with the experimental values in Table 3.

Table 3. Vertical, Adiabatic Excitation Energies (eV) and Oscillator Strengths of C_5H_3 Isomers Calculated with MS-CASPT2 (13,13) and the Absorptions in Neon Matrixes

species	transition	vert.	ad.	f	experiment
A	**1** $^2A' \leftarrow X\ ^2A'$	4.01	3.80	0.002	3.36
	3 $^2A' \leftarrow$	5.85	5.44	0.089	
	1 $^2A'' \leftarrow$	4.13		0.001	
B	**1** $^2B_1 \leftarrow X\ ^2B_1$	3.46	2.82	0.015	2.85
	2 $^2B_1 \leftarrow$	4.97		0.004	
	3 $^2B_1 \leftarrow$	5.39		0.002	
	4 $^2B_1 \leftarrow$	5.75	5.00	0.043	
C	**1** $^2A_2 \leftarrow X\ ^2B_1$	3.52	3.13	0.045	3.11
	1 $^2B_1 \leftarrow$	4.76		0.005	
D	**1** $^2A'' \leftarrow X\ ^2A''$	4.80		0.005	
	2 $^2A'' \leftarrow$	4.92		0.005	
	3 $^2A'' \leftarrow$	5.80	4.84	0.078	4.64
	4 $^2A' \leftarrow$	5.28		0.011	
F	**1** $^2A_2 \leftarrow X\ ^2A_2$	5.94		0.006	
	4 $^2B_1 \leftarrow$	5.08	4.45	0.033	
G	**3** $^2A'' \leftarrow X\ ^2A''$	4.46	3.78	0.003	
	5 $^2A'' \leftarrow$	5.57		0.003	
H	**2** $^2A' \leftarrow X\ ^2A'$	3.13	3.03	0.021	
	3 $^2A' \leftarrow$	4.67		0.012	
	5 $^2A' \leftarrow$	5.92		0.009	
J	**1** $^2A' \leftarrow X\ ^2A'$	2.45		0.006	
	2 $^2A' \leftarrow$	3.46		0.004	
	3 $^2A' \leftarrow$	4.67		0.002	
	3 $^2A'' \leftarrow$	3.98		0.003	
	4 $^2A'' \leftarrow$	4.52		0.001	

One can expect that some absorptions in Figures 3 and 4 originate from isomers **B** and **C** because their charged counterparts are identified. The ground state of **B** and **C** is X $^2B_1$. Calculations give the lowest-energy electronic transition to the **1** $^2B_1$ and **1** $^2A_2$ states close to each other at 3.46 and 3.52 eV, respectively. The predicted vertical excitation energy of **B** and **C** overestimates the absorption onset at 434.5 nm (2.85 eV) around 0.6 eV. Neutral **H** possesses an excitation energy closer, 3.13 eV, but is excluded from consideration because $\mathbf{H}^+$ lies 428.8 kJ/mol above $\mathbf{A}^+$ and is thus unlikely to be formed. For the same reason, isomer **J** can be excluded; in addition, its strongest transition is predicted at 2.45 eV, in disagreement with the experimental data. Therefore, structures **B** and **C** remain the best candidates for the absorption in the visible range (Figure 3).

Adiabatic excitation energies of **B** and **C**, calculated with MS-CASPT2 using a smaller active space (11 electrons on 11 orbitals) and the orbitals optimized for the average energy of four electronic states, are red shifted by 0.4−0.5 eV in comparison to the vertical ones. The adiabatic excitation energy of the **1** $^2B_1 \leftarrow X\ ^2B_1$ electronic transition of **B** (2.82 eV) agrees well with the 434.5 nm (2.85 eV) system; therefore, the absorptions are assigned to this. Similar calculations for isomer **C** provide the adiabatic excitation energy of 3.13 eV (396 nm), which identifies the **1** $^2A_2 \leftarrow X\ ^2B_1$ transition shown in Figure 3. Spectra recorded in this region using different precursors for production of $C_5H_3^+$ show a slight difference in the relative intensities of the absorption bands. Another system starts at 398.3 nm (3.11 eV), which agrees with the allowed electronic transition of **C** to the **1** $^2A_2$ state. A vibrational analysis of the 434.5 and 398.3 nm systems based on the calculated harmonic frequencies of **B** and **C** in the **1** $^2B_1$ and **1** $^2A_2$ states supports the assignment. A weak absorption at 444.7 nm belongs to isomer **B** and is interpreted as a vibronically induced transition to the **1** $^2B_2$ state. Calculations predict a vertical energy at 3.20 eV, 0.26 eV below the **1** $^2B_1$ state. A signature of state mixing is also seen in the 427 nm region, with multiple bands apparent. The wavelengths of the absorption band maxima of **B** and **C** and the assignments are summarized in Table 1.

Two weaker absorption systems of neutral C_5H_3 are also detected in the UV (Figure 4). The one with onset at 369 nm is the most intense, with cyclopropylacetylene as a precursor of the cations. This suggests that the carrier has a carbon three-membered ring motif with a hydrocarbon chain attached. Among the eight neutrals, only **A**, **D**, and **J** possess the right structure. **J** was already excluded from consideration because of the high energy of $\mathbf{J}^+$. The MS-CASPT2 calculations of the vertical excitation energies of **D** predict several electronic transitions above 4.8 eV. Calculation of the adiabatic energy of the strongest one at 5.8 eV red shift this to 4.84 eV, still ∼1.50 eV from the 369 nm system. Only **A** is a plausible candidate for this absorption. Vertical excitation energies of 4.01 eV for the **1** $^2A' \leftarrow X\ ^2A'$ transition and 3.80 eV for the adiabatic one (Table 3) are predicted. The latter overestimates the observed energy by approximately 0.4 eV. The reason for this could be that the structure of **A** is not fully optimized. The geometry of **A** differs significantly from the one of the cation, for which a planar structure was predicted, whereas **A** in the ground state adopts a nonplanar structure with the ethynyl chain ∼64° above the carbon ring plane. Because the difference between the predicted energy of the **1** $^2A' \leftarrow X\ ^2A'$ transition of **A** and the observation at 369 nm is large, the assignment remains tentative.

The best candidate for the neutral responsible for the 276 nm (4.64 eV) system is isomer **D**. The calculated vertical excitation energy of the strongest **3** $^2A'' \leftarrow X\ ^2A''$ transition is 5.80 eV, and the adiabatic value is 4.84 eV, showing a large geometry change upon excitation. The adiabatic energy is 0.2 eV larger than the observation.

CONCLUDING REMARKS

Though the electronic spectra of smaller $C_3H_3^+$ and larger $C_7H_3^+$ members of the $C_{2n+1}H_3^+$ family are known, the C_5H_3 cations and the neutrals escaped hitherto spectral characterization. The present study fills this gap for the electronic transitions of some $C_5H_3^+$ and C_5H_3 isomers.

The $C_5H_3^+$ cations were produced from several cyclic and acyclic precursors in a hot cathode ion source. The absorptions of two isomers of $C_5H_3^+$ were detected in 6 K neon matrixes in the UV range following deposition of m/z = 63 ions and are assigned to isomers $\mathbf{B}^+$ and $\mathbf{C}^+$ on the basis of the adiabatic excitation energies calculated with the CASPT2 method. The absorptions of the neutral counterparts have also been detected in the visible region after photobleaching of the cations with

dx.doi.org/10.1021/jp506706f | J. Phys. Chem. A 2015, 119, 2338−2343

UV radiation. The adiabatic excitation energies of **B** and **C** calculated at the CASPT2 level of theory agree with the observations. Apart from the absorptions of **B** and **C**, also weaker ones were detected in the UV range and are tentatively associated with structures **A** and **D**.

The spectroscopic data presented can be used as the starting point for gas-phase studies and can help in hydrocarbon combustion chemistry in oxygen-deficient environments via in situ monitoring.

AUTHOR INFORMATION

Corresponding Author

*E-mail: j.p.maier@unibas.ch. Tel.: +41 612673826. Fax: +41 612673855.

Notes

The authors declare no competing financial interest.

ACKNOWLEDGMENTS

This work is supported by the Swiss National Science Foundation (Project 200020-124349/1).

REFERENCES

(1) Homann, K.-H. Fullerenes and Soot Formation — New Pathways to Large Particles in Flames. *Angew. Chem., Int. Ed.* **1998**, *37*, 2434−2451.

(2) Kohse-Höinghaus, K.; Atakan, B.; Lamprecht, A.; Alatorre, G. G.; Kamphus, M.; Kasper, T.; Liu, N.-N. Contributions to the Investigation of Reaction Pathways in Fuel-Rich Flames. *Phys. Chem. Chem. Phys.* **2002**, *4*, 2056−2062.

(3) Hansen, N.; Kasper, T.; Klippenstein, S. J.; Westmoreland, P. R.; Law, M. E.; Taatjes, C. A.; Kohse-Höinghaus, K.; Wang, J.; Cool, T. A. Initial Steps of Aromatic Ring Formation in a Laminar Premixed Fuel-Rich Cyclopentene Flame. *J. Phys. Chem. A* **2007**, *111*, 4081−4092.

(4) McCarthy, M. C.; Thaddeus, P. Microwave and Laser Spectroscopy of Carbon Chains and Rings. *Chem. Soc. Rev.* **2001**, *30*, 177−185.

(5) Trainer, M. G.; Pavlov, A. A.; DeWitt, H. L.; Jimenez, J. L.; McKay, C. P.; Toon, O. B.; Tolbert, M. A. Organic Haze on Titan and the Early Earth. *Proc. Natl. Acad. Sci. U.S.A.* **2006**, *103*, 18035−18042.

(6) Chassefière, E.; Cabane, M. Two Formation Regions for Titan's Hazes: Indirect Clues and Possible Synthesis Mechanisms. *Planet Space Sci.* **1995**, *43*, 91−103.

(7) Korth, A.; Krueger, F. R.; Mendis, D. A.; Mitchell, D. L. Organic Ions in the Coma of Comet Halley. In *Asteroids, Comets, Meteors III. Proceedings of a meeting (AMC 89) held at the Astronomical Observatory of the Uppsala University*; Uppsala Universitet, Uppsala, Sweden, June 12−16, 1989; Lagerkvist, C. I., Rickman, H., Lindblad, B. A., Eds.; 1990; pp 373−376.

(8) Holland, D. M. P.; Shaw, D. A.; Sumner, I.; Bowler, M. A.; Mackie, R. A.; Shpinkova, L. G.; Cooper, L.; Rennie, E. E.; Parker, J. E.; Johnson, C. A. F. A Time-of-Flight Mass Spectrometry Study of the Fragmentation of Valence Shell Ionised Benzene. *Int. J. Mass Spectrom.* **2002**, *220*, 31−51.

(9) da Silva, G.; Trevitt, A. J. Chemically Activated Reactions on the C_7H_5 Energy Surface: Propargyl + Diacetylene, i-C_5H_3 + Acetylene, and n-C_5H_3 + Acetylene. *Phys. Chem. Chem. Phys.* **2011**, *13*, 8940−8952.

(10) Dannacher, J.; Heilbronner, E.; Stadelmann, J.-P.; Vogt, J. Fragmentation of Energy Selected Butadiyne- and 1,3-Pentadiyne Radical Cations. *Helv. Chim. Acta* **1979**, *62*, 2186−2201.

(11) Öztürk, F.; Moini, M.; Brill, F. W.; Eyler, J. R.; Buckley, T. J.; Lias, S. G.; Ausloos, P. J. Reactions of $C_5H_3^+$ and $C_5H_5^+$ Ions with Acetylene and Diacetylene. *J. Phys. Chem.* **1989**, *93*, 4038−4044.

(12) Mebel, A. M.; Lin, S. H.; Yang, X. M.; Lee, Y. T. Theoretical Study on the Mechanism of the Dissociation of Benzene. The C_5H_3 + CH_3 Product Channel. *J. Phys. Chem. A* **1997**, *101*, 6781−6789.

(13) Parker, D. S. N.; Zhang, F.; Kim, Y. S.; Kaiser, R. I.; Mebel, A. M. On the Formation of Resonantly Stabilized C_5H_3 Radicals — A Crossed Beam and Ab Initio Study of the Reaction of Ground State Carbon Atoms with Vinylacetylene. *J. Phys. Chem. A* **2011**, *115*, 593−601.

(14) Guo, Y.; Gu, X.; Zhang, F.; Mebel, A. M.; Kaiser, R. I. Unimolecular Decomposition of Chemically Activated Pentatetraene ($H_2CCCCCH_2$) Intermediates: A Crossed Beams Study of Dicarbon Molecule Reactions with Allene. *J. Phys. Chem. A* **2006**, *110*, 10699−10707.

(15) Gu, X.; Guo, Y.; Kaiser, R. I. Mass Spectra of the 2,4-Pentadiynylidyne (n-C_5H; X $^2\Pi$) and 2,4-Pentadiynyl-1 (n-C_5H_3; X $^2B_1$) Radicals. *Int. J. Mass Spectrom.* **2007**, *261*, 100−107.

(16) Yang, B.; Huang, C.; Wei, L.; Wang, J.; Sheng, L.; Zhang, Y.; Qi, F.; Zheng, W.; Li, W.-K. Identification of Isomeric C_5H_3 and C_5H_5 Free Radicals in Flame with Tunable Synchrotron Photoionization. *Chem. Phys. Lett.* **2006**, *423*, 321−326.

(17) Hansen, N.; Klippenstein, S. J.; Miller, J. A.; Wang, J.; Cool, T. A.; Law, M. E.; Westmoreland, P. R.; Kasper, T.; Kohse-Höinghaus, K. Identification of C_5H_x Isomers in Fuel-Rich Flames by Photoionization Mass Spectrometry and Electronic Structure Calculations. *J. Phys. Chem. A* **2006**, *110*, 4376−4388.

(18) Schmidt, T. W.; Boguslavskiy, A. E.; Pino, T.; Ding, H.; Maier, J. P. Optical Detection of C_9H_3, $C_{11}H_3$, and $C_{13}H_3$ from a Hydrocarbon Discharge Source. *Int. J. Mass Spectrom.* **2003**, *228*, 647−654.

(19) Ding, H.; Pino, T.; Güthe, F.; Maier, J. P. Isomeric Structures and Visible Electronic Spectrum of the C_7H_3 Radicals. *J. Am. Chem. Soc.* **2003**, *125*, 14626−14630.

(20) Chakraborty, A.; Fulara, J.; Dietsche, R.; Maier, J. P. Spectroscopic Characterization of $C_7H_3^+$ and $C_7H_3^\bullet$: Electronic Absorption and Fluorescence in 6 K Neon Matrices. *Phys. Chem. Chem. Phys.* **2014**, *16*, 7023−7030.

(21) Wyss, M.; Riaplov, E.; Maier, J. P Electronic and Infrared Spectra of $H_2C_3H^+$ and Cyclic $C_3H_3^+$ in Neon Matrices. *J. Chem. Phys.* **2001**, *114*, 10355−10361.

(22) Fulara, J.; Nagy, A.; Garkusha, I.; Maier, J. P. Higher Energy Electronic Transitions of $HC_{2n+1}H^+$ (n=2−7) and $HC_{2n+1}H$ (n=4−7) in Neon Matrices. *J. Chem. Phys.* **2010**, *133*, 024304/1−024304/9.

(23) Batalov, A.; Fulara, J.; Shnitko, I.; Maier, J. P. Electronic Absorption Spectra of the Protonated Polyacetylenes $H_2C_nH^+$ (n = 4, 6, 8) in Neon Matrixes. *J. Phys. Chem. A* **2006**, *110*, 10404−10408.

(24) Frisch, M. J.; Trucks, G. W.; Schlegel, H. B.; Scuseria, G. E.; Robb, M. A.; Cheeseman, J. R.; Scalmani, G.; Barone, V.; Mennucci, B.; Petersson, G. A.; et al. *Gaussian 09*, revision D.01; Gaussian, Inc.: Wallingford, CT, 2009.

(25) Andesson, K.; Malmqvist, P.-A.; Roos, B. O.; Sadlej, A. J.; Wolinski, K. Second-Order Perturbation Theory with a CASSCF Reference Function. *J. Phys. Chem.* **1990**, *94*, 5483−5488.

(26) Andesson, K.; Malmqvist, P.-A.; Roos, B. O. Second-Order Perturbation Theory with a Complete Active Space Self-Consistent Field Reference Function. *J. Chem. Phys.* **1992**, *96*, 1218−1226.

8. SUMMARY & OUTLOOK

This doctoral thesis focused on the electronic characterization of astrophysically relevant molecules in neon matrices. The unambiguous structural assignments of the detected absorption systems have been accomplished by mass-selection in a combination with theoretical calculations. Several ionic isomers are deposited in solid neon and are distinguished by calculated ground-state stabilities, computed excitation energies, and in some cases on the basis of the geometry of precursor molecules.

In order to record spectra with a high signal-to-noise ratio, adequate production of transient species is needed. Due to high reactivity, production and analysis of interstellar molecules are not experimentally trivial. In this dissertation exotic species are generated in electrical discharge from respective precursors. The essence of bi-component molecular gas mixtures for the production of complex molecules has been exemplified. The generation of O-containing hydrocarbons in an ion source was the primary challenge in their spectroscopic exploration. The 1:1 mixture of C_3O_2 and HC_4H served the role in generation of $H_2C_6O^+$. According to theory, the production of $H_2C_6O^+$ has been achieved by an exothermic reaction between HC_4H^+ and C_2O. Such reactions should be included in the astrochemical models as a mechanism of oxygen incorporation into hydrocarbon moieties.

In other experiments predominant production of dehydrogenated fluorene cation ($C_{13}H_9^+$) from fluorene or the formation of phenalenylium in a naphthalene and propyne mixture shows the precursor dependency on the relative abundance of isomers in the matrix. The greatest advantage of the MI technique is that the experimental species can be confined for long time scales to execute many spectroscopic studies. Therefore, even after 60 years of its discovery, this technique is still continuously used. MI is a bridge between intermolecular interaction dominated liquid-phase and non-interactive gas-phase environment.

Bare carbon chains and unsaturated hydrocarbons have been a topic of research since Douglas hypothesis suggested them as probable DIB carriers. The incentive of spectroscopic characterization of these carbonaceous ions and radicals is that they possess immense importance in combustion chemistry. Absorptions of fulvenallenyl radical (HC≡C-cyc-C_5H_4) have been recorded, and it is considered as the precursor of PAHs in flames. The m/z=63 ($C_5H_3^+$) peak is

very strong in the mass spectra of various unsaturated hydrocarbons which demonstrates stability of this fragment. This molecule is also conceived to be present in flames. *In situ* detection of $C_5H_3^+$ or fulvenallenyl radical in combustion can be carried out by using the reported electronic transitions. The matrix study on $C_7H_3^+$ has revealed that one of its isomer $HCCCCCCCH_2^+$ has potential to be the carrier of 438.77 nm DIB. All the $C_7H_3^+$ isomers identified in the matrix possess large oscillator strengths suggesting that they could be detected in the ISM even at low column densities.

The photo-instability of oxygen containing polycarbon cations has been identified. It could lead a very low column densities for such systems in harsh galactic environments, and therefore, hard to identify in the diffuse ISM.

Electronic spectra of a new class of molecules, protonated PAHs, have been carried out. The photo-instability of polycyclic O-containing species has been observed, similar to acyclic organic ketones. 2,3,6,7-dibenzotropone cation fragments with UV irradiation to phenanthrene cation. γ- and α-protonated species are generated upon protonation of fluoranthene *via* chemical ionization. The detection of C_{60}^+ in diffuse cloud has raised many questions about the interstellar processing of molecules. Scientists believe that C_{60} forms in the surrounding of late-type stars and planetary nebulae. Thereafter, *via* photoionization dissociates to relatively smaller organics and becomes hydrogenated to generate PAHs. According to a top-down speculation, one could expect the existence of fluoranthene type species (combination of six and five member rings) in the ISM.

Alongside astrophysical purposes matrix isolation plays pivotal role in trapping and spectroscopic characterization of organic reaction intermediates. Compared to radiolysis and flashphotolysis, matrix isolation combined with mass-selection provides vibrationally resolved electronic spectra which are more viable for *in situ* detection of reaction intermediates.

This dissertation has shown a multi-disciplinary research employing the matrix isolation technique and measurements of electronic transitions of various astrophysically important molecules – ions and radicals, which will be used in the future for finer spectroscopic studies in gas-phase.

Database: List of molecules studied during this doctoral thesis. Cations and radicals are listed along with the origin (0_0^0) band maxima.

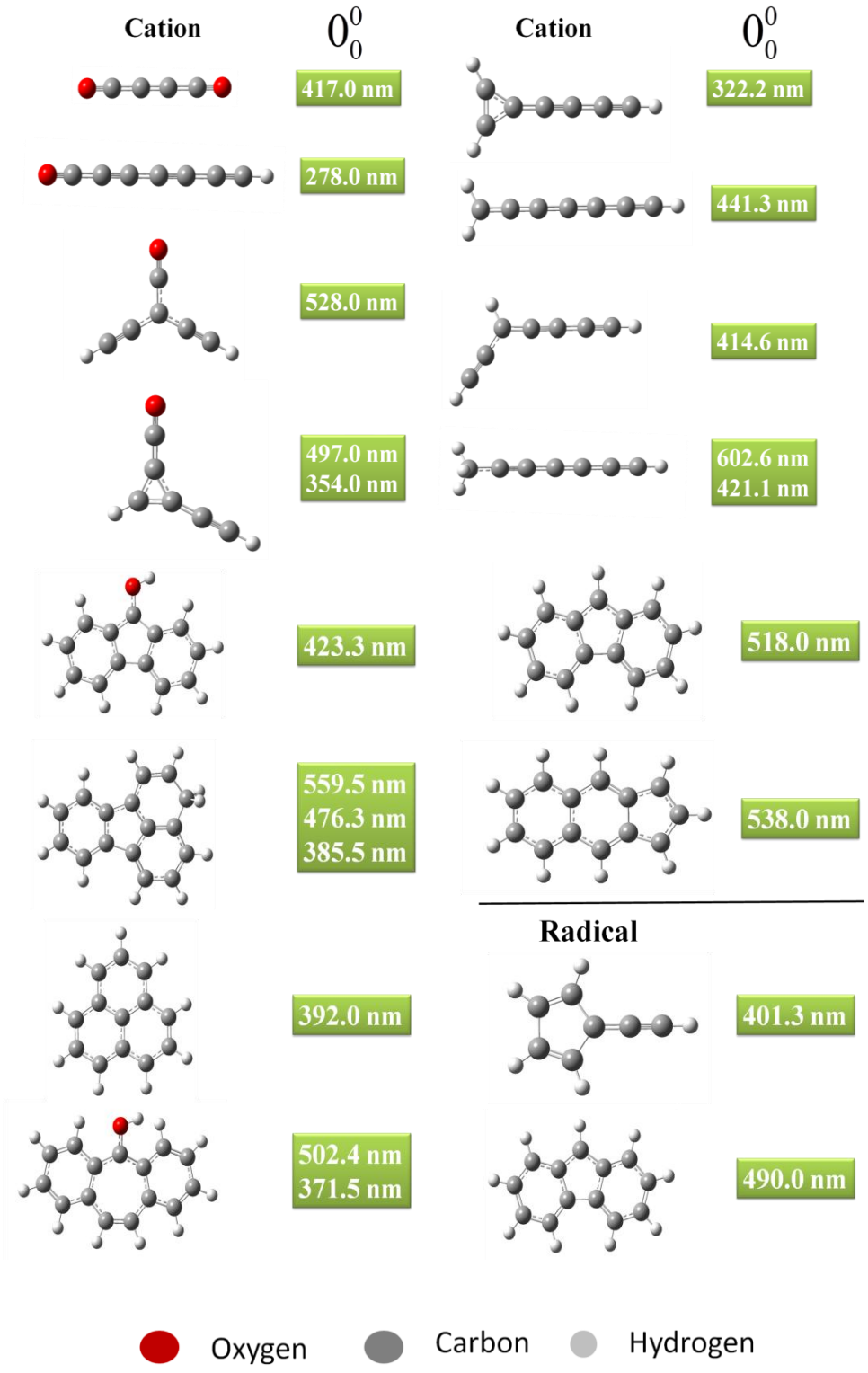

CURRICULUM VITAE

Name **ARGHYA CHAKRABORTY**
Date of Birth **27th July 1989**
Citizen **Indian**
Email *deep.chem27@gmail.com*
Current Address Johanniterstrasse 13
Basel, CH-4056

Education

Doctor of Philosophy (in Electronic Spectroscopy) ***Oct, 2011—Feb, 2016***
Physical Chemistry Department, University of Basel
Thesis Adviser: ***Prof. John P. Maier***
Thesis Title: ***Electronic Characterization of Mass-selected longer Chain Hydrocarbon Cations/Neutrals and Protonated Polycyclic Aromatic Species in Cryogenic Neon Matrices.***

Master of Science (M.Sc. in Chemistry) ***July, 2009—May, 2011***
Indian Institute of Technology Kanpur (IITK), Kanpur, India
Master's Thesis: ***Exploring Marcus Inverted Region in Binary Solvent Mixtures.***
Thesis Adviser: ***Prof. Pratik Sen***
CPI:8.4/10

Bachelor of Science (B.Sc. in Chemistry) ***July, 2006—May, 2009***
University of Burdwan, West Bengal, India
Score: 66.4% (First Class)

Internship

Summer Internship (Solvation Dynamics) ***May-July, 2010***
University of Hyderabad, Hyderabad, India
Thesis: ***Solvation Dynamics in a Di-imidazolium Ionic Liquid.***
Thesis Advisor: ***Prof. Annunay Samanta,*** *J C Bose National Fellow*

Invited Talk

• *PhD Chemistry Community, University of Basel (PCC @ unibas) Meeting 2014* : **Electronic Absorption Spectra of Astrochemically Important Mono-Oxygenated Hydrocarbon Cations : Produced in Hot Cathode via Ion-Molecule Reactions.**

Teaching Assistantship

• Physical Chemistry Lab — **Fall and Spring Semester**

Experiments: **1)** *Measurement of Surface Tension by Wilhelmy Plate Method,* **2)** *Differential Scanning Calorimetry (DSC),* **3)** *Vapor Pressure Measurement Experiment* — ***Oct, 2011—Dec,2015***

Publications

1. Arghya Chakraborty, Jan Fulara and John P. Maier; **2015**. *The Electronic Transition of the Fulvenallenyl Radical.* ***Angew. Chem. Int. Ed.*** 55, 228.

2. Jan Fulara, Arghya Chakraborty, and John P. Maier; 2016 *Electronic Characterization of Reaction Intermediates: Fluorenylium, Phenalenylium and Benz[f]indenylium Cations and the Radicals.* ***Angew. Chem. Int. Ed.*** 55, 3424.

3. Arghya Chakraborty**,** Jan Fulara, Rainer Dietsche and John P. Maier; **2014.** *Spectroscopic Characterization of $C_7H_3^+$ and $C_7H_3^{\bullet}$: Electronic Absorption and Fluorescence in 6 K Neon Matrices.* **Physical Chemistry Chemical Physics**, 16, 7023.

4. Arghya Chakraborty, Jan Fulara and John P. Maier; **2015.** *Electronic Absorption Spectra of $H_2C_6O^+$ Isomers: Produced by Ion-Molecule Reactions.* **Journal of Physical Chemistry A** 119, 50.

5. Arghya Chakraborty, Jan Fulara and John P. Maier; **2015.** *Electronic Spectra of Oxygen Containing Polycyclic Hydrocarbon Cations and the Protonated Analogues.* **Journal of Chemical Physics.** *143,* 084312.

6. Arghya Chakraborty, Jan Fulara and John P. Maier; **2013**. *Electronic Spectroscopy of a $C_7H_4^+$ Isomer in a Neon Matrix: Methyltriacetylene Cation.* **Australian Journal of Chemistry** 67, 416.

7. Jan Fulara, Arghya Chakraborty, Adam Nagy, Karol Filipkowski, and John P. Maier; **2014.** *Electronic Transitions of $C_5H_3^+$ and C_5H_3: Neon Matrix and CASPT2 Studies.* **Journal of Physical Chemistry A** 119, 2338.

8. Arghya Chakraborty, Corey Rice, F-X Hardy, Jan Fulara and John P. Maier; *Electronic Spectra of Protonated Fluoranthene in a 6 K Neon Matrix and in an Ion Trap at 10 K.* **Accepted in Journal of Physical Chemistry A** 10.1021/acs.jpca.5b12232

9. Arghya Chakraborty, Jan Fulara and John P. Maier; Electronic Spectrum of HC_7O^+. **Accepted in Journal of Molecular Physics** 10.1080/00268976.2016.1177218

10. F-X Hardy, Corey Rice, Arghya Chakraborty, Jan Fulara and John P. Maier; *Electronic Absorption spectra of $C_4O_2^+$: Study in Neon matrix and 22-pole ion trap*. Submitted to **The Astrophysical Journal.**

11. Jan Fulara, Adam Nagy, Arghya Chakraborty and J.P.Maier. Electronic Absorption spectra of C_5H^+: Neon Matrices and CASPT2 studies. Submitted to **Journal of Chemical Physics**

Conference

Poster Presentations

- *The Warm Universe Astrochemistry at Intermediate and Elevated Temperatures***.** (Tallinn, Estonia, 2012)
  Electronic Absorption Spectra of Mono-Oxygenated Hydrocarbon Cations ($H_2C_6O^+$, $H_2C_7O^+$, HC_7O^+) in 6 K Neon Matrices.

- *The 23rd International Conference on High Resolution Molecular Spectroscopy, Bologna 2014***.** (Bologna, Italy 2014)
  Spectroscopic Characterization of Oxygenated Hydrocarbon Cation, $H_2C_6O^+$: Produced via Ion-Neutral Reactions in Hot Cathode.

- Conditions and Impact of Star Formation: From Lab to Space (Zermatt, Switzerland, 2015**)**
  Electronic Transitions of $C_7H_n^{+/\bullet}$ (n=3-5) Species: Probable Precursor of PAHs in Sooting Environment
- Poster presentation on the Master's thesis: **Exploring Marcus Inverted Region in Binary Solvent Mixtures.**
  Kanpur, India 2011